Inter-Agency Space Debris Coordination Committee

Attitude motion characterization of LEO upper stages using different observation techniques

IADC Action Item 38.2

Working Group 1

Abstract

Active debris removal is one of the most promising solutions to clean up space for leftovers of activities in the past. Understanding the motions of the rocket bodies, which are the potential targets of the active debris removal, in the low earth orbits is necessary for the research and development of the active debris removal system. As a result of the AI31.2, a number of LEO upper stages presenting unexpected attitude motion were identified. The causes have not yet been fully explained and deserve further investigation. These particular objects should be analyzed by fusing data collected from different sensors to better characterize their attitude motion and evolution of this motion with time. In this AI38.2, 9 objects were selected as the targets of the campaign observation that show the unexpected attitude motion. Six space agencies joined the campaign observation and a lot of lightcurve data were obtained. These data will be shared with all the space agencies of IADC and will be analyzed for future investigation in the near future.

1 Introduction

Space debris is becoming a serious problem in low earth orbit (LEO). It is thought that a chain reaction of cascading collisions, in which many pieces of space debris created by a collision become sources of other collisions, have begun in the 1000 km region. Humanity must cope with this situation as soon as possible to protect its space programs. The active debris removal (ADR) systems which remove relatively large objects such as rocket bodies and inactive satellites from the precious orbits, is one of the most promising solutions because it reduces the risk to create enormous amounts of debris. Many space agencies are studying and developing various method for the ADR system. Rocket bodies will be good targets since their shapes are relatively simple which help the ADR system to access them. Understanding the motions of the rocket bodies are very important to design the ADR system. As AI31.2, the working group 1 (WG1) of IADC performed the observation campaign targeting 137 rocket bodies to understand the overall situations of the rocket bodies in LEO. As a result, the visual inspection of the light curves showed 6.6% of the objects indicated clear periodic brightness variations and 8.3% did ambiguous ones. Large part of the objects indicating clear periodicity get and/or lose their periodicities arbitrarily. The understanding of this phenomenon would be of great use for the future ADR missions and could also be useful for the improvement of the reentry predictions. In order to understand the phenomenon, WG1 selected 9 objects as the observation targets which include a subset from the previous AI32.1 that showed the phenomenon. Five space delegations (ASI, CNES, ESA, JAXA, SSAU) had joined the campaign observation and provided the lightcurves. The detail of the observations of each agency is described in the section 2. The obtained lightcurves are shown in the section 3.

2 Observation

WG1 selected 9 rocket bodies (SSC number: 11804, 18340, 23088, 23405, 25637, 39198, 40879, 41847, 41858) for the campaign observation targets which include a subset from the previous AI32.1 that showed the phenomenon. Five delegations, ASI, CNES, ESA, JAXA and SSAU joined the campaign observation. We did not set the detailed observation and analysis strategies since each

delegation has different equipment, observation method, and analysis processes. Unifying these parameters is very time-consuming and ruin the main objective of the campaign observation sometimes. The details of the observation of each delegation are described in the section 2.1, 2.2, 2.3, 2.4, and 2.5 respectively. CSA has a very unique observation asset, NEOSSat in the orbit. Although CSA could not joint the campaign observation, the satellite will provide great contribution to this kind of campaign in the near future. The details of the NEOSSat are shown in section 2.6.

2.1 Observation and data analysis at ASI

The light-curve presented for this AI were acquired with the Remote Space Debris Observation System (RESDOS) and the Sapienza Coupled University Debris Observatory (SCUDO) observatories, located in Rome (RM) and Collepardo (FR), respectively. In both systems, a scientific Complementary Metal-Oxide Semiconductor (sCMOS) sensor is installed integrally with the main telescope and its mount, so the systems can track the satellite and acquire the video in real time. Both systems are equipped with the same sCMOS sensor and mount. The sCMOS have a resolution of 5.5 Mpx and a sensor diagonal 22 mm. The maximum fps achievable is 100. The optical tube has a focal length of 750 mm and a diameter of 150 mm. The mount type is equatorial. These two observatories were used also to produce simultaneous light-curve.

Figure 1. RESDOS observatory (left) and SCUDO observatory (right)

The light-curve of the object is retrieved starting from the computation of the object and stars intensity (i.e. the luminous flux) for each frame. In the frame, all the objects (stars and satellite) are identified, and a preliminary position is assigned through the use of a segmentation algorithm. This preliminary position is corrected evaluating the proprieties of the object (shape, flux, background, etc.) not in the whole frame but in a small region of interest (ROI). Once the object is correctly discriminated from the background, an aperture photometry procedure is applied to calculate the object position (centroid) and intensity.

Once the centroid and the intensity of the stars and of the object in each frame are extracted, the

magnitude is calculated comparing the intensity of the object respect to each star in the FoV. The magnitude of the object is evaluated respect to all the stars in the frame, so a vector of possible values is obtained, and it is assumed that the object's magnitude is equal to the median of these values and the error is the standard deviation of these magnitudes. Some positions can be affected by a wrong segmentation procedure due to the star crossing of the object or to the overexposure of the object itself. These data are excluded. All the relevant data (datetime, pixel position, celestial coordinates, brightness intensity, magnitude, background) for each frame are then stored in the Tracking Data Message (TDM) standard.

2.2 Observation and data analysis at CNES

CNES contributed to AI38.2 using the TAROT Réunion telescope located on Reunion Island in Indian Ocean. TAROT Réunion is owned and operated by CNRS.

Figure 2. TAROT telescopes

2.2.1 Cnes Images capture method

The TAROT telescopes are observing higher orbits every night as part of the French and European Union Space Surveillance and Tracking programs. As we optimized the telescope command and control software for these operational activities, we had few possibilities of adaptation of the observation scheme for this new type of activity. So, the best observation method we found in the context of those constraints was to make a sidereal picture of 10 seconds at an approximate pace of one every 40 to 90 seconds.

As the information we can provide with this system is very fragmented (see figure below), we decided to make a few observation to better understand the constraints and needs of this type of observations but not to use a lot of telescope time for so few information. In consequence, we limited this campaign to 4 light curves of norad 39198 and 31 light curves of norad 23405.

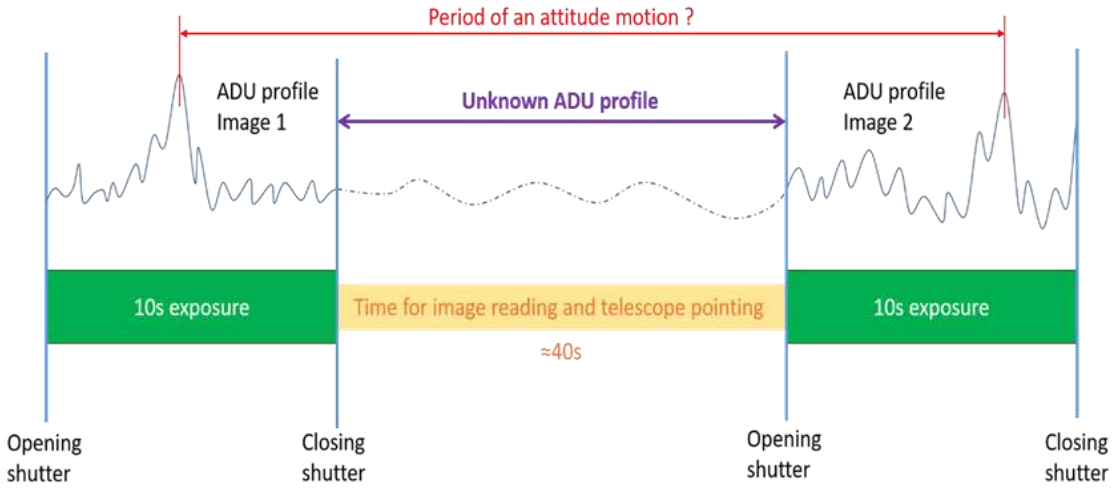

Figure 3. Image sequencing schema

2.2.2 Cnes images analysis

To extract the light curves from the images, our extraction software followed the following scheme:

- detection of the ends of the trail,
- fitting of a curve linking both ends of the trail,
- performs a bilinear interpolation to extract the ADU value of pixels surrounding the curve.

This gives us the ADU variation over the 10 seconds of the picture.

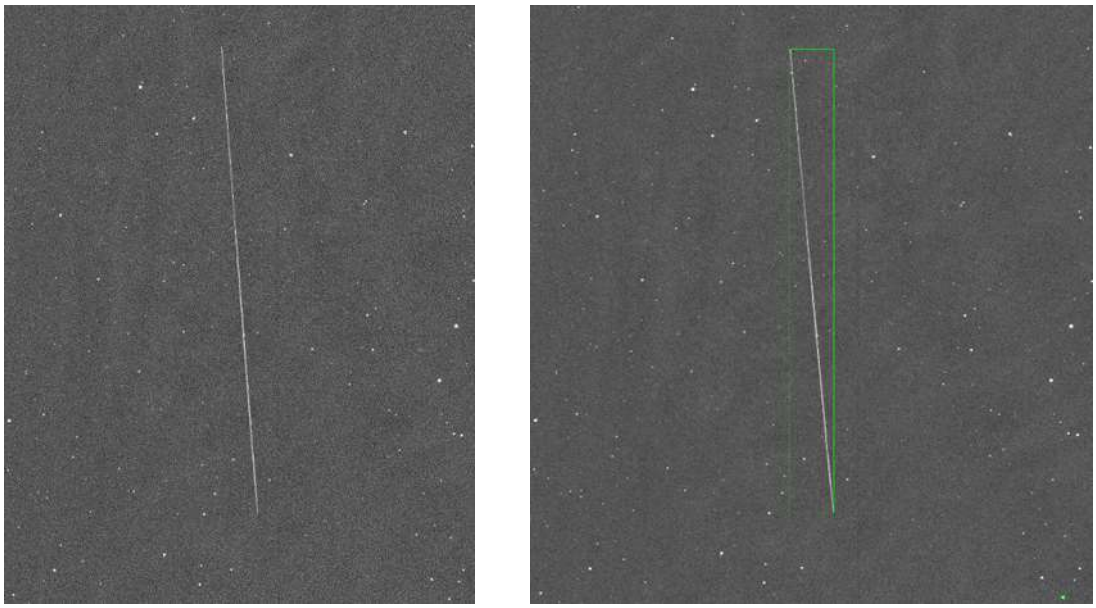

Figure 4. Light trail detection

2.2.3 Cnes observations of PEGASUS R/B NORAD 39198

The norad 39198 object is very interesting as its light curves presents very bright peaks. This object is the third stage of the PEGASUS XL rocket that launched the satellite IRIS (SMEX 12, Explorer 94).

Figure 5. Image of an Orion 38 (Pegasus XL third stage, source http://www.b14643.de)

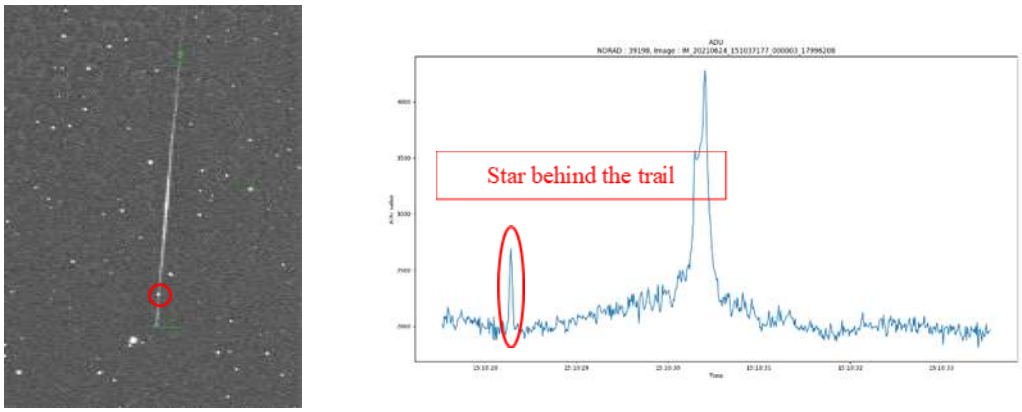

Figure 6. First image of PEGASUS light trail and its ADU profile

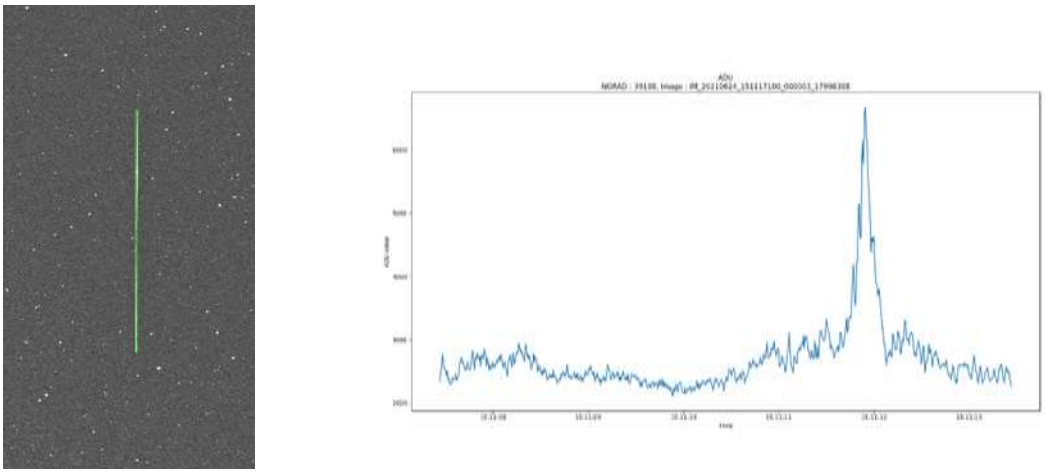

Figure 7. Second image of PEGASUS light trail and its ADU profile

We took the two images presented consecutively as shown in the following graph:

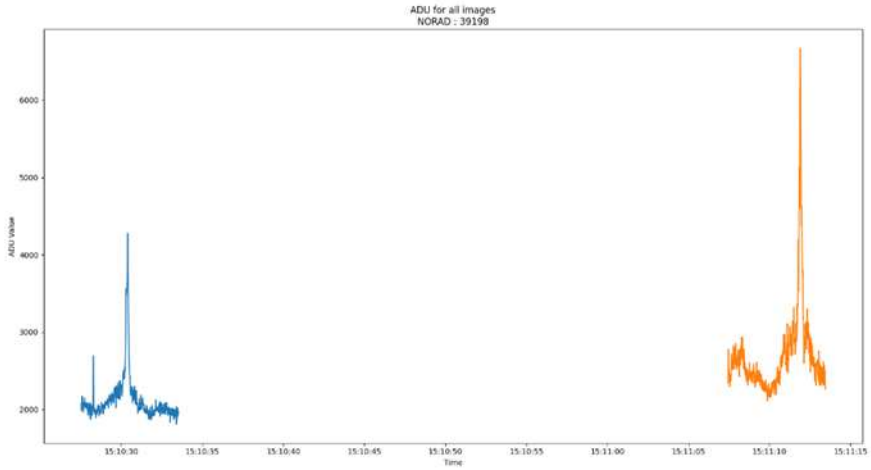

Figure 8. ADU profile in sequence

As the interval of time between the two light curves is too long, we cannot infer a periodicity from this sequence of light curves.

2.2.4 Observations of norad 23405

The figure below shows the dates when we obtained lightcurves from norad 23405 object. During those 6 passes of the satellite above TAROT Réunion, we extracted 31 light curves of 10 seconds.

The figure below shows the dates when we obtained lightcurves from norad 23405 object. During those 6 passes of the satellite above TAROT Réunionn, we extracted 31 light curves of 10 seconds.

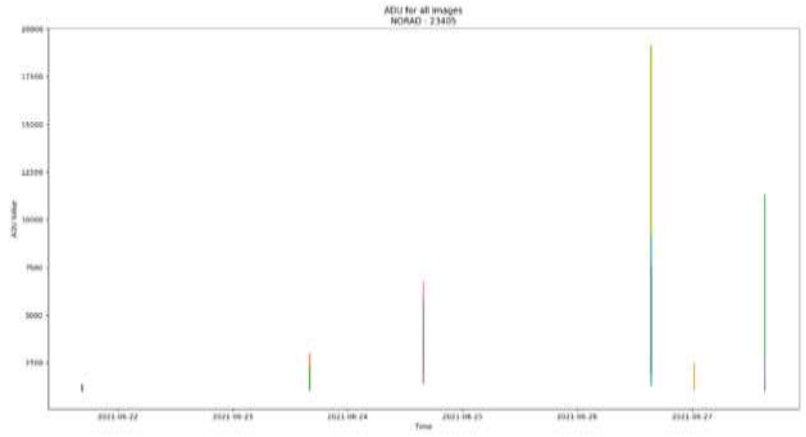

Figure 9. dates of the N23405 observed passes

The figure below shows an example of a lightcurves series taken during a pass of the satellite.

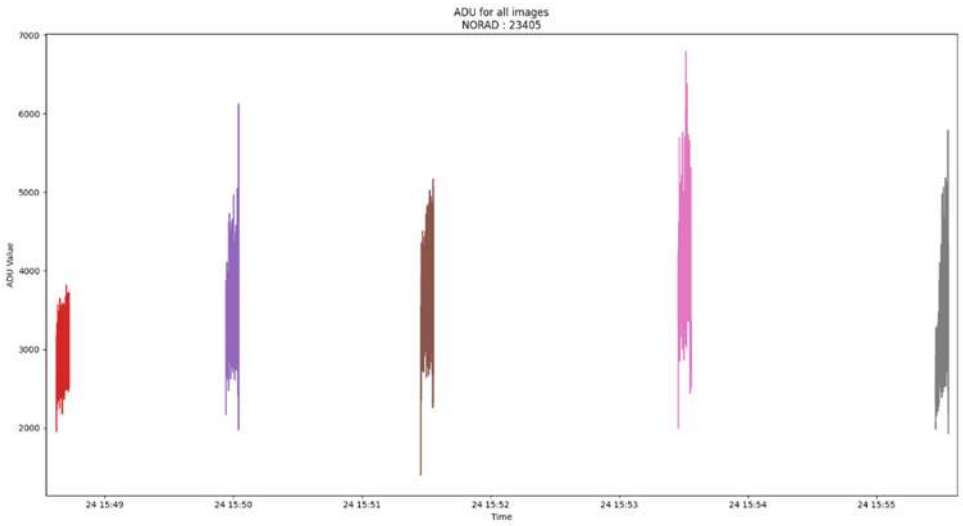

Figure 10. example of a sequence of light curves during a pass of norad 23405

For this second object, we did not observed any bright peak on the lightcurves. Some of the variations seen on the light curves has been interpreted by the analyst as the partial masking of the streak by a cloud during a part of the exposure time.

2.2.5 Conclusions on the Cnes campaign

The OSMOSE/TAROT system is able to provide ADU profiles from long exposure images. As of today, the information provided is very fragmented because of the lack of versatility of the current observatory's supervision software which is optimized for higher orbits observation.

The informative content of the lightcurves sequences we can produce being poor, we decided not to use much telescope time for this activity and limit the production to about 30 lightcurves. In 2023, or new observatory supervision software named PyROS and the use of CMOS Camera will give us the ability to produce more informative lightcurves.

One of the lessons learned during this campaign is that variability of the brightness of the detection can be due to a variability of the brightness of the object observed, but also to clouds attenuating the light crossing the atmosphere. Attenuation varying both temporally and spatially, the correction of this effect on the lightcurves seems not easy. This fact should be taken into account when using lightcurves.

2.3 Observation and data analysis at ESA

ESA data in support of AI38.2 was collected in the time frame from March 2021 to March 2023. For some objects archive data from previous years has been added. All observations were acquired by the Astronomical Institute of the University of Bern (AIUB) at the Swiss Optical Ground Station and Geodynamics Observatory Zimmerwald, Switzerland. The photometric light curves were obtained using either a CCD camera with frame rates of about 0.3 frames/s or a sCMOS camera with frame rates of up to 70 frames/s. The CCD light curves were acquired at the 1-m Zimmerwald Laser and Astrometry Telescope ZIMLAT (see Fig. 10), and all the CMOS data was taken at the 0.8-m Zimmerwald Multiple Applications Instrument ZimMAIN (see. Fig. 11).

Light curves with the ZIMLAT CCD camera are obtained by taking series of small sub-frames (200x200 pixels or 2.60' x 2.60') centered on the objects. Real time centroiding of the target object is used to feed an active tracking loop to prevent the object from leaving the sub-frames due to poor orbit predictions. The exposure time may be chosen from 0.2s (due to the shutter limits) on upwards, and filters can be used (e.g. B- and V-filter), depending on the brightness of the object. The sampling interval is about twice the exposure time. After 500 sub-frame images are acquired, a full frame with 2064x2048 pixels (26.6' x 26.6') is acquired for photometric recalibration purposes, resulting in a gap of around 20s between every two series of 500 sub-frames. The observation data is stored in form of the original images. The intensity of the object is measured on the sub-frames in an automated real-time process. Some images are excluded, e.g. if a star is present in the sub-frame or if the object is over- or underexposed. A text file containing the measured intensities and epochs, as well as additional information from the photometric reduction, is generated from the data of the remaining sub-frames and used for further analysis of the light curve.

For targets which show high frequency signals or which are clearly under-sampled in the CCD observations, a high frame rate Andor Neo sCMOS-camera may be used. In this case series of full frames of 2560 x 2160 pixels (7.5’ x 6’) with frame rates between 5 to 100 frames/s are acquired. No active tracking is performed.

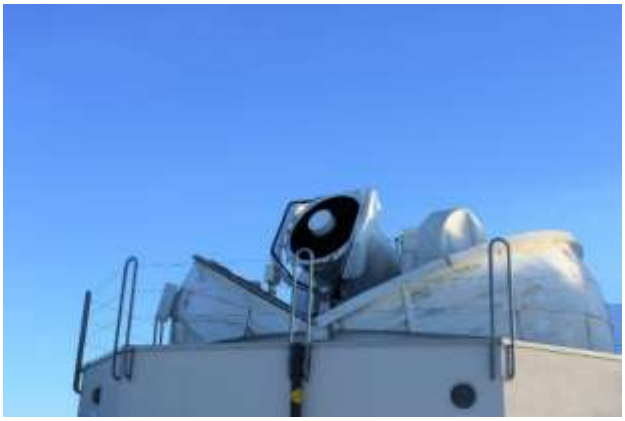

Fig.10. AIUB’s 1-meter Zimmerwald Laser and Astrometry Telescope ZIMLAT jointly used for passive optical measurements (photometry and astrometry) and satellite laser ranging (SLR).

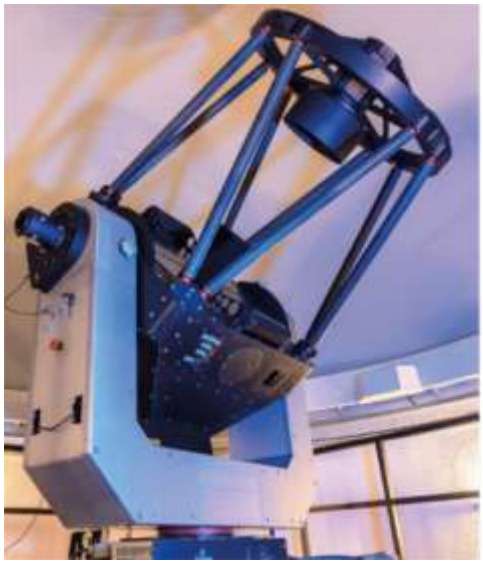

Fig.11. AIUB’s 0.8-meter Zimmerwald Multiple Applications Instrument ZimMAIN used for passive optical measurements (Astrometry, photometry, and spectroscopy).

A summary of the observations acquired for the various targets of interest is presented in Table 1. In this table, the stability of a light-curve is defined as “Stable” or “Slow-tumbler” for objects which show no clear signs of rotation within the time interval of observation (length of the pass). For a rotating object, the range of estimated periods is listed. Periods have been determined with a phase dispersion minimization method.

A “stable” light-curve refers to the case where the observed pattern of the brightness is simple enough that it appears to be a function of the target’s orbital motion around the Earth only. On the other hand, a “slow-tumbler” light-curve refers to the case where the pattern is not as simple as in the previous case and it appears to be a function of the target’s attitude motion along with its orbital motion.

However, it should be noted that such a classification into these two categories is purely empirical. It is based on the inspection of several parameters such as the object’s elevation, sky-background (presence of clouds), object’s entry into Earth’s shadow etc. Moreover, a “stable” light-curve for an object does not indicate that the object is always stable. It merely indicates that the estimated behaviour of the object based on that particular light-curve is stable. On some occasion, it is possible to observe a light-curve for the same object that has "slow-tumbler" nature.

Table 1

Target No.	**COSPAR ID**	**NORAD**	**Target name**	**Light-curves details**	
				# of light curves Observation interval	**Comments on the period / Light-curve / stability of the light-curve**
2	1987-074G	18340	SL-14 R/B	29 light curves 12 Apr 2021 - 16 Mar 2023	*periodic* period = 36 to 95 sec 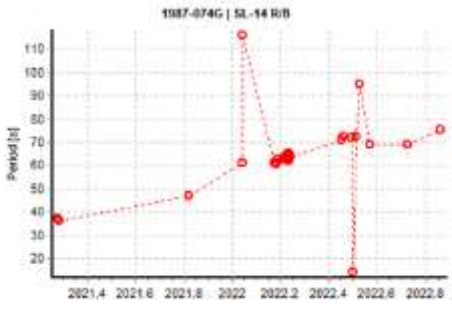
3	1994-023B	23088	SL-16 R/B	28 light curves 14 Dec 2014 – 15 Feb 2023	*periodic in 2014 and 2015!* *slow-tumbler or stable else*

4	1994-077B	23405	SL-16 R/B	10 light curves 06 Apr 2021 – 11 Jul 2022	*slow-tumbler or stable*
5	1999-008D	25637	DELTA 2 R/B	3 light curves 06 Apr 2021 – 11 Jul 2021	slow-tumbler
6	2013-33B	39198	Pegasus R/B	17 light curves 9 Jan 2021 – 20 Mar 2023	*slow-tumbler or stable*
7	2015-040B	40879	CZ-4C R/B	6 light curves 13 Apr 2021 – 6 Jul 2022	*slow-tumbler or stable*
8	2016-066G	41847	CZ-11 R/B	19 light curves 14 Apr 2021 – 19 Jul 2022	*slow-tumbler or stable*
9	2016-068B	41858	CZ-2D R/B	12 light curves 14 Apr 2021 – 5 Mar 2022	*slow-tumbler*

Individual light curves are provided in Section 3.3. The figures are annotated with labels like "azimuth = [xx yy zz]" where xx, yy, zz are the values for the beginning, the middle, and the end of the light curves. Values are given for the azimuth, elevation, phase angle, exposure time, and range. All observations were performed without filters and the magnitudes are instrumental magnitudes, i.e. not individually calibrated.

2.4 Observation and data analysis at JAXA

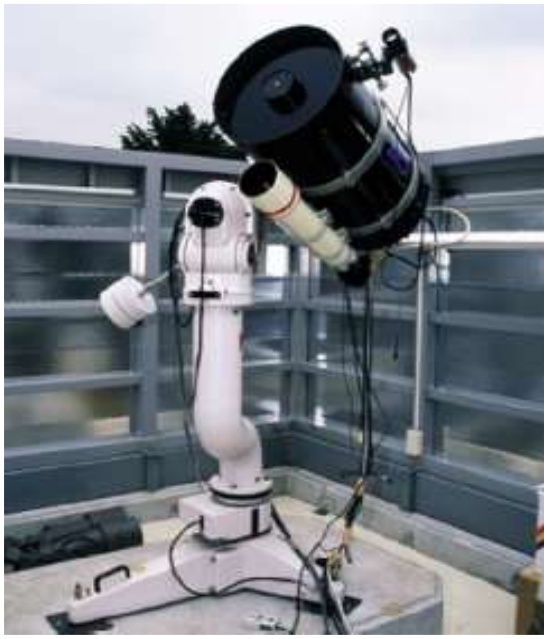

Fig.5. JAXA's 35cm telescope for LEO object. A Schmidt Cassegrain telescope with diameter of 350 mm and focal length of 3910 mm with a tri-axial equatorial mount. Mounted at the focal plane is a fast-readout CCD camera (NIL ICC-40M) able to take 10 images every second.

The 35 cm LEO observation telescope at the Aerospace Center of JAXA in Chofu, Tokyo was used for the campaign. Fig.5 shows the telescope, which is a 35 cm Schmidt–Cassegrain

telescope on a tri-axial equatorial mount. Since the tri-axial equatorial mount does not have any singular points in the sky it can easily track any type of orbit. A fast-readout CCD camera (NIL ICC-40M) that can acquire 10 images per second is mounted at the telescope's focal plane. The observations were carried out for 55 days from July 2nd, 2020 to February 1st, 2022 totaling 55 light curves. Between 500 and 1000 images were acquired during each pass depending on the observable time. The LEO observation telescope shown in Fig.5 can start observations automatically by calculating the target's position from up-to-date orbital elements. The difference between the calculated and actual orbits was corrected for manually using the guide telescope attached to the main telescope.

From the image data acquired from the telescope, the brightness of a target on each image is measured and a light curve is created. Measuring the brightness of a target in a few thousand images manually would be extremely time-consuming, so an algorithm was developed to recognize a target and measure its brightness automatically. The algorithm identifies a group of pixels in an image with a value higher than a threshold as the target. It then sums the value of 100 pixels around that group of pixels and subtracts 100 times the median value of the surrounding pixels to correct for the sky value. The brightness of the target in each image is measured automatically by these processes. The algorithm can avoid false detection of thermal noise and cosmic ray events that manifest as isolated high-value pixels. As the field of view of the telescope is relatively narrow (6.7 by 8.9 arc minutes) and the telescope tracks at high speed the probability of stars entering the field of view is very low. Even if this should occur the light from the stars would be spread along lines parallel to the telescope's motion, which would usually result in star streaks dimmer than the target. For safety, single "spiky" events whose values exceeded those of neighboring points by more a factor of two were discarded.

2.5 Observation and data analysis at SSAU

In total, since the beginning of the campaign, Ukrainian observers (the location and characteristics of telescopes were given earlier) have received 153 light curves (LC) for 8 objects of the campaign (1 LC from Astronomical Observatory of Lviv National University, 14 LC for 4 objects from Wide FoV telescope of SSAU Quantum Ooptical Station (QOS) in Khmelnytskyi region, other LC from KT-50 telescope of RI "Astronomical Observatory", Odessa National University (AO ONU)). The largest contribution (138 LC) was made by observations with the KT-50 (Fig. 6) telescope of the Odessa Astronomical Observatory. Since the main results were obtained at the AO ONU, and the results of the QOS observations generally correspond to them, here the main attention will be focused precisely on the results of the AO ONU.

Fig. 6 KT-50 telescope of AO ONU. A Maksutov telescope with diameter of 500 mm and focal length of 2000 mm with an alt-azimuth mount. Mounted at the focal plane is a TV-CCD camera Watec-902H2 able to take 50 TV halfframes every second.

KT-50 is a Maksutov telescope on a semi-automatic alt-azimuth mount (maximum slew rate is 4

deg/s). It is equipped with a TV-CCD camera Watec-902H2. This setup runs at a fixed rate of 50 TV half-farmes/s. All processing of the received data is carried out using software developed in AO ONU. The brightness values were taken taking atmospheric extinction into account and recalculated to a single topocentric distance (1000 km).

The analysis of the light curves of the observed objects, made by the specialists of AO ONU, made it possible to detect only one relatively rapidly rotating object - USSC ID 18340 (COSPAR ID 1987-074G). This analysis was sent separately. To save space, here in Section 3.5 only those light curves that were shown in this report, as well as all the light curves of the object 18340, are presented.

2.6 Contribution of CSA

The Canadian Space Agency (CSA) owns and operates, in collaboration with Defence Research & Development Canada (DRDC), the Near-Earth Object Surveillance Satellite (NEOSSat). NEOSSat is a 75-kg microsatellite space telescope, launched in February 2013 to a 780km sun-synchronous low-Earth orbit. The satellite's primary payload is a 15-cm aperture Maksutov telescope with 0.8º field of view and associated read-out electronics providing 3 arcsecond/pixel resolution on a E2V 1024x1024 charge-coupled devices (CCD). NEOSSat splits its observation time evenly between two core missions: space astronomy (e.g., near-Earth asteroids/comet astrometry and exoplanet transit photometry) and space surveillance (e.g., space situational awareness, tracking of resident space objects in various orbit regimes). NEOSSat was originally designed track deep space geosynchronous space objects but was adapted to track LEO objects in 2017.

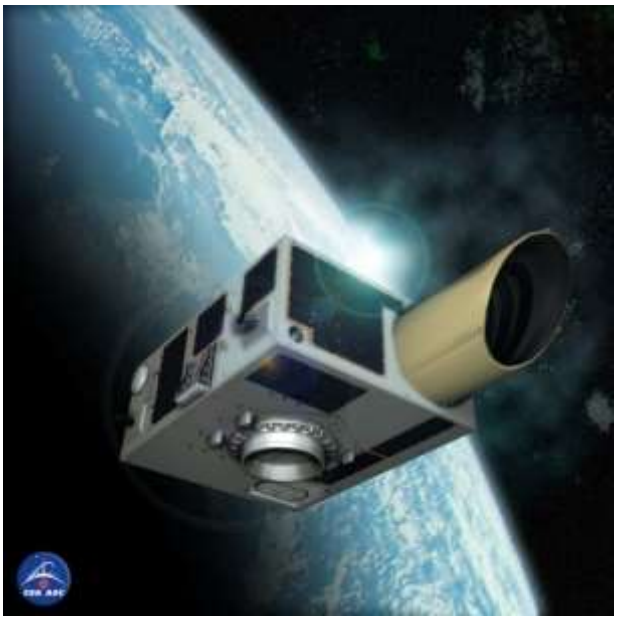

Fig.7. Artists rendition of Canada's NEOSSat space telescope on-orbit. NEOSSat provides a 15-cm aperture Maksutov telescope with 0.8º field of view and 3 arcseconds/pixel.

LEO to LEO tracking is possible from NEOSSat as long as the target object's relative angular rate is within the control authority of NEOSSat's attitude determination and control system (ADCS). The target object must also be at least 11 degrees above the illuminated portion of Earth's limb for NEOSSat's co-boresighted star tracker to detect background stars for its fine slew tracking. There is

no constraint on tracking over the dark limb if guide stars are available for NEOSSat' s ADCS. Typically, the angular rate and Earth limb angle constraints on NEOSSat limits tracking of objects to ~2-4 minute intervals in LEO depending on target altitude.

While rocket bodies tend to be large making them well-suited for detection by NEOSSat, light curves detailing rocket body rotational motion are more challenging for NEOSSat to achieve. NEOSSat's frame rate when tracking LEO objects is approximately 1 image / 15 seconds (0.067 Hz). This sampling rate suboptimal for characterizing fast-rotating bodies to support light curve analysis tools such as light curve folding, Fast Fourier Transforms or Lomb-Scargle periodograms. Given that NEOSSat can only really perform 1-2 tracks on LEO space objects due to ADCS constraints, full rotational characterization of rotating rocket bodies is challenging. In this experiment, NEOSSat collected range normalized photometric characterization of select rocket bodies in both time, phase angle and time during track.

NEOSSat collected tracks on selected rocket bodies shown in Table 2.

Table 2. NEOSSat rocket body targets for IADC AI 38.2 campaign

SSN ID	Object Name	Int. Number	Country	Launch Date	Period (mins)	Incl. (deg)	Apogee (km)	Perigee (km)
11804	SL-8 R/B	1980-039B	CIS	1980-05-20	104.62	82.94	992	962
18340	SL-14 R/B	1987-074G	CIS	1987-09-07	114.69	82.57	1472	1411
23088	SL-16 R/B	1994-023B	CIS	1994-04-23	101.78	71	844	842
23405	SL-16 R/B	1994-077B	CIS	1994-11-24	101.74	70.98	845	838
39198	PEGASUS R/B	2013-033B	US	2013-06-28	97.22	97.94	642	610
40879	CZ-4C R/B	2015-040B	PRC	2015-08-27	108.01	100.41	1204	1065

Figure 8 shows the tracks on rocket bodies detected from orbit by day of year in 2020. Range normalization uses a 1000 km range as a comparison basis for LEO objects when observed from orbit. This helps compare ground-based observers which have a different perspective on the orbiting targets. The range normalized magnitude range of detection spans magnitude 2 through magnitude 8. In this view, rotational motion is not inferable. However, the span of the brightness observations exceeding 1 magnitude or more, if often an indication of rotational motion of space objects.

Figure 9 shows the phase angle vs range normalized behavior of the space objects detected in LEO. Note that several observations were collected over the dayside of the Earth where the phase angle (the angle subtending Sun/target/observer) exceeds 90 degrees. In such cases, back-reflected sunlight from the Earth onto the rocket body acts as a secondary illumination source making the object somewhat brighter than if it were observed over Earth's night side. This effect is somewhat small compared to the brightness of the Sun but may have the impact of brightening the rocket bodies. NEOSSat's space-based perspective adds the ability to observe such objects over the dayside of the Earth where ground-based observers normally cannot.

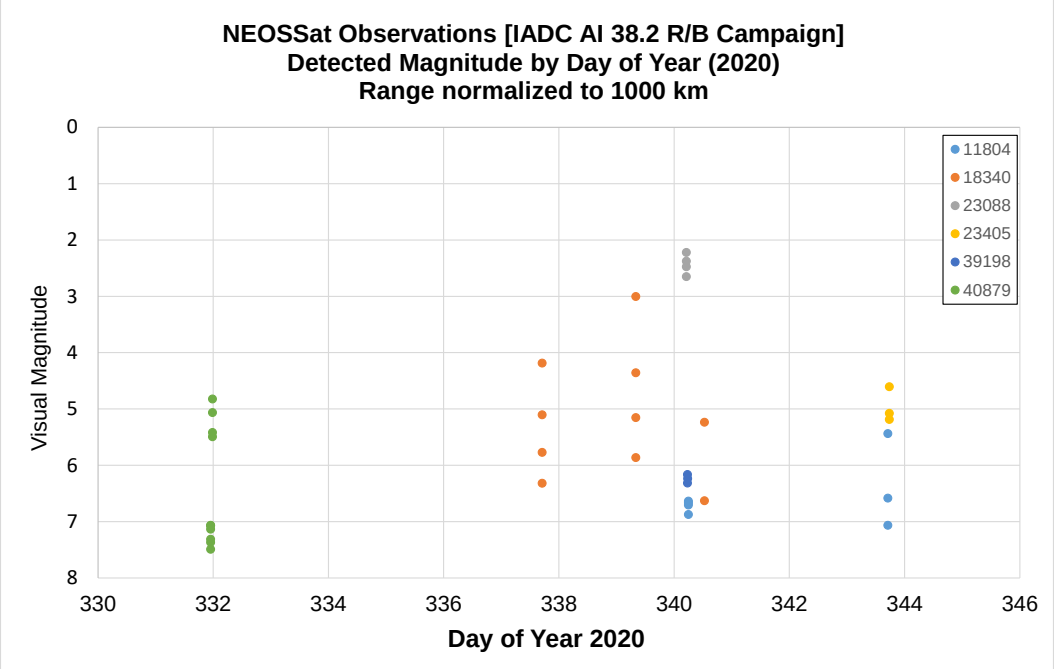

Figure 8. Time vs magnitude of AI 38.2 rocket bodies detected by NEOSSat in 2020.

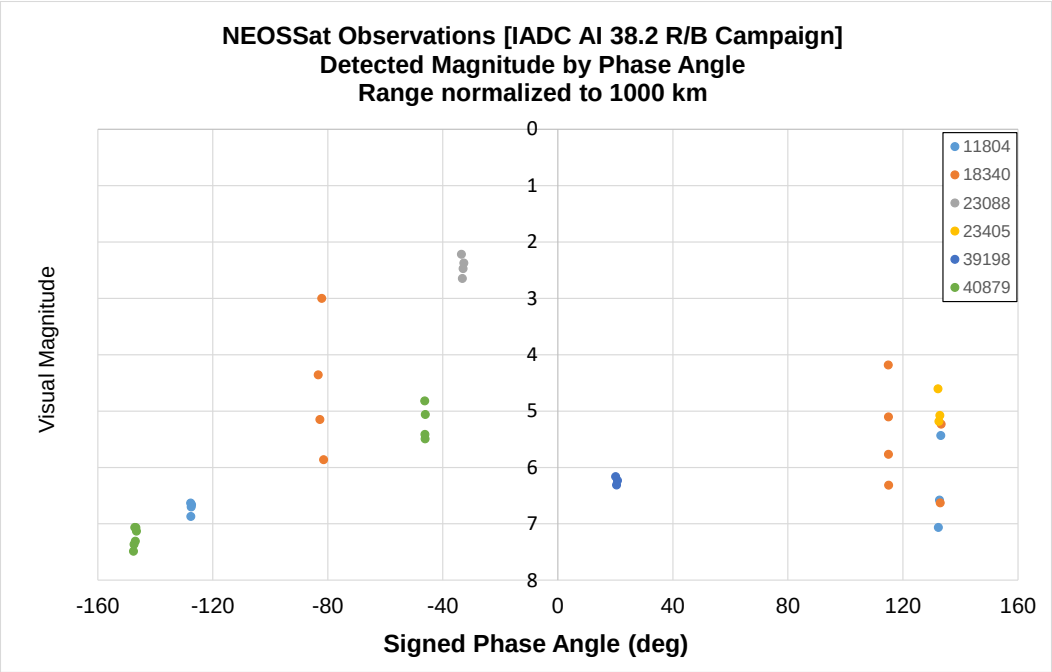

Figure 9. Phase angle versus magnitude of AI 38.2 rocket bodies detected by NEOSSat in 2020.

Figures 10 and 11 show the time during track of the rocket bodies for objects suspected to have slow to little rotational motion. Slow rotation is typically identified by the degree of variability of the target's photometry where objects exhibiting less than 1 magnitude of variation are generally considered to be slowly rotating. Objects with variability greater than 1 magnitude are generally considered to be faster rotating. Figure 10 also shows that the majority of NEOSSat tracks are short

duration (< 75 seconds) with few samples per track. While NEOSSat is not optimal for light curve analysis, some degree of target angular motion of the detected objects can be inferred by the degree of variability of the target's photometry when tracked from orbit.

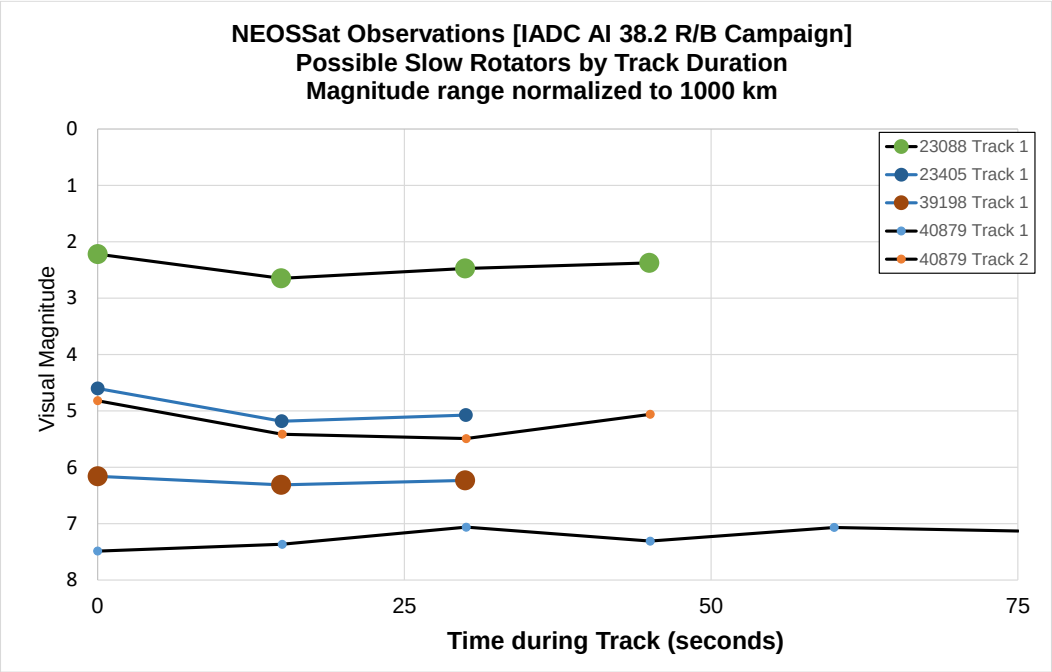

Figure 10. Time within track vs magnitude of AI 38.2 objects (suspected slow rotators).

Figure 11 shows a similar plot, but with objects suspected of having rapid rotational motion and contrasts the behavior of objects in Figure 10. Figures 10 and 11 give some indication of their prospective attitude motion based on their photometric behavior.

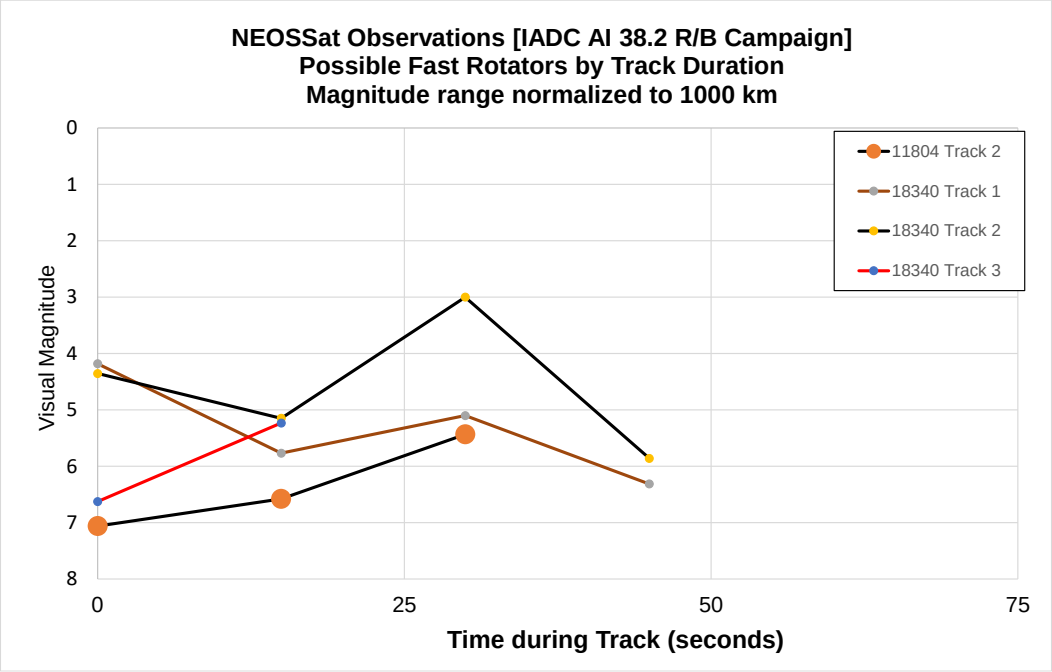

Figure 11. Time within track vs magnitude of AI 38.2 objects (suspected fast rotators).

3 Lightcurves from each delegation

3.1 Lightcurve graphs from ASI

3.1.1 Norad 11804

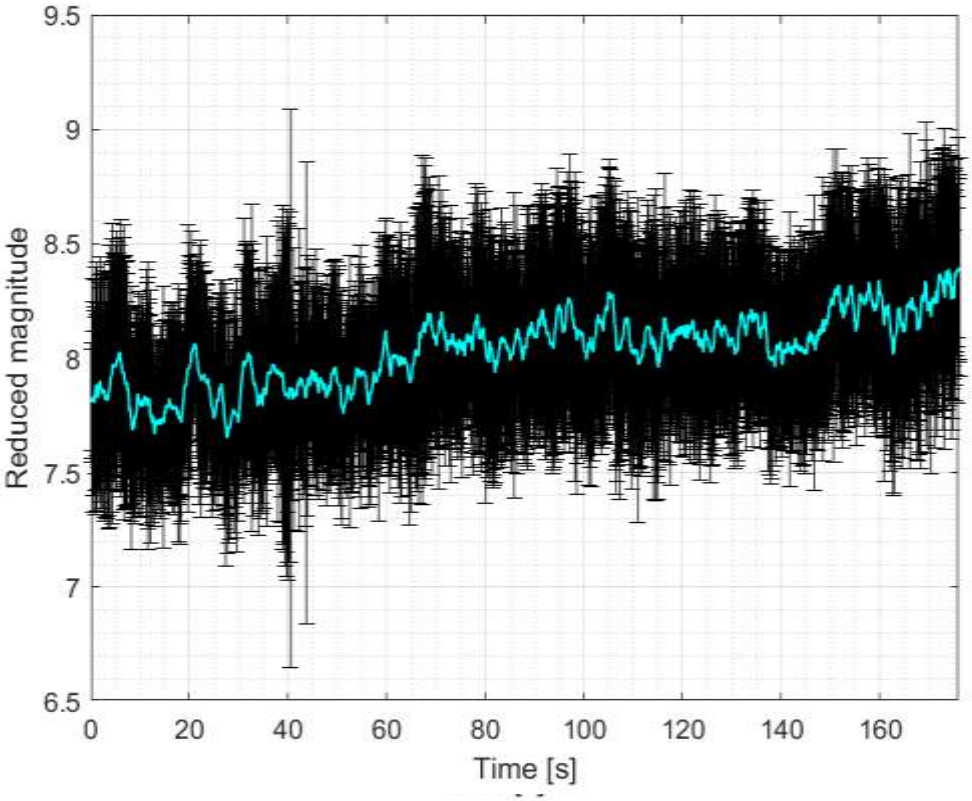

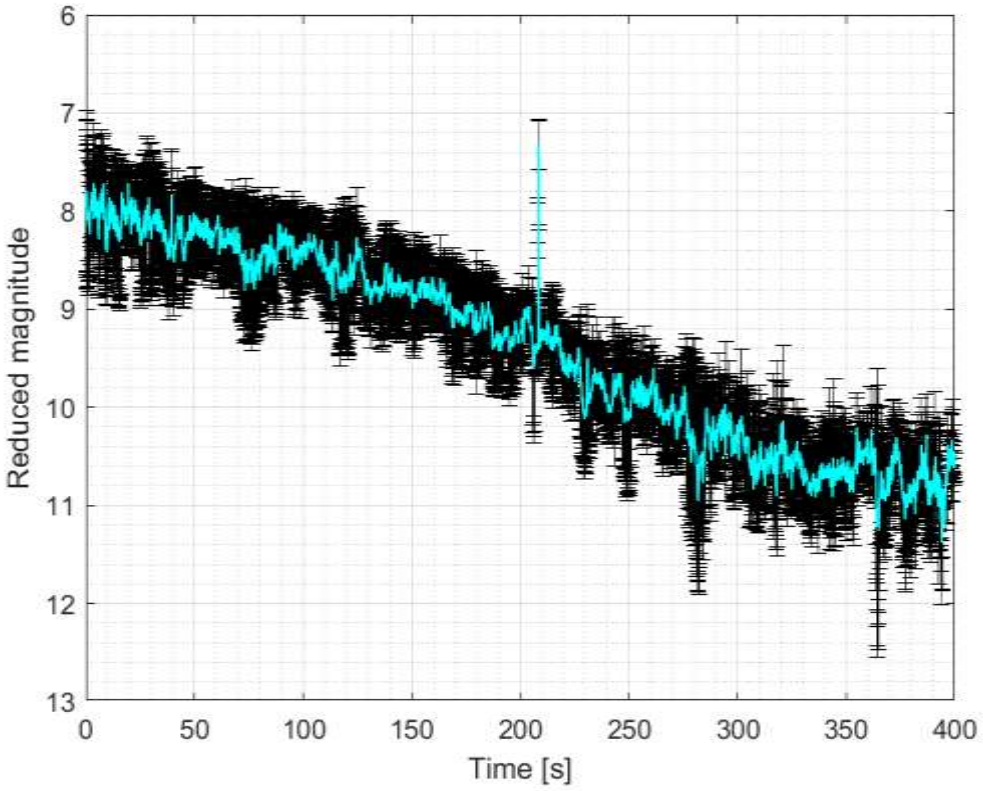
Reduced magnitude
Time [s]
6
7
8
9
10
11
12
13
0
50
100
150
200
250
300
350
400

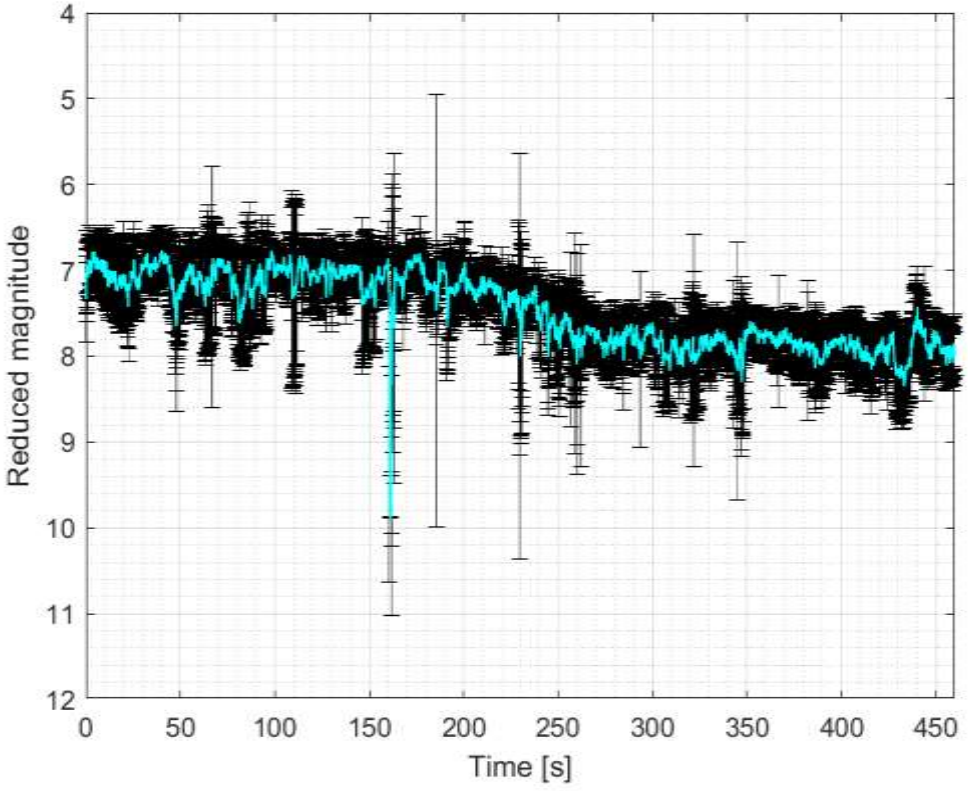
Reduced magnitude
Time [s]
4
5
6
7
8
9
10
11
12
0
50
100
150
200
250
300
350
400
450

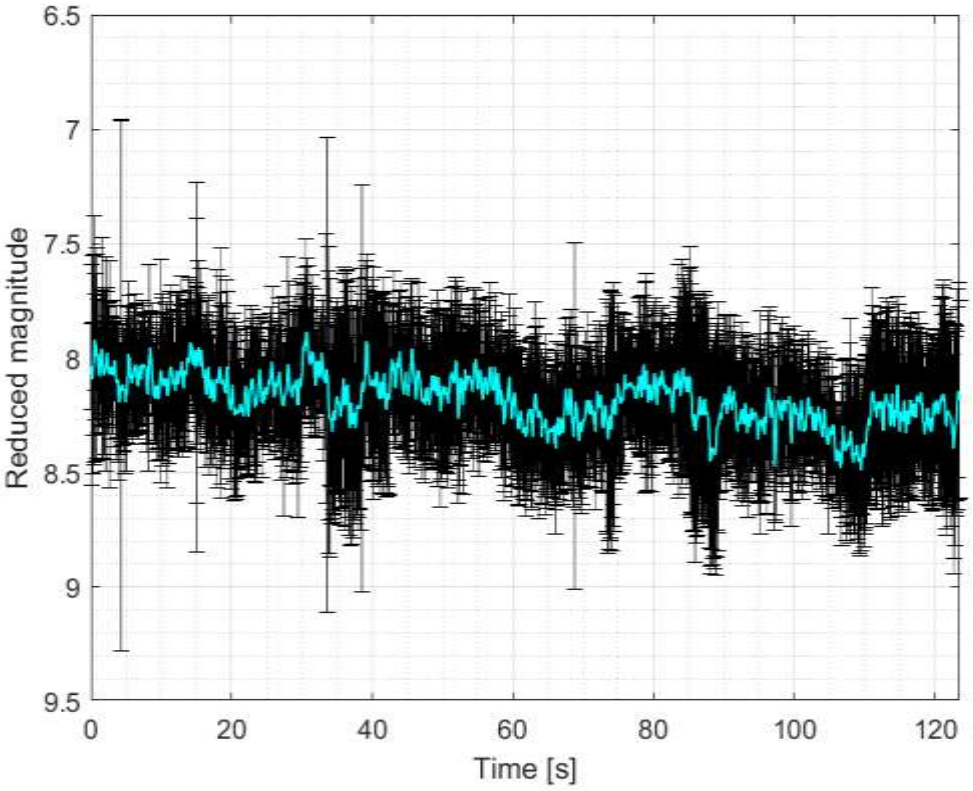
Reduced magnitude
Time [s]
6.5
7
7.5
8
8.5
9
9.5
0
20
40
60
80
100
120

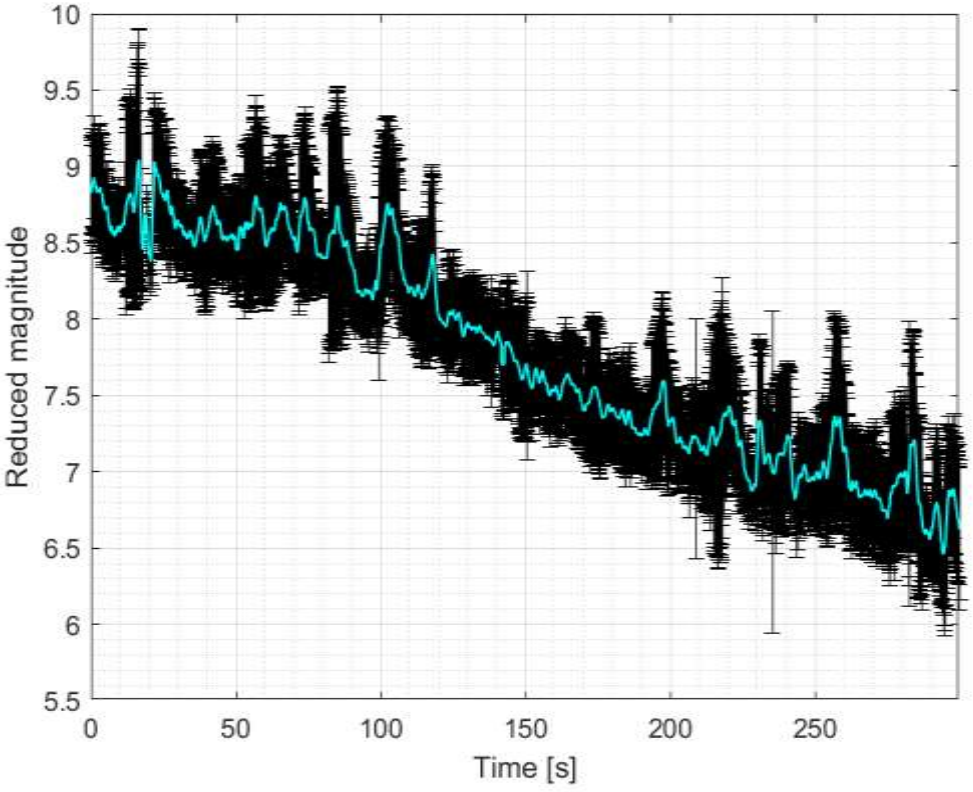
Reduced magnitude
Time [s]
10
9.5
9
8.5
8
7.5
7
6.5
6
5.5
0
50
100
150
200
250

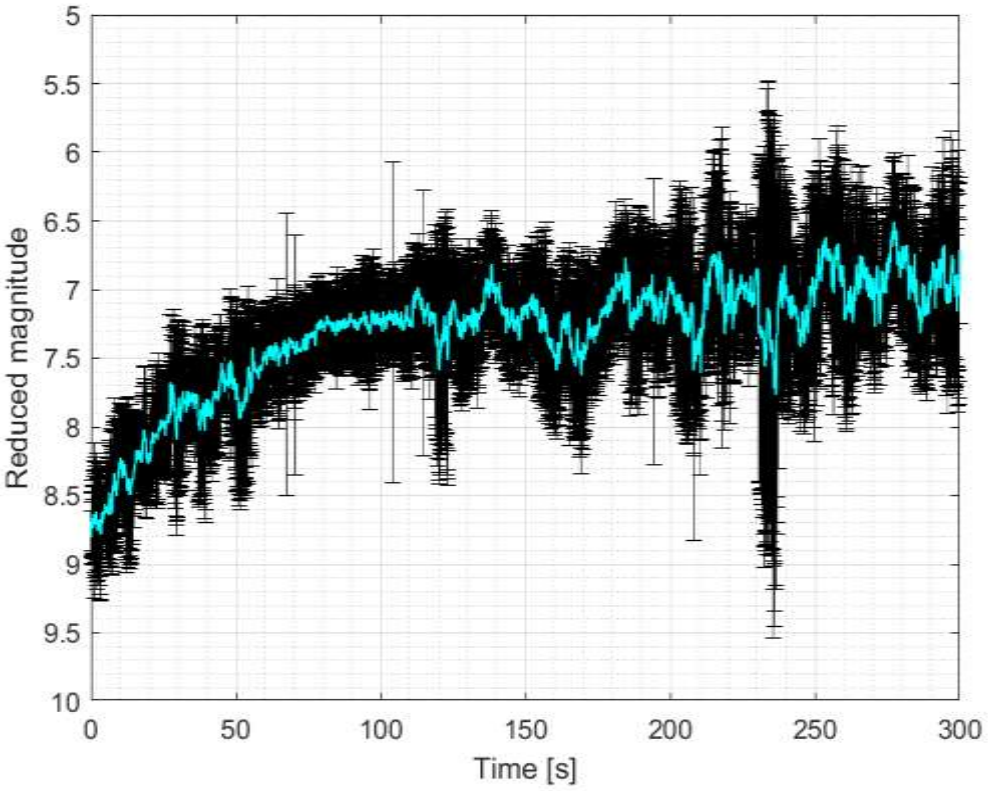
Reduced magnitude
Time [s]
5
5.5
6
6.5
7
7.5
8
8.5
9
9.5
10
0
50
100
150
200
250
300

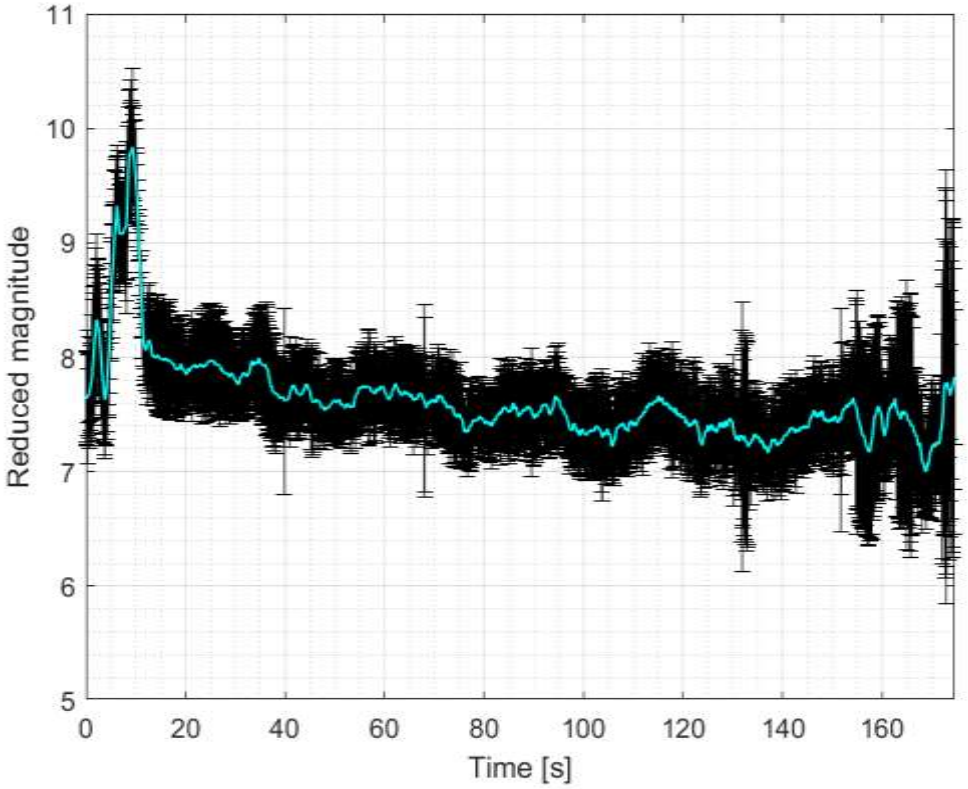
Reduced magnitude
Time [s]
11
10
9
8
7
6
5
0
20
40
60
80
100
120
140
160

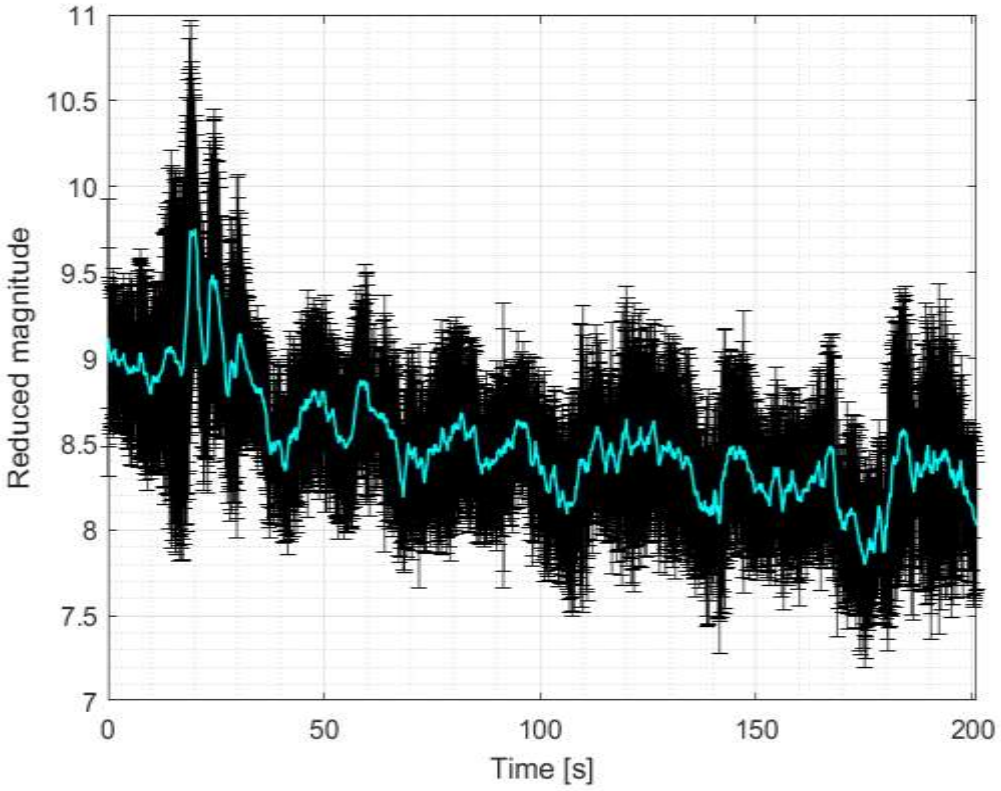

3.1.2 Norad 18340

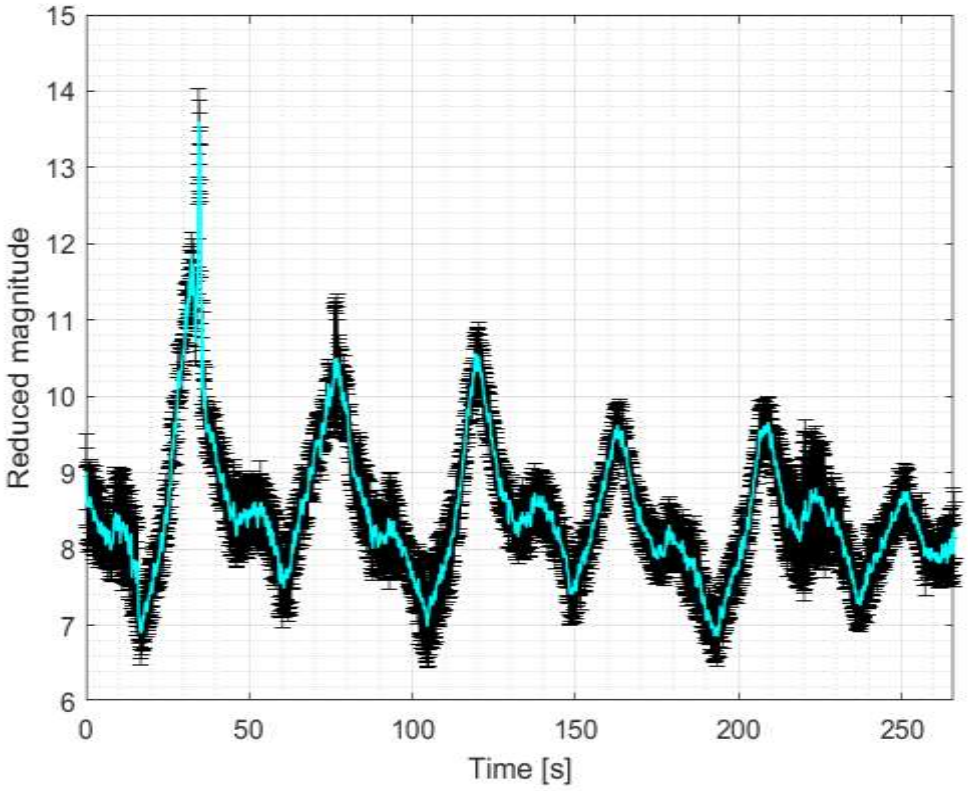
Reduced magnitude
Time [s]
15
14
13
12
11
10
9
8
7
6
0
50
100
150
200
250

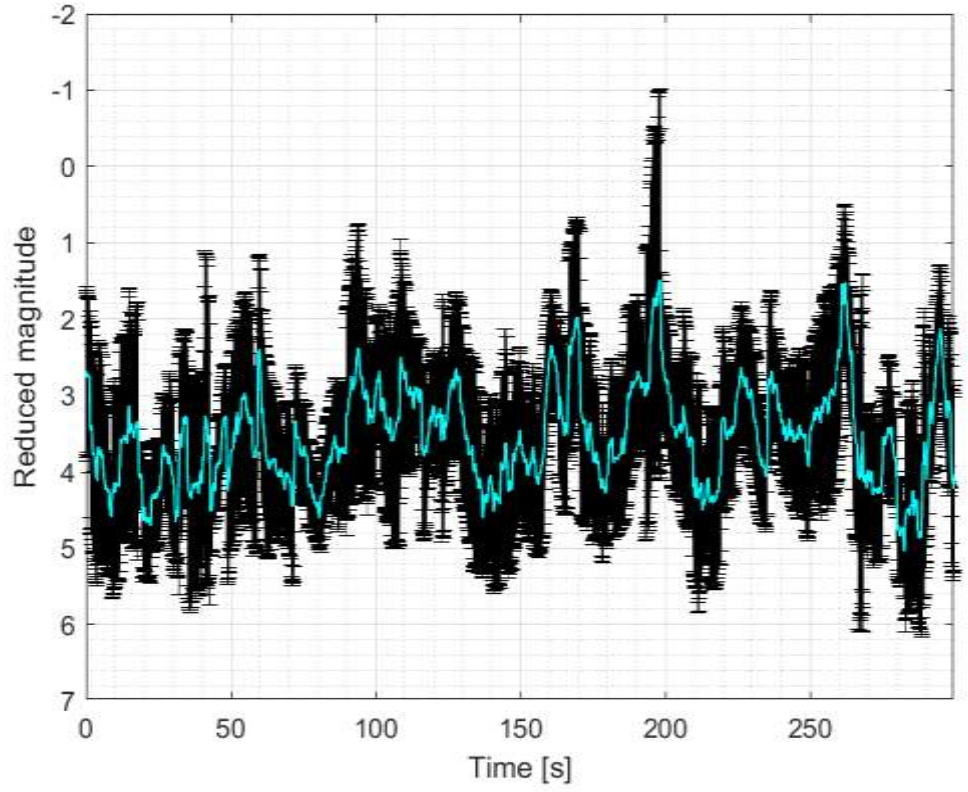
Reduced magnitude
Time [s]
-2
-1
0
1
2
3
4
5
6
7
0
50
100
150
200
250

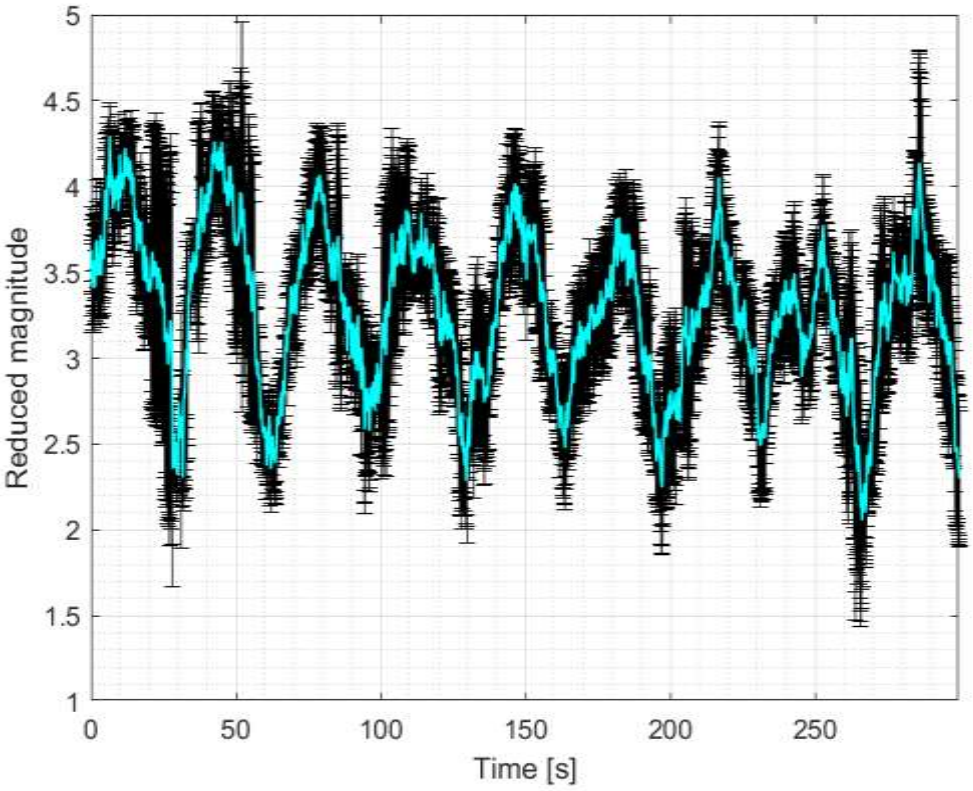
Reduced magnitude
Time [s]
5
4.5
4
3.5
3
2.5
2
1.5
1
0
50
100
150
200
250

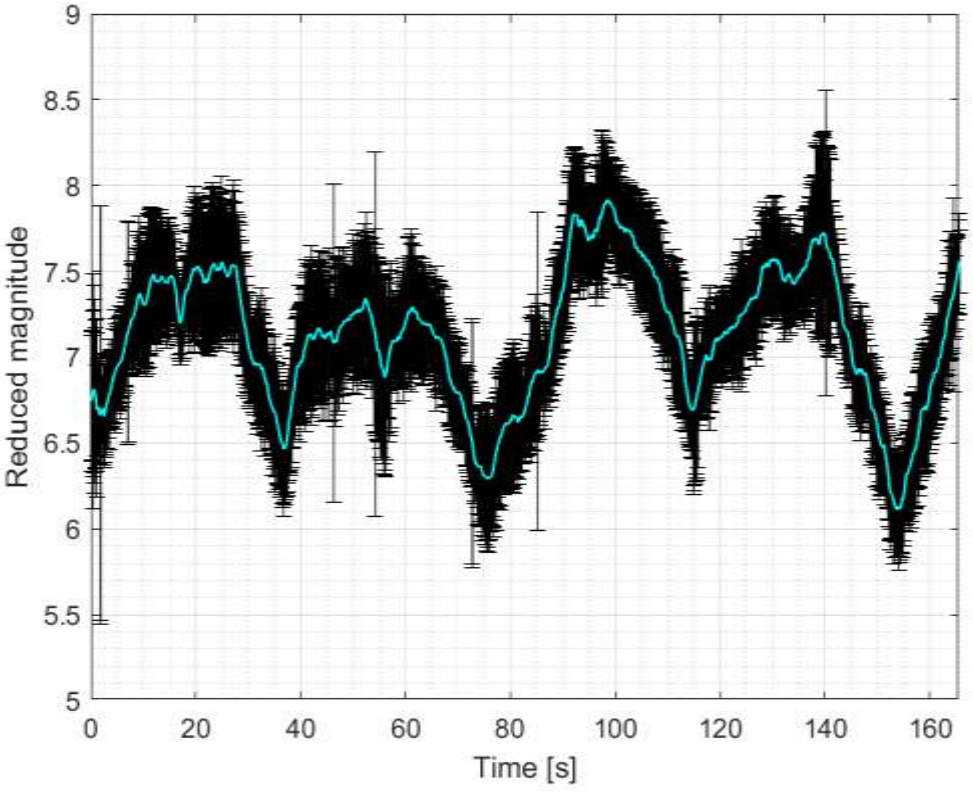
Reduced magnitude
Time [s]
9
8.5
8
7.5
7
6.5
6
5.5
5
0
20
40
60
80
100
120
140
160

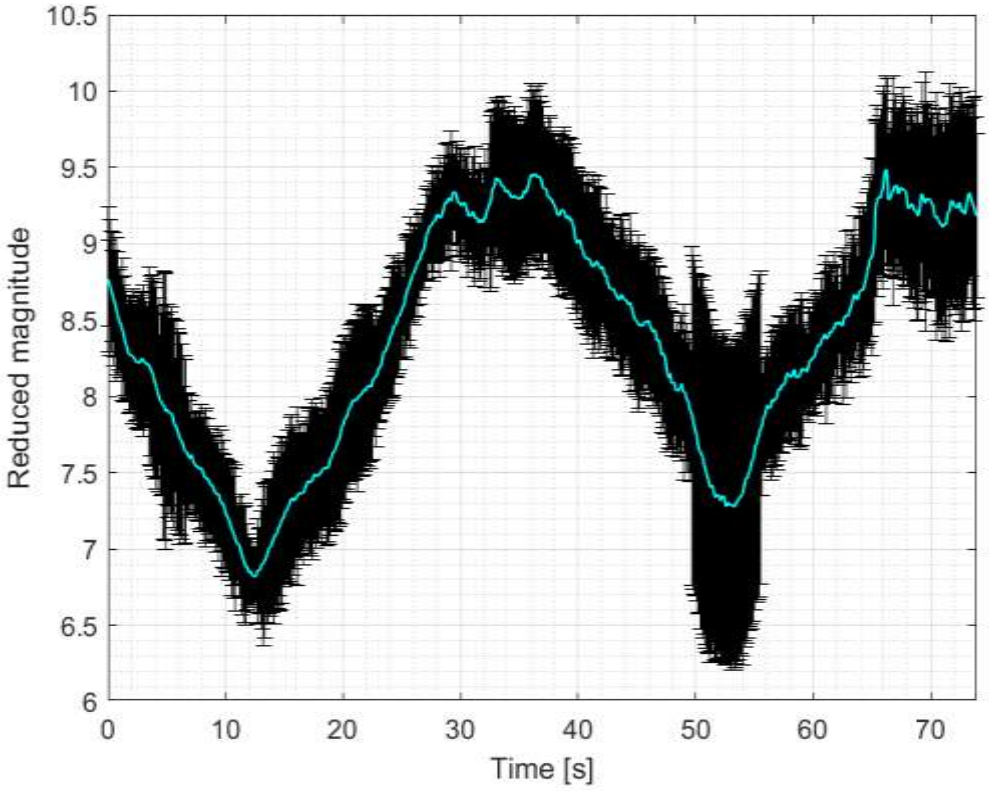
Reduced magnitude
Time [s]
10.5
10
9.5
9
8.5
8
7.5
7
6.5
6
0
10
20
30
40
50
60
70

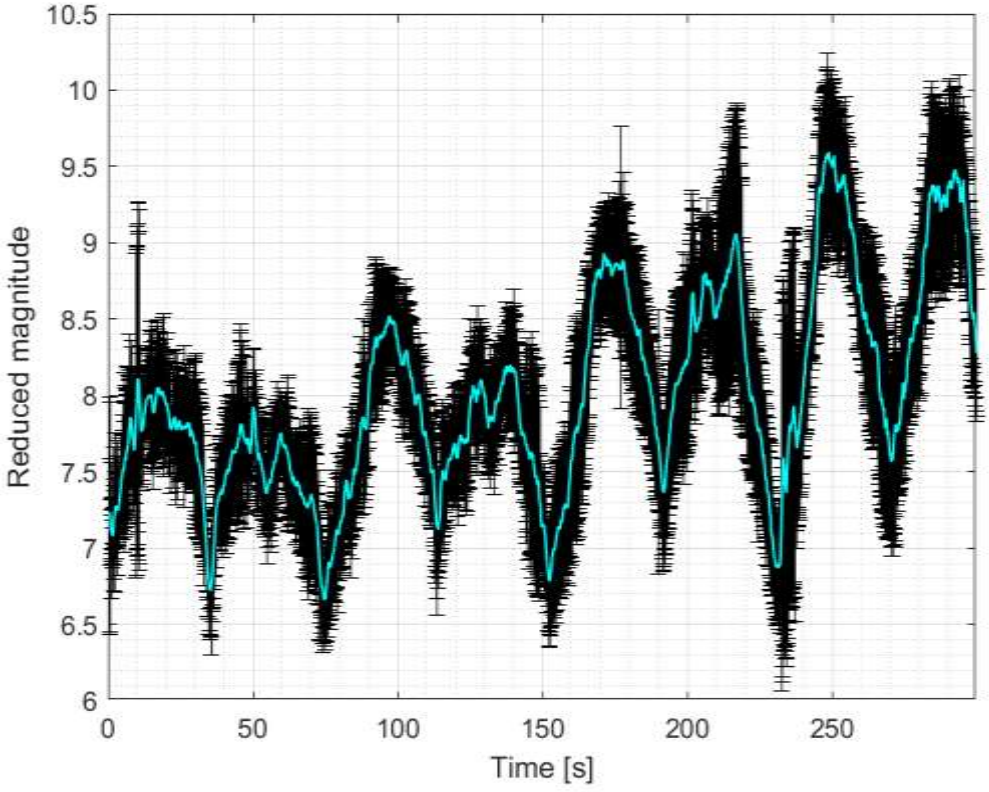
Reduced magnitude
Time [s]
10.5
10
9.5
9
8.5
8
7.5
7
6.5
6
0
50
100
150
200
250

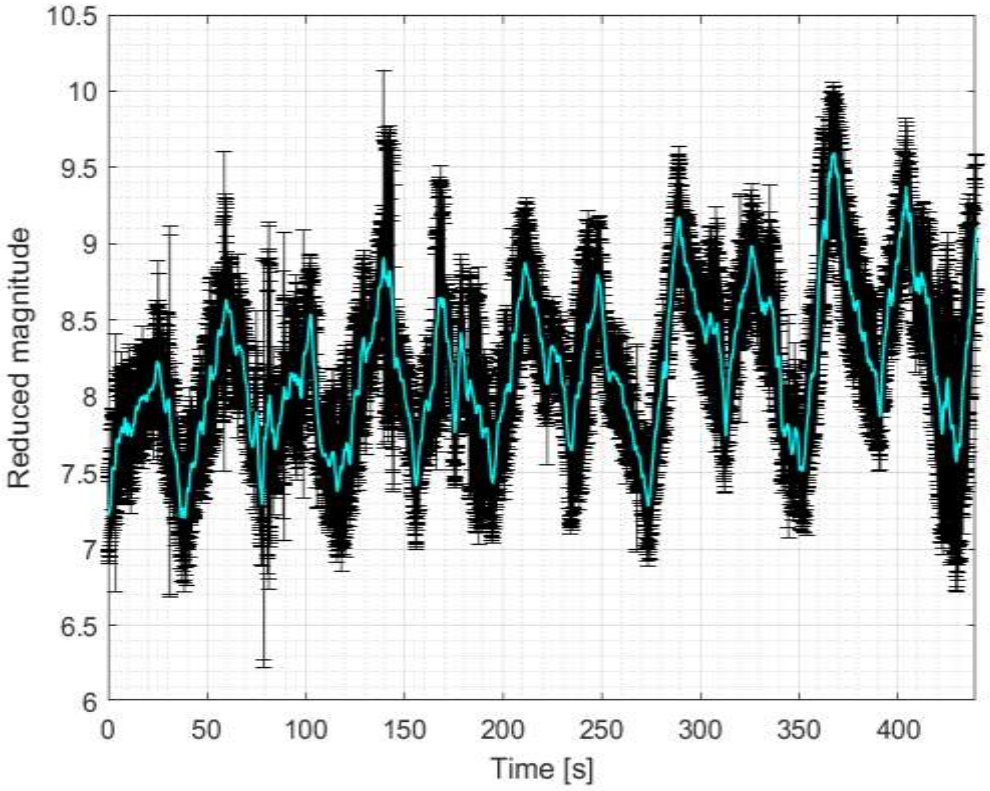
Reduced magnitude
Time [s]
10.5
10
9.5
9
8.5
8
7.5
7
6.5
6
0
50
100
150
200
250
300
350
400

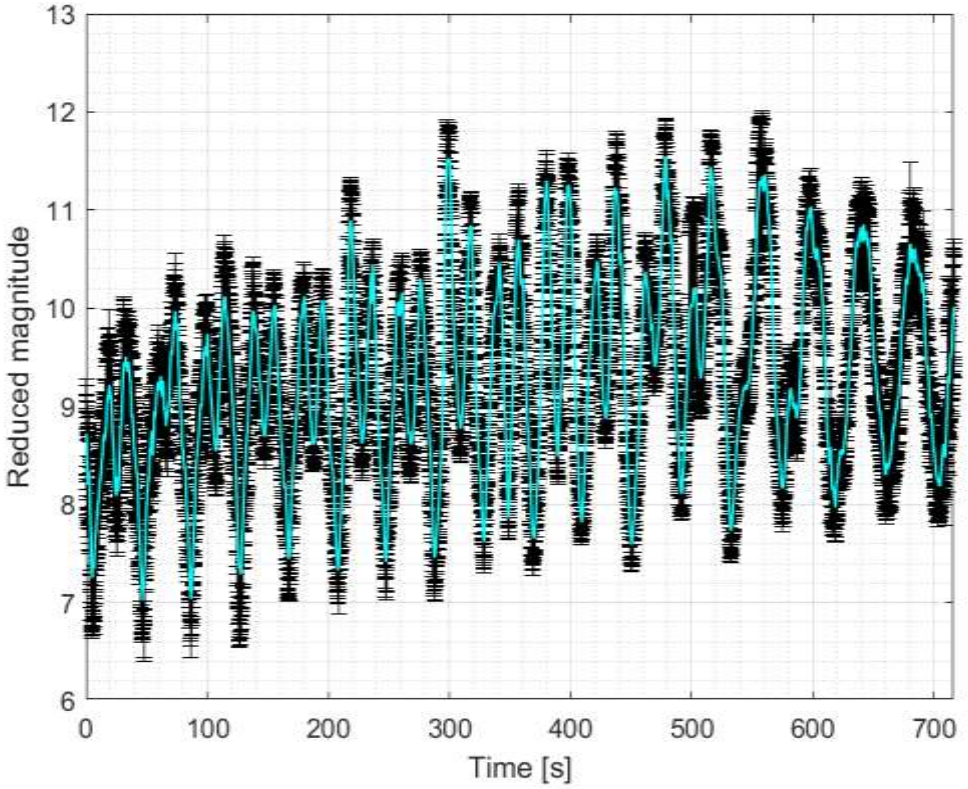
Reduced magnitude
Time [s]
13
12
11
10
9
8
7
6
0
100
200
300
400
500
600
700

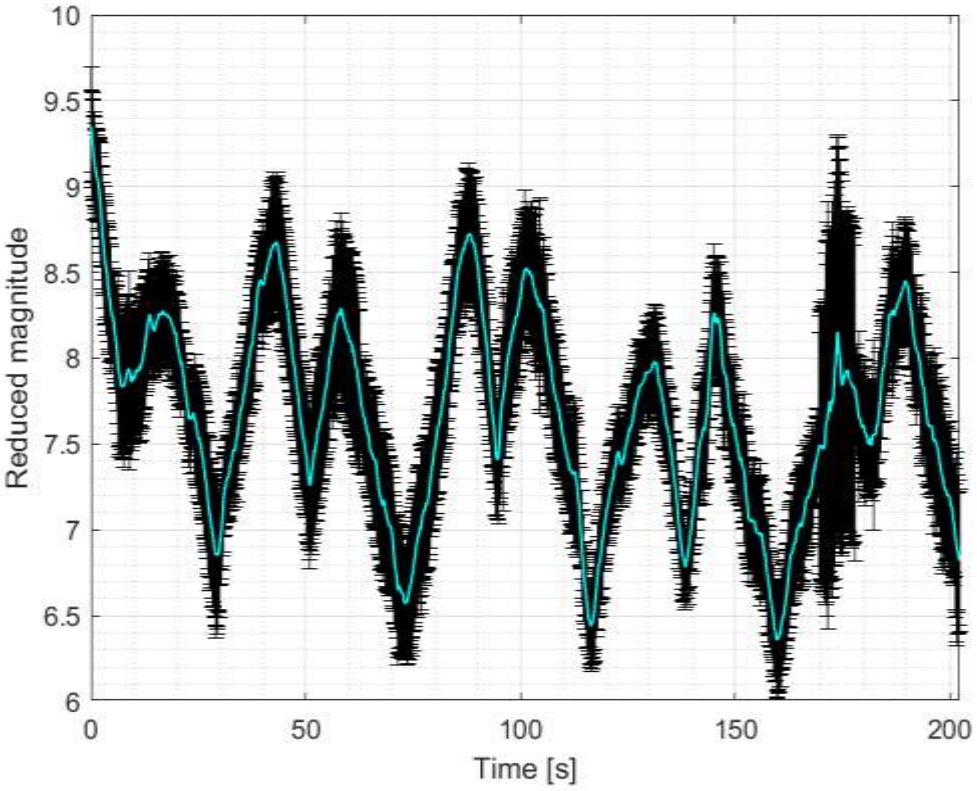
Reduced magnitude
Time [s]
10
9.5
9
8.5
8
7.5
7
6.5
6
0
50
100
150
200

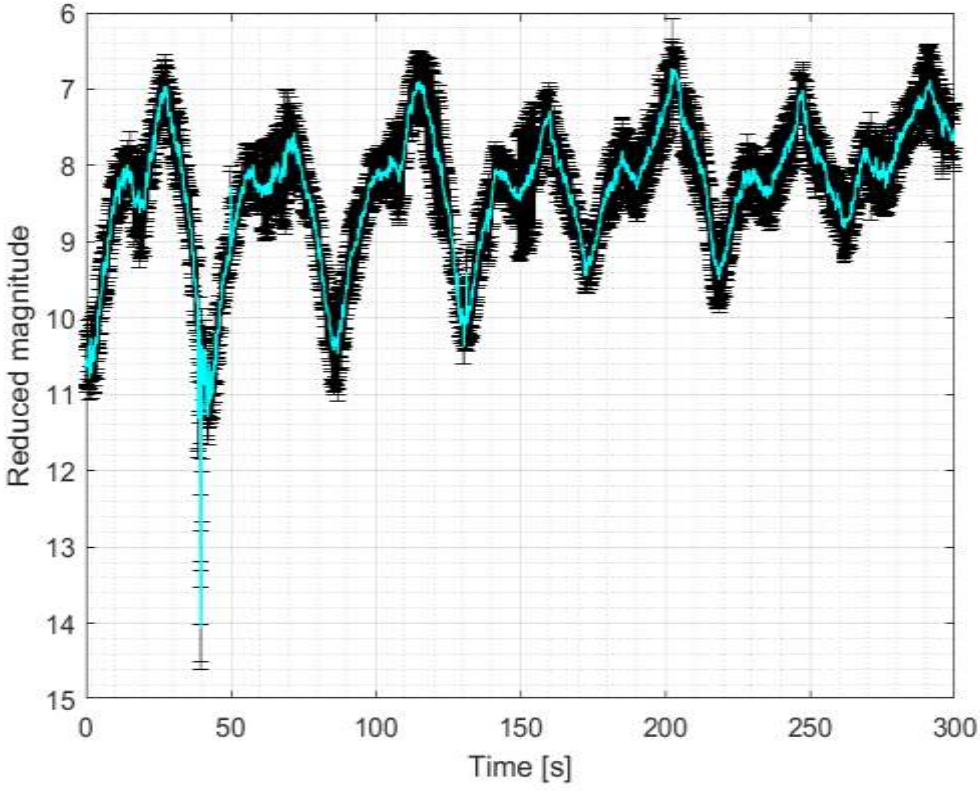
Reduced magnitude
Time [s]
6
7
8
9
10
11
12
13
14
15
0
50
100
150
200
250
300

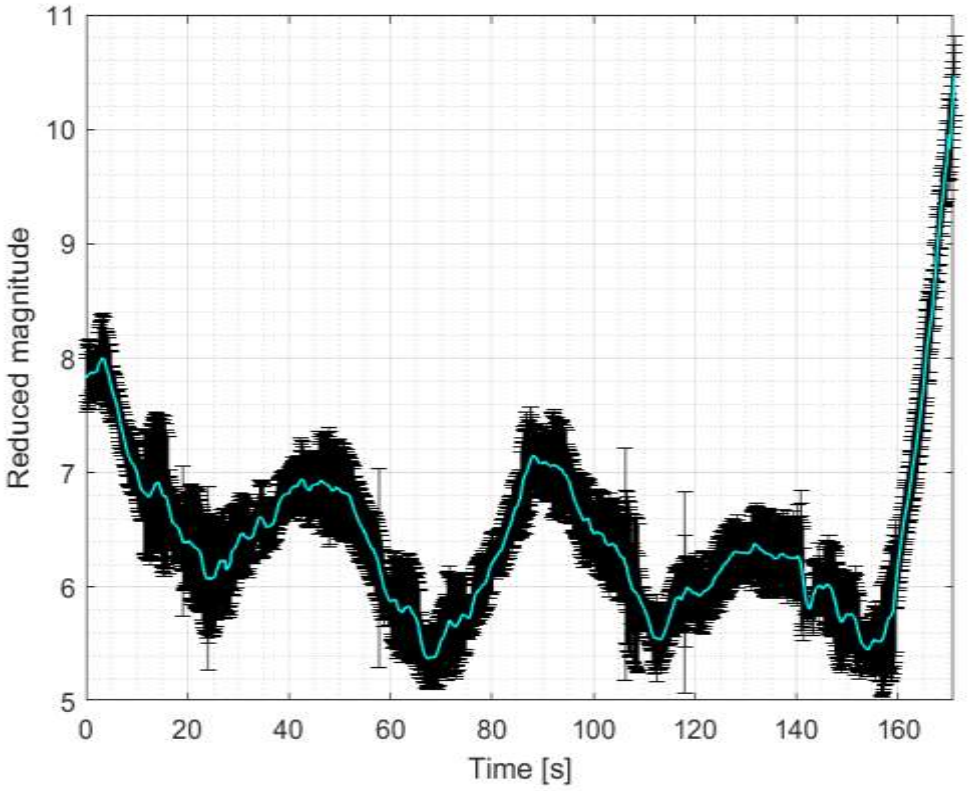
Reduced magnitude
Time [s]
11
10
9
8
7
6
5
0
20
40
60
80
100
120
140
160

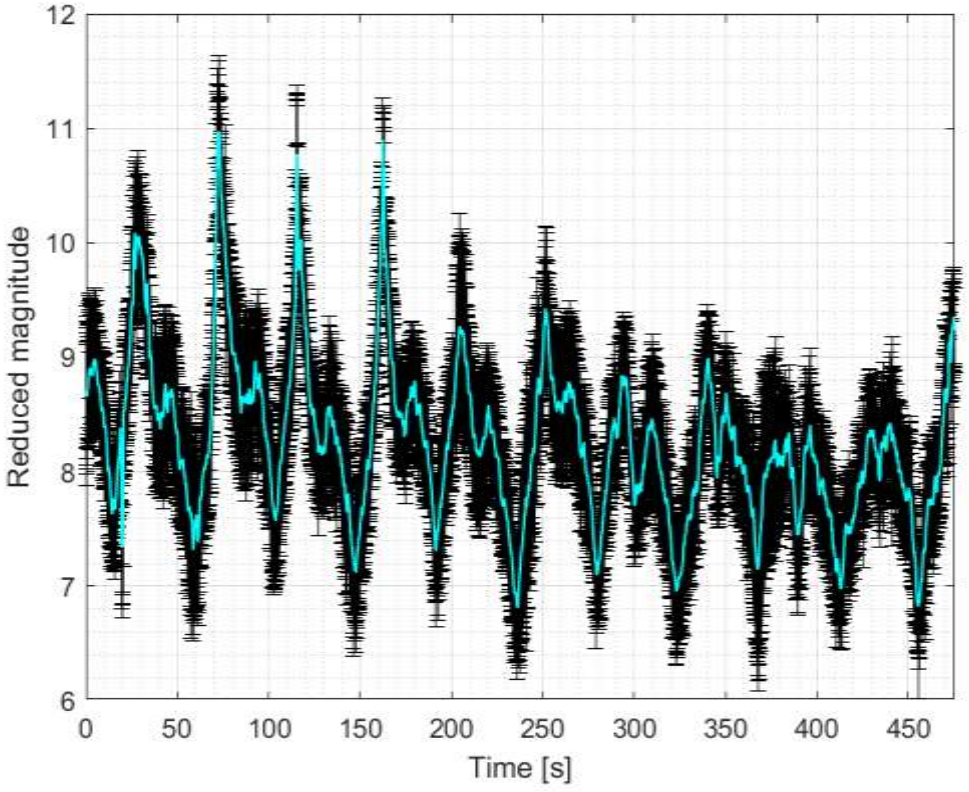
Reduced magnitude
Time [s]
12
11
10
9
8
7
6
0
50
100
150
200
250
300
350
400
450

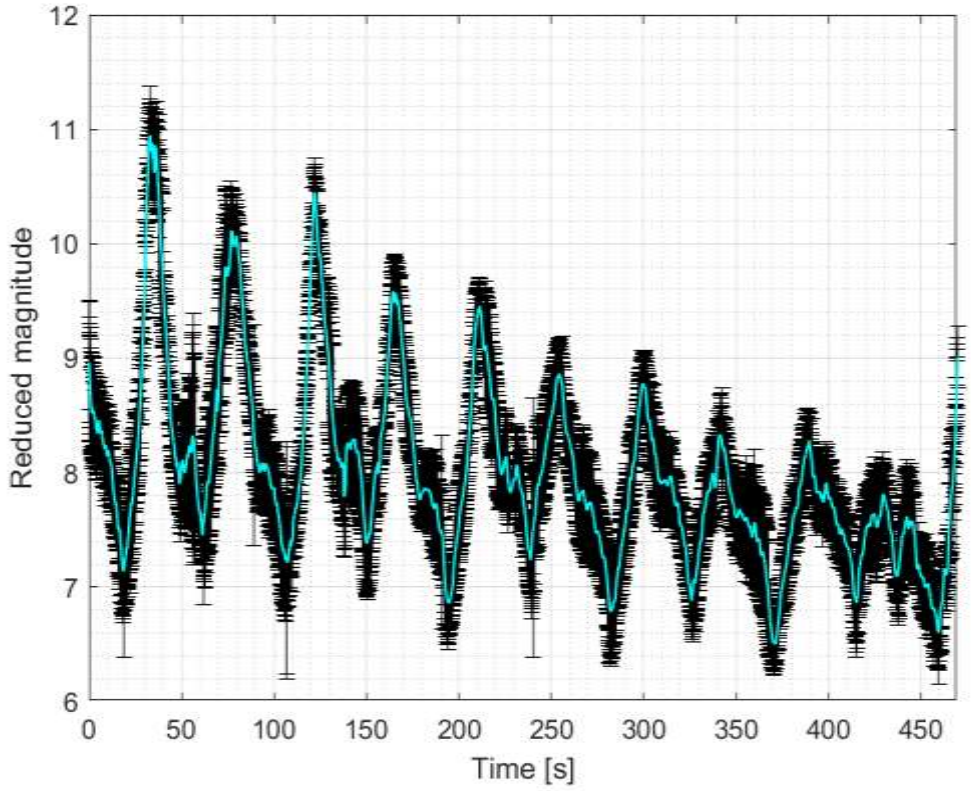
Reduced magnitude
Time [s]
12
11
10
9
8
7
6
0
50
100
150
200
250
300
350
400
450

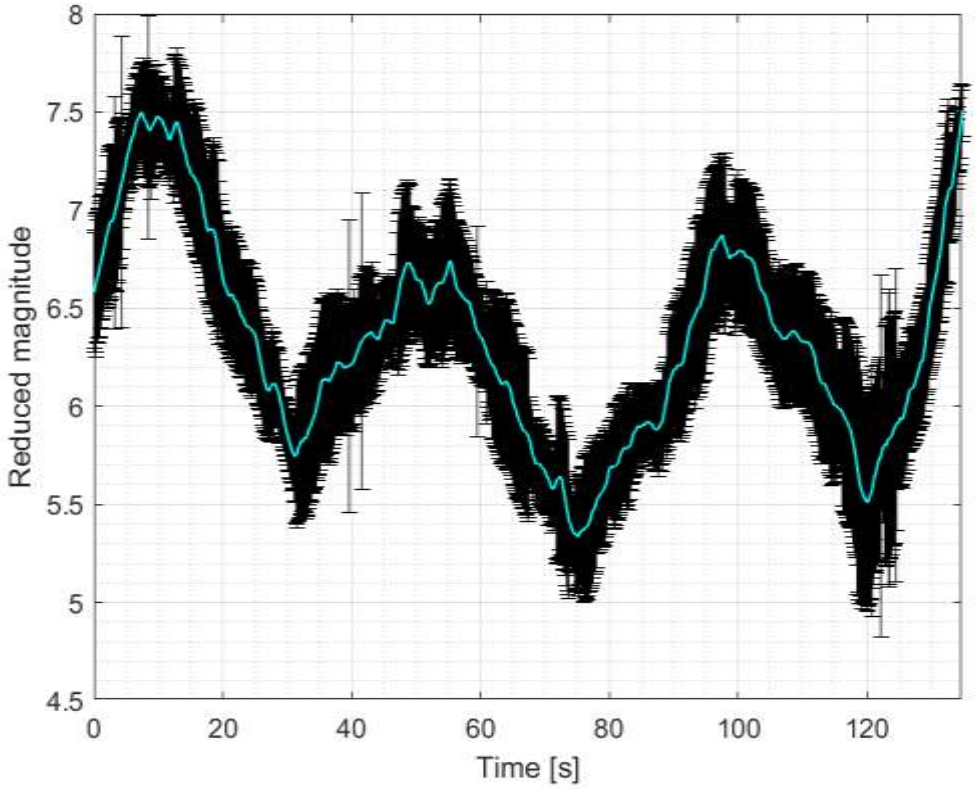
Reduced magnitude
Time [s]
8
7.5
7
6.5
6
5.5
5
4.5
0
20
40
60
80
100
120

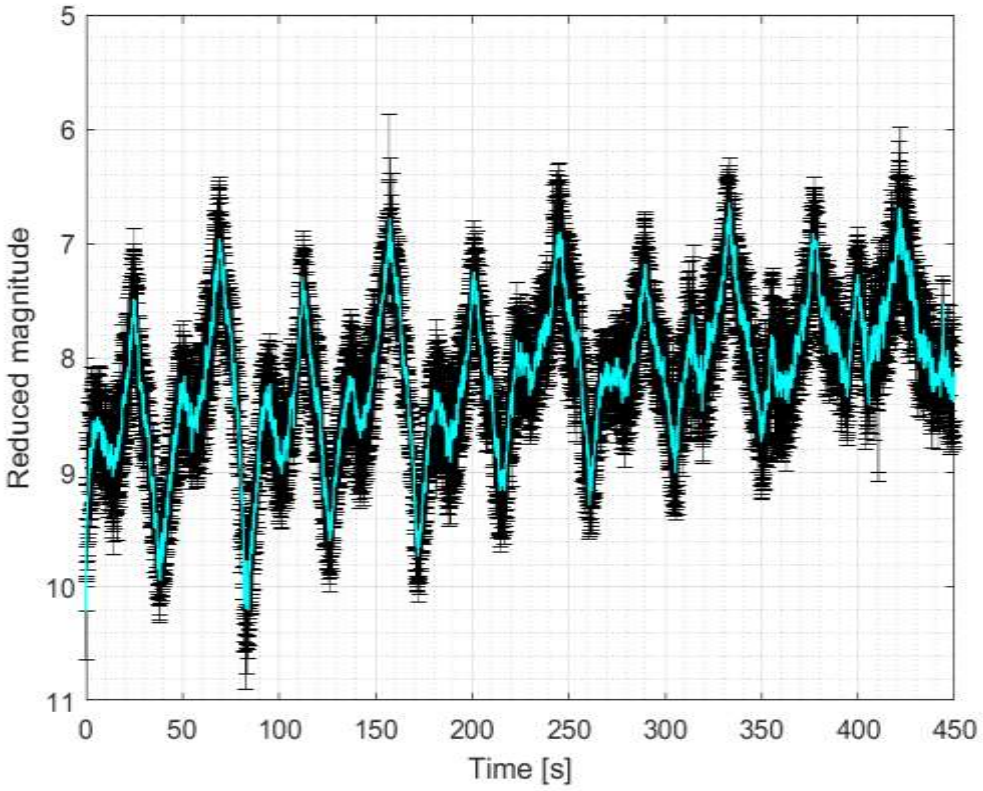
Reduced magnitude
Time [s]
5
6
7
8
9
10
11
0
50
100
150
200
250
300
350
400
450

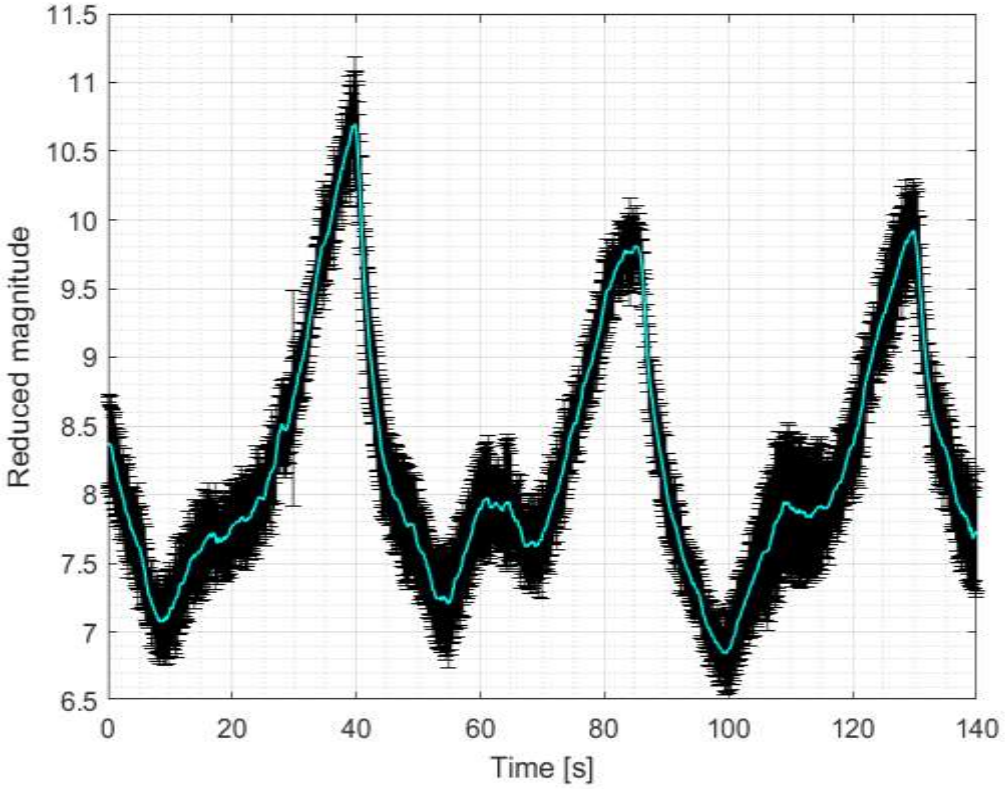
Reduced magnitude
Time [s]
11.5
11
10.5
10
9.5
9
8.5
8
7.5
7
6.5
0
20
40
60
80
100
120
140

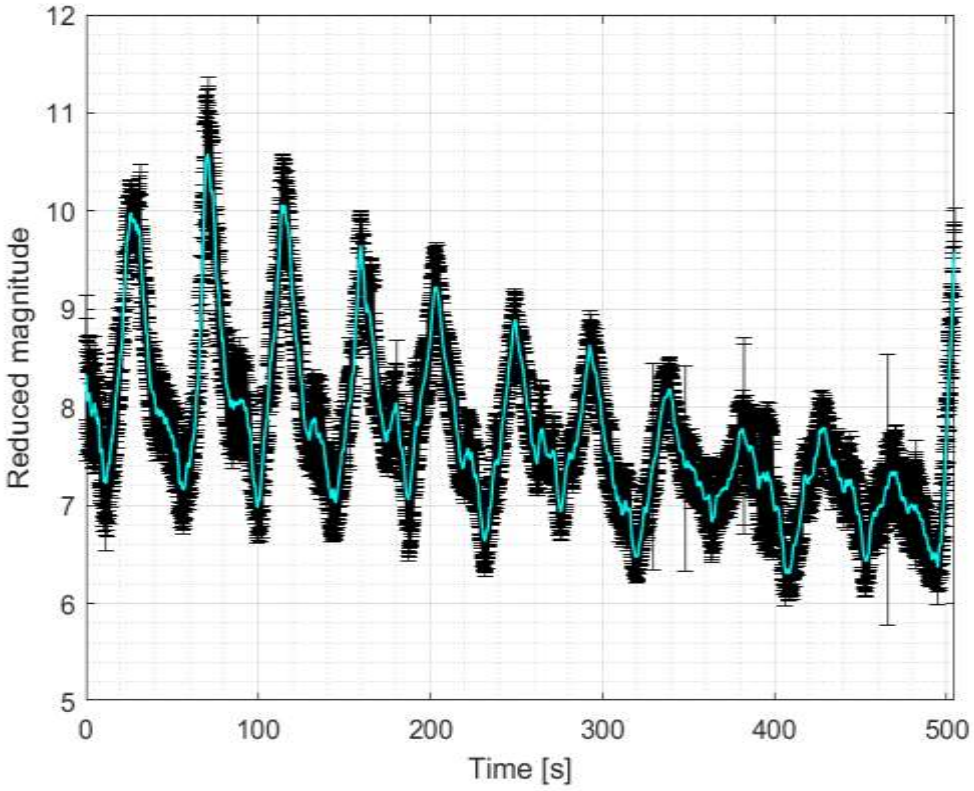
Reduced magnitude
Time [s]
12
11
10
9
8
7
6
5
0
100
200
300
400
500

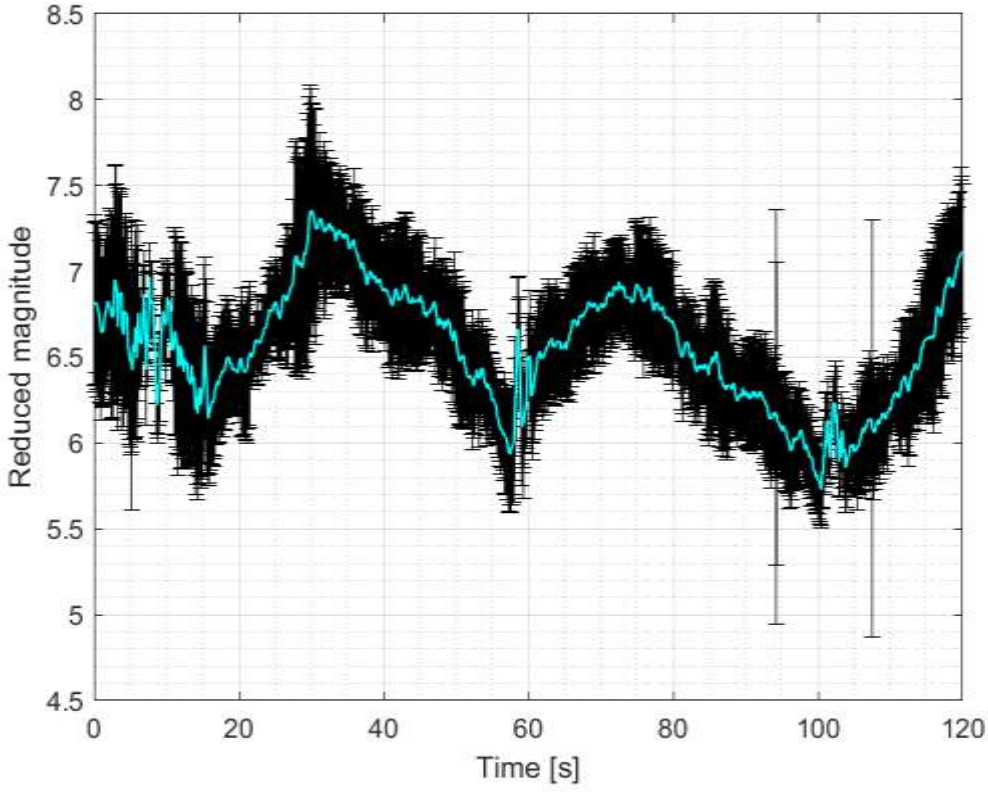
Reduced magnitude
Time [s]
8.5
8
7.5
7
6.5
6
5.5
5
4.5
0
20
40
60
80
100
120

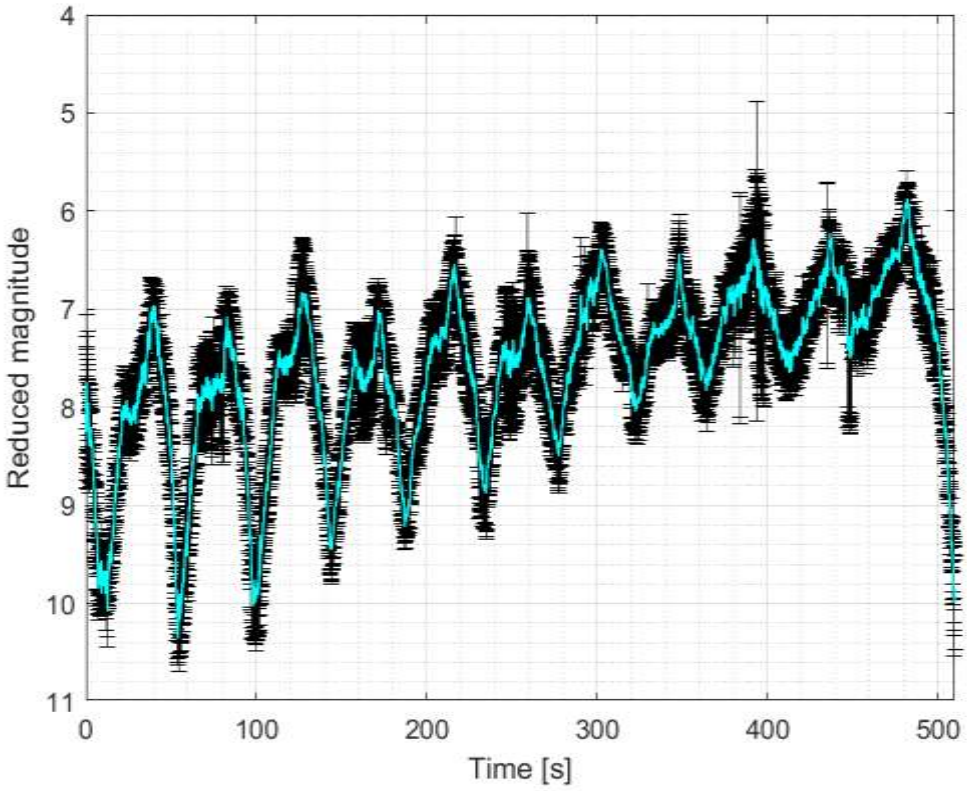
Reduced magnitude
Time [s]
4
5
6
7
8
9
10
11
0
100
200
300
400
500

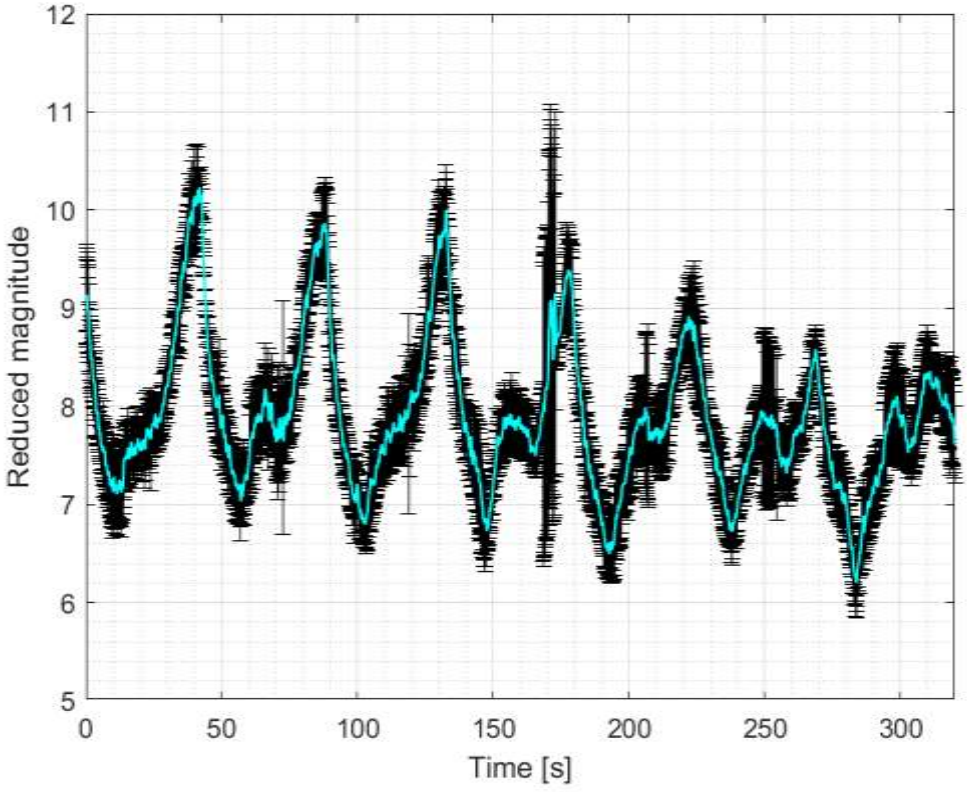
Reduced magnitude
Time [s]
5
6
7
8
9
10
11
12
0
50
100
150
200
250
300

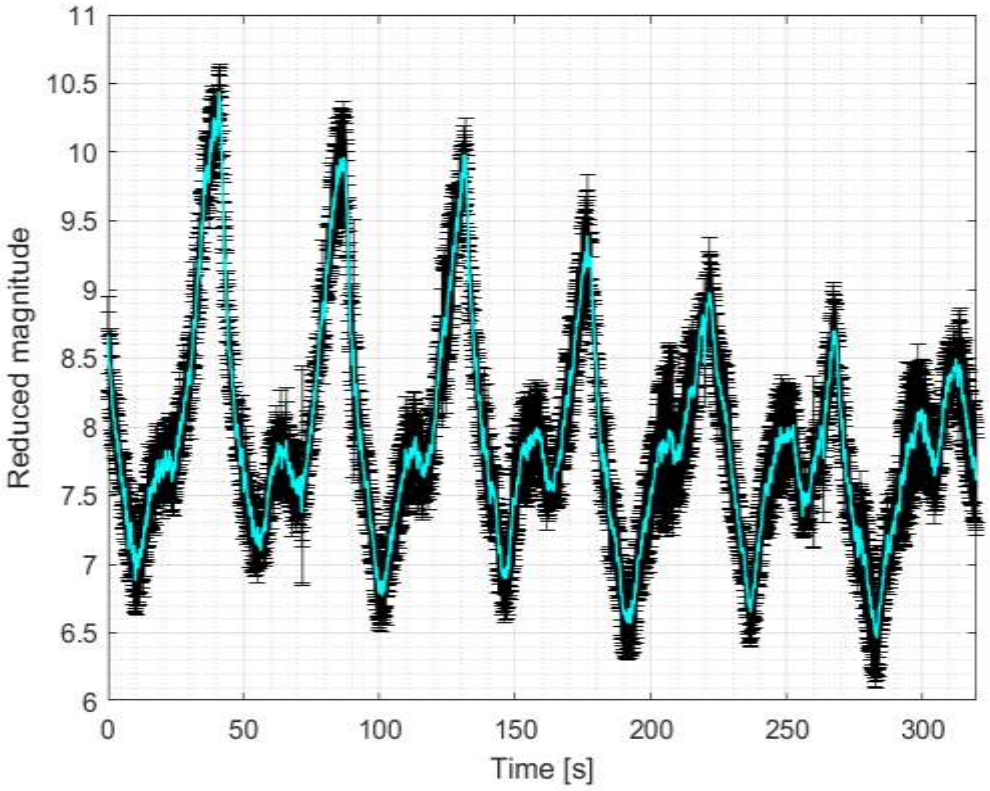
Reduced magnitude
Time [s]
11
10.5
10
9.5
9
8.5
8
7.5
7
6.5
6
0
50
100
150
200
250
300

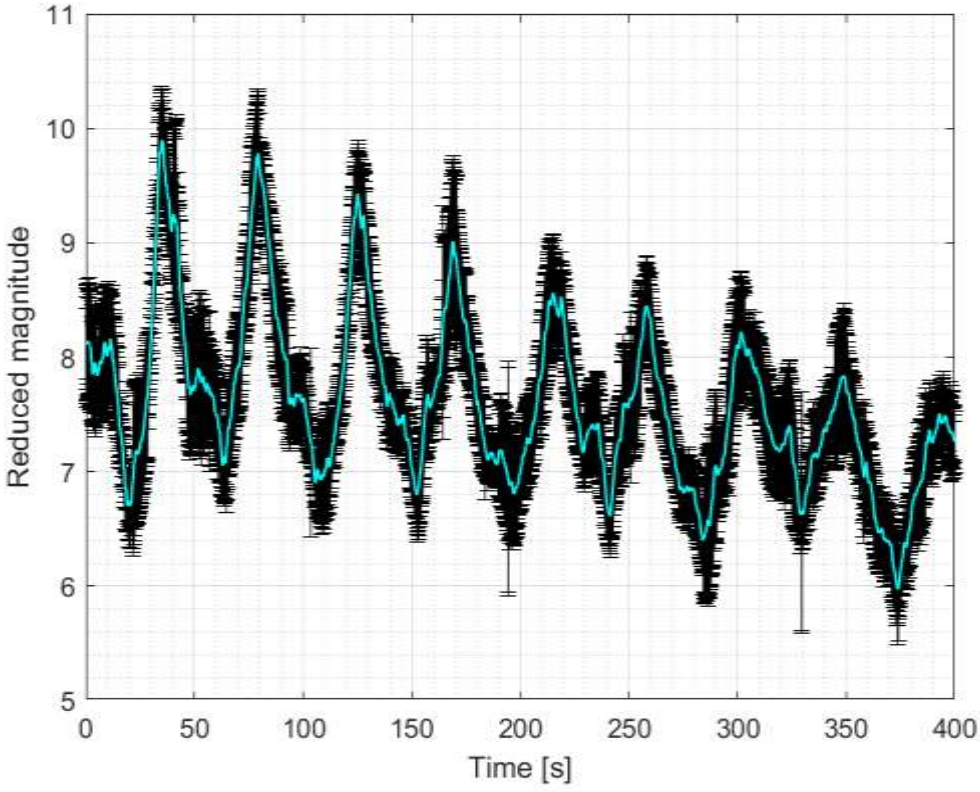
Reduced magnitude
Time [s]
11
10
9
8
7
6
5
0
50
100
150
200
250
300
350
400

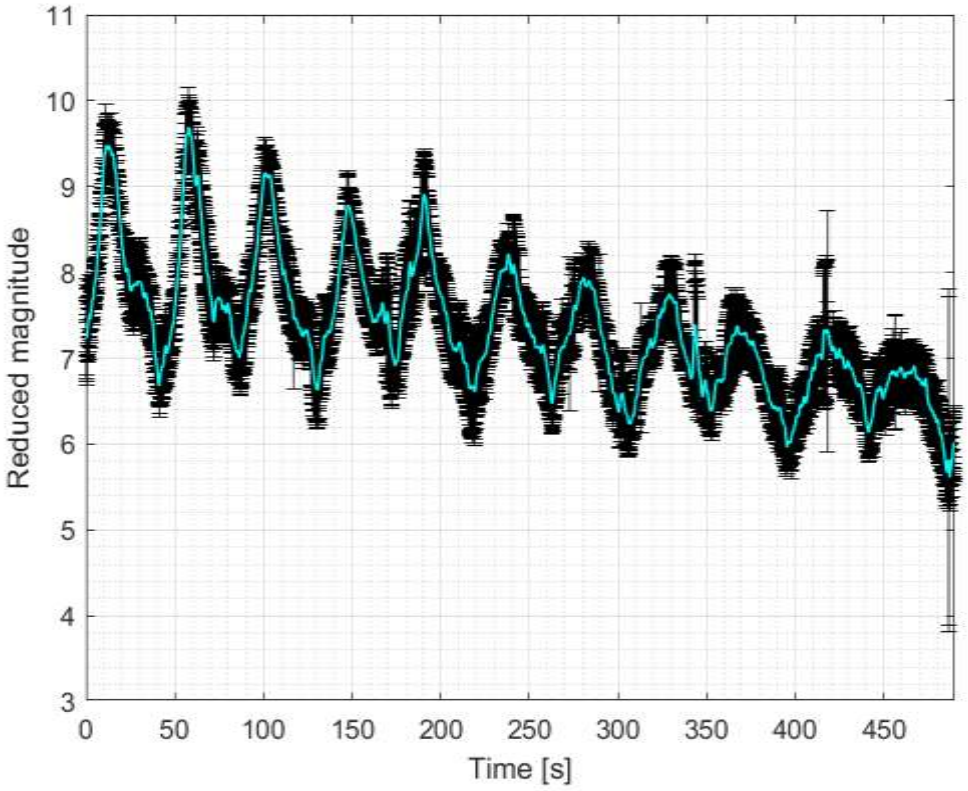
Reduced magnitude
Time [s]
11
10
9
8
7
6
5
4
3
0
50
100
150
200
250
300
350
400
450

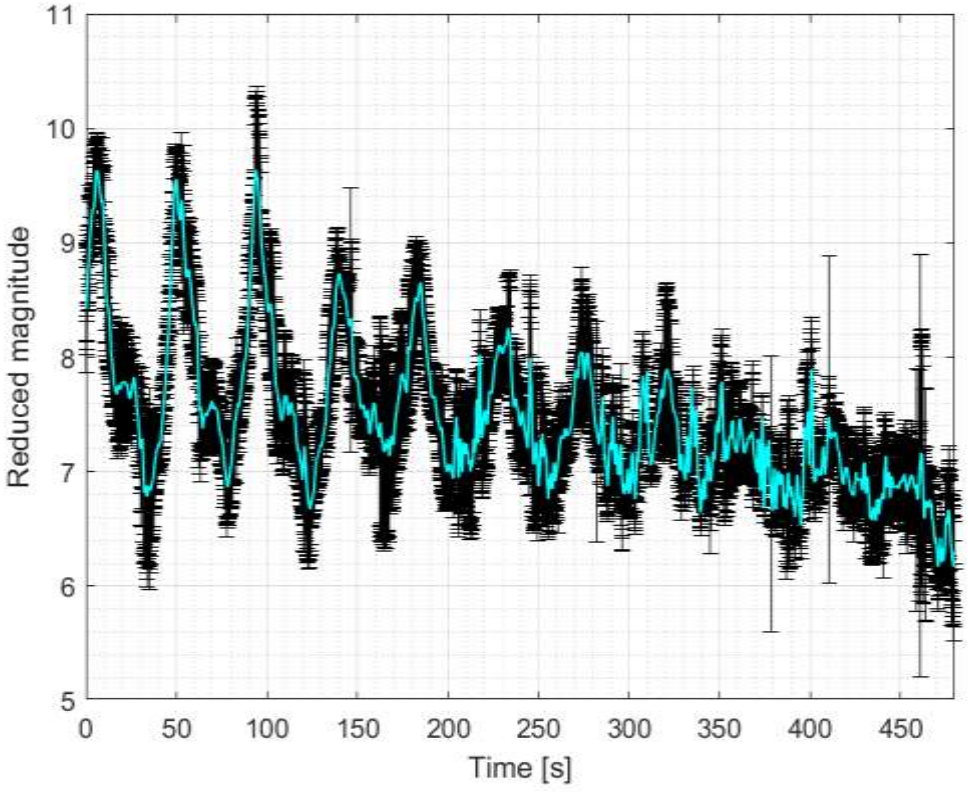
Reduced magnitude
Time [s]
11
10
9
8
7
6
5
0
50
100
150
200
250
300
350
400
450

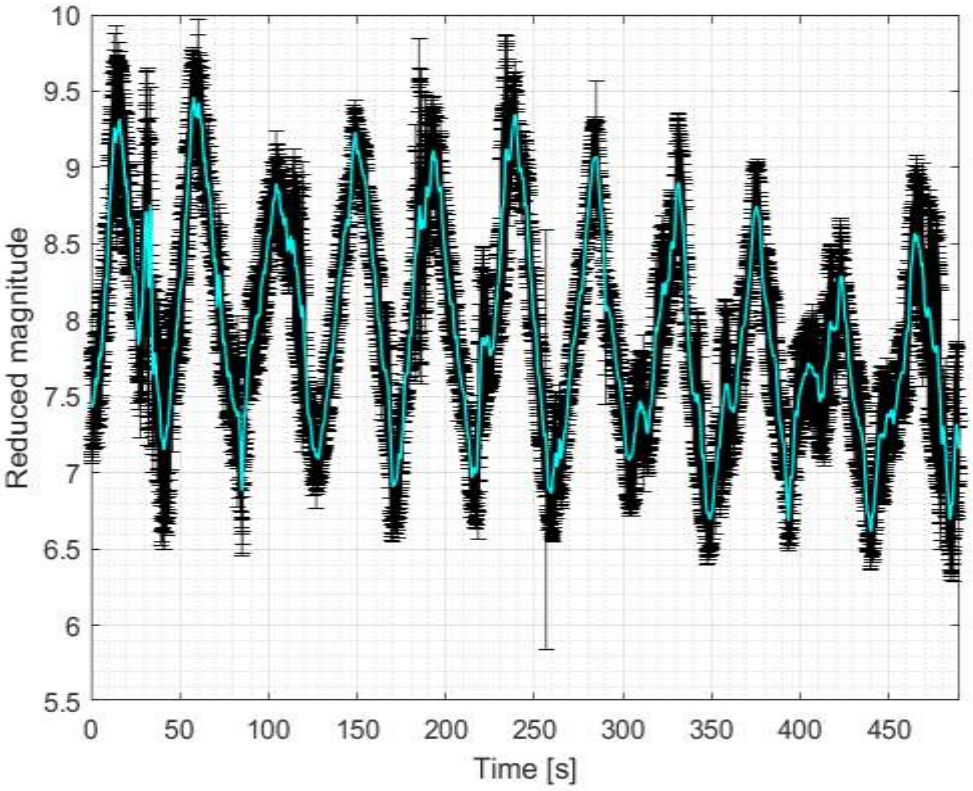
Reduced magnitude
Time [s]
10
9.5
9
8.5
8
7.5
7
6.5
6
5.5
0
50
100
150
200
250
300
350
400
450

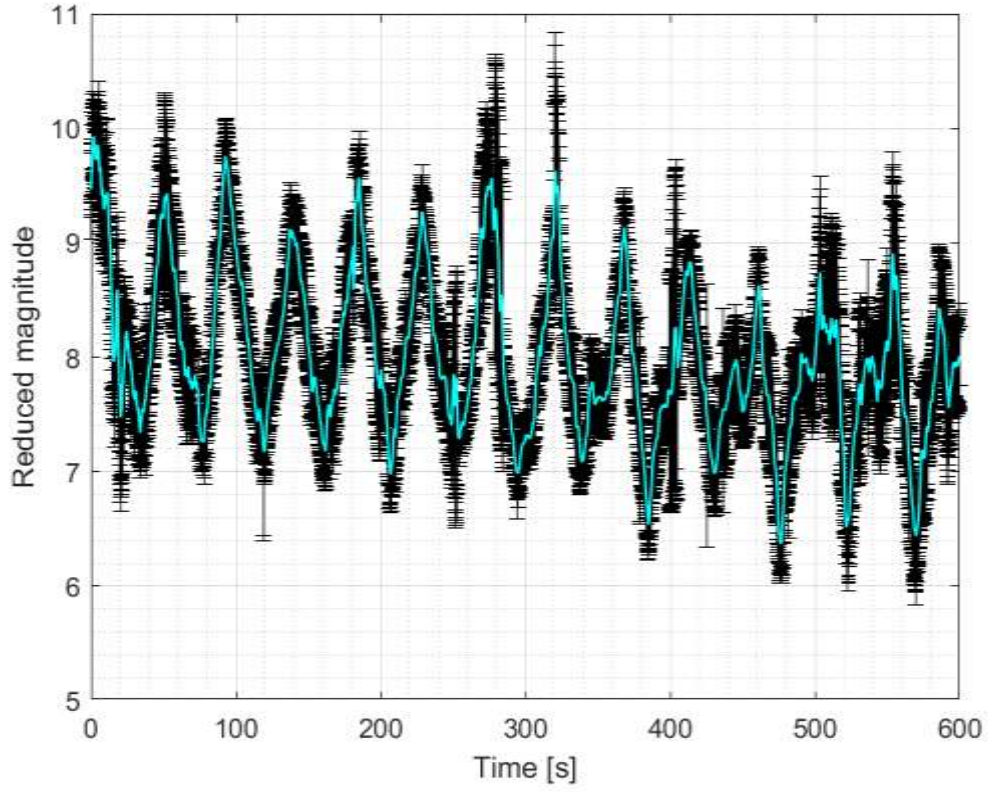
Reduced magnitude
Time [s]
11
10
9
8
7
6
5
0
100
200
300
400
500
600

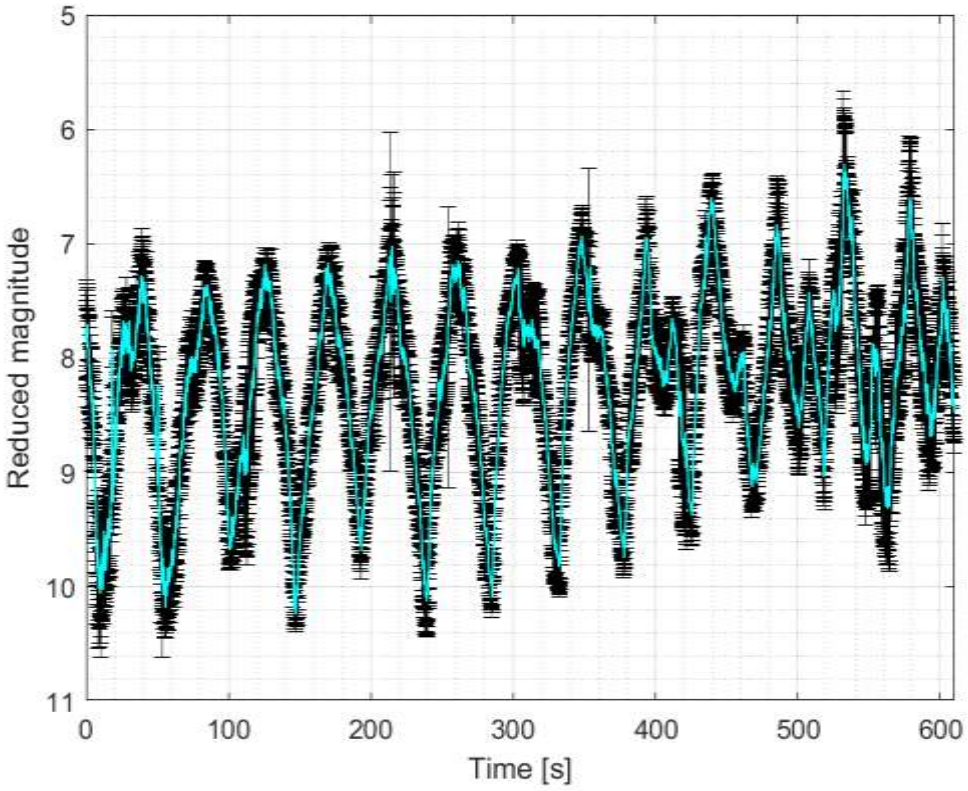

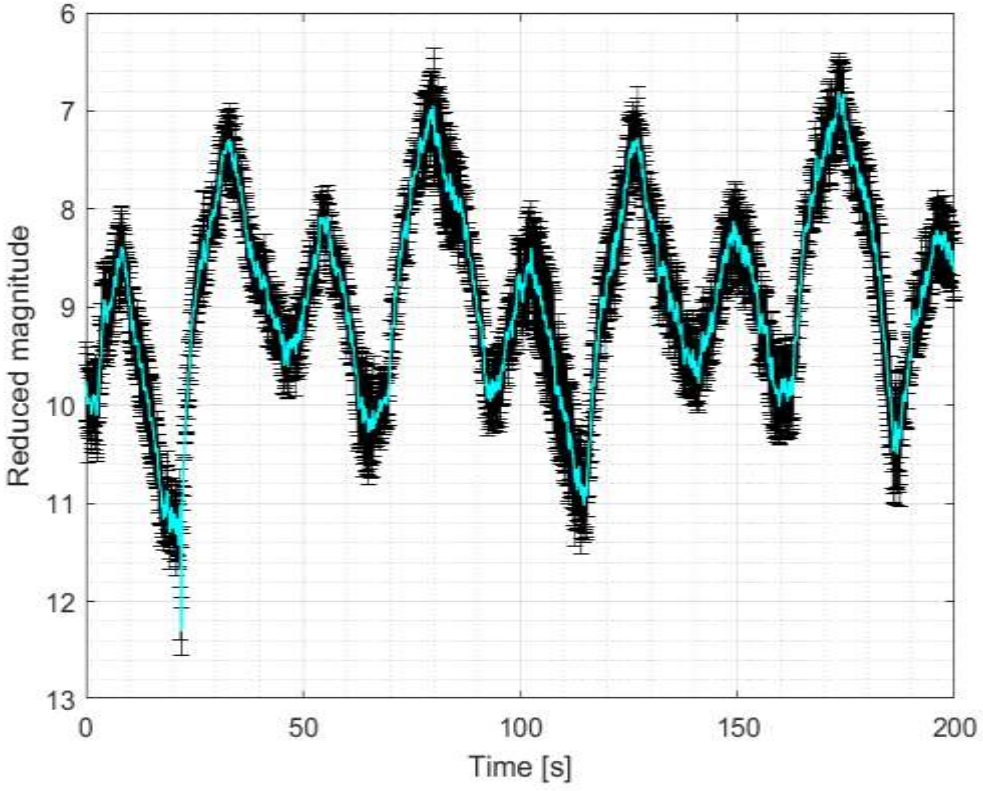

3.1.3 Norad 23088

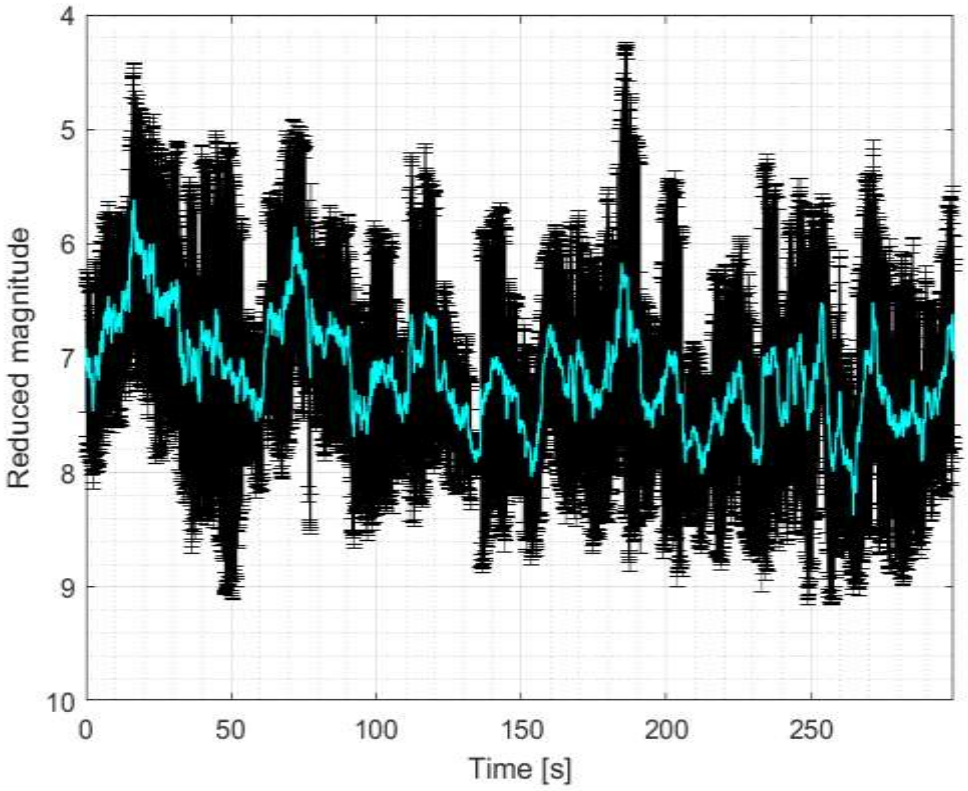
Reduced magnitude
4
5
6
7
8
9
10
0
50
100
150
200
250
Time [s]

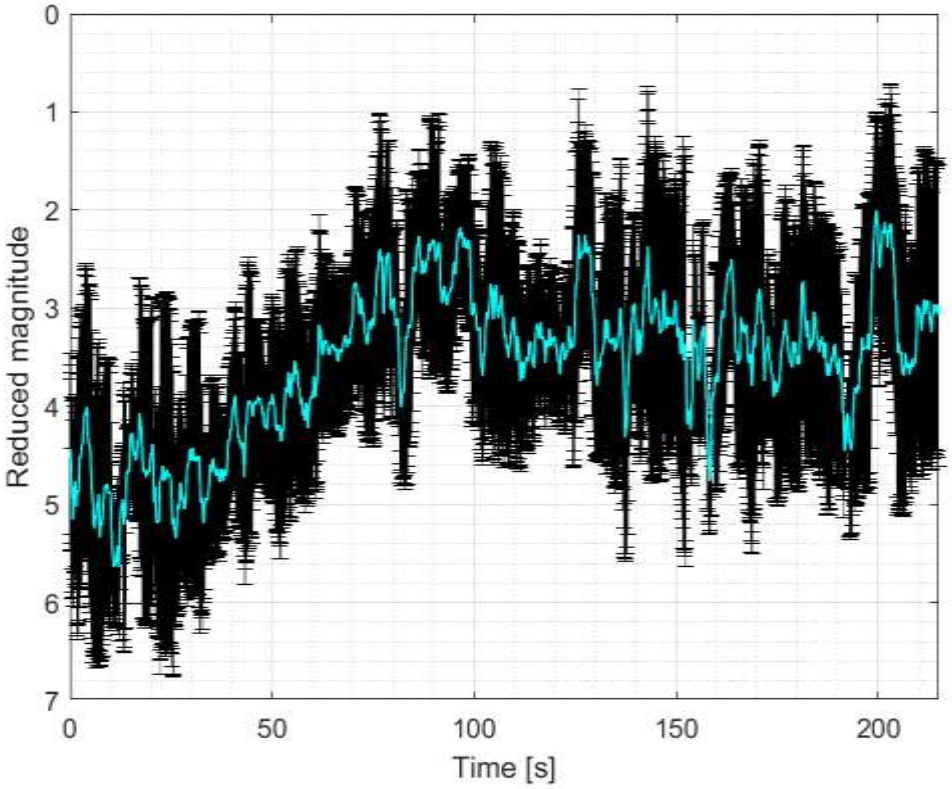
Reduced magnitude
0
1
2
3
4
5
6
7
0
50
100
150
200
Time [s]

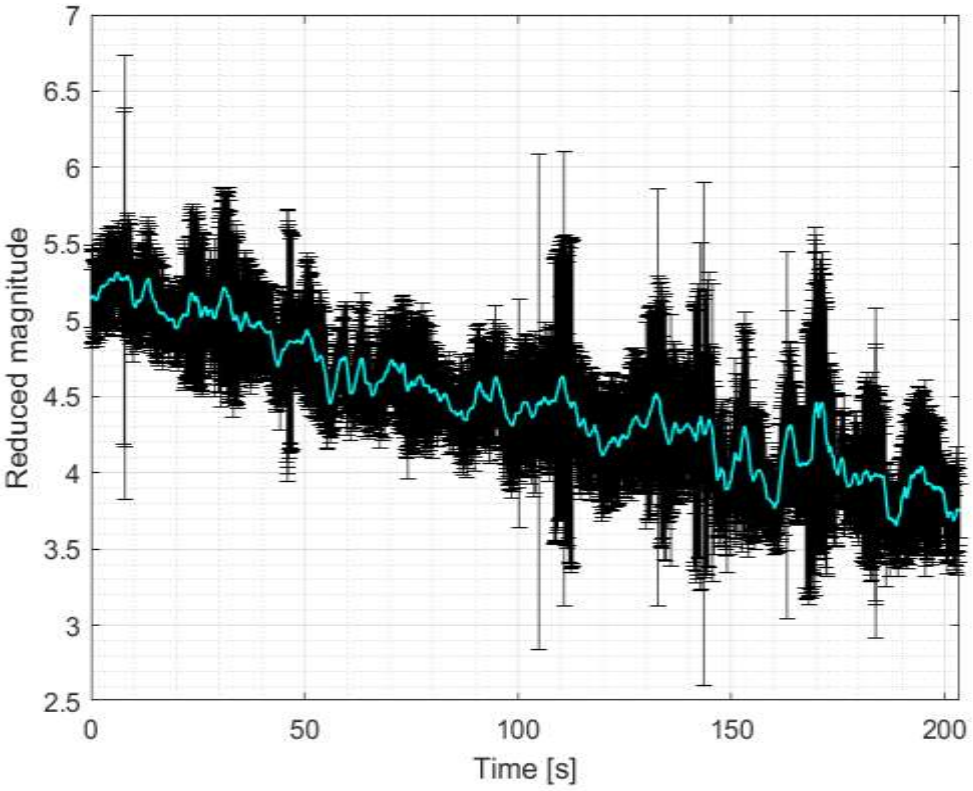
Reduced magnitude
Time [s]
7
6.5
6
5.5
5
4.5
4
3.5
3
2.5
0
50
100
150
200

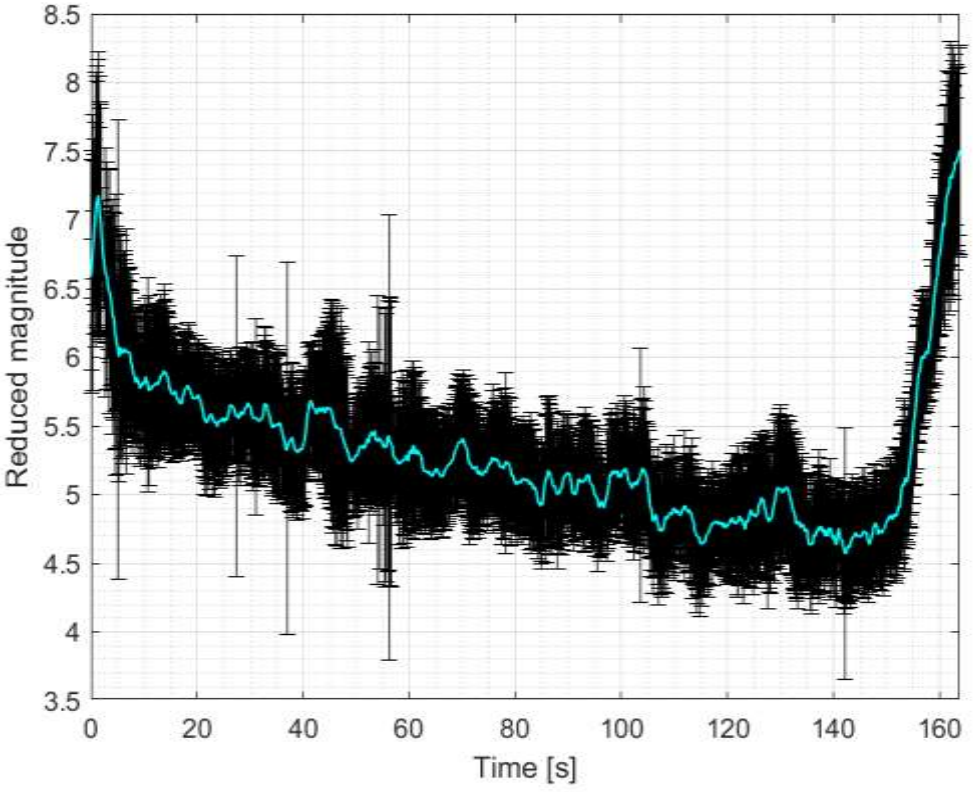
Reduced magnitude
Time [s]
8.5
8
7.5
7
6.5
6
5.5
5
4.5
4
3.5
0
20
40
60
80
100
120
140
160

3.1.4 Norad 23405

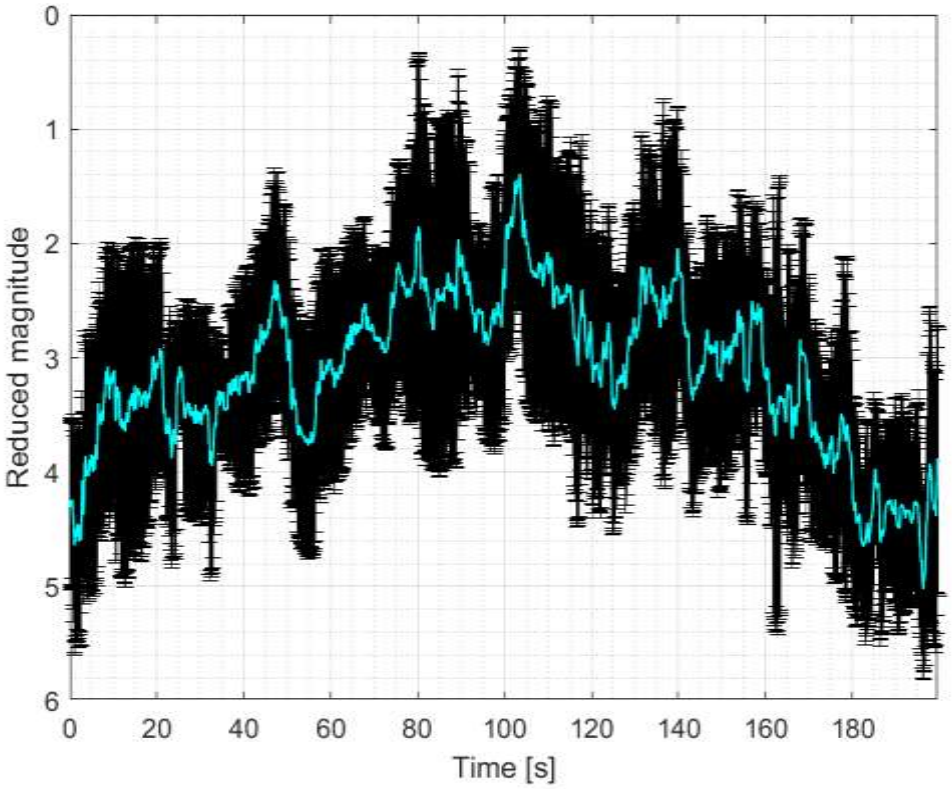

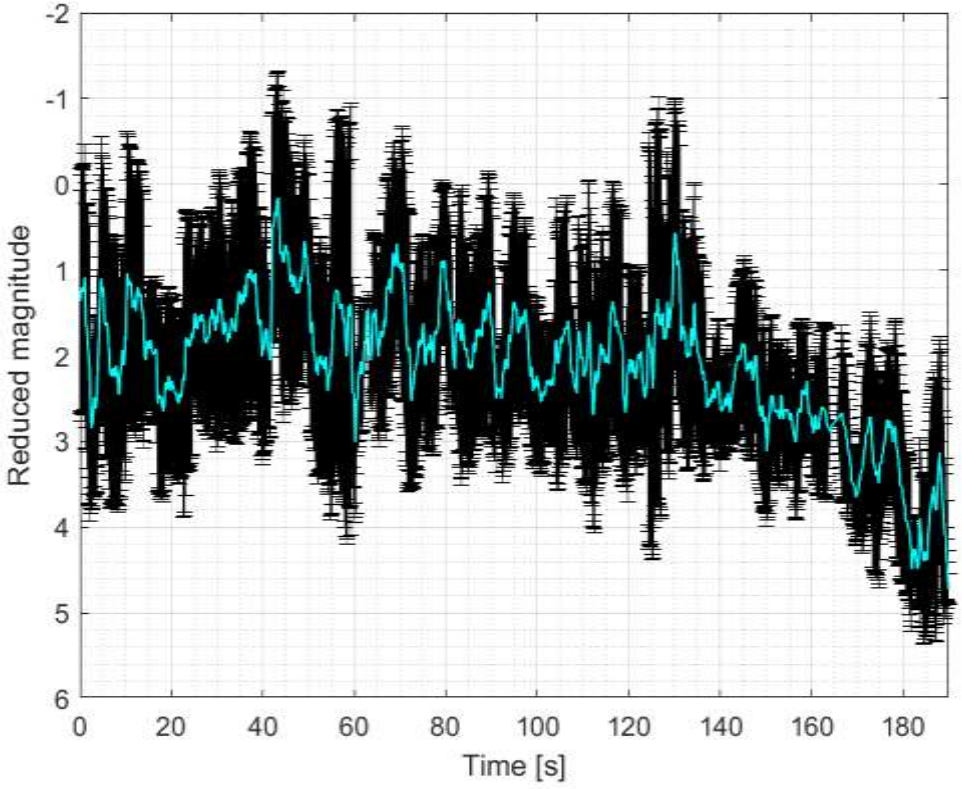

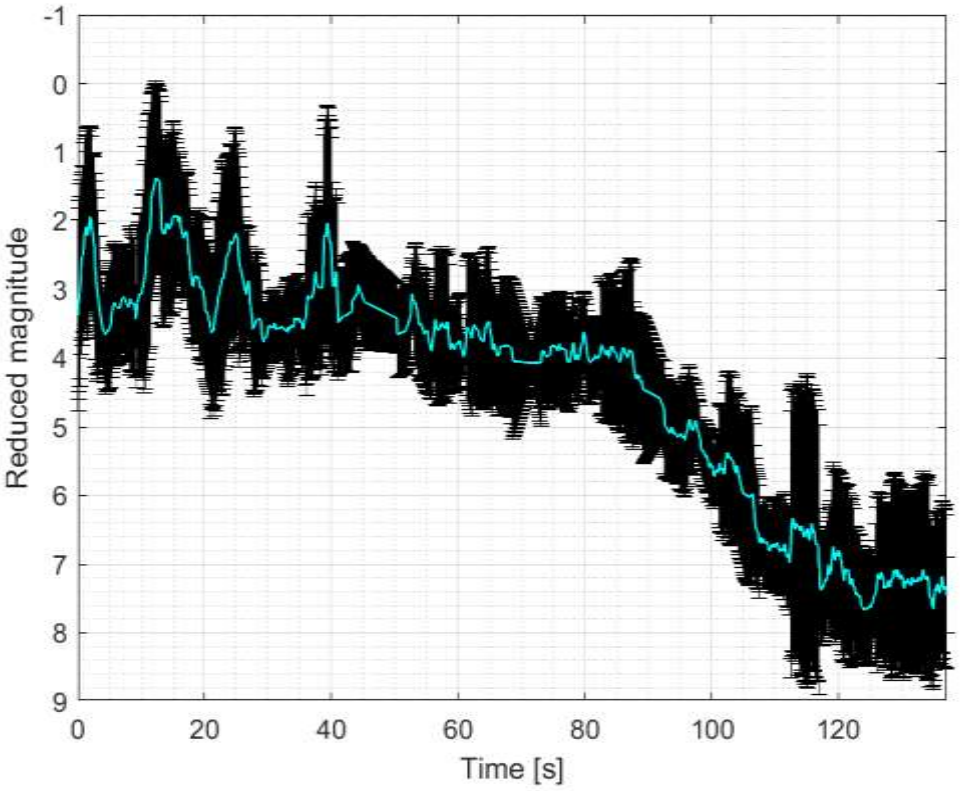
Reduced magnitude
-1
0
1
2
3
4
5
6
7
8
9
0
20
40
60
80
100
120
Time [s]

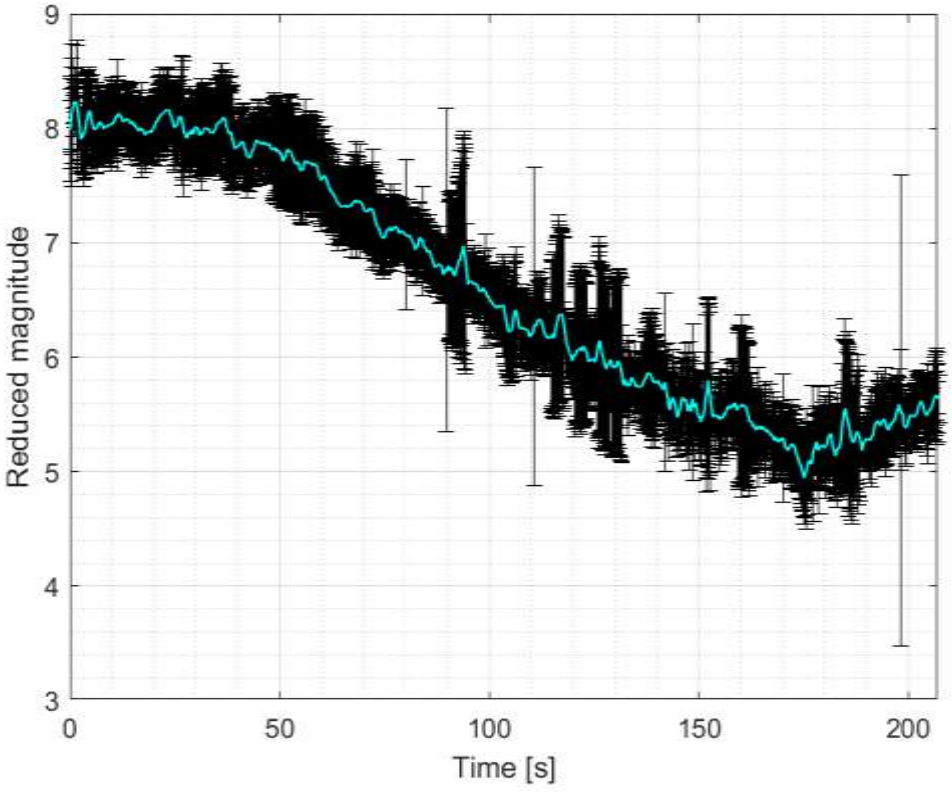
Reduced magnitude
9
8
7
6
5
4
3
0
50
100
150
200
Time [s]

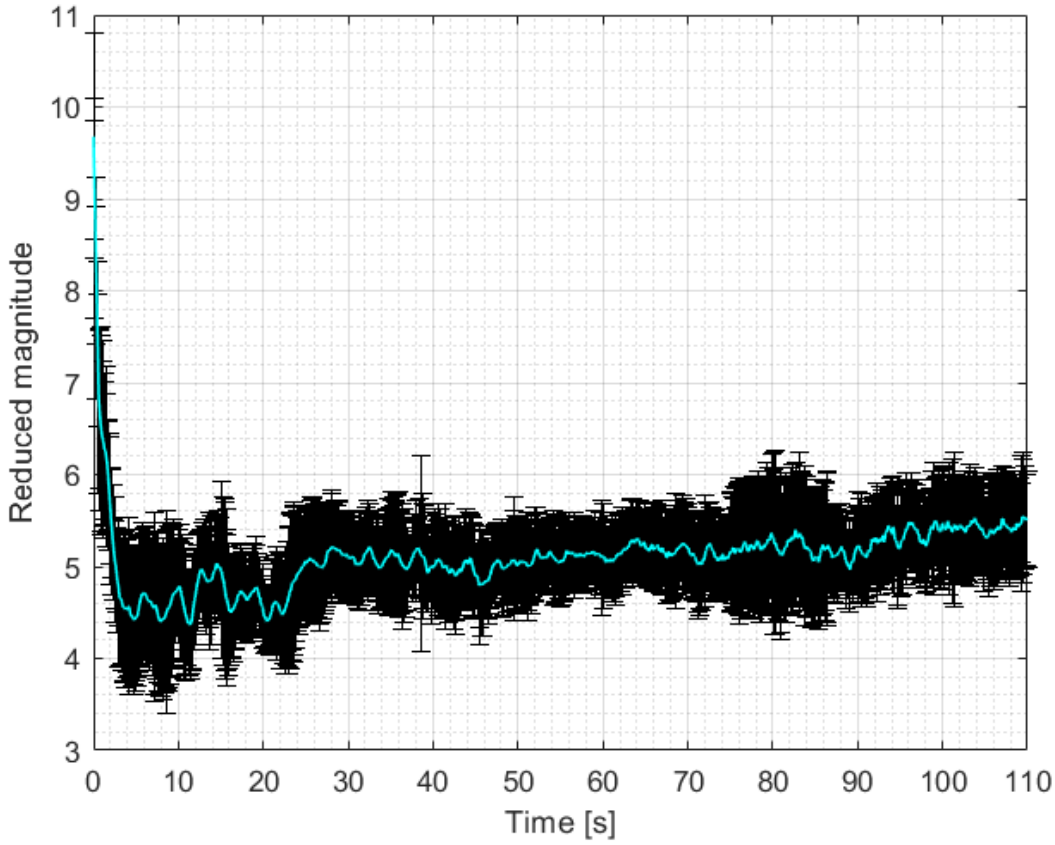
Reduced magnitude
Time [s]
11
10
9
8
7
6
5
4
3
0
10
20
30
40
50
60
70
80
90
100
110

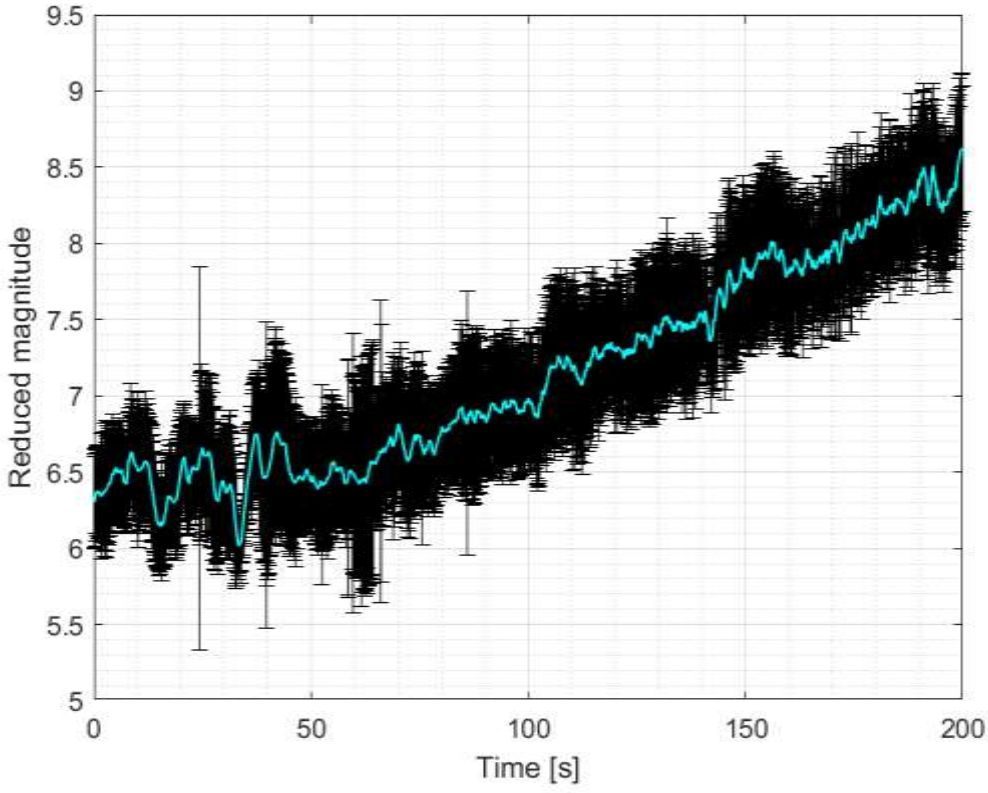
Reduced magnitude
Time [s]
9.5
9
8.5
8
7.5
7
6.5
6
5.5
5
0
50
100
150
200

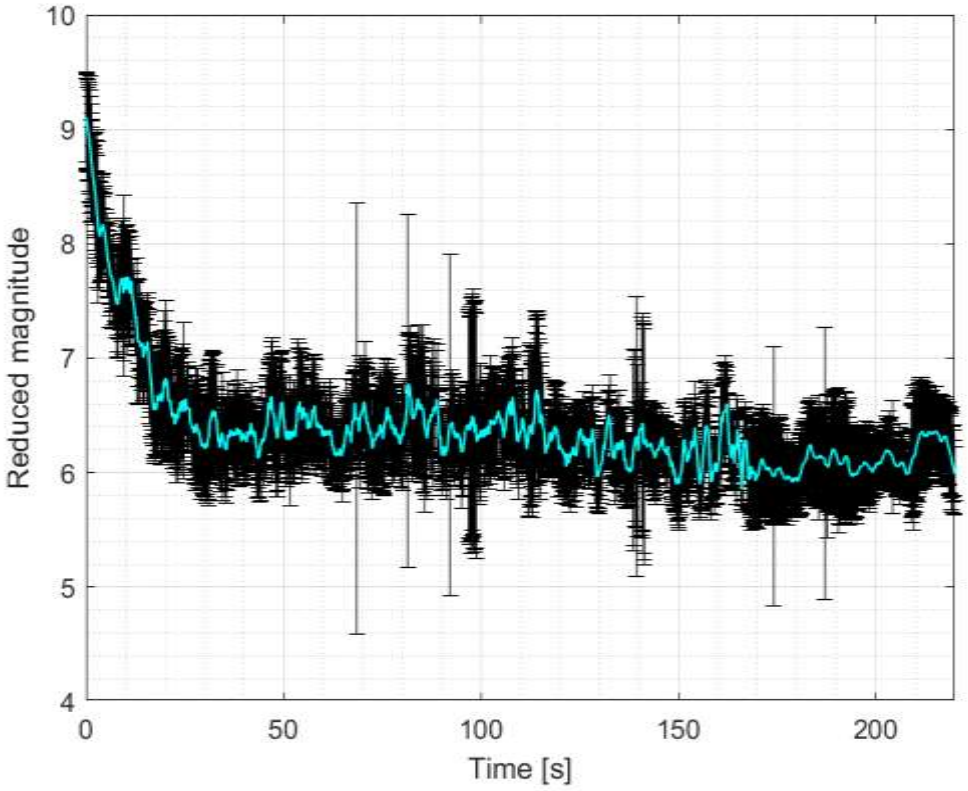
Reduced magnitude
Time [s]
10
9
8
7
6
5
4
0
50
100
150
200

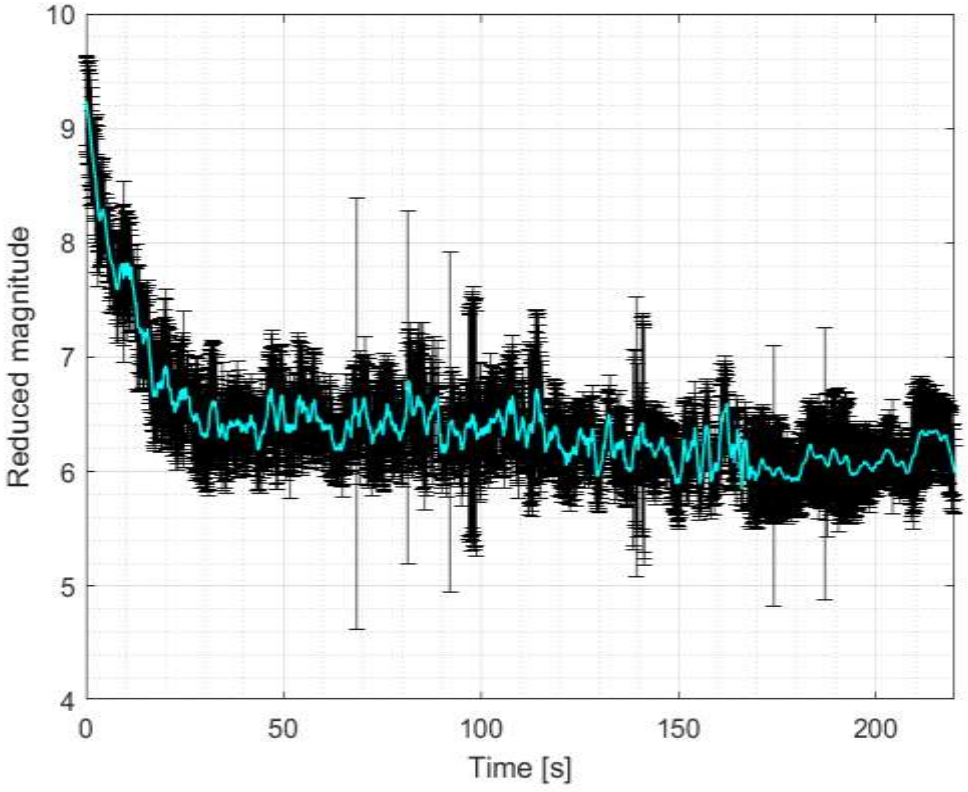
Reduced magnitude
Time [s]
10
9
8
7
6
5
4
0
50
100
150
200

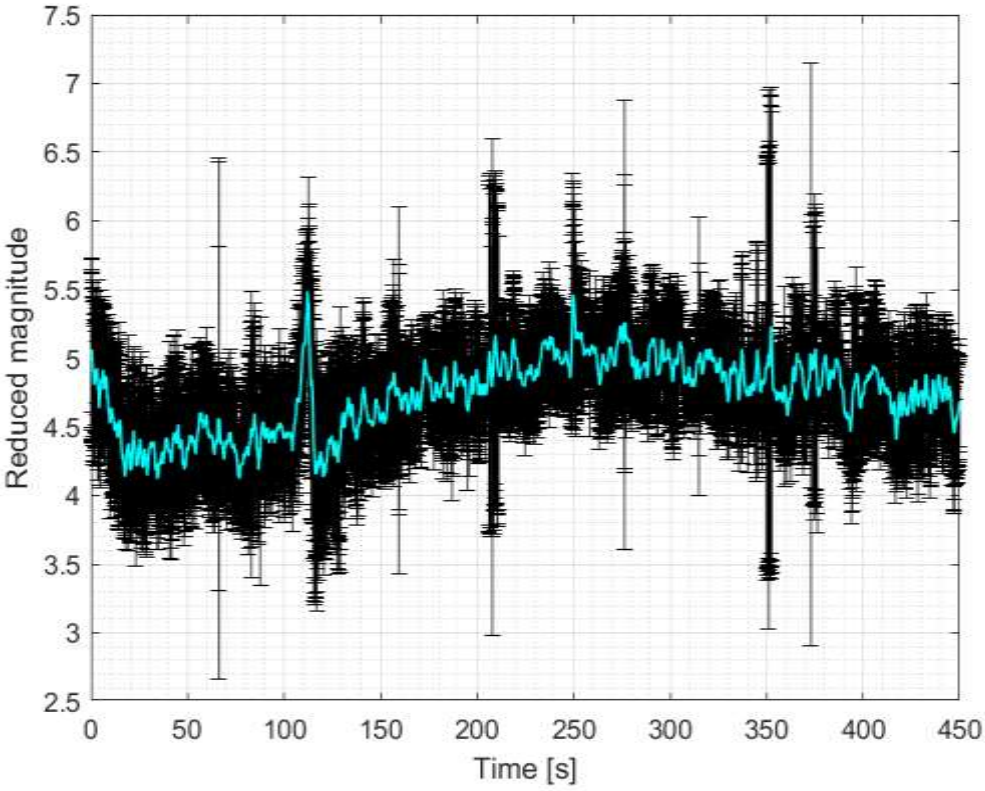
Reduced magnitude
Time [s]
7.5
7
6.5
6
5.5
5
4.5
4
3.5
3
2.5
0
50
100
150
200
250
300
350
400
450

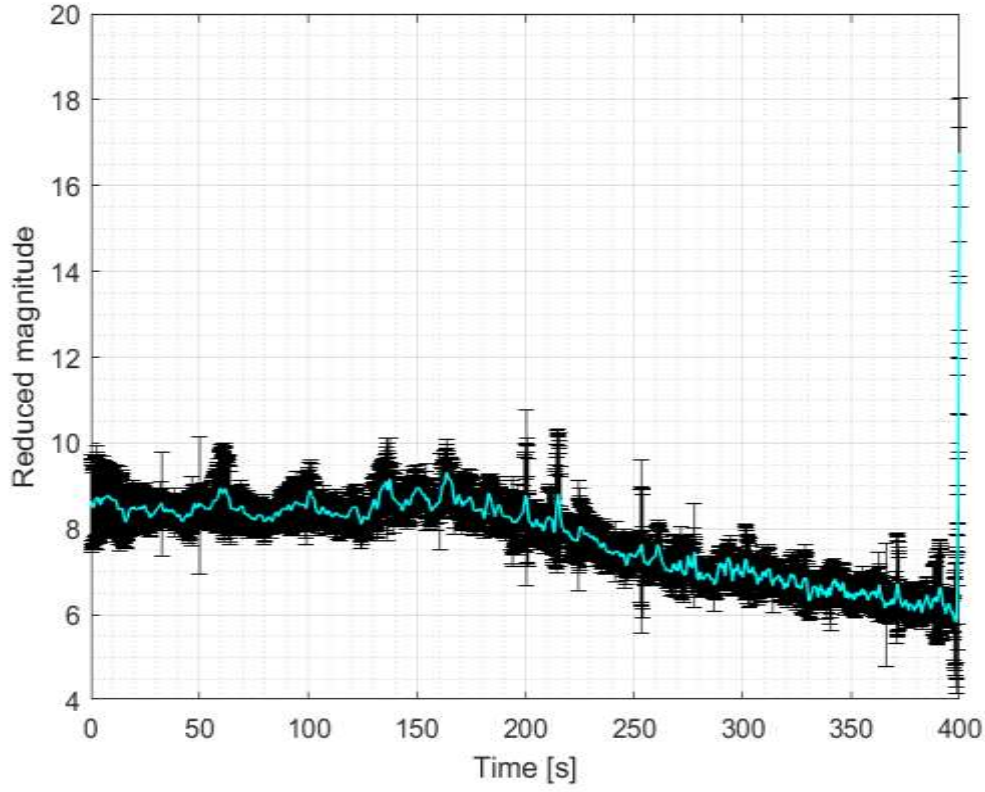
Reduced magnitude
Time [s]
20
18
16
14
12
10
8
6
4
0
50
100
150
200
250
300
350
400

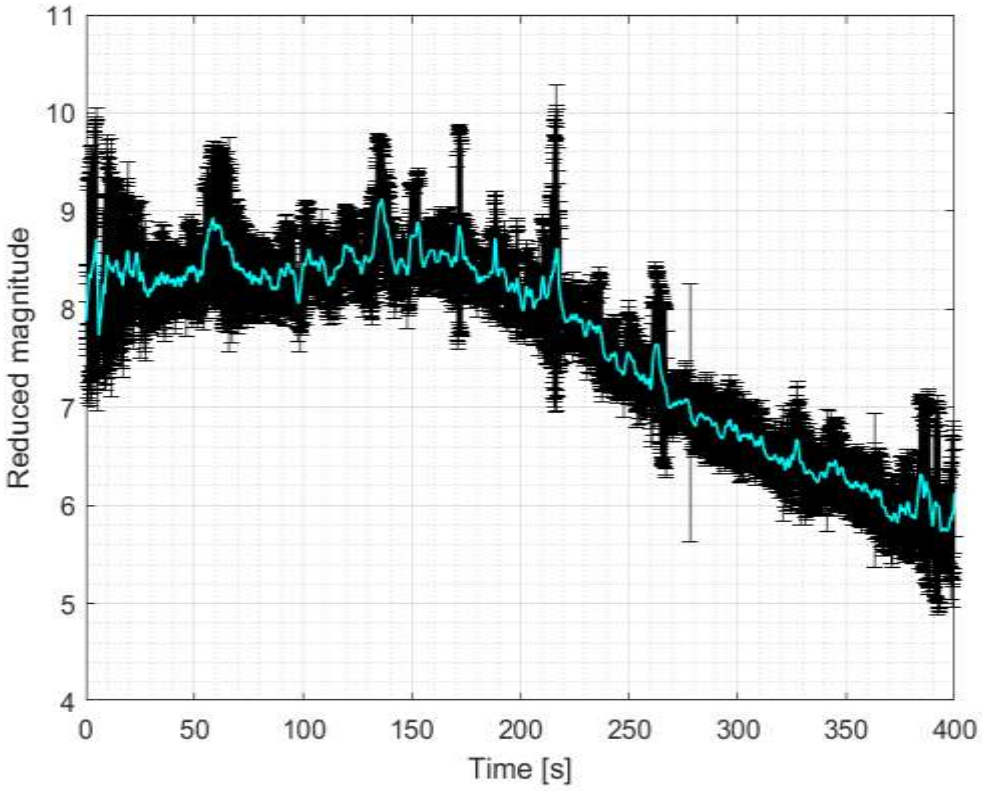

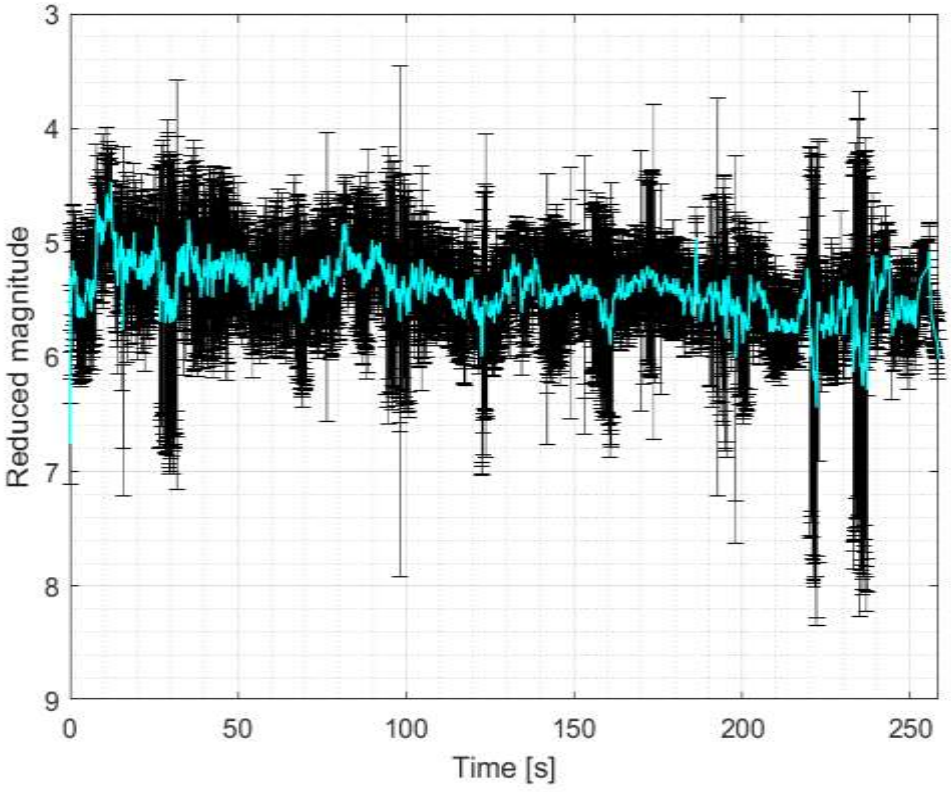

3.1.5 Norad 39198

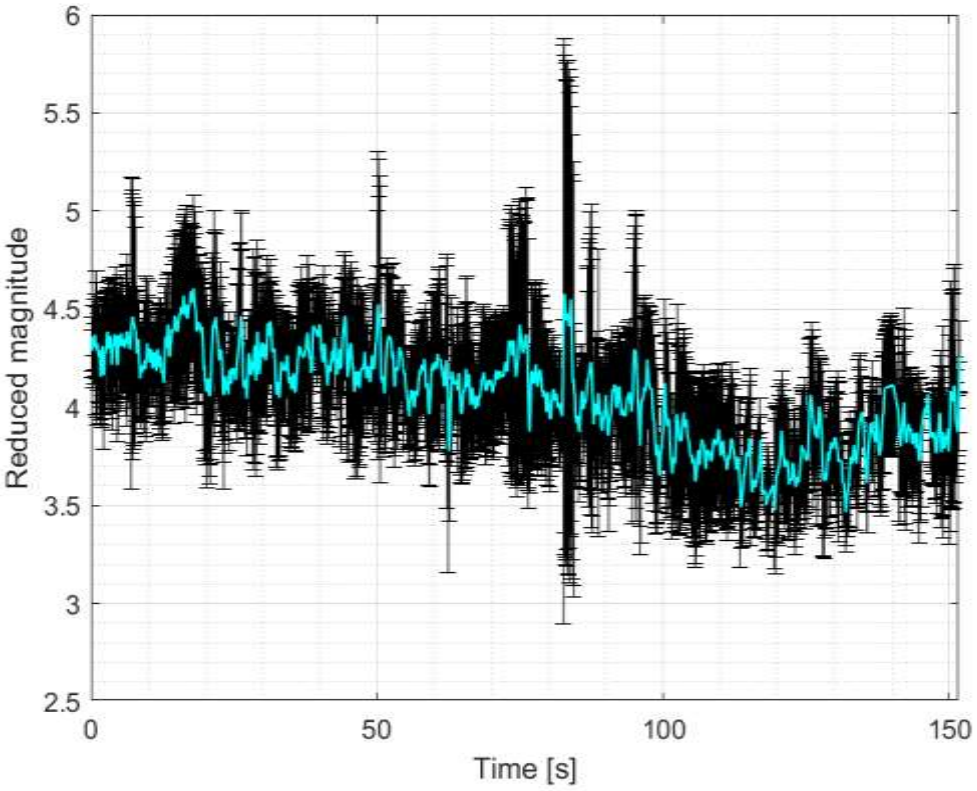
Reduced magnitude
Time [s]
6
5.5
5
4.5
4
3.5
3
2.5
0
50
100
150

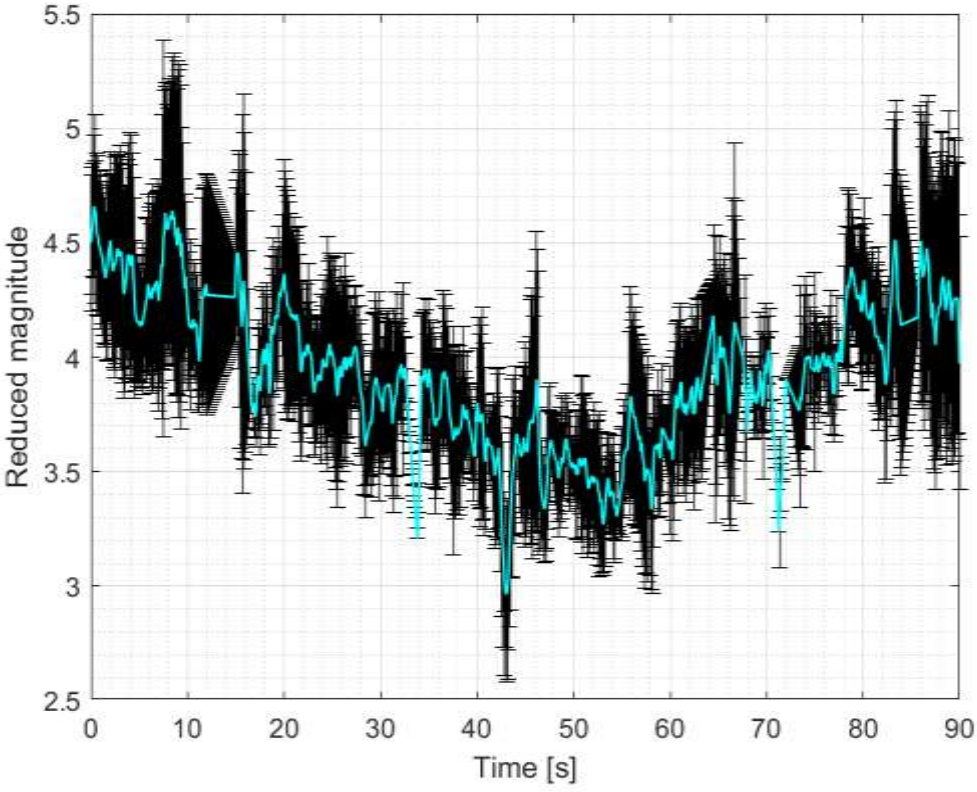
Reduced magnitude
Time [s]
5.5
5
4.5
4
3.5
3
2.5
0
10
20
30
40
50
60
70
80
90

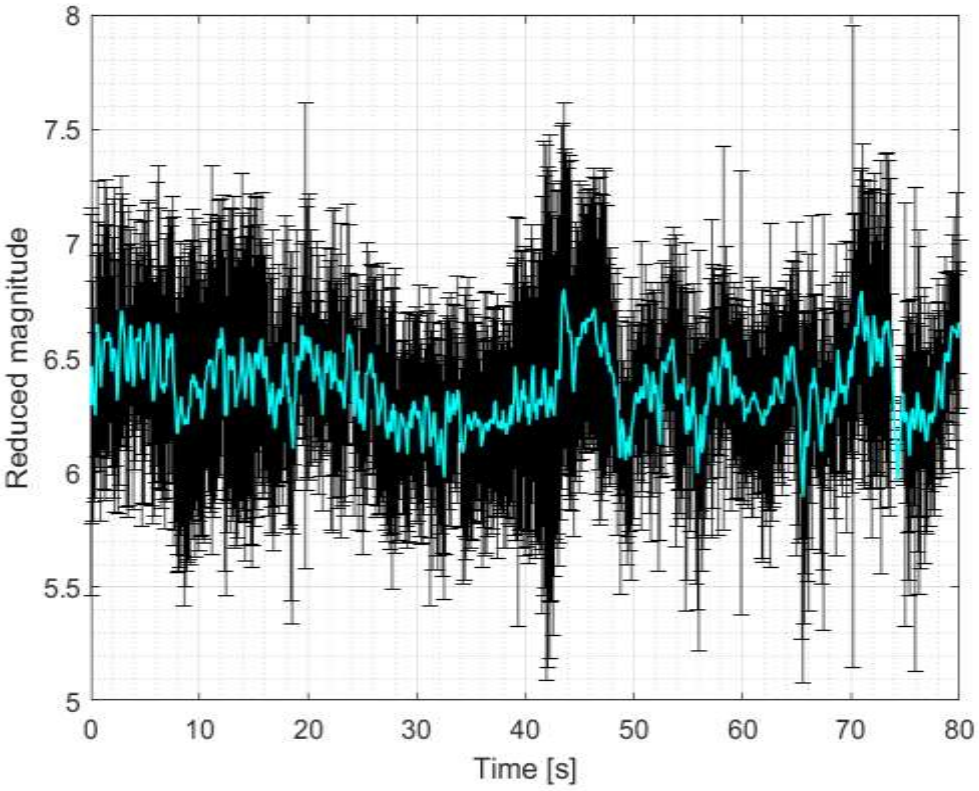
Reduced magnitude
Time [s]
8
7.5
7
6.5
6
5.5
5
0
10
20
30
40
50
60
70
80

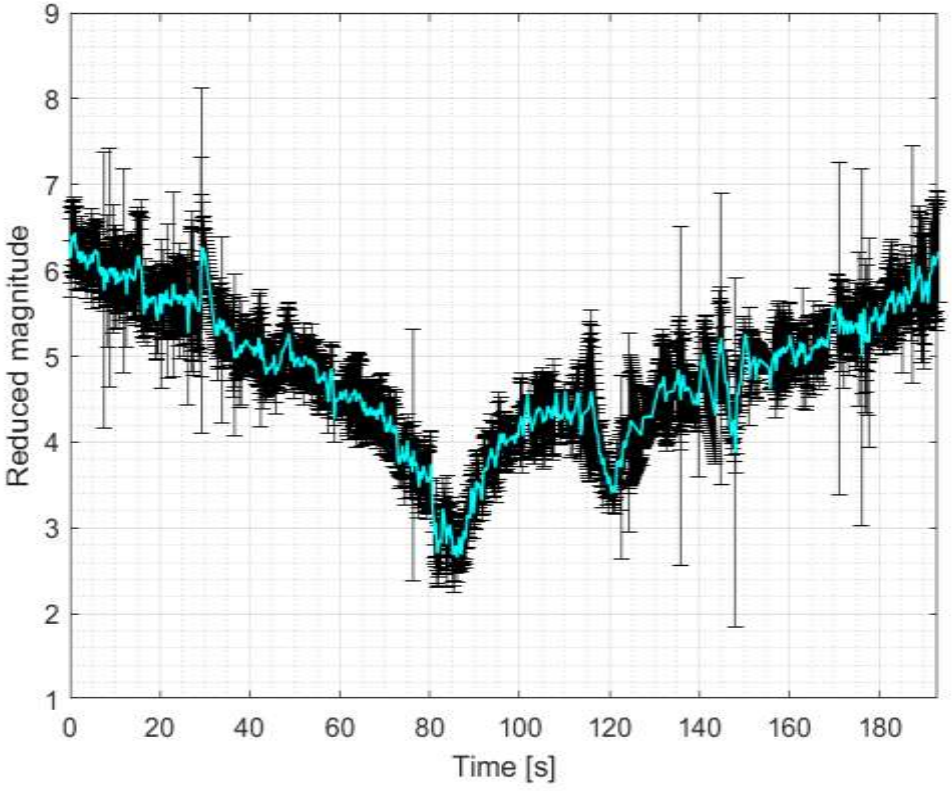
Reduced magnitude
Time [s]
9
8
7
6
5
4
3
2
1
0
20
40
60
80
100
120
140
160
180

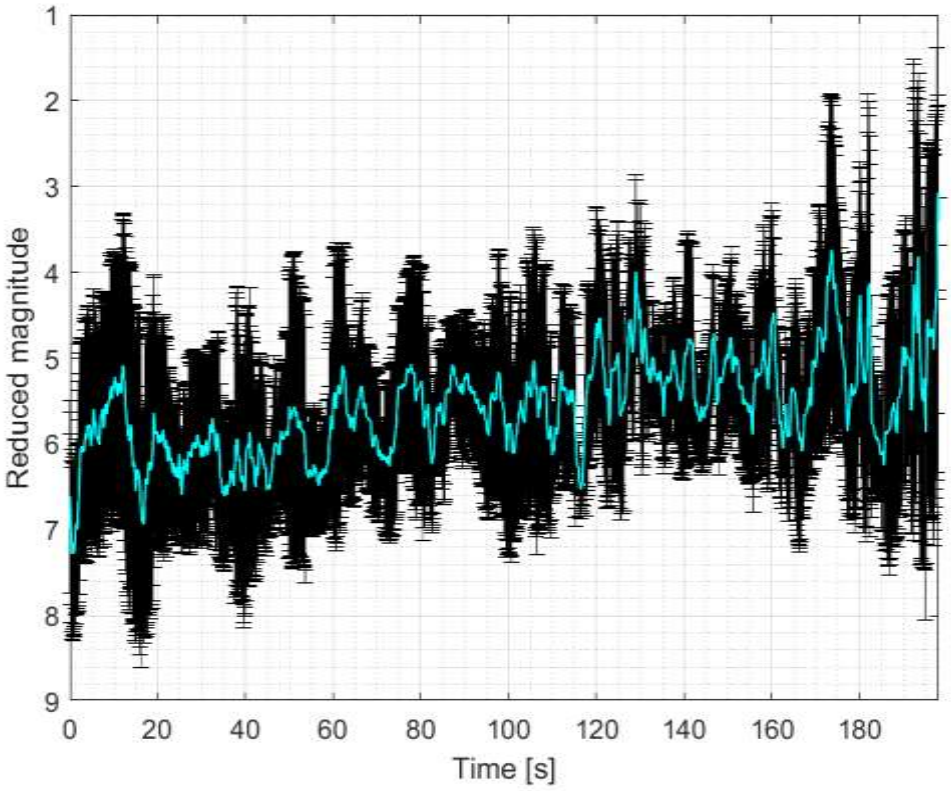
Reduced magnitude
Time [s]
1
2
3
4
5
6
7
8
9
0
20
40
60
80
100
120
140
160
180

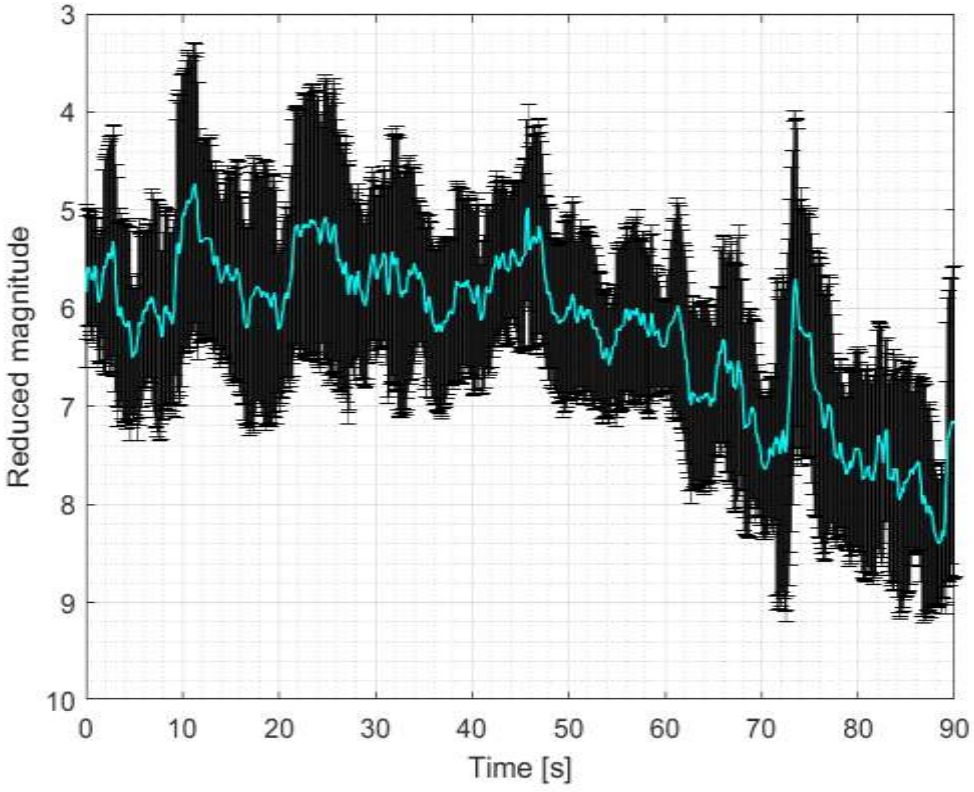
Reduced magnitude
Time [s]
3
4
5
6
7
8
9
10
0
10
20
30
40
50
60
70
80
90

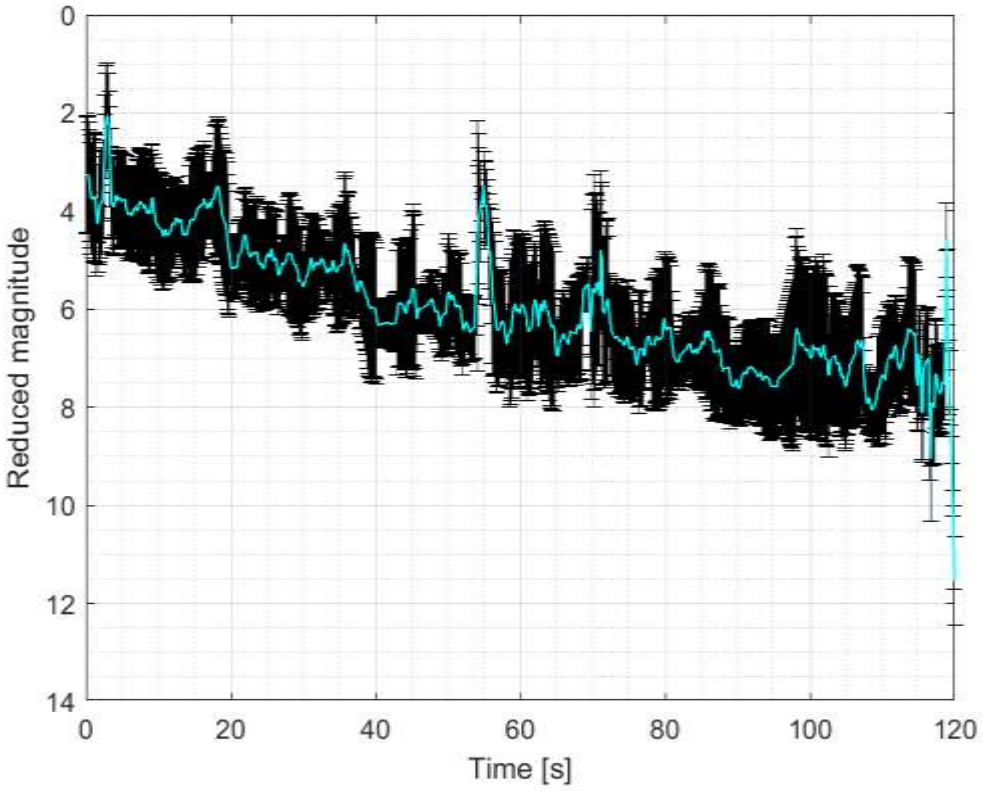
Reduced magnitude
Time [s]
0
2
4
6
8
10
12
14
0
20
40
60
80
100
120

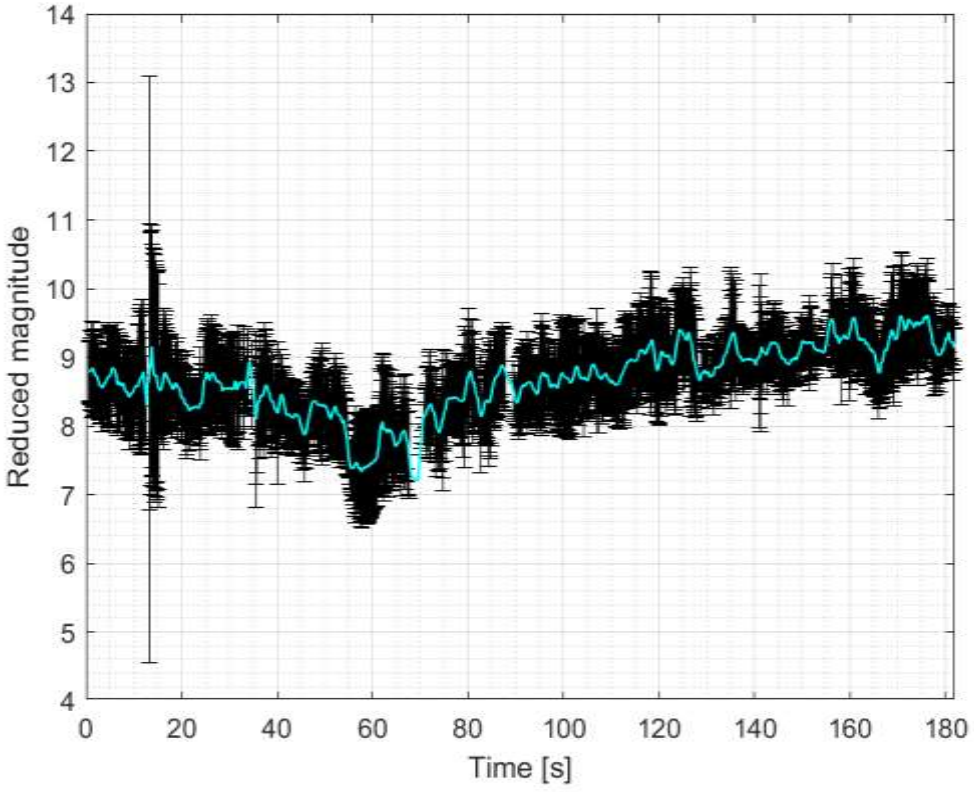
Reduced magnitude
Time [s]
4
5
6
7
8
9
10
11
12
13
14
0
20
40
60
80
100
120
140
160
180

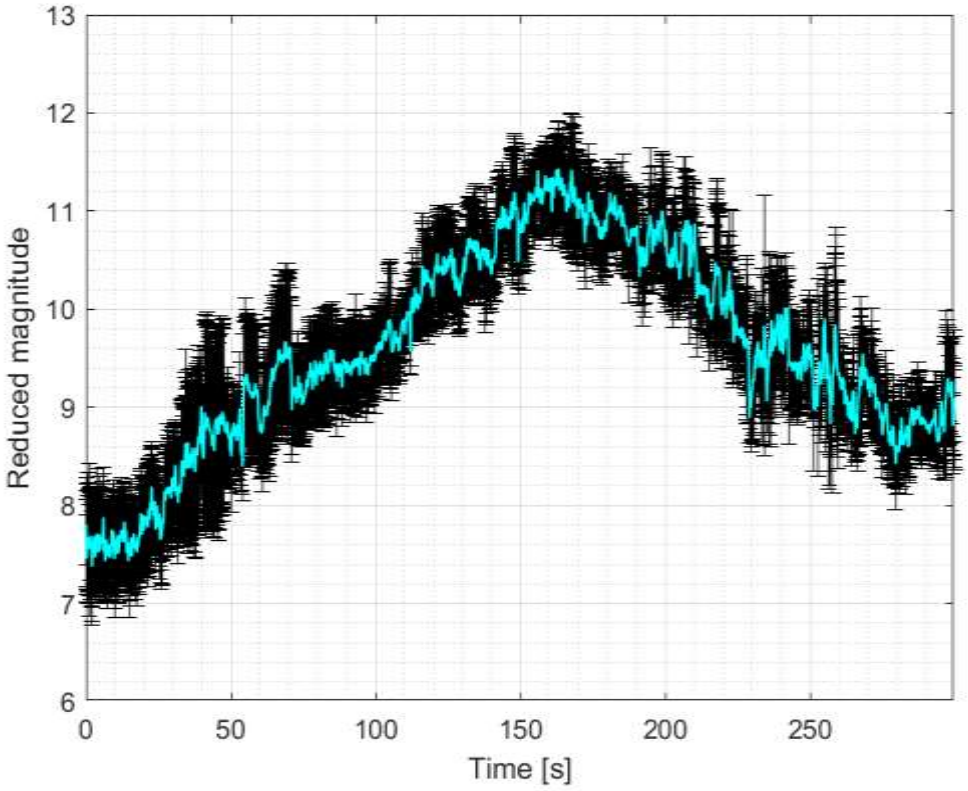

3.1.6 Norad 40879

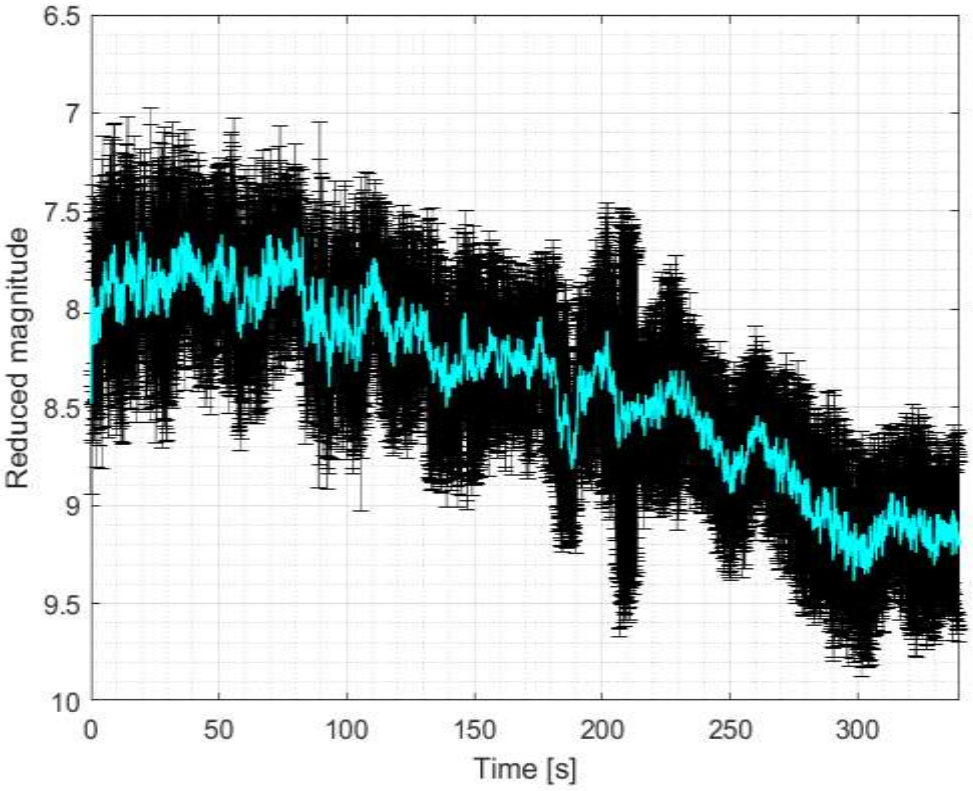
6.5
7
7.5
8
8.5
9
9.5
10
Reduced magnitude
0
50
100
150
200
250
300
Time [s]

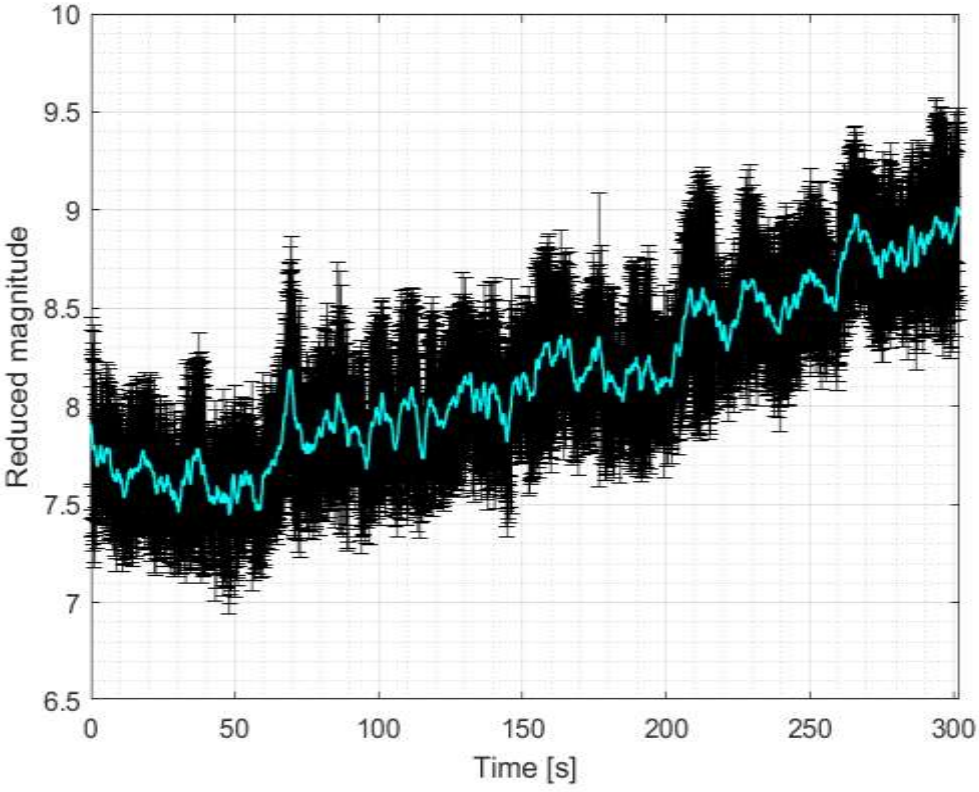
10
9.5
9
8.5
8
7.5
7
6.5
Reduced magnitude
0
50
100
150
200
250
300
Time [s]

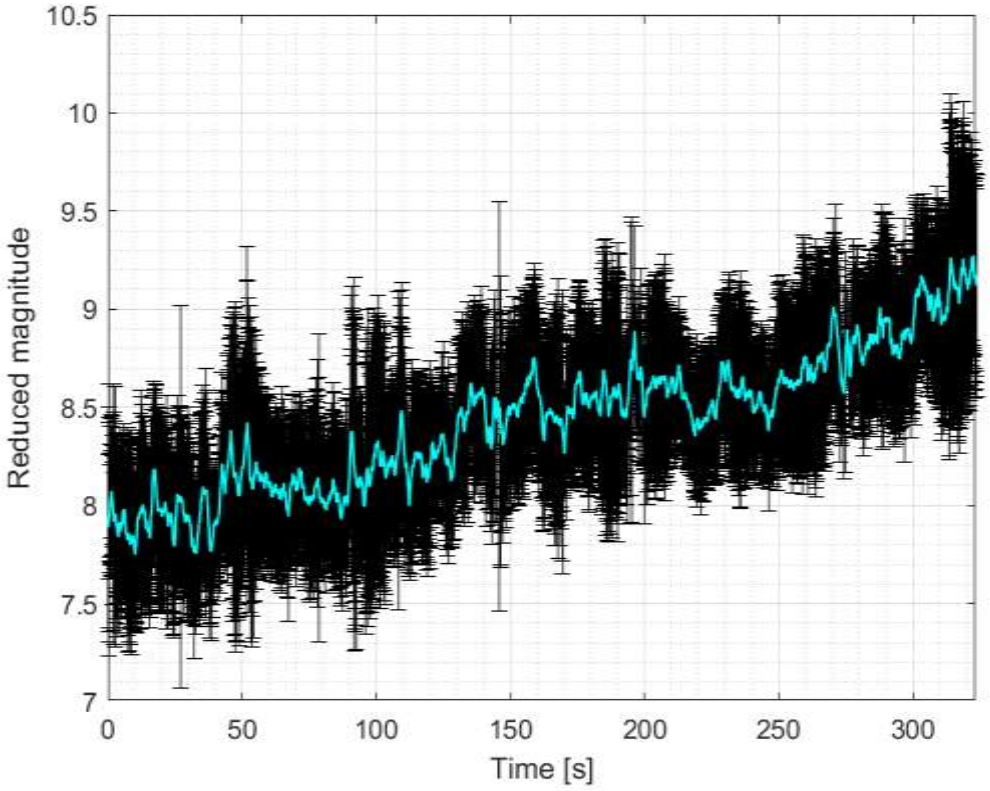
10.5
10
9.5
9
8.5
8
7.5
7
Reduced magnitude
0
50
100
150
200
250
300
Time [s]

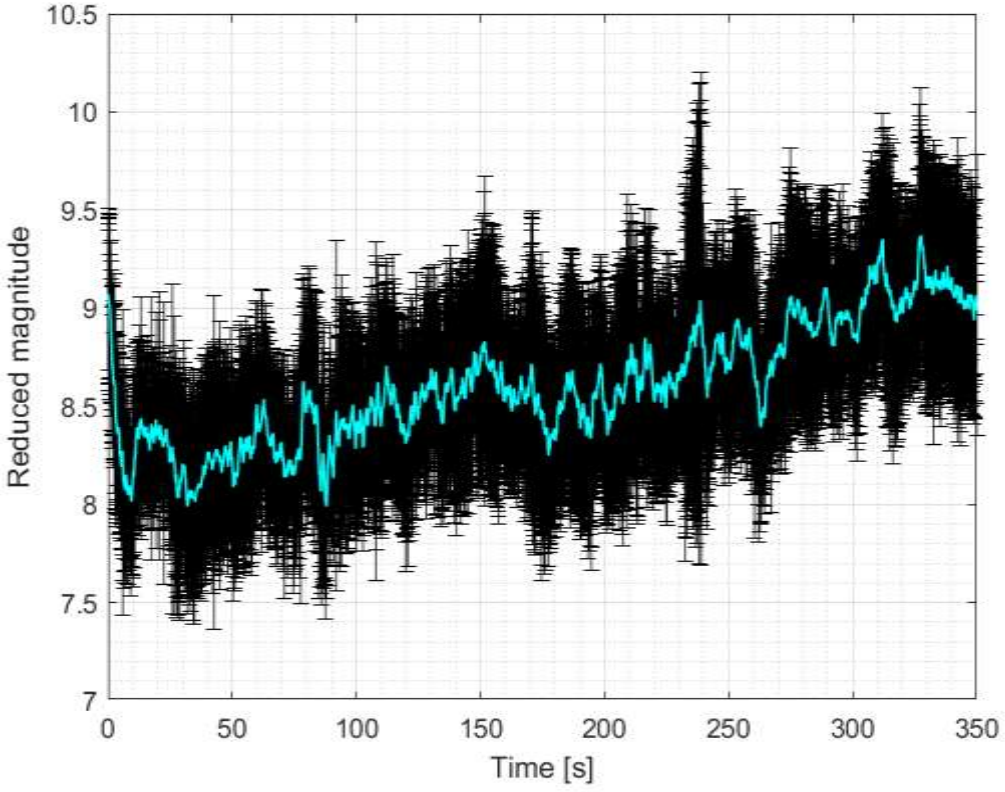
10.5
10
9.5
9
8.5
8
7.5
7
Reduced magnitude
0
50
100
150
200
250
300
350
Time [s]

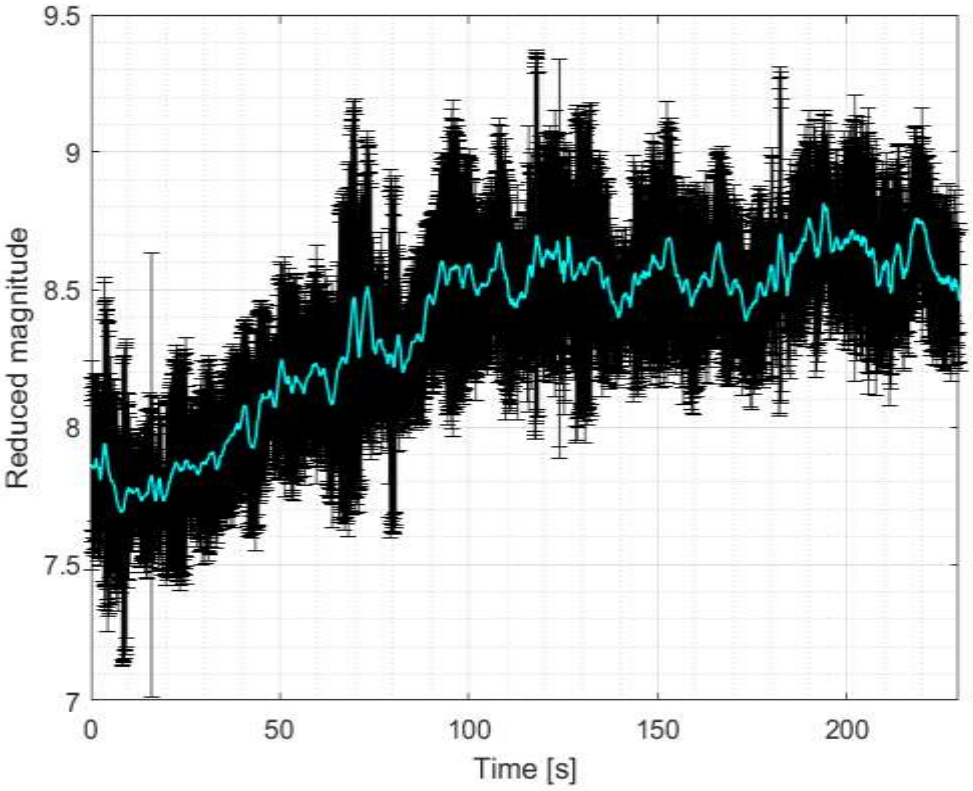
9.5
9
8.5
8
7.5
7
Reduced magnitude
0
50
100
150
200
Time [s]

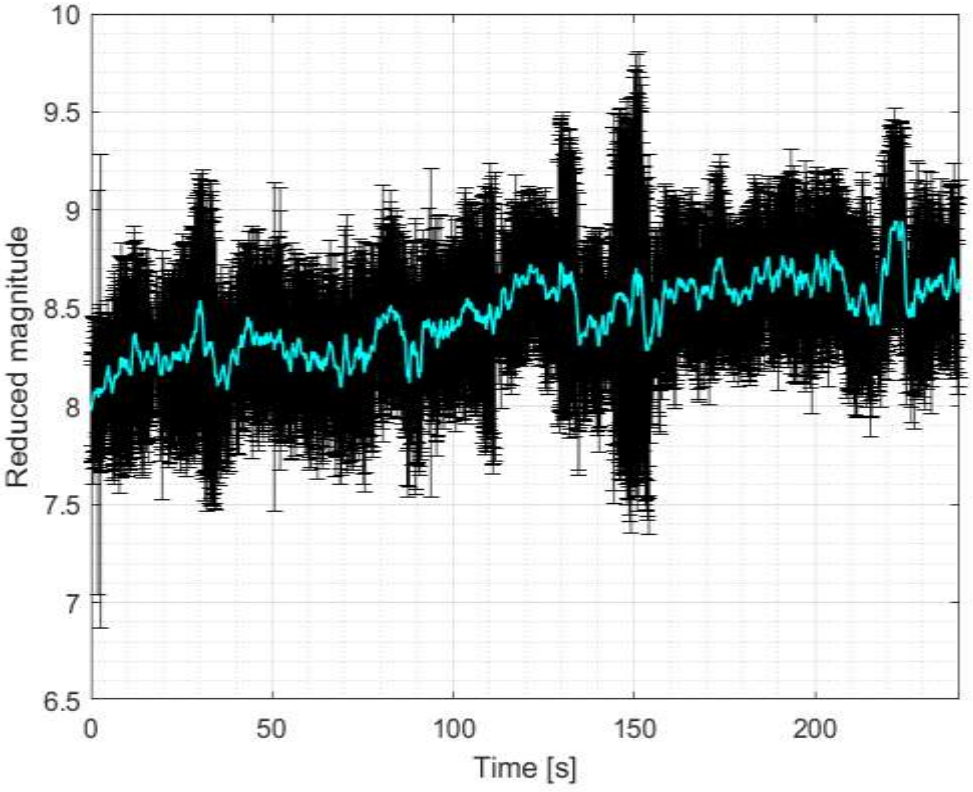
10
9.5
9
8.5
8
7.5
7
6.5
Reduced magnitude
0
50
100
150
200
Time [s]

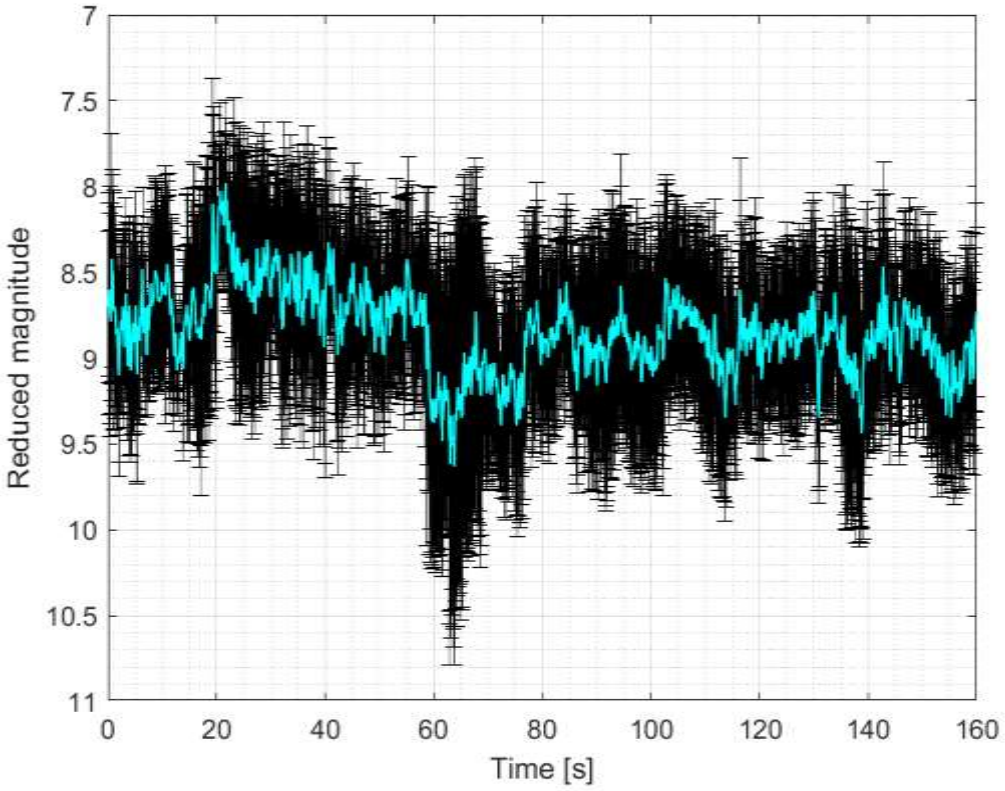

3.1.7 Norad 41847

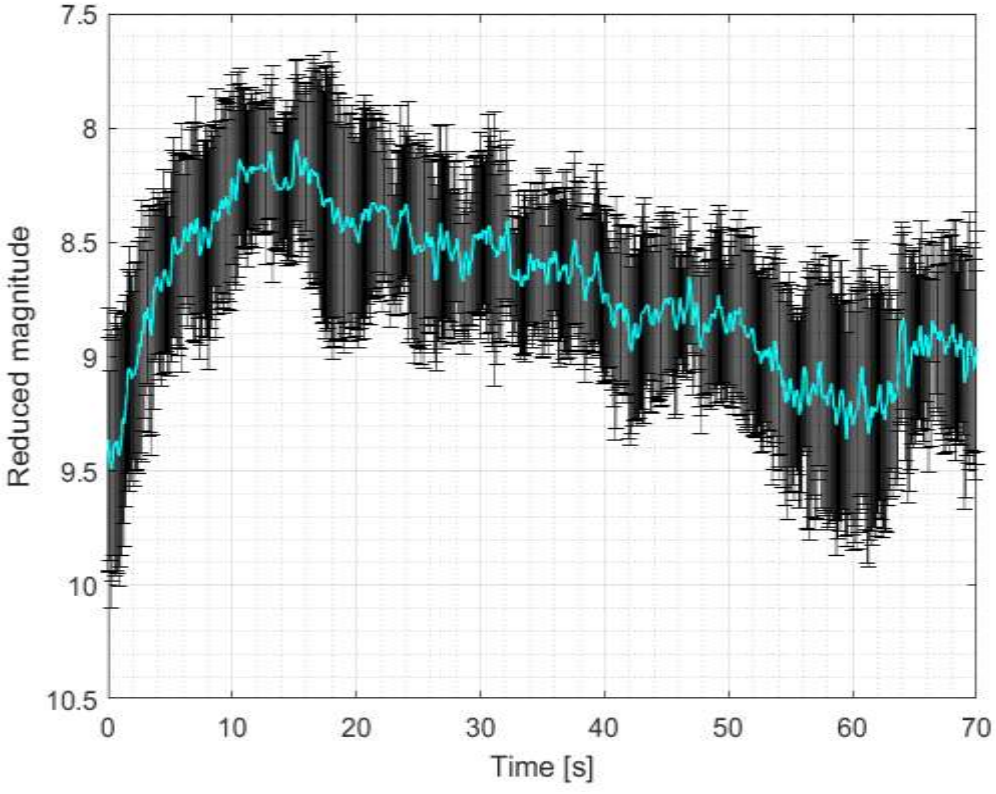

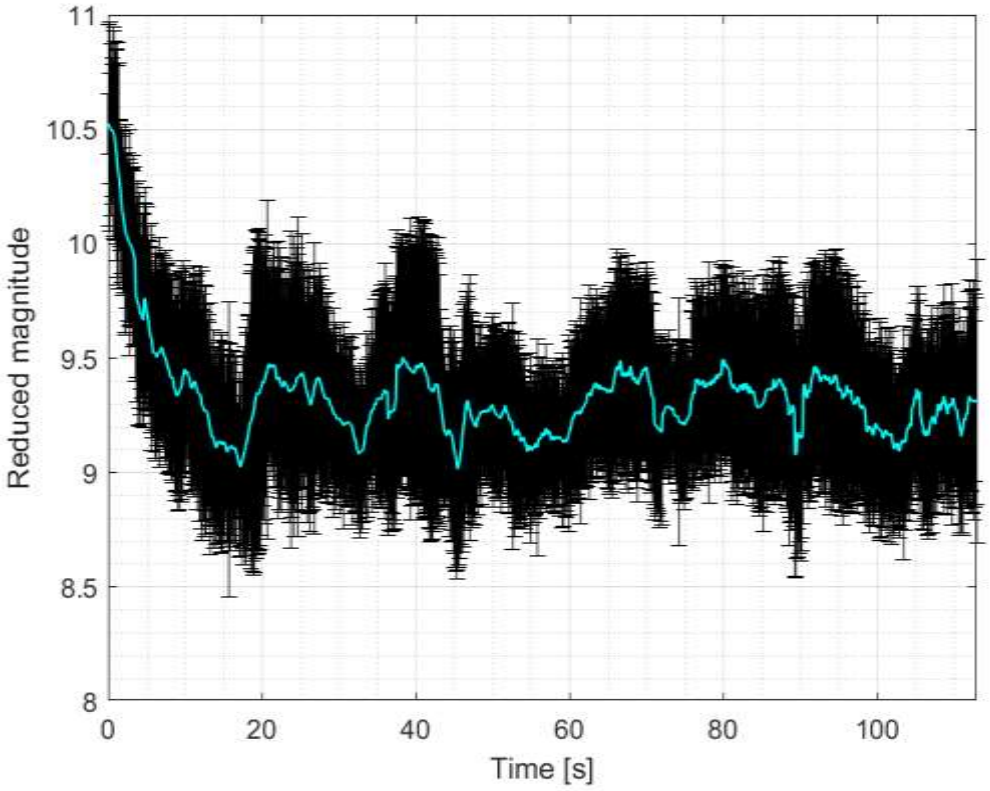
Reduced magnitude
Time [s]
11
10.5
10
9.5
9
8.5
8
0
20
40
60
80
100

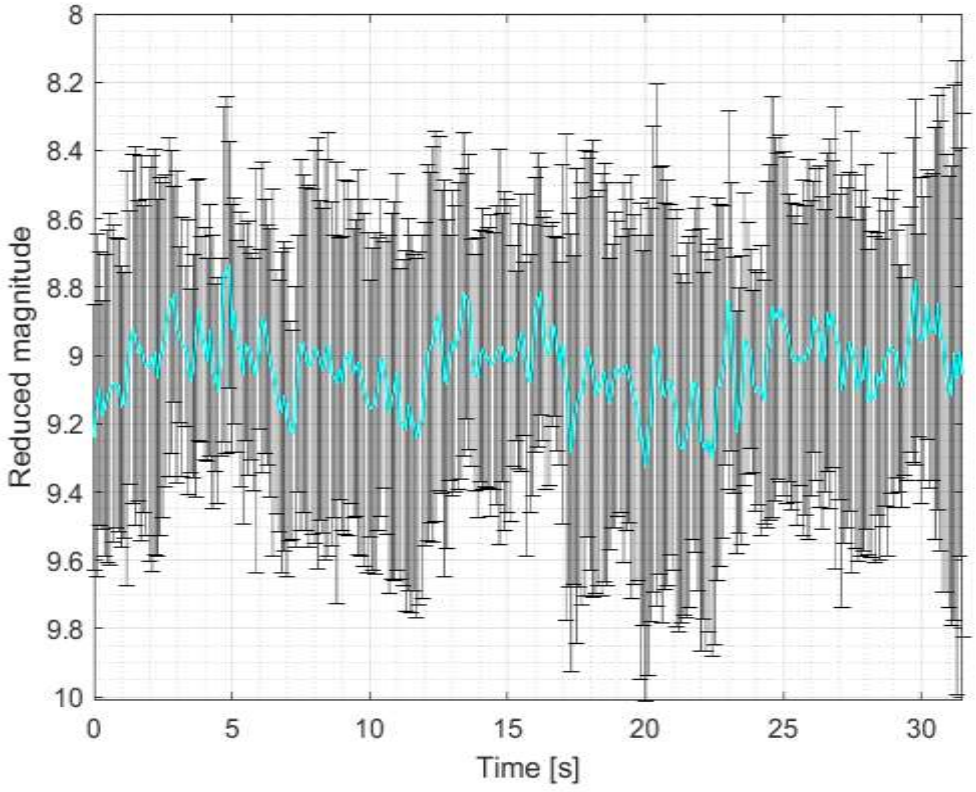
Reduced magnitude
Time [s]
8
8.2
8.4
8.6
8.8
9
9.2
9.4
9.6
9.8
10
0
5
10
15
20
25
30

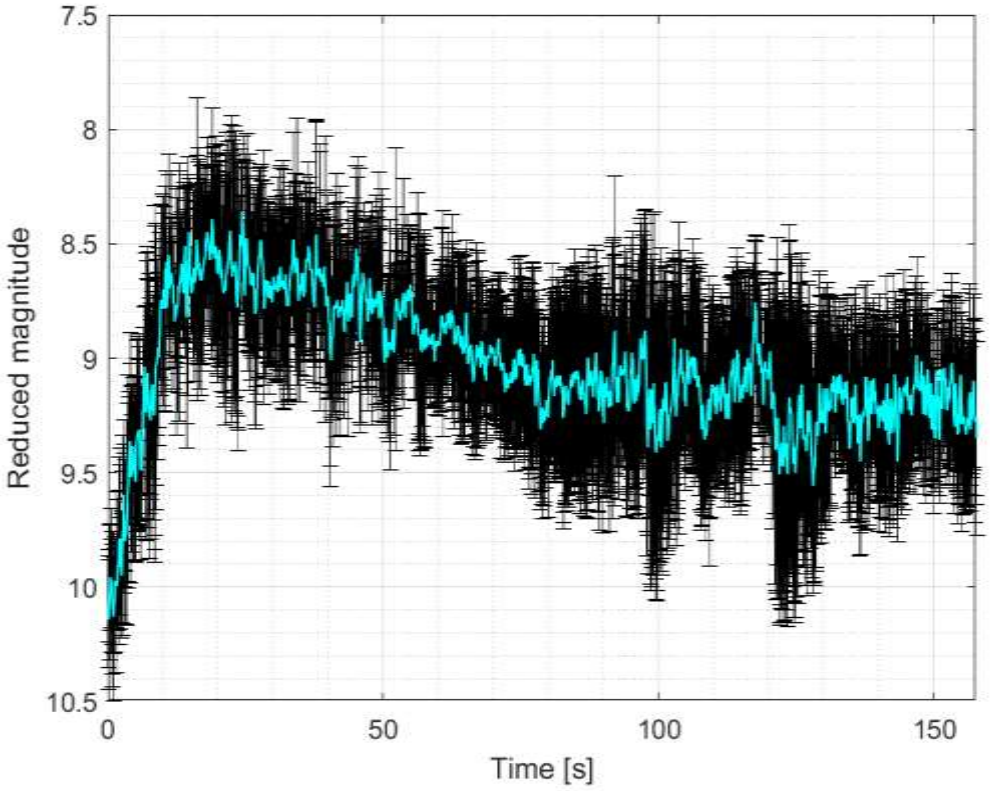
7.5
8
8.5
9
9.5
10
10.5
Reduced magnitude
0
50
100
150
Time [s]

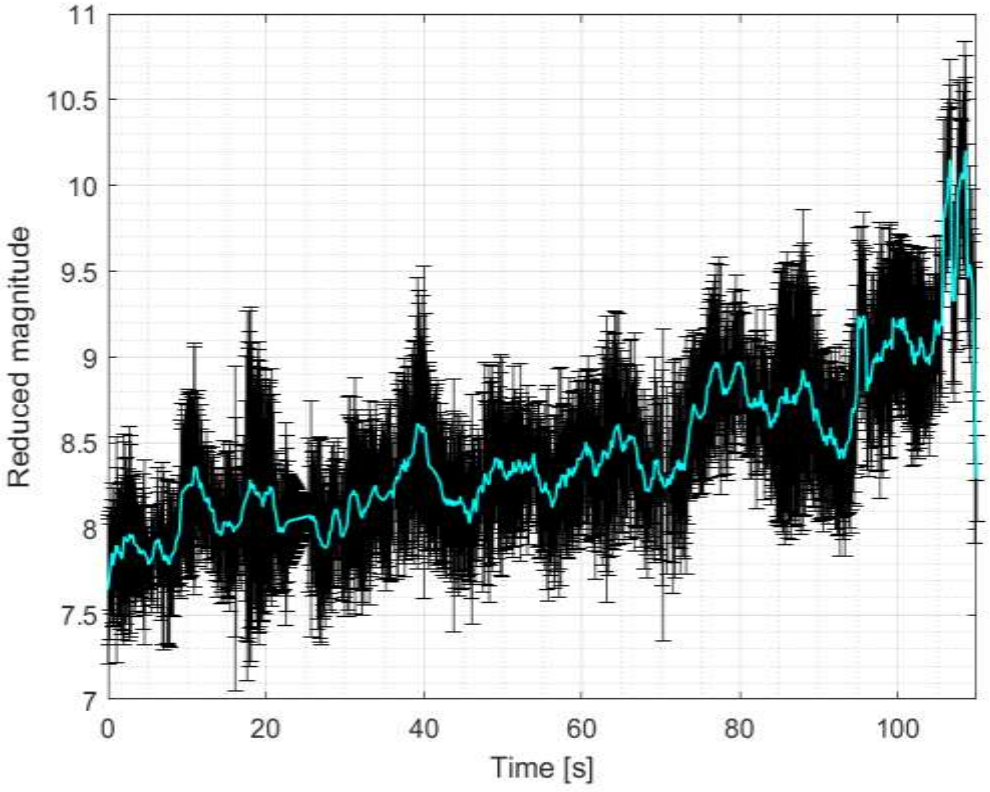
11
10.5
10
9.5
9
8.5
8
7.5
7
Reduced magnitude
0
20
40
60
80
100
Time [s]

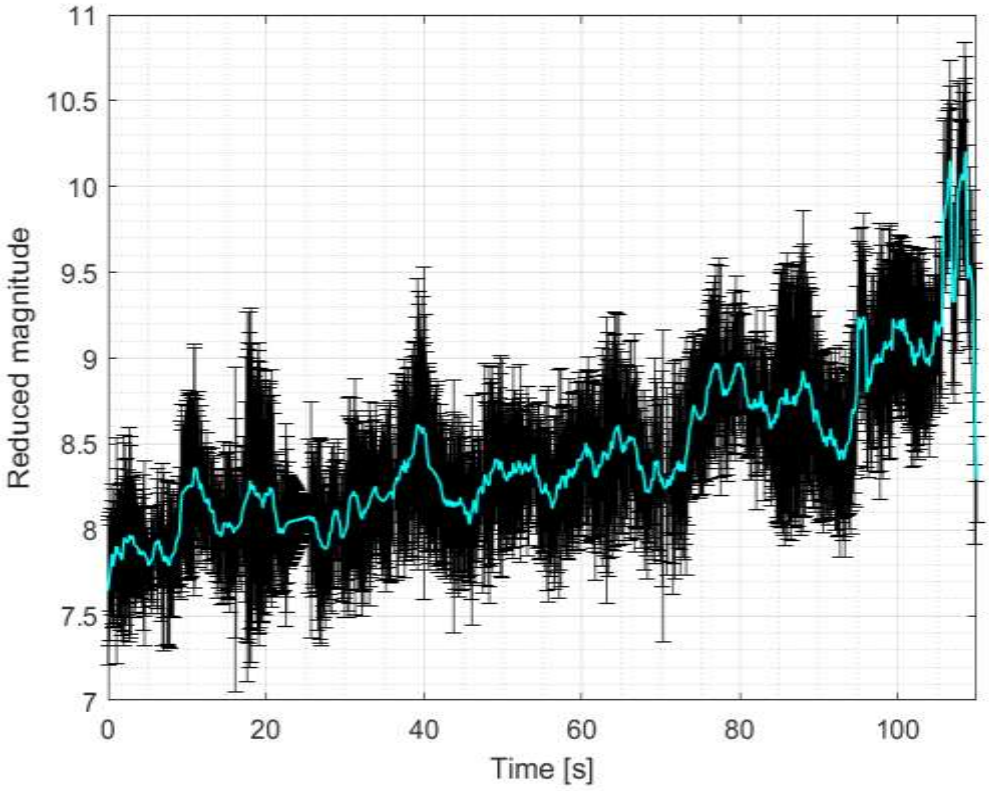
Reduced magnitude
Time [s]
11
10.5
10
9.5
9
8.5
8
7.5
7
0
20
40
60
80
100

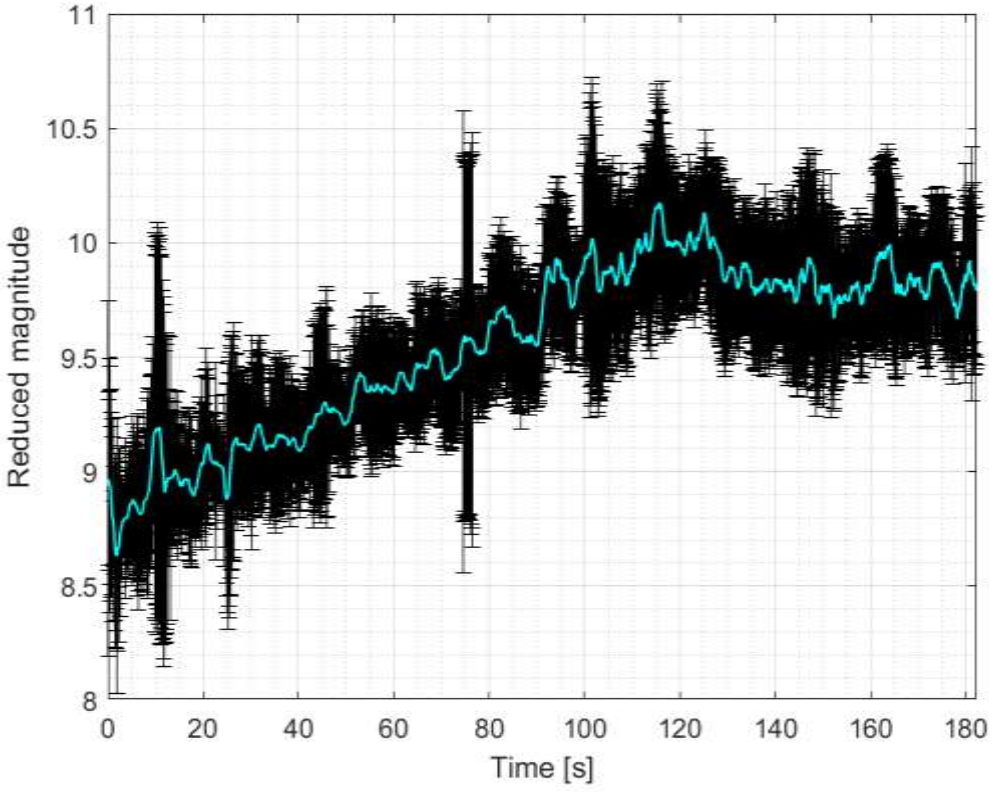
Reduced magnitude
Time [s]
11
10.5
10
9.5
9
8.5
8
0
20
40
60
80
100
120
140
160
180

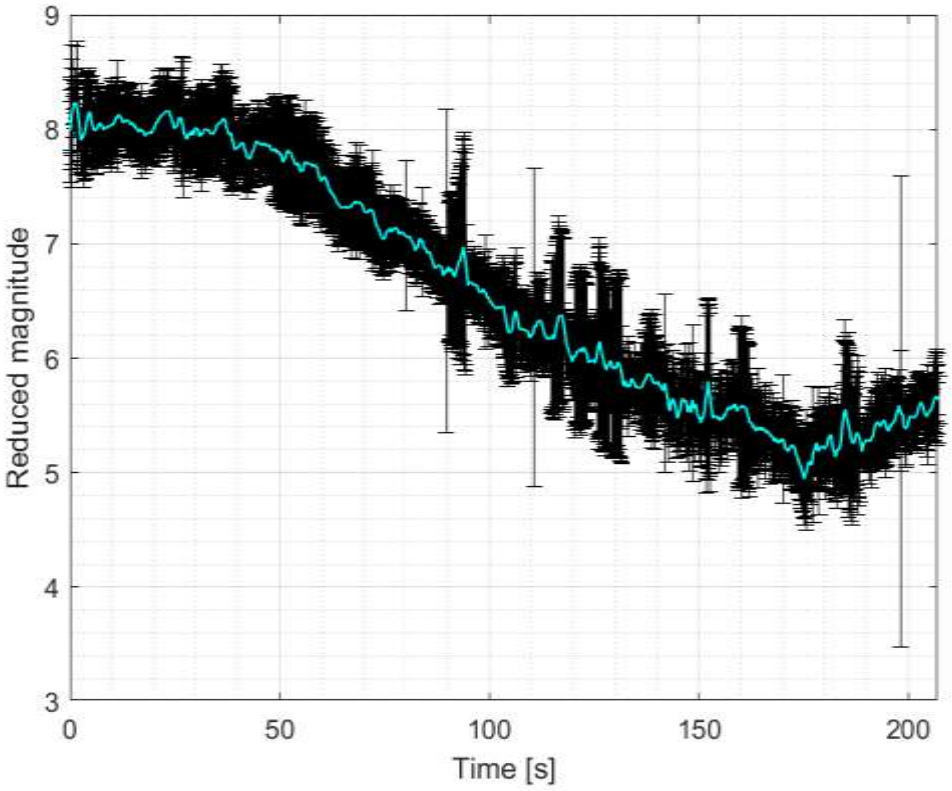
Reduced magnitude
Time [s]
9
8
7
6
5
4
3
0
50
100
150
200

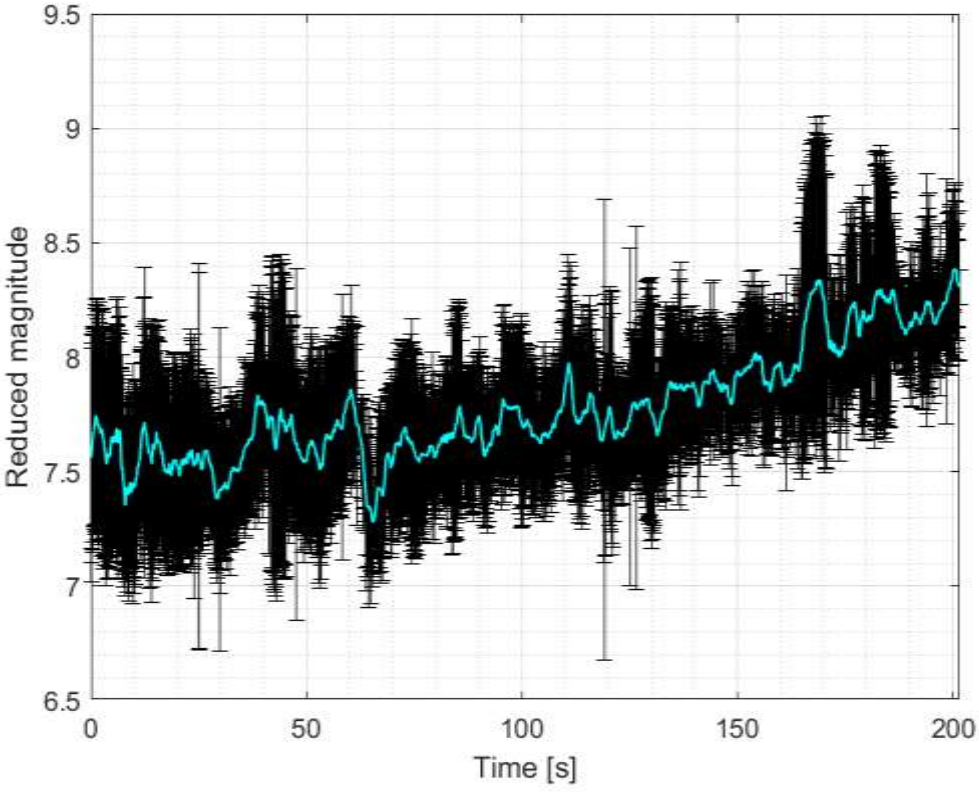
Reduced magnitude
Time [s]
9.5
9
8.5
8
7.5
7
6.5
0
50
100
150
200

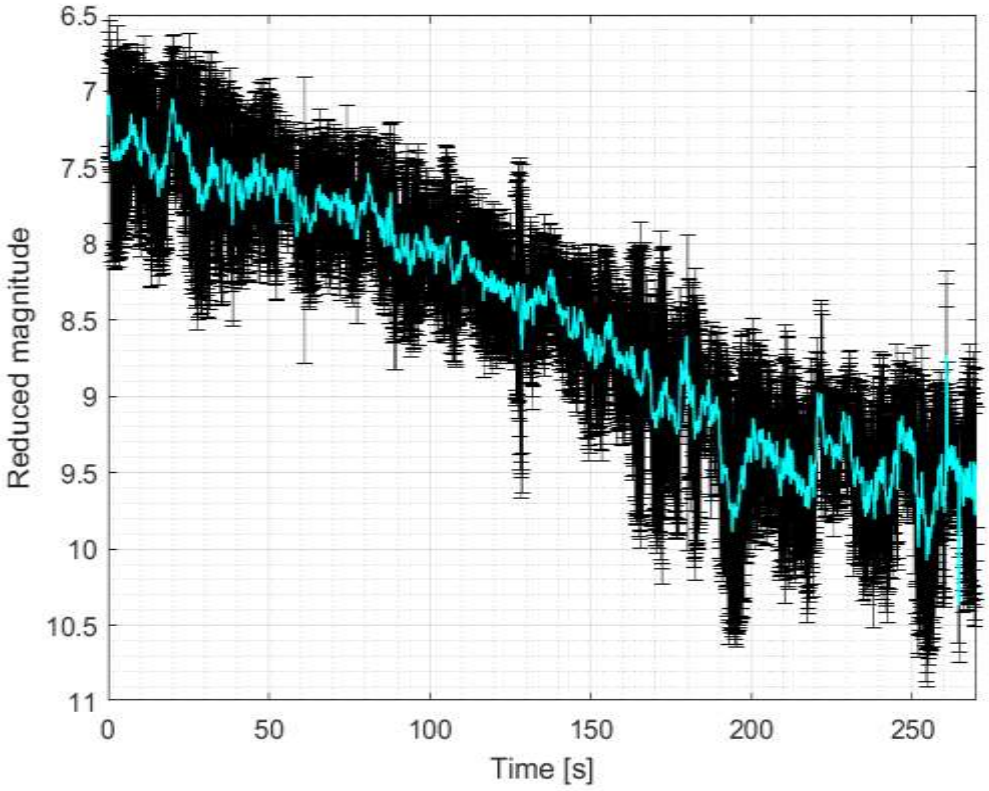
Reduced magnitude
Time [s]
6.5
7
7.5
8
8.5
9
9.5
10
10.5
11
0
50
100
150
200
250

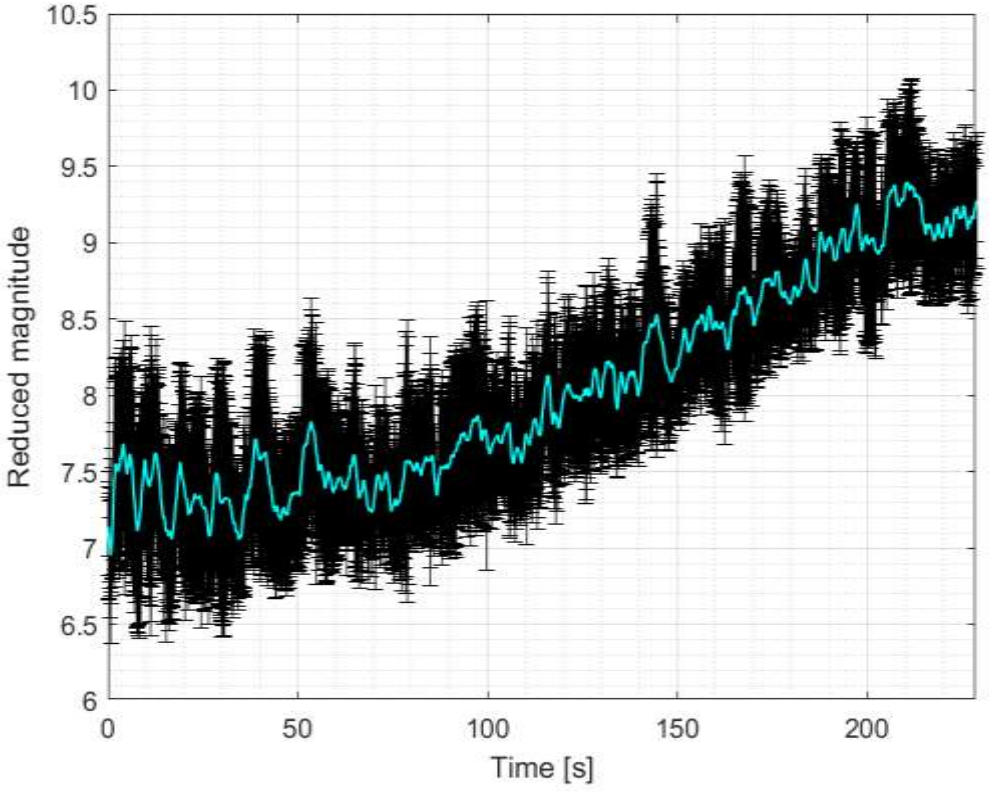
Reduced magnitude
Time [s]
10.5
10
9.5
9
8.5
8
7.5
7
6.5
6
0
50
100
150
200

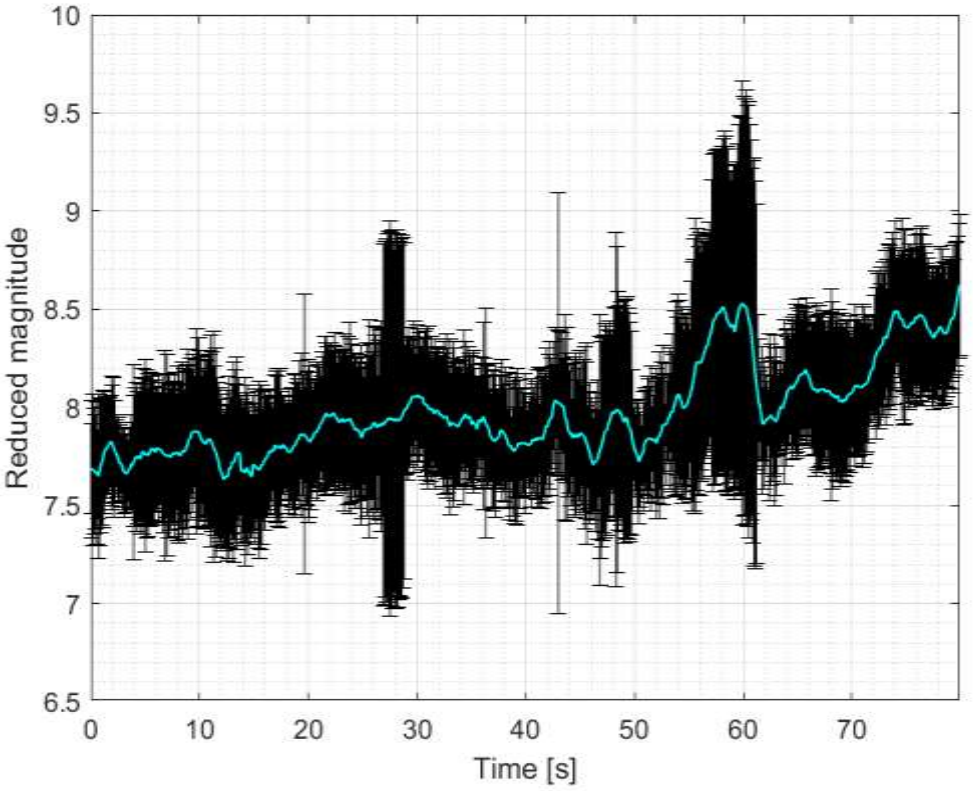
Reduced magnitude
Time [s]
10
9.5
9
8.5
8
7.5
7
6.5
0
10
20
30
40
50
60
70

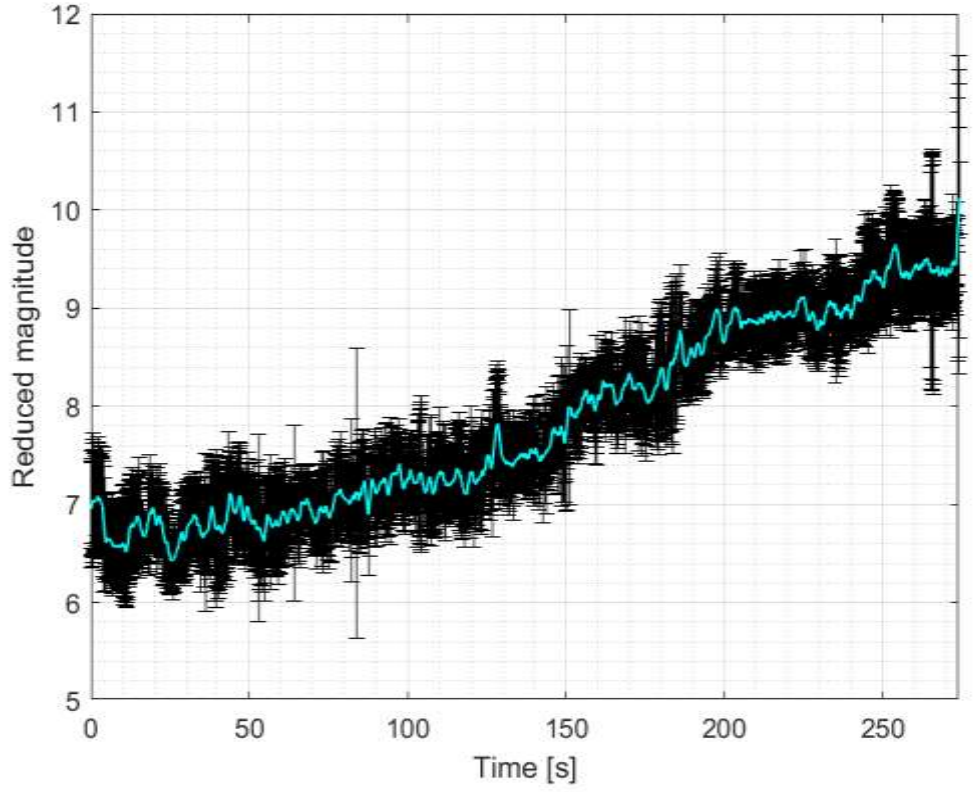
Reduced magnitude
Time [s]
12
11
10
9
8
7
6
5
0
50
100
150
200
250

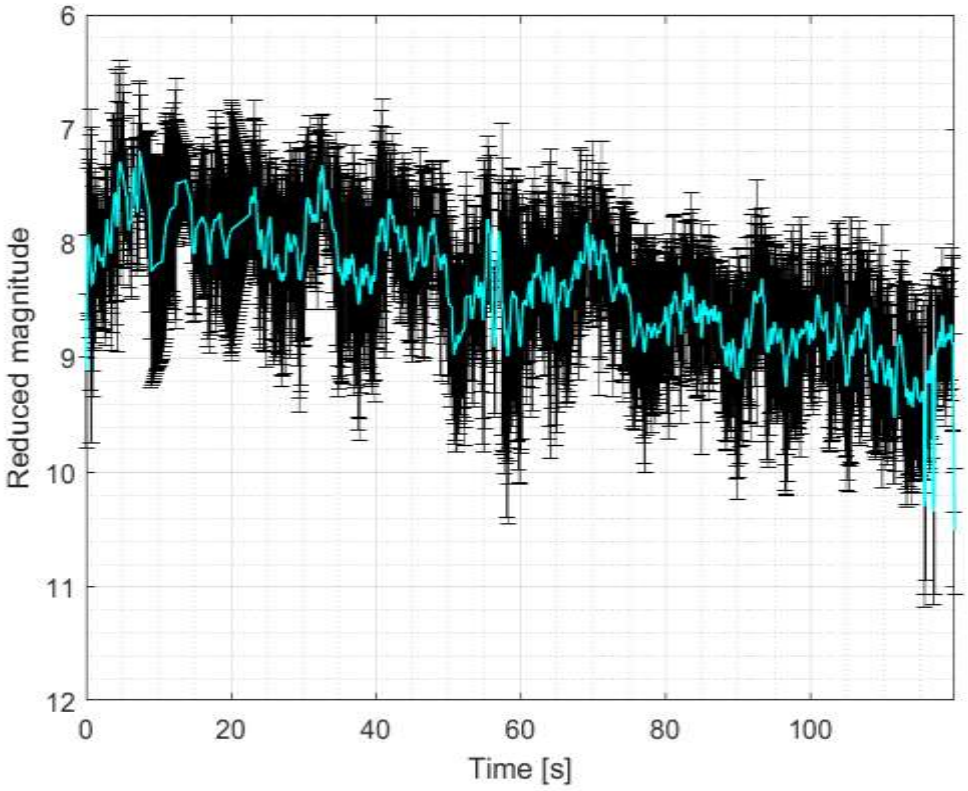
Reduced magnitude
Time [s]
6
7
8
9
10
11
12
0
20
40
60
80
100

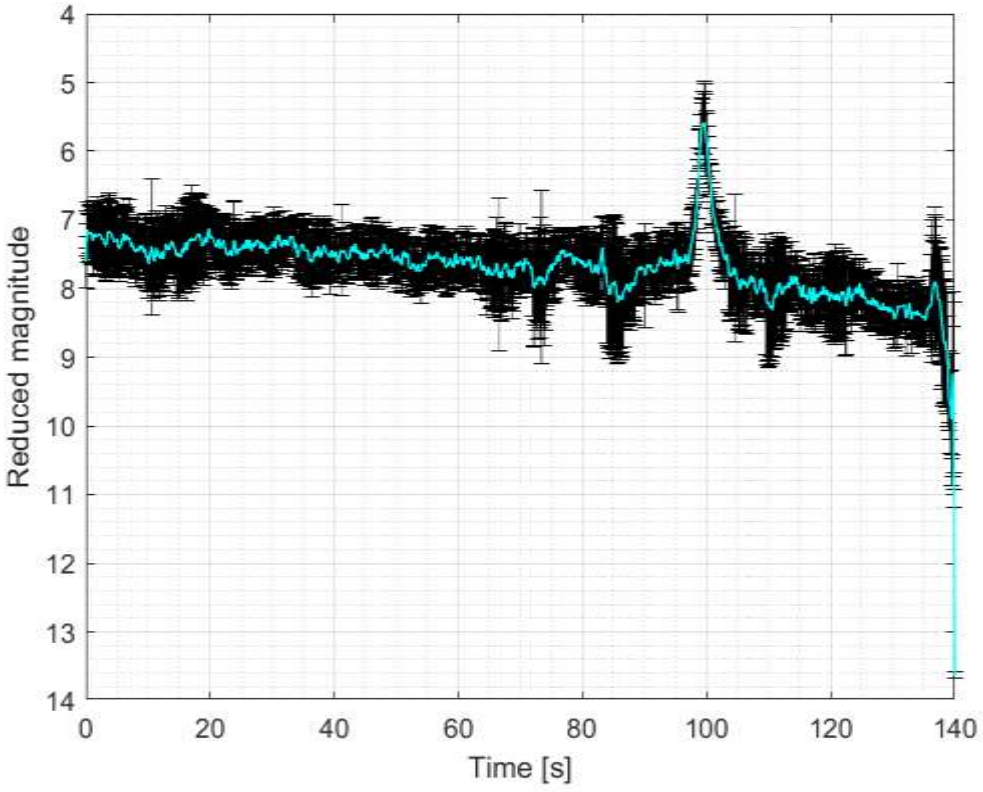
Reduced magnitude
Time [s]
4
5
6
7
8
9
10
11
12
13
14
0
20
40
60
80
100
120
140

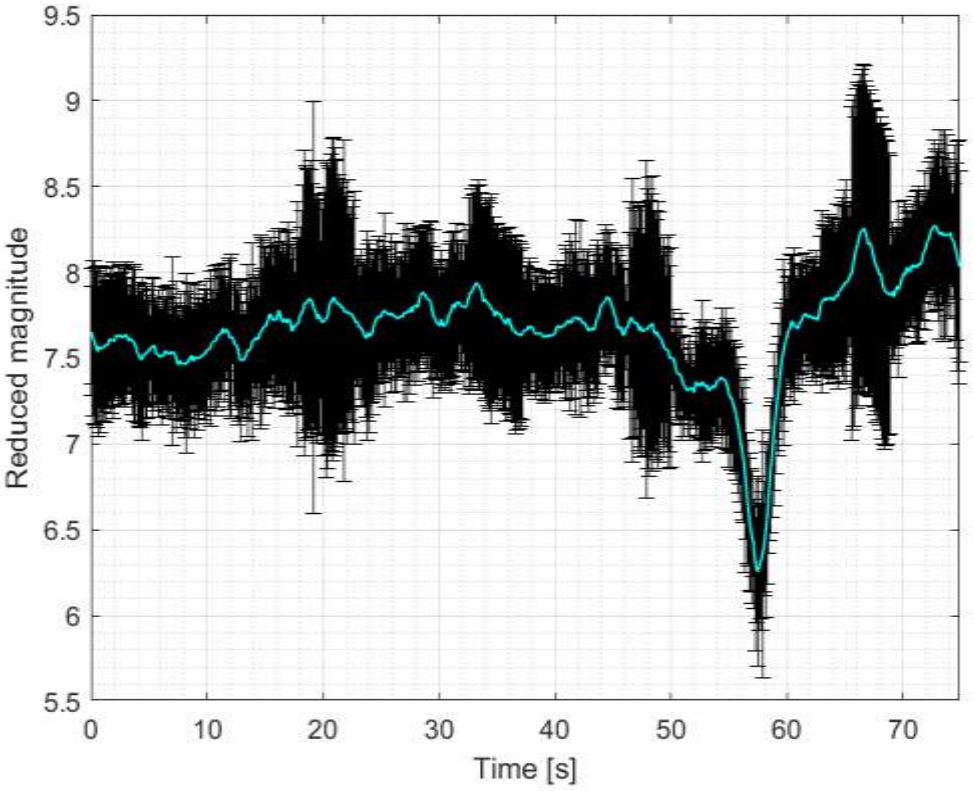
Reduced magnitude
Time [s]
9.5
9
8.5
8
7.5
7
6.5
6
5.5
0
10
20
30
40
50
60
70

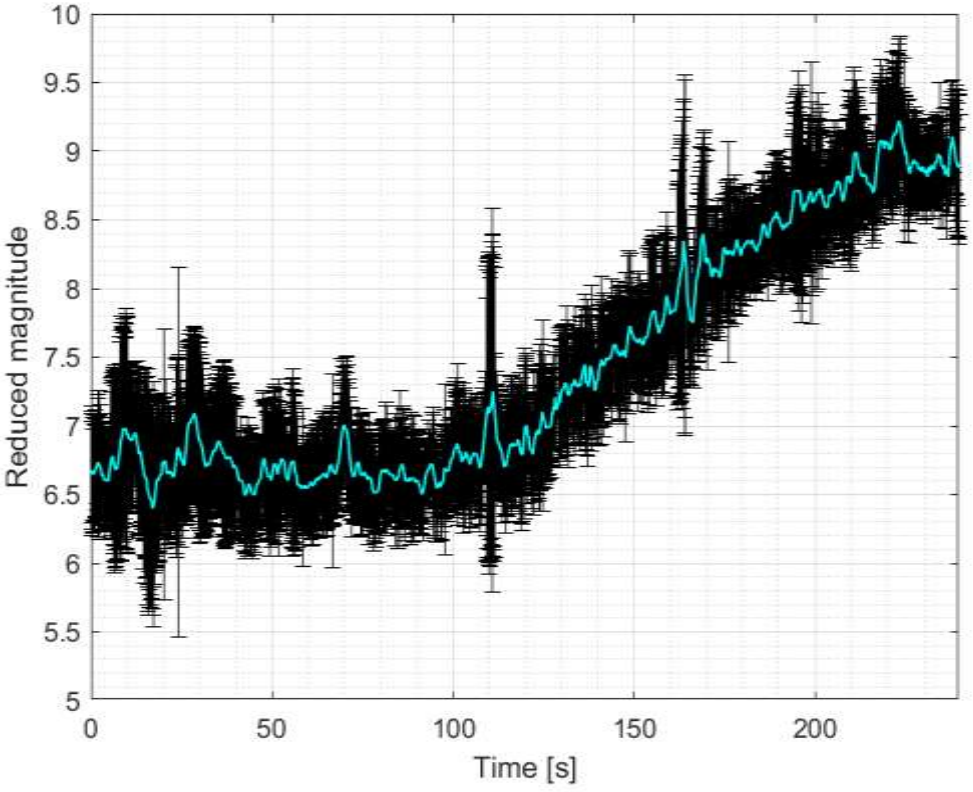
Reduced magnitude
Time [s]
10
9.5
9
8.5
8
7.5
7
6.5
6
5.5
5
0
50
100
150
200

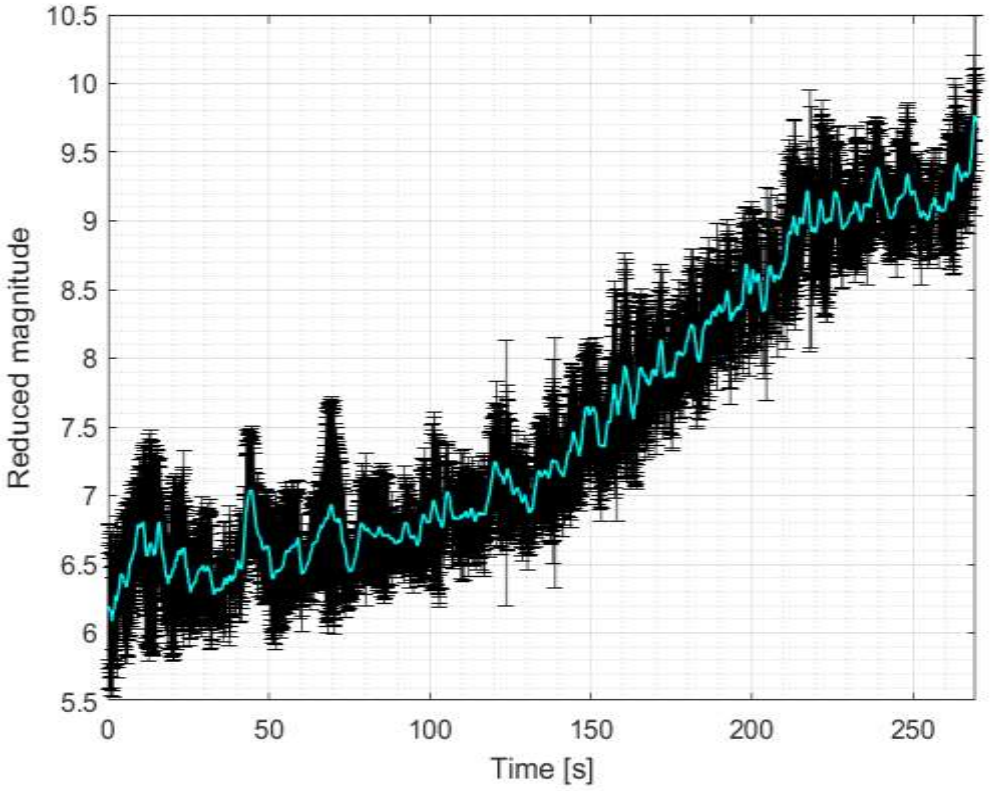
Reduced magnitude
Time [s]
10.5
10
9.5
9
8.5
8
7.5
7
6.5
6
5.5
0
50
100
150
200
250

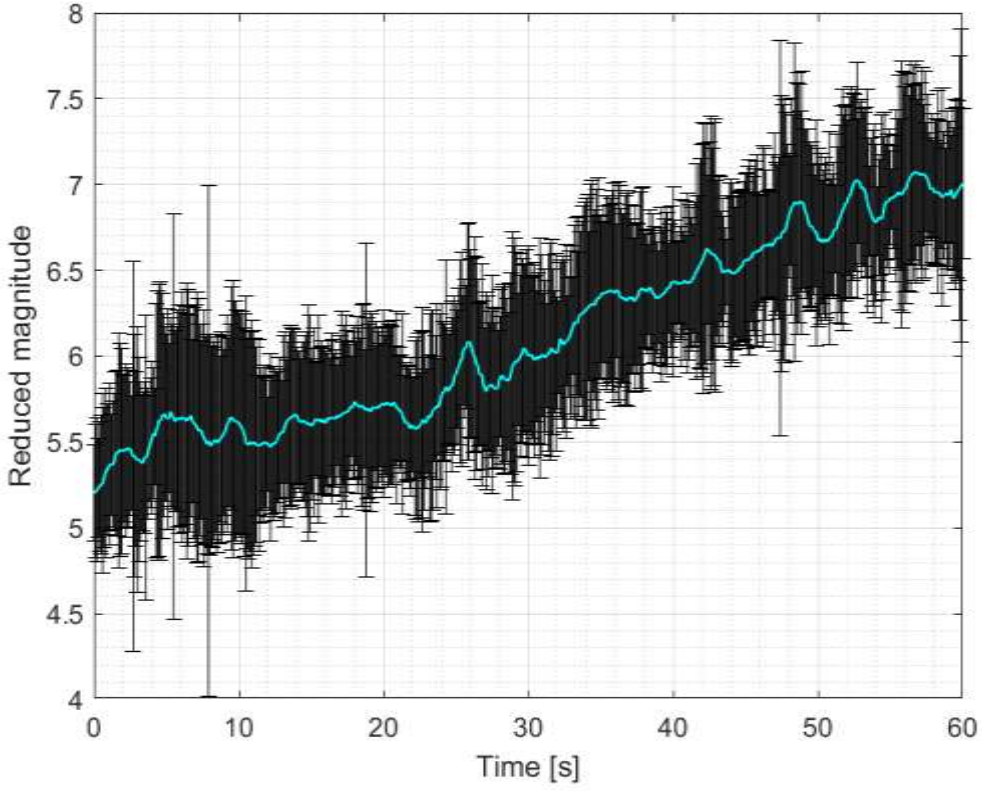
Reduced magnitude
Time [s]
8
7.5
7
6.5
6
5.5
5
4.5
4
0
10
20
30
40
50
60

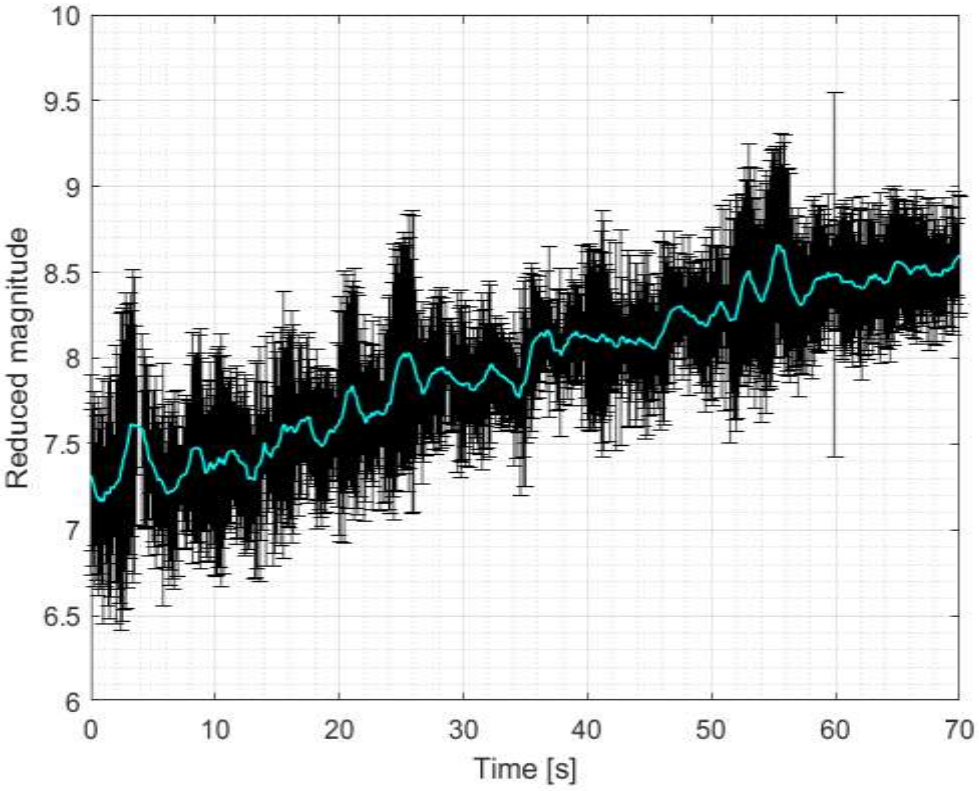
Reduced magnitude
Time [s]
10
9.5
9
8.5
8
7.5
7
6.5
6
0
10
20
30
40
50
60
70

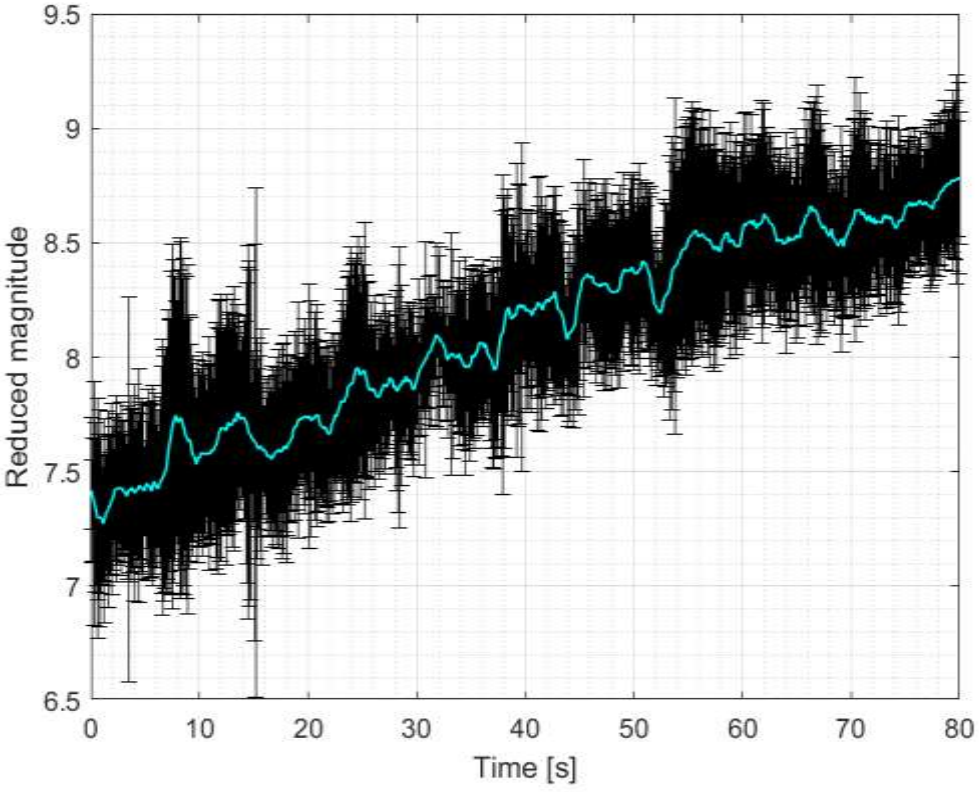
Reduced magnitude
Time [s]
9.5
9
8.5
8
7.5
7
6.5
0
10
20
30
40
50
60
70
80

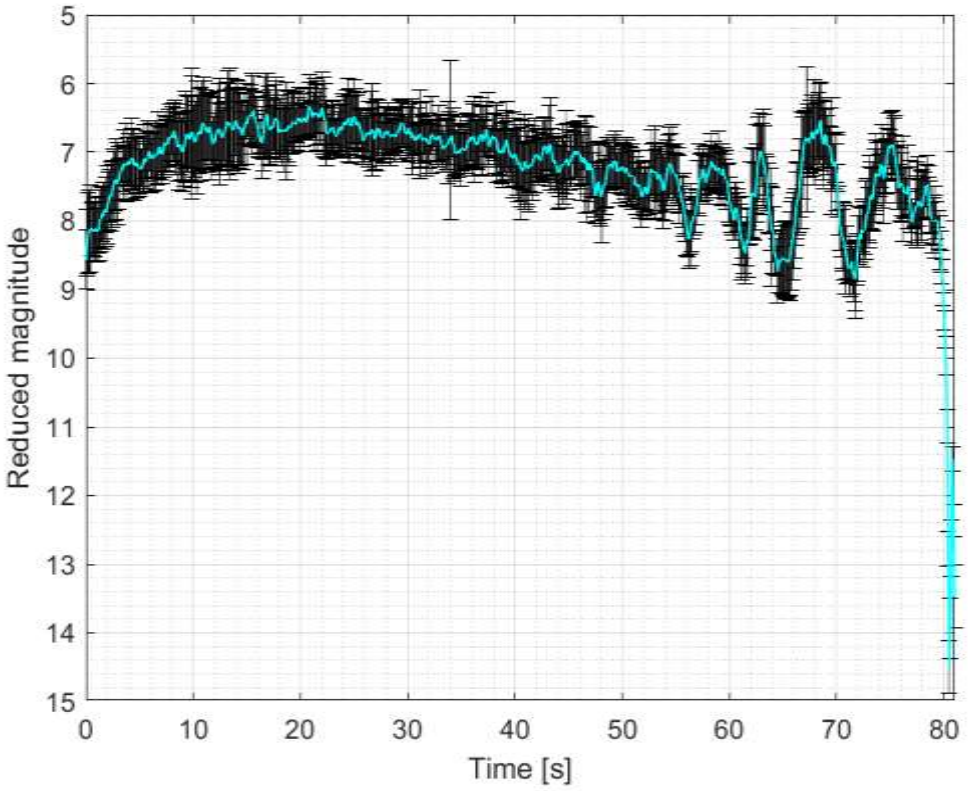
Reduced magnitude
Time [s]
5
6
7
8
9
10
11
12
13
14
15
0
10
20
30
40
50
60
70
80

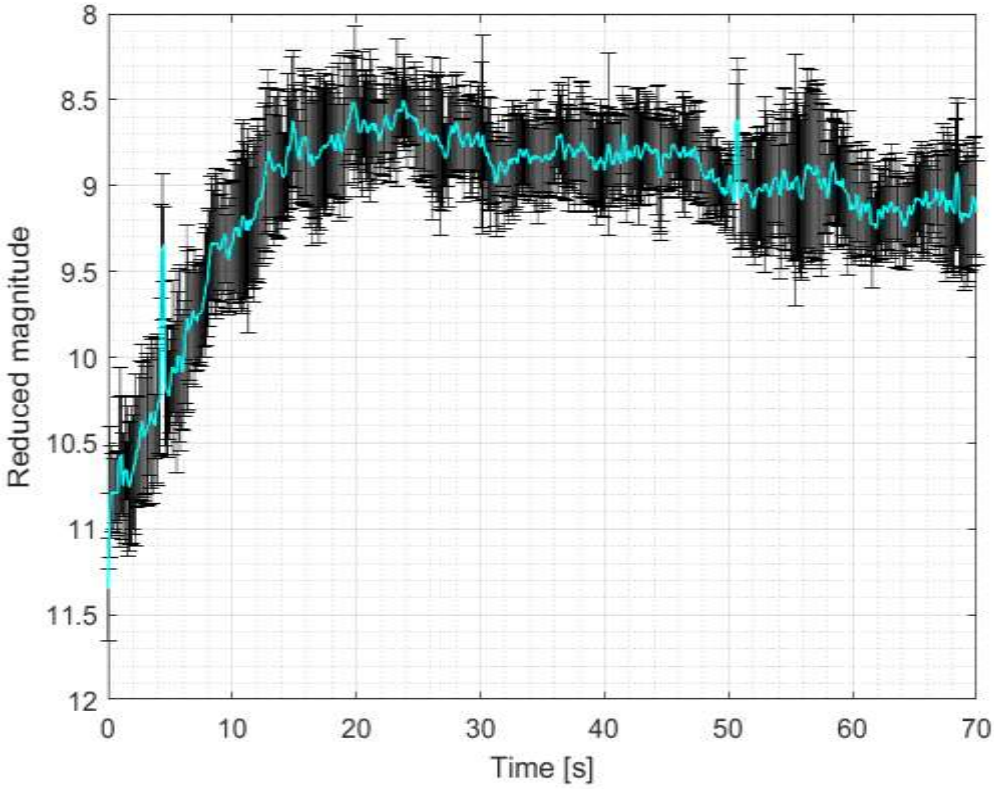
Reduced magnitude
Time [s]
8
8.5
9
9.5
10
10.5
11
11.5
12
0
10
20
30
40
50
60
70

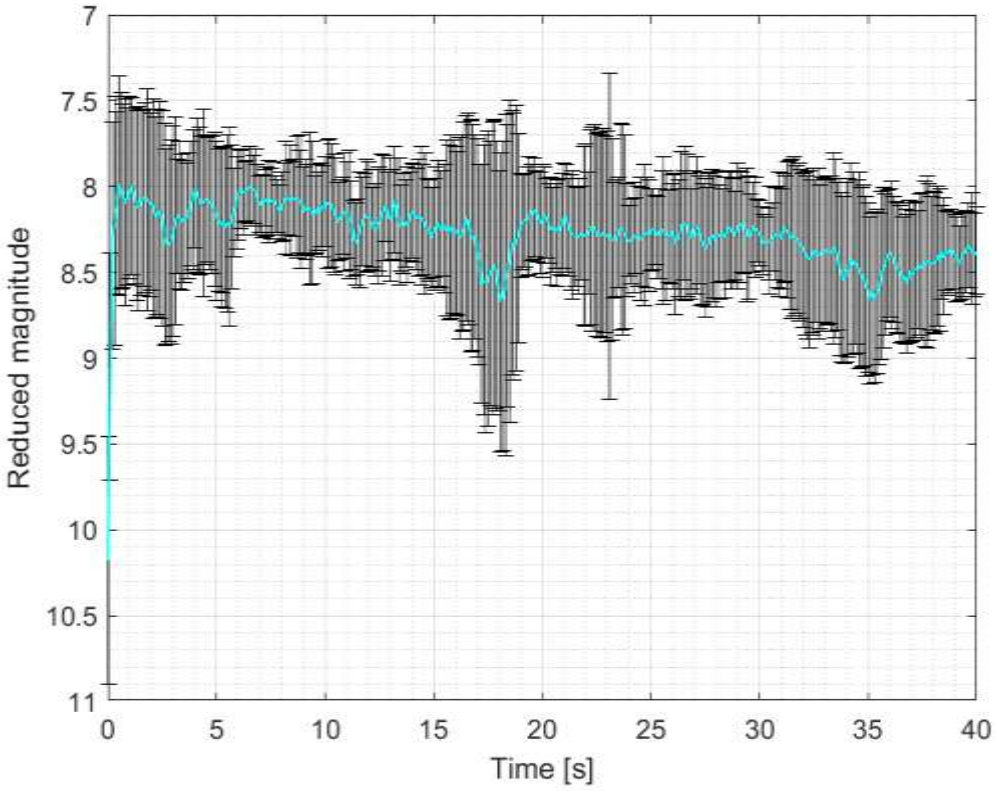

3.2 Lightcurve graphs from CNES

3.2.1 Norad 23405

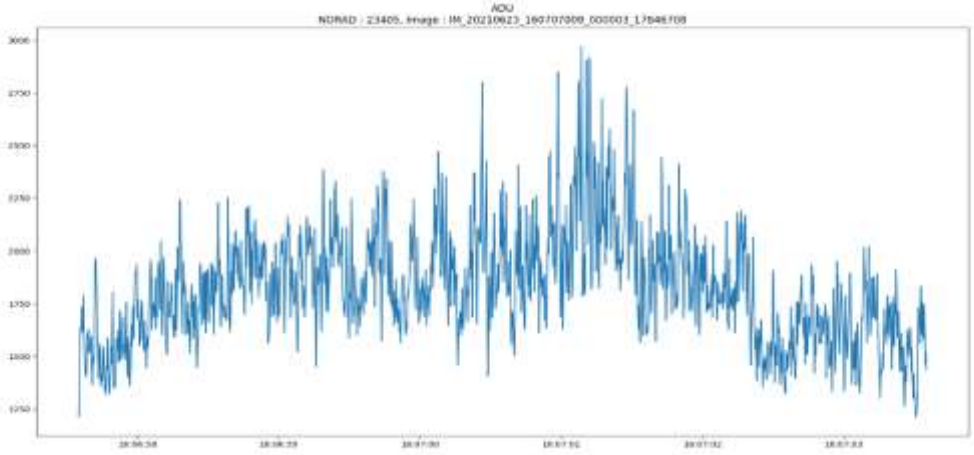

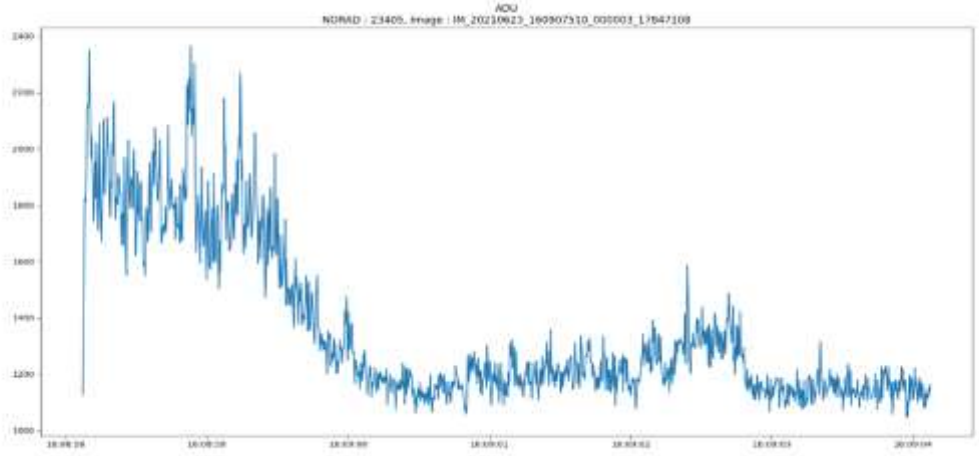
AOU
NORAD : 23405, Image : IM_20210923_160907510_000003_17847108

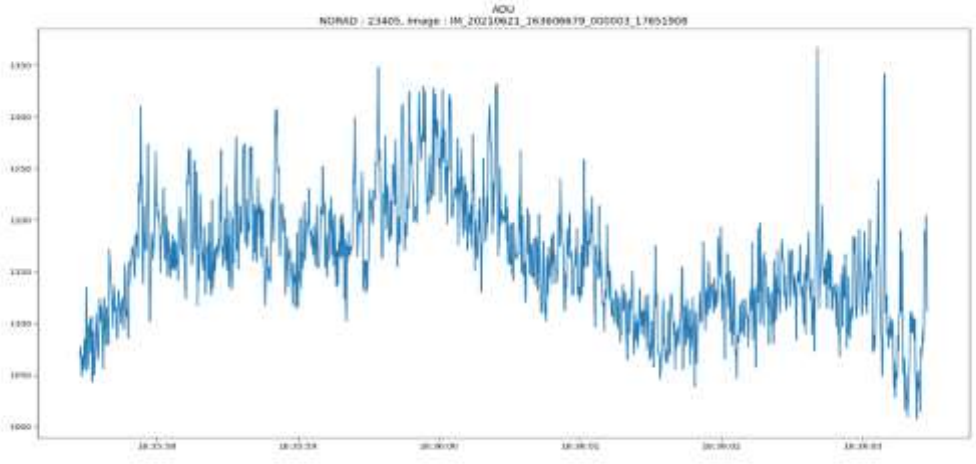
AOU
NORAD : 23405, Image : IM_20210923_163609879_000003_17851908

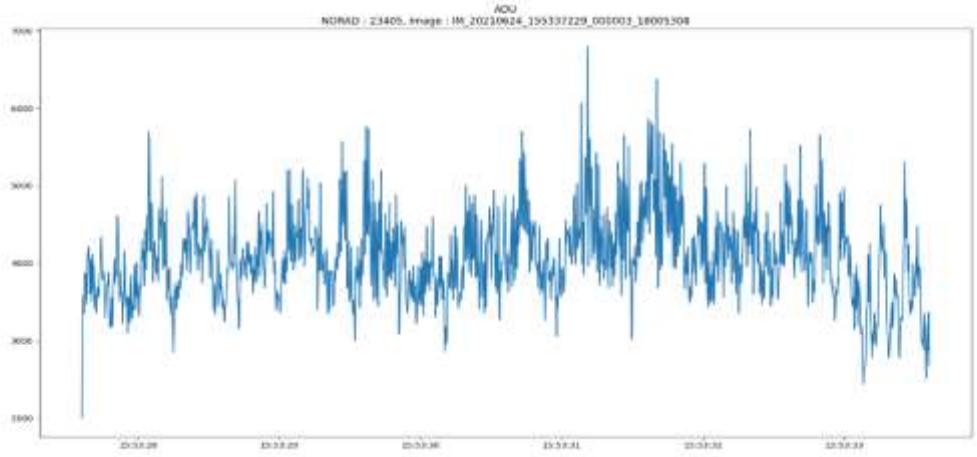
ADU
NORAD : 23405, Image : IM_20210624_155337229_000003_18005304

ADU
NORAD : 23405, Image : IM_20210624_155337211_000003_18005708

ADU
NORAD : 23405, Image : IM_20210626_152306202_000003_18314908

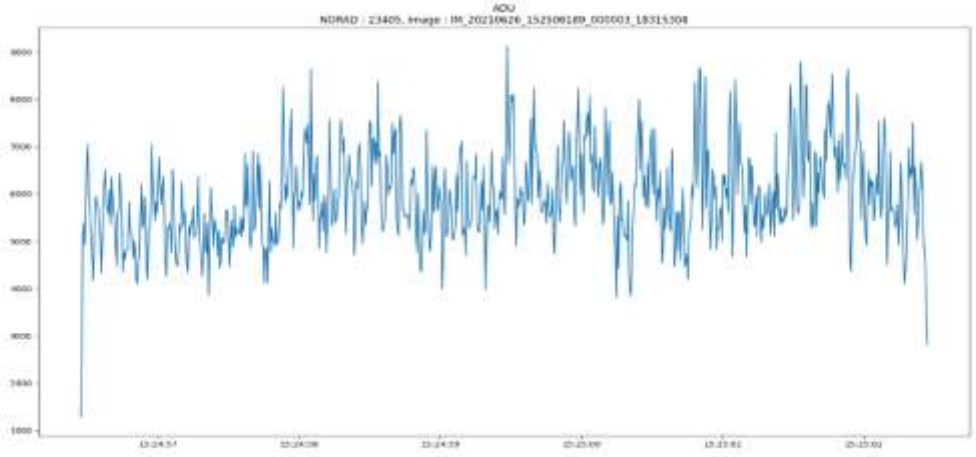
ADU
NORAD : 23405, Image : IM_20210626_152306189_000003_18315308

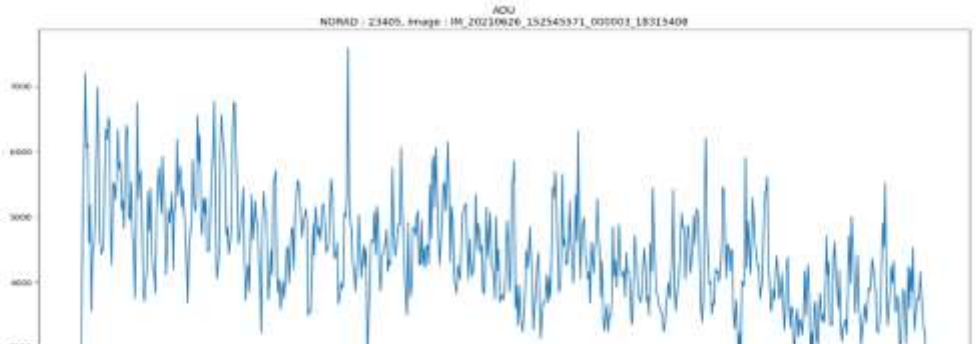
ADU
NORAD : 23405, Image : IM_20210626_152545571_000003_18315408

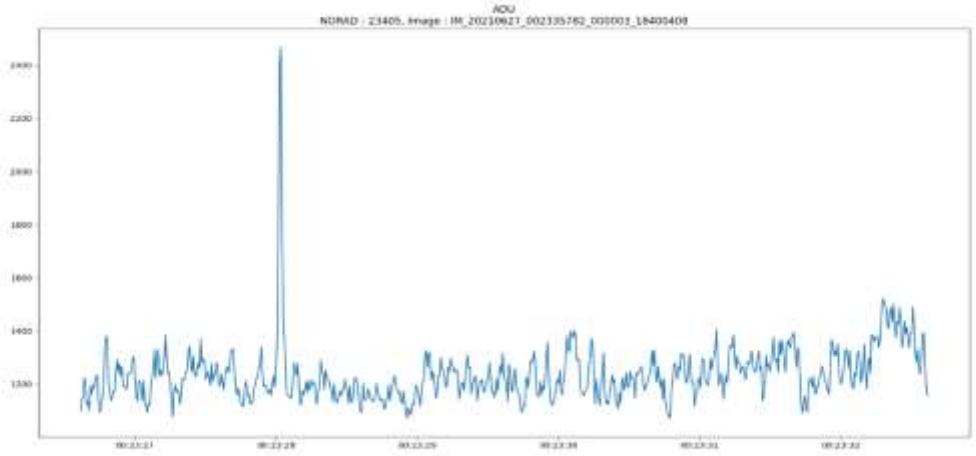
AOU
NORAD : 23405, Image : IM_20210627_002335762_000003_18400408

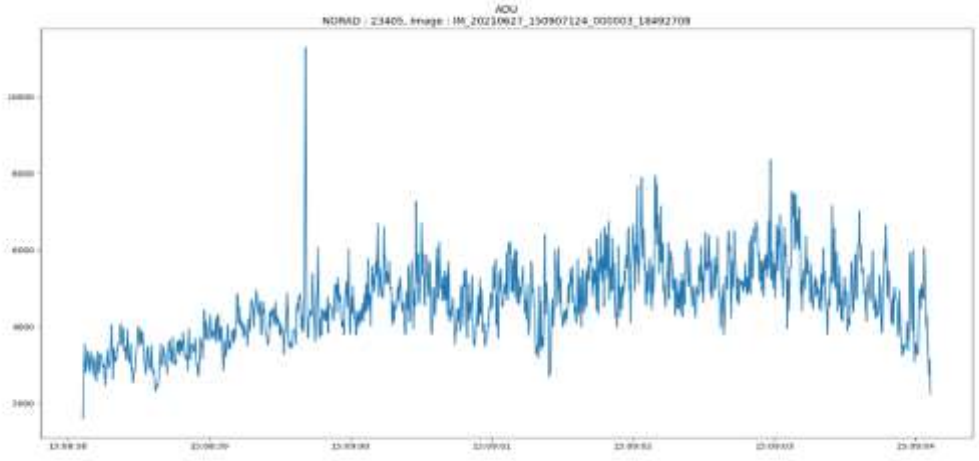
AOU
NORAD : 23405, Image : IM_20210627_150907124_000003_18492709

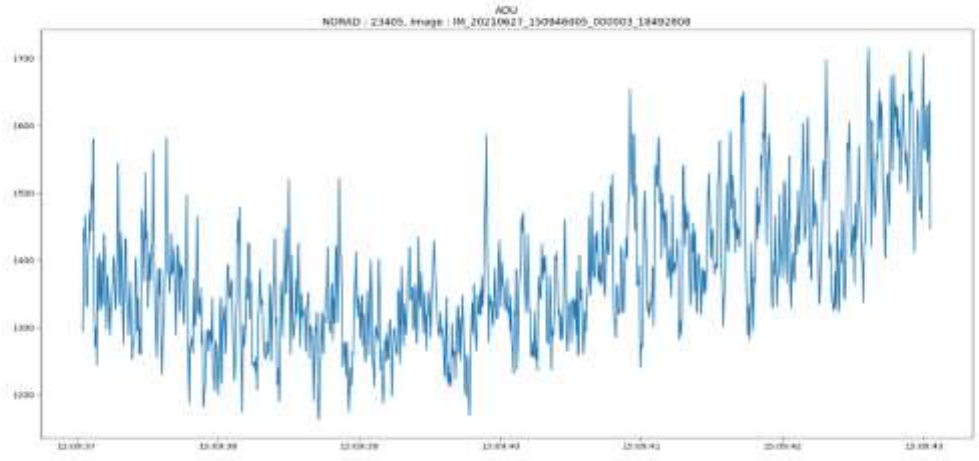
AOU
NORAD : 23405, Image : IM_20210627_150946005_000003_18492808

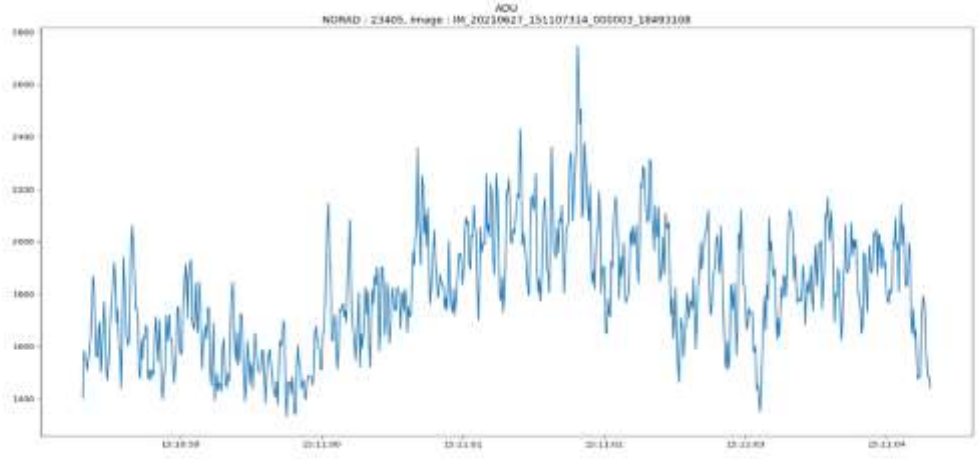
AOU
NORAD : 23405, Image : IM_20210627_151107314_000003_18493108

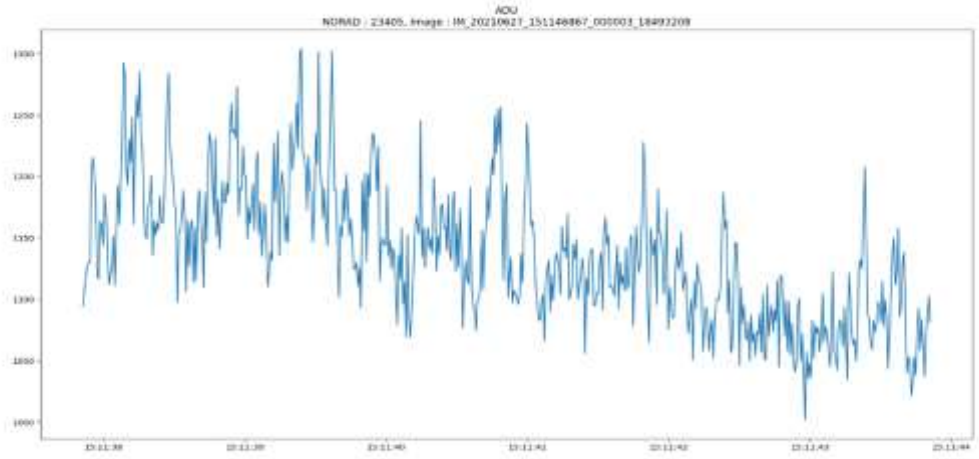
AOU
NORAD : 23405, Image : IM_20210627_151146867_000003_18493209

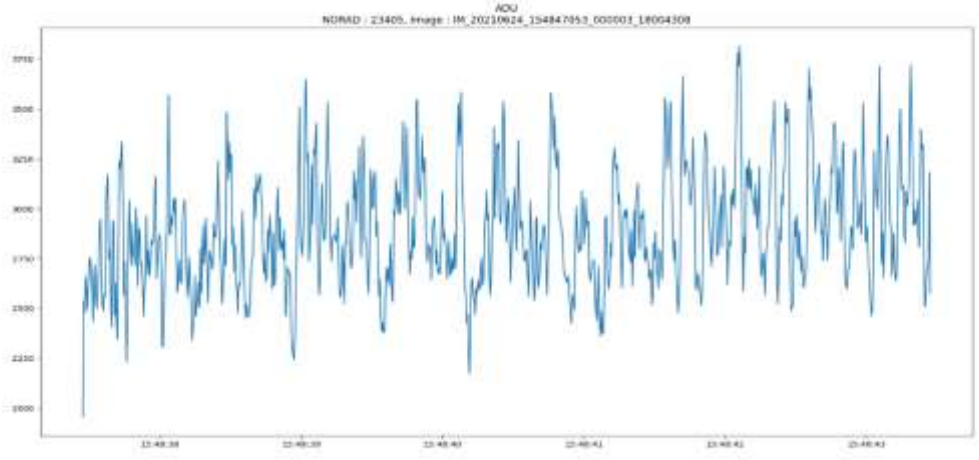
AOU
NORAD : 23405, Image : IM_20210624_154847053_000003_18004308

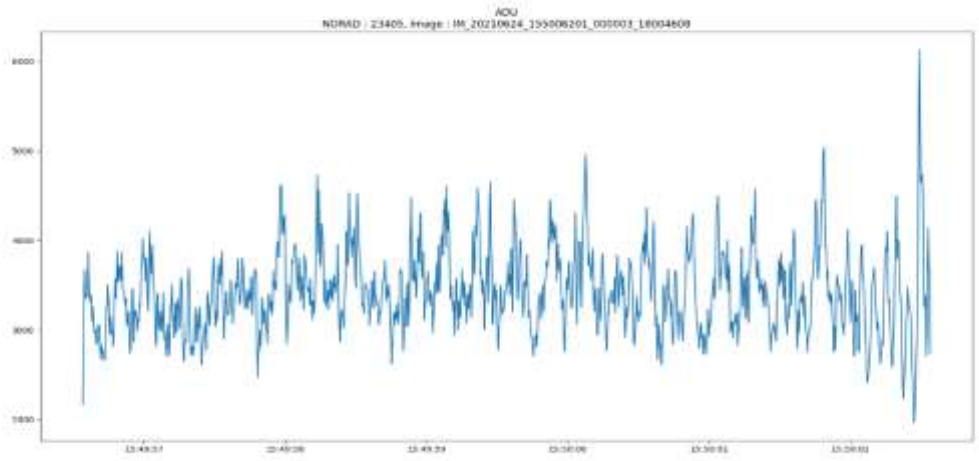
AOU
NORAD : 23405, Image : IM_20210624_155006201_000003_18004608

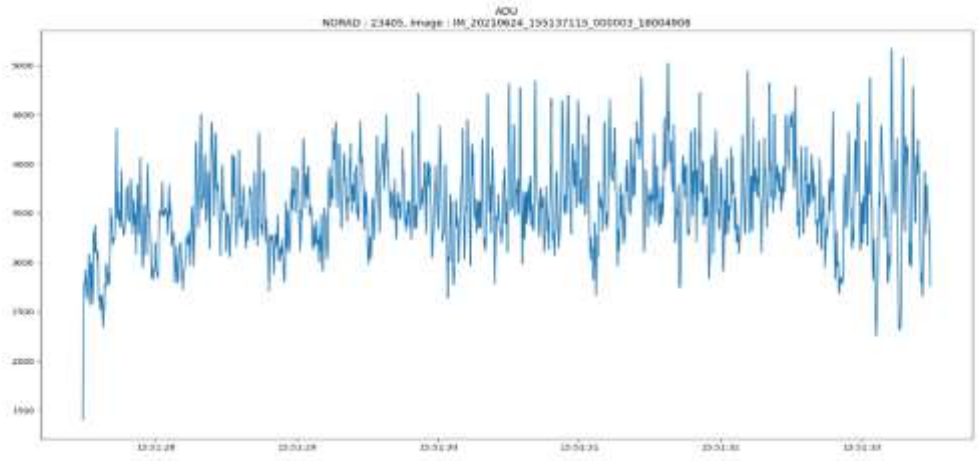
AOU
NORAD : 23405, Image : IM_20210624_155137115_000003_18004808

3.2.2 Norad 39198

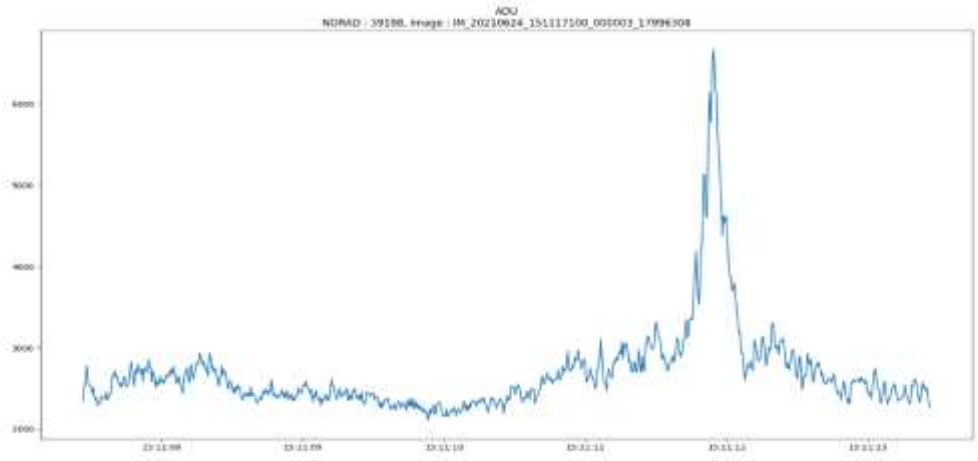

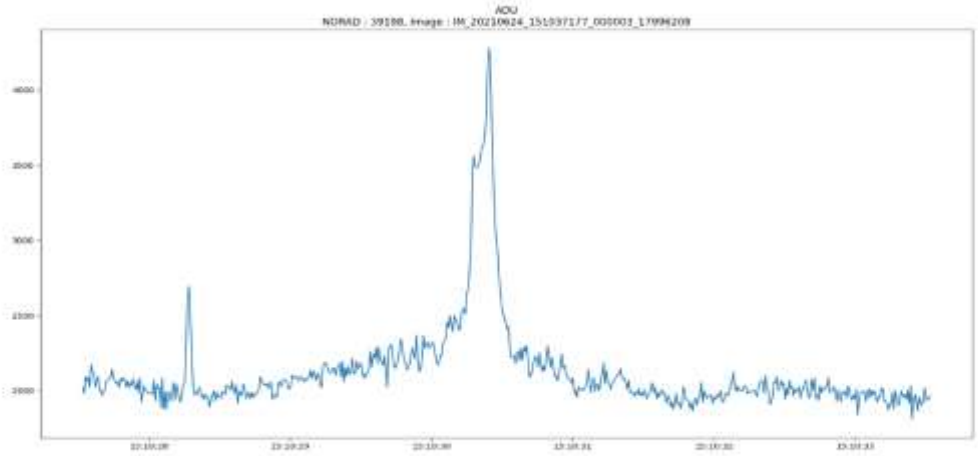

3.3 Lightcurve graphs from ESA

3.3.1 Norad 11840

3.3.2 Norad 18340 (78047G)

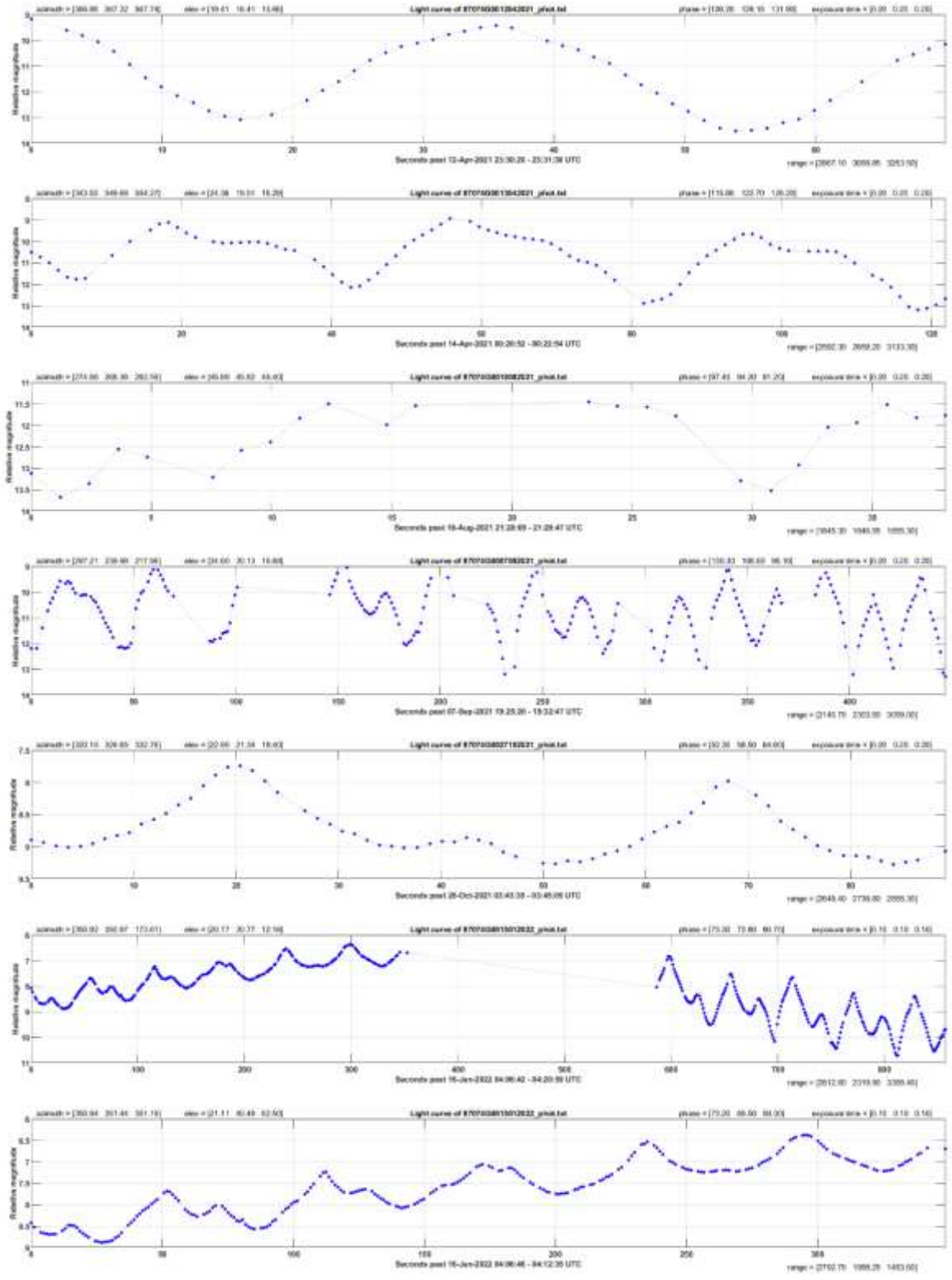

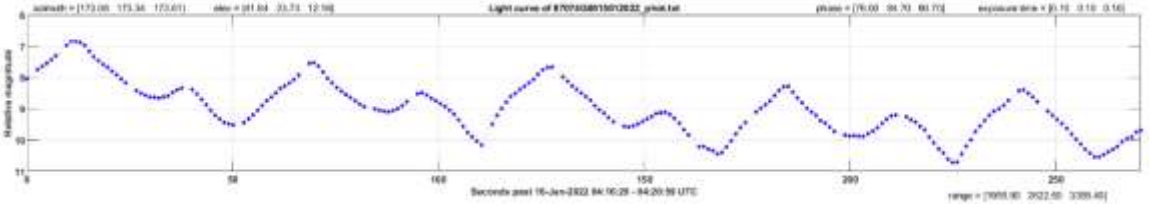
Relative magnitude
Seconds past 16-Jan-2022 04:00:29 - 04:20:59 UTC

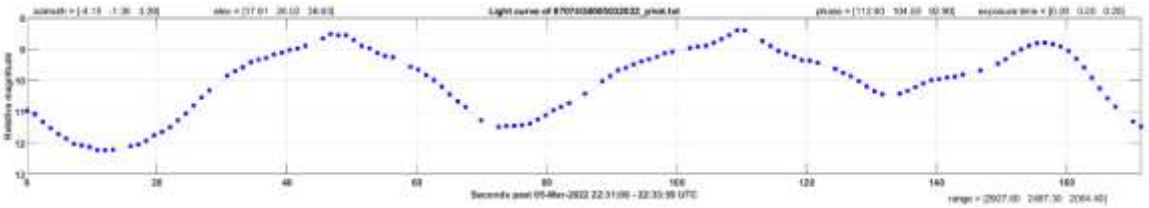
Relative magnitude
Seconds past 05-Mar-2022 22:31:09 - 22:33:59 UTC

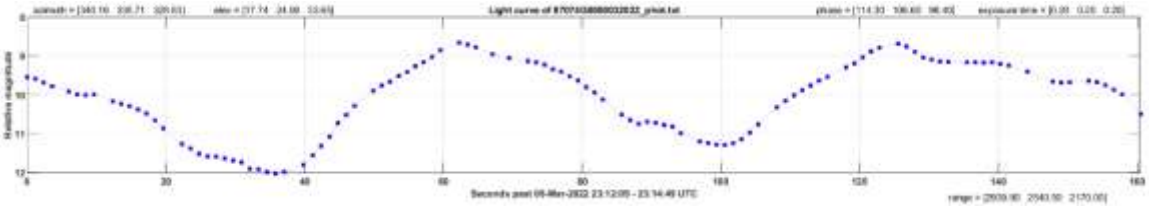
Relative magnitude
Seconds past 05-Mar-2022 23:12:09 - 23:14:49 UTC

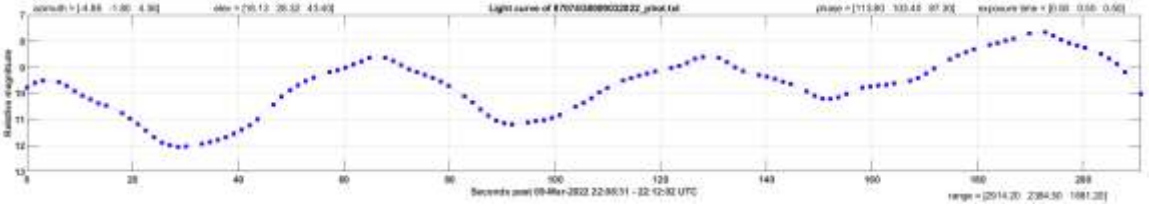
Relative magnitude
Seconds past 09-Mar-2022 22:00:31 - 22:12:32 UTC

Relative magnitude
Seconds past 10-Mar-2022 23:00:47 - 23:03:54 UTC

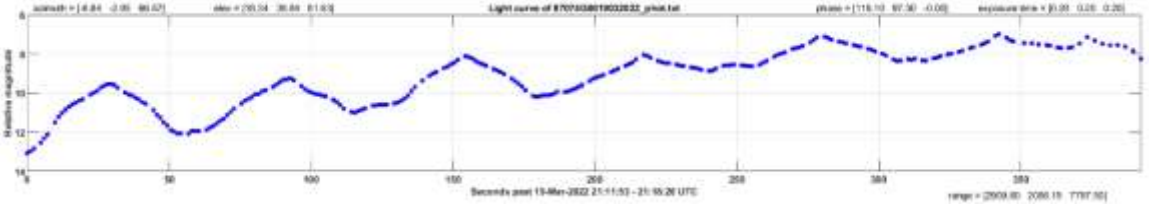
Relative magnitude
Seconds past 13-Mar-2022 21:11:53 - 21:15:26 UTC

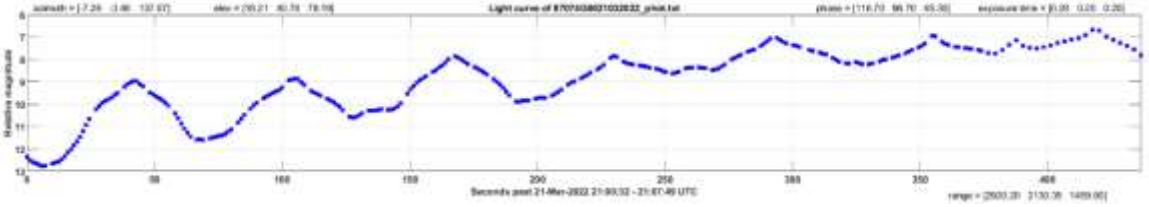
Relative magnitude
Seconds past 21-Mar-2022 21:00:32 - 21:07:49 UTC

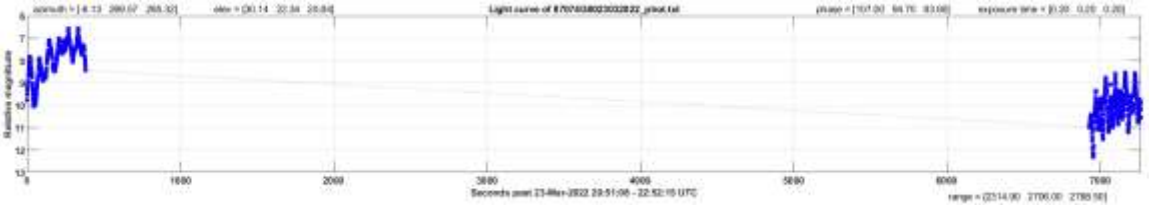
Relative magnitude
Seconds past 23-Mar-2022 20:51:08 - 22:52:15 UTC

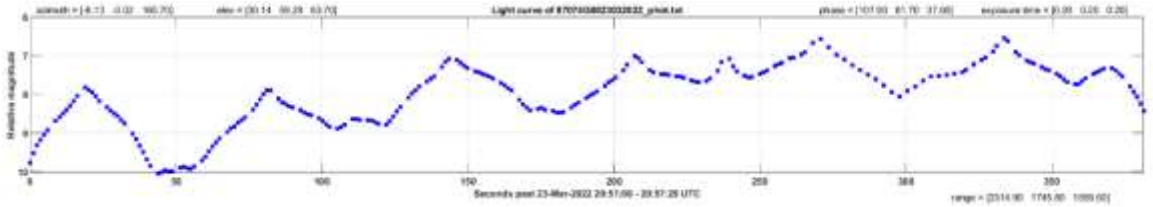

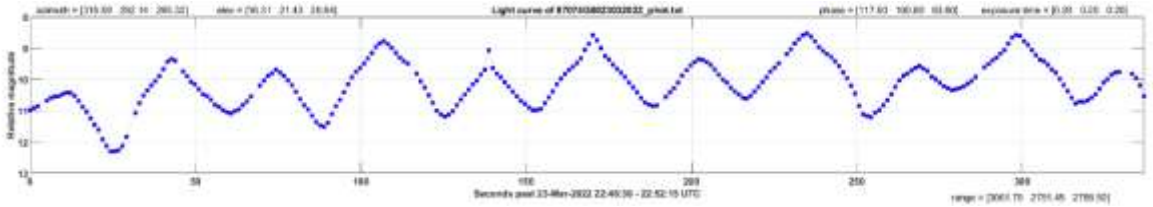

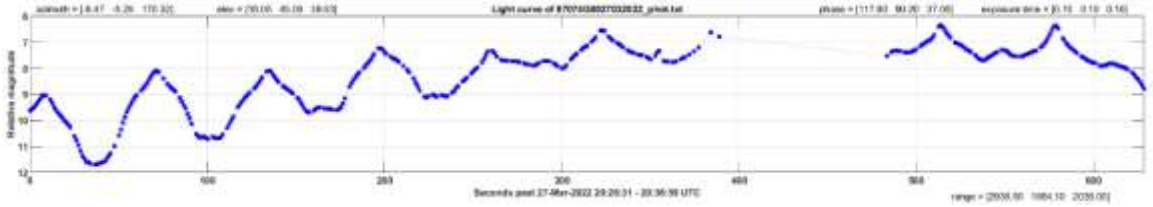

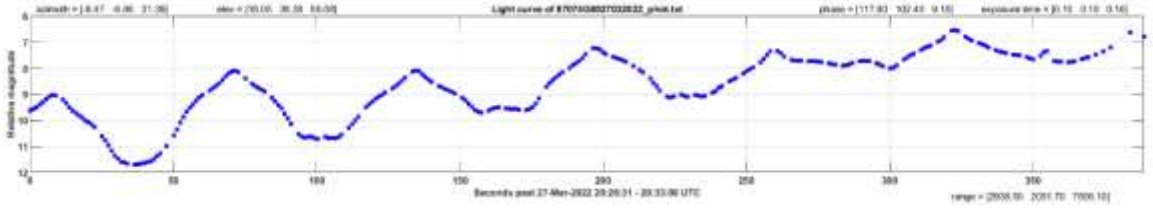

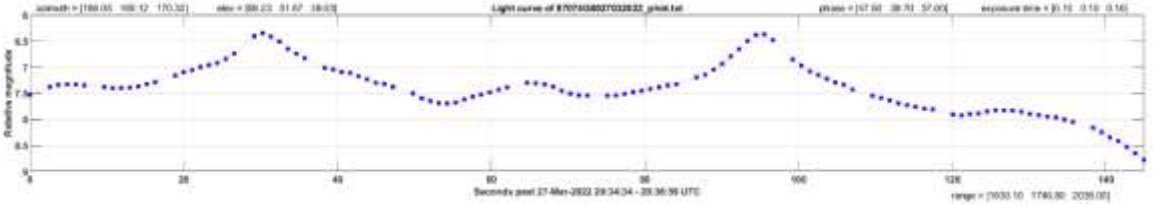

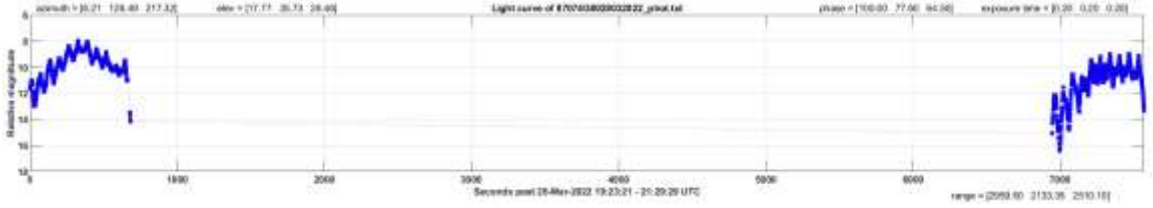

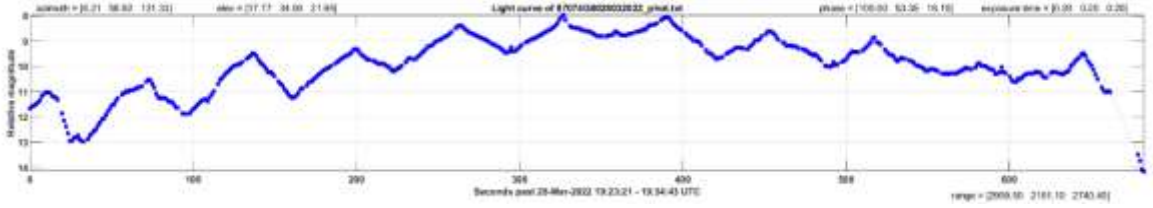

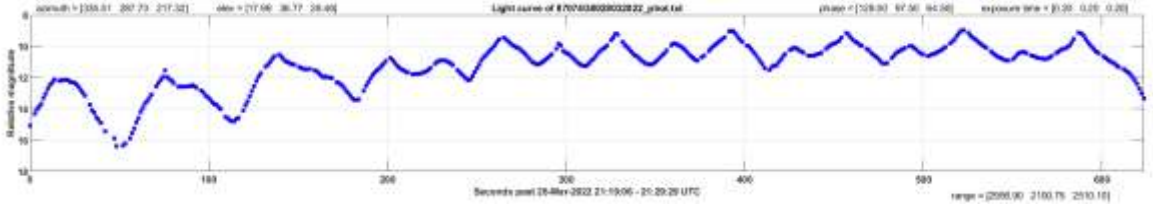

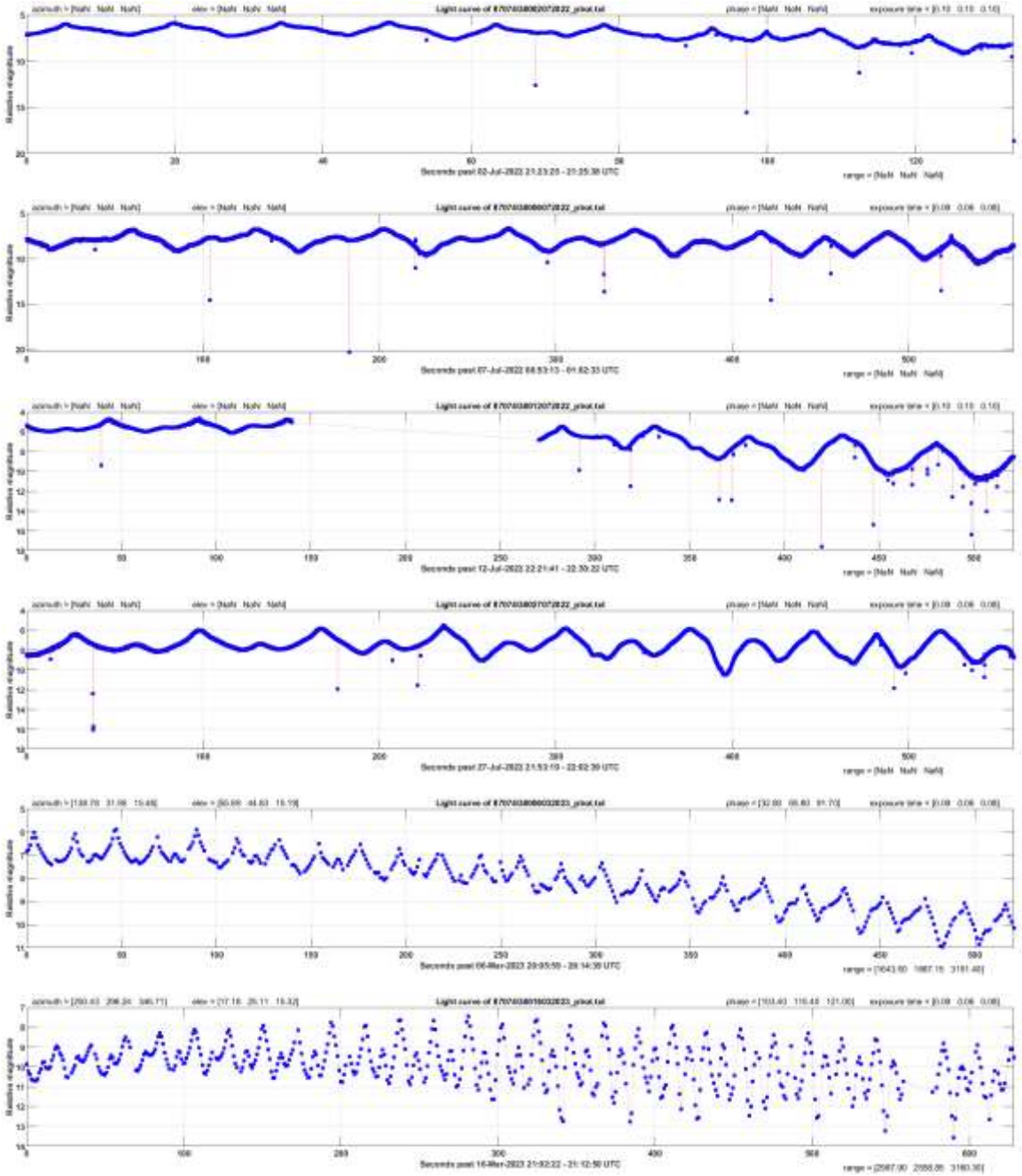

3.3.3 Norad 23088 (94023B)

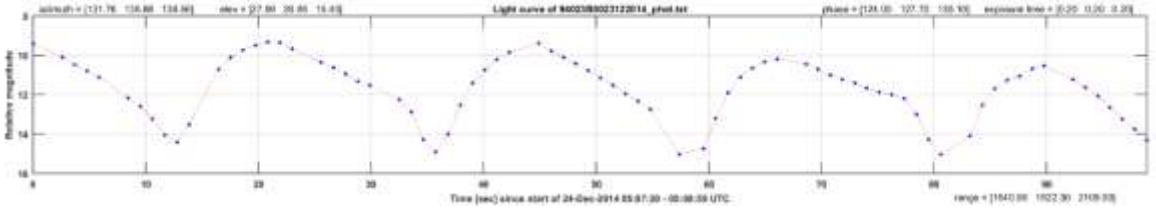

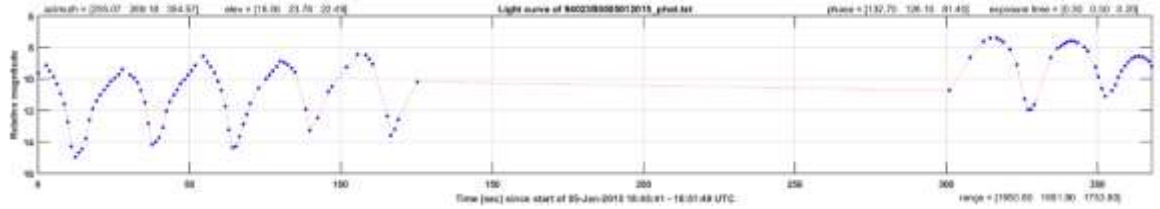
Relative magnitude
Time [sec] since start of 05-Jan-2015 16:03:01 - 16:01:49 UTC

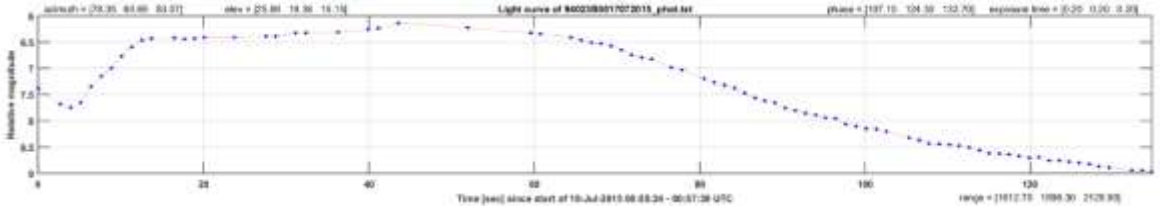
Relative magnitude
Time [sec] since start of 10-Jul-2015 06:03:24 - 06:57:38 UTC

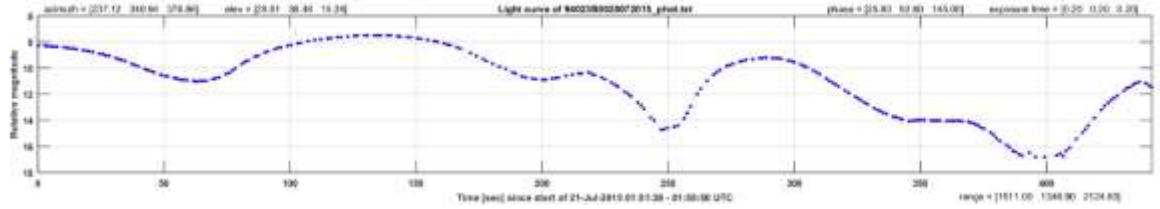
Relative magnitude
Time [sec] since start of 21-Jul-2015 01:01:39 - 01:08:06 UTC

Relative magnitude
Time [sec] since start of 20-Apr-2016 22:23:35 - 23:28:15 UTC

Relative magnitude
Time [sec] since start of 30-Aug-2016 21:28:42 - 21:28:16 UTC

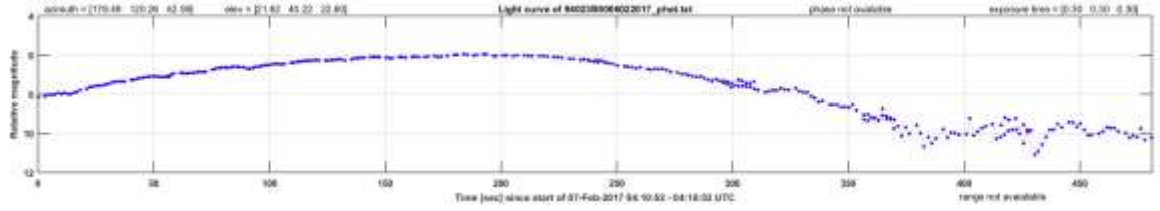
Relative magnitude
Time [sec] since start of 07-Feb-2017 04:10:52 - 04:18:02 UTC

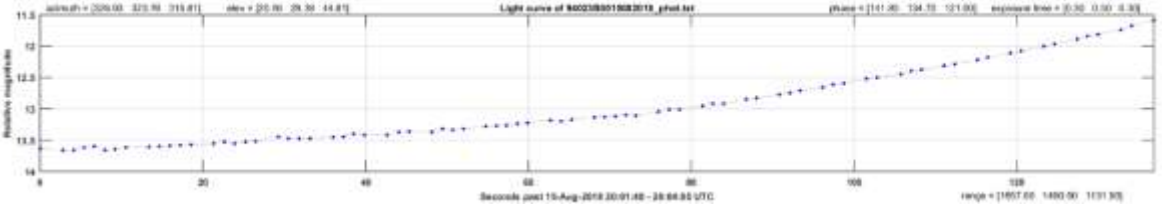
Relative magnitude
Seconds past 15-Aug-2018 20:01:48 - 20:04:55 UTC

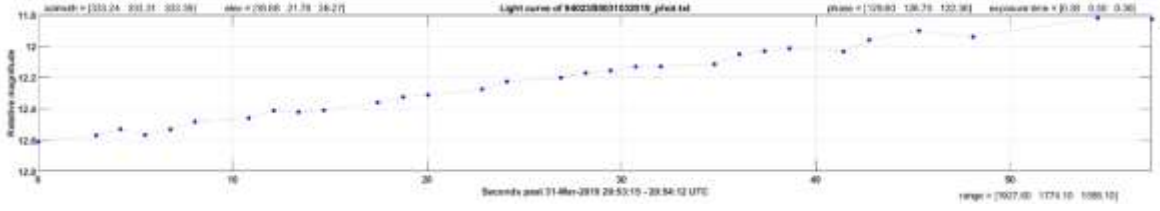
Relative magnitude
Seconds past 31-Mar-2018 29:53:15 - 29:54:12 UTC

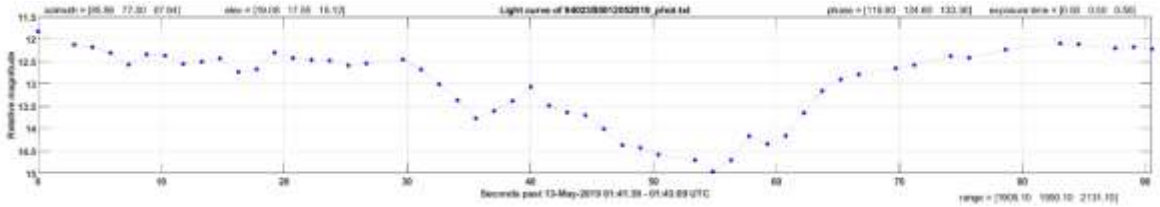
Relative magnitude
Seconds past 13-May-2019 01:41:39 - 01:43:59 UTC

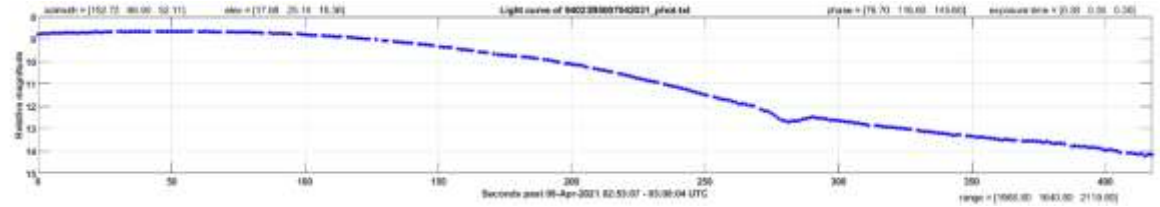
Relative magnitude
Seconds past 06-Apr-2021 02:53:07 - 02:56:04 UTC

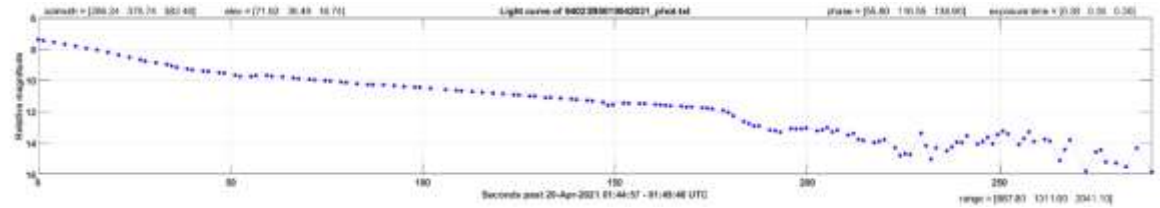
Relative magnitude
Seconds past 26-Apr-2021 01:44:57 - 01:48:46 UTC

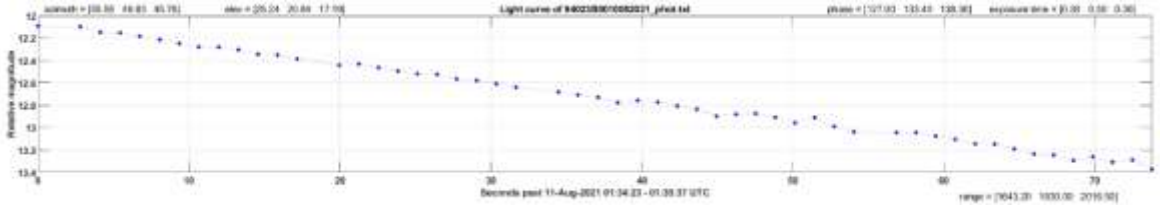
Relative magnitude
Seconds past 11-Aug-2021 01:34:23 - 01:35:37 UTC

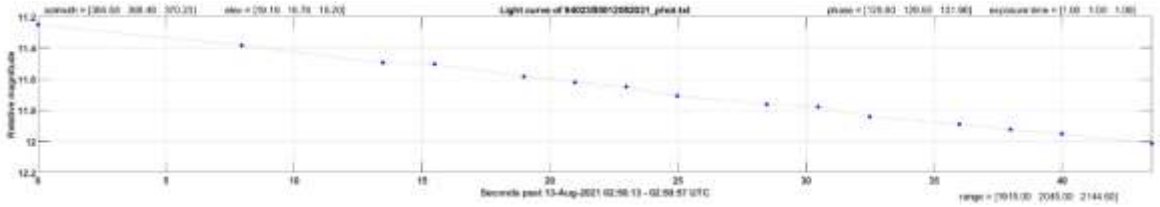
Relative magnitude
Seconds past 13-Aug-2021 02:56:13 - 02:56:57 UTC

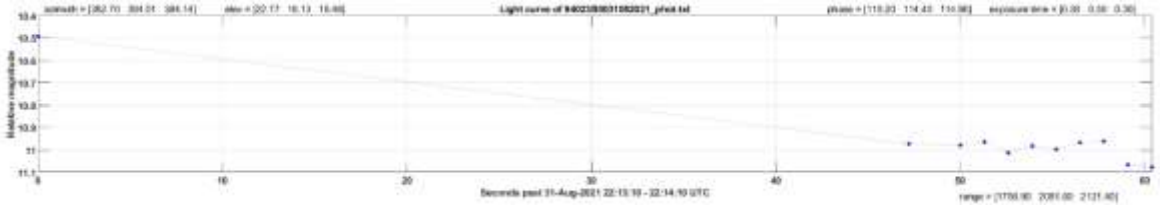
Relative magnitude
Seconds past 31-Aug-2021 22:13:10 - 22:14:10 UTC

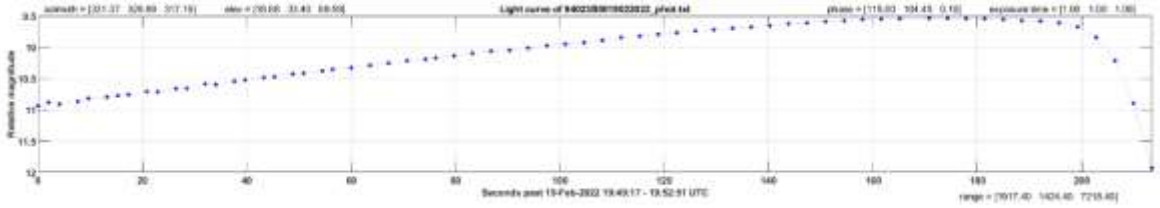
Relative magnitude
Seconds past 15-Feb-2022 19:49:17 - 19:52:51 UTC

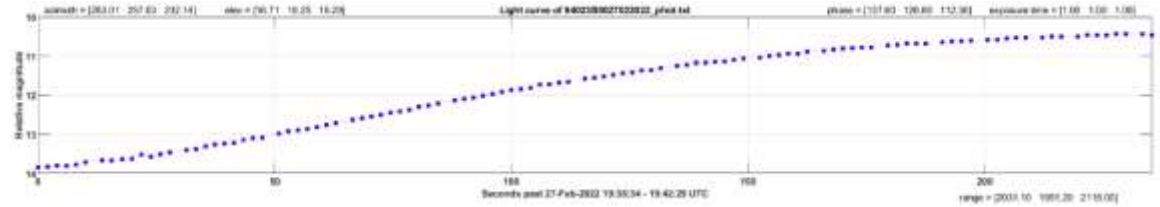
Relative magnitude
Seconds past 27-Feb-2022 19:39:34 - 19:42:29 UTC

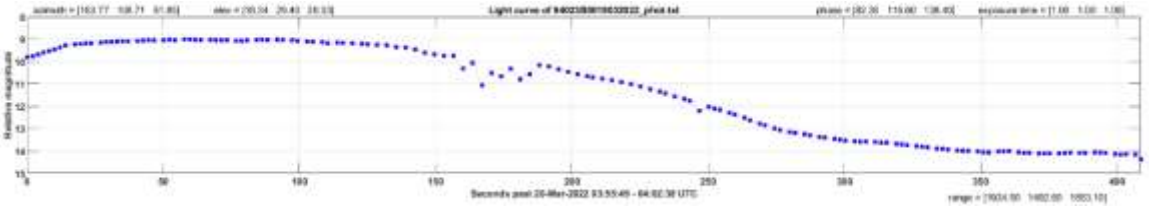
Relative magnitude
Seconds past 26-Mar-2022 03:55:49 - 04:02:38 UTC

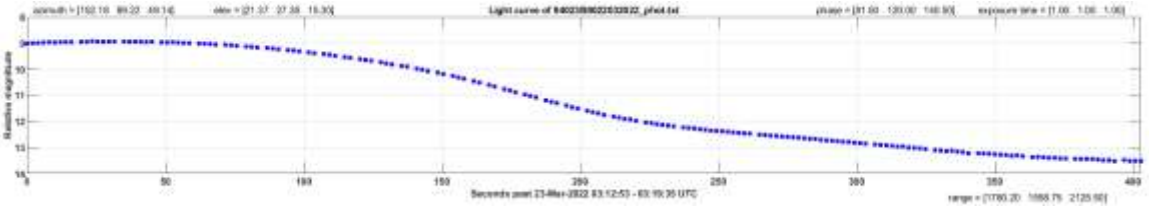
Relative magnitude
Seconds past 23-Mar-2022 03:12:53 - 03:19:35 UTC

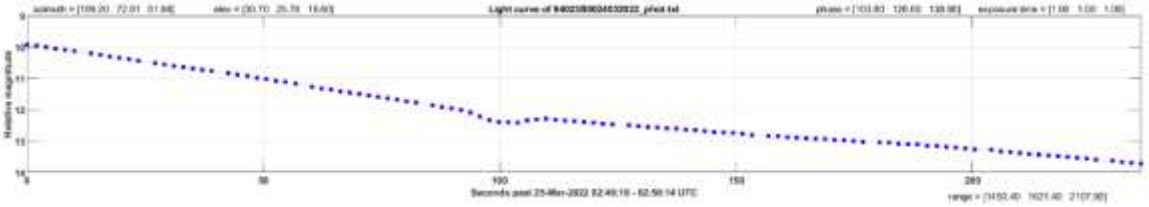
Relative magnitude
Seconds past 25-Mar-2022 02:49:16 - 02:56:14 UTC

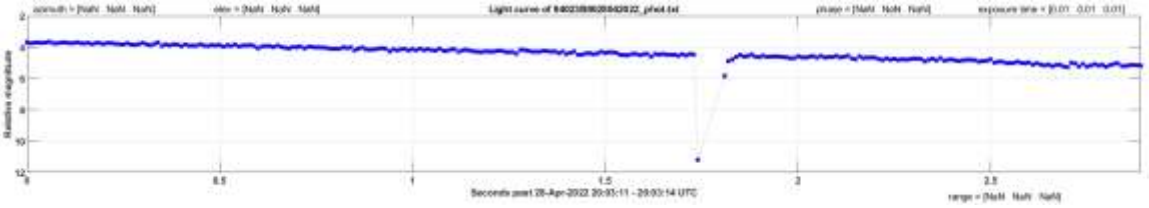
Relative magnitude
Seconds past 28-Apr-2022 20:03:11 - 20:03:14 UTC

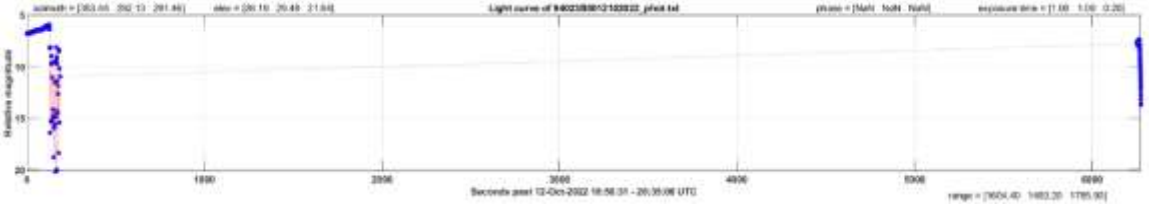
Relative magnitude
Seconds past 12-Oct-2022 18:58:31 - 20:35:06 UTC

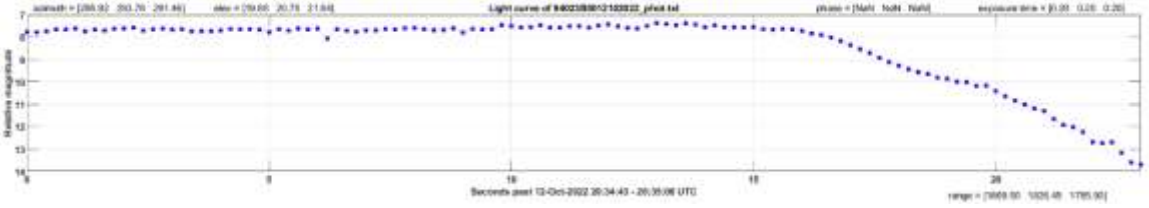
Relative magnitude
Seconds past 12-Oct-2022 20:34:43 - 20:35:06 UTC

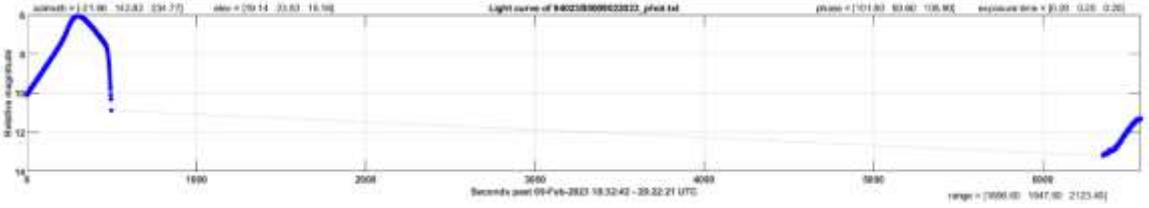
Relative magnitude
Seconds past 09-Feb-2023 18:32:42 - 20:22:21 UTC

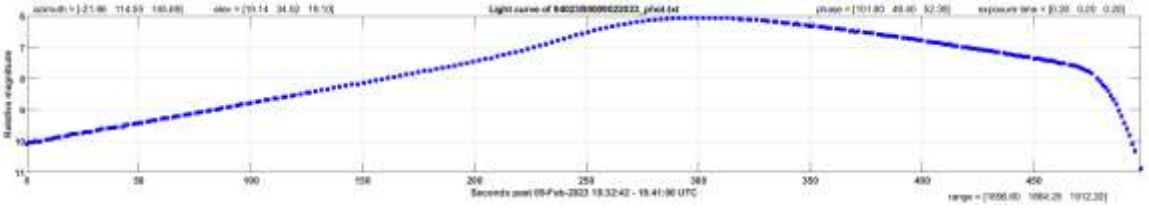
Relative magnitude
Seconds past 09-Feb-2023 18:32:42 - 18:41:00 UTC

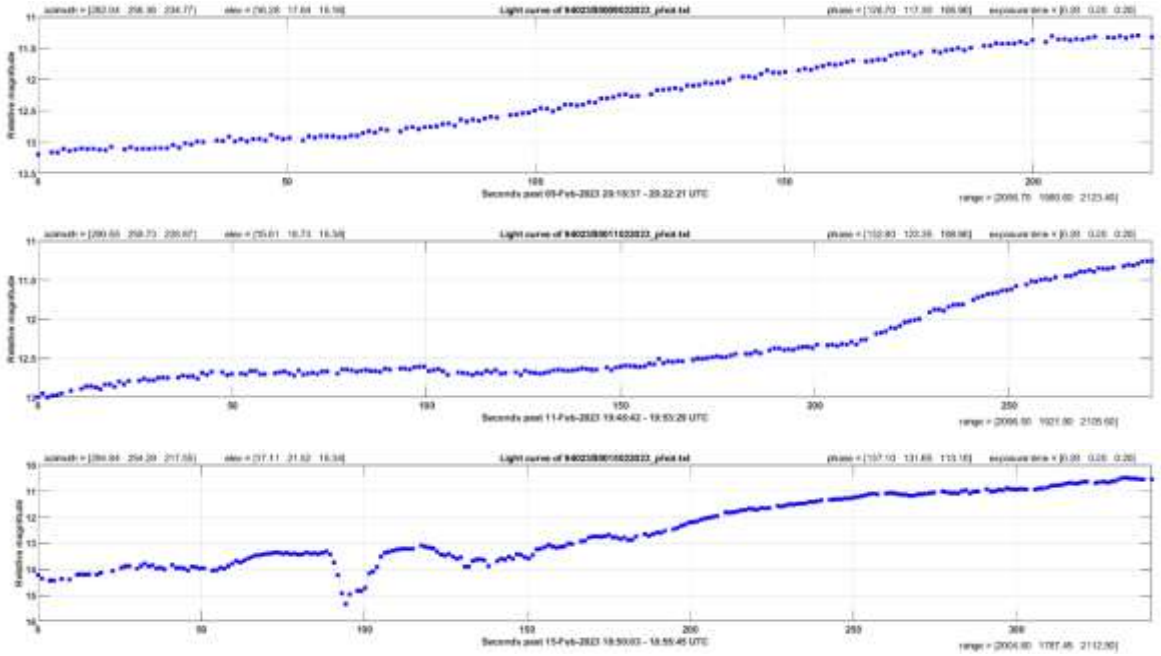

3.3.4 Norad 23405 (94077B

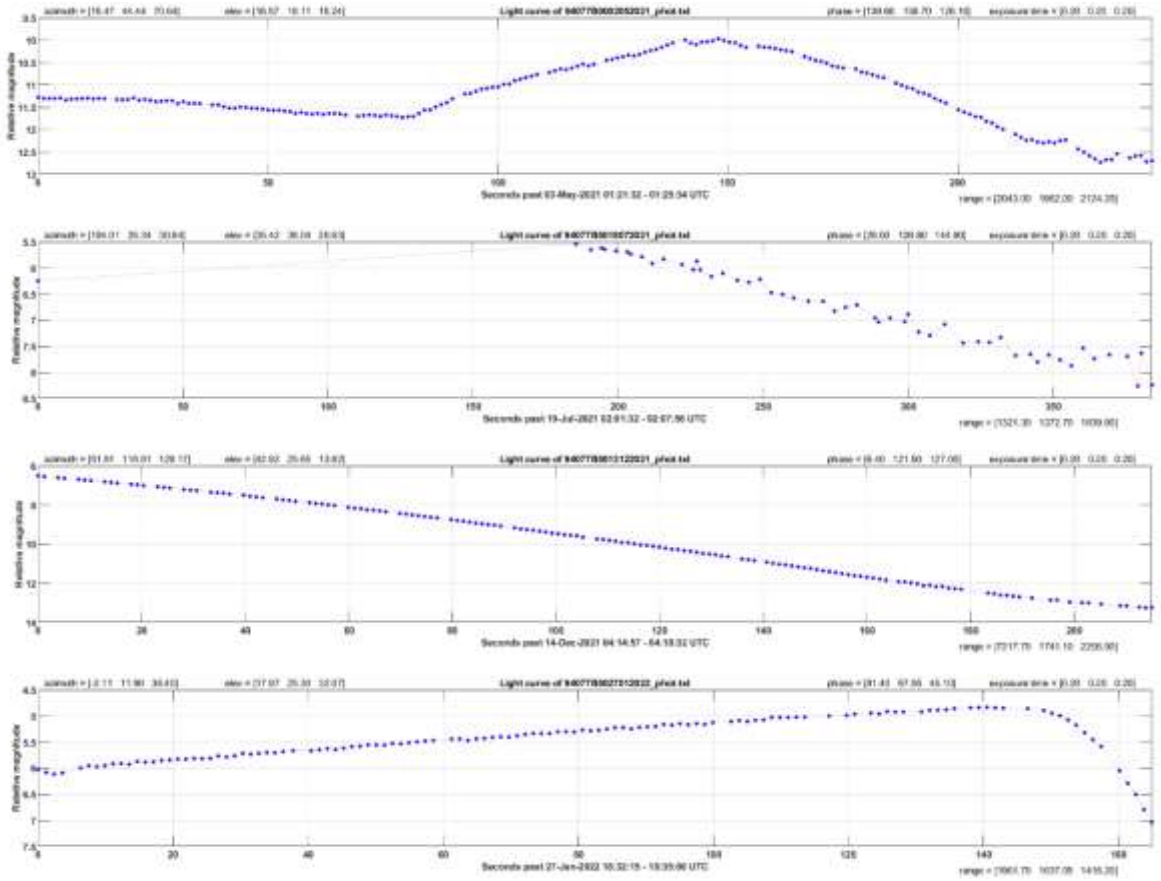

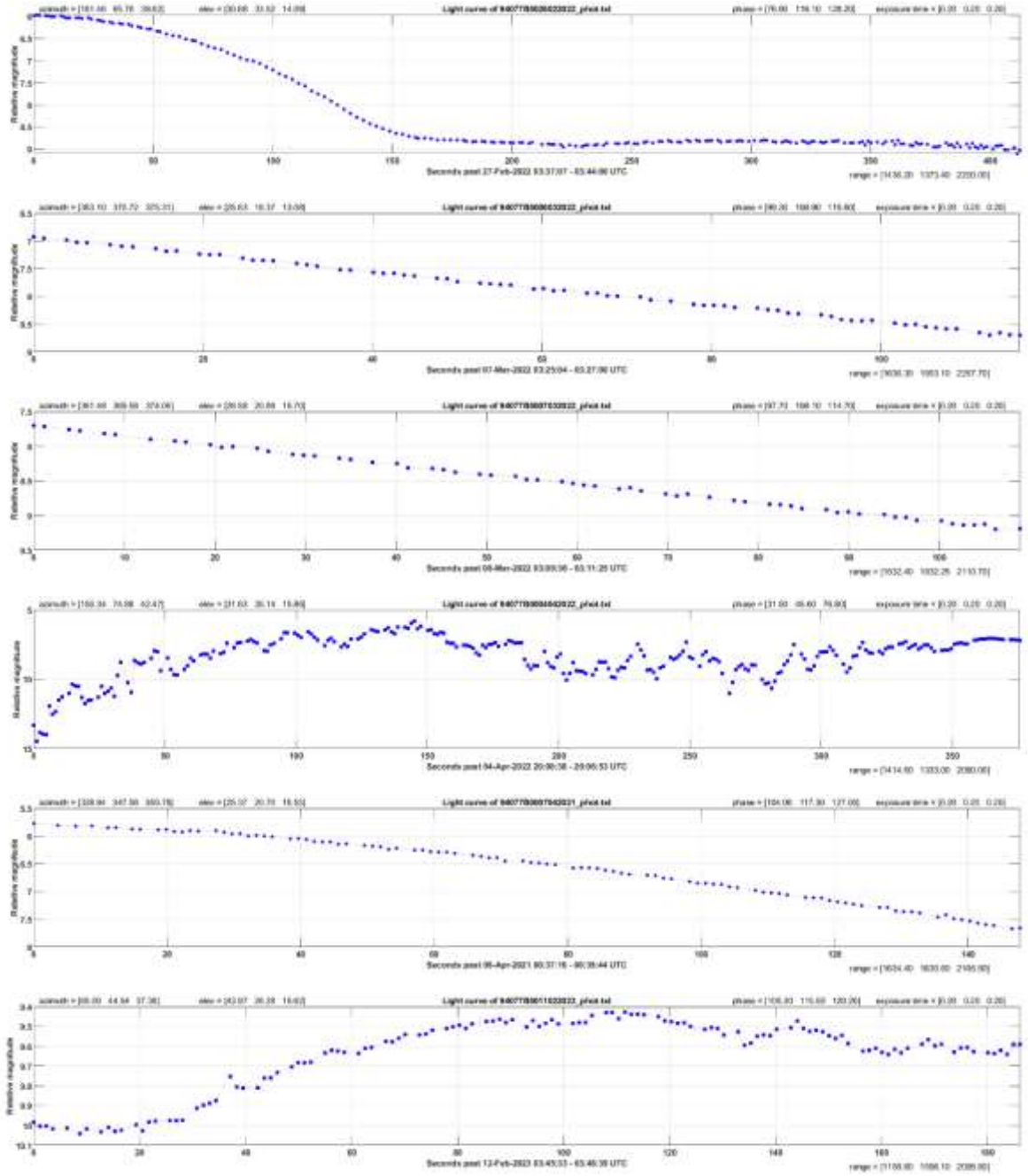

3.3.5 Norad 25637 (99008D)

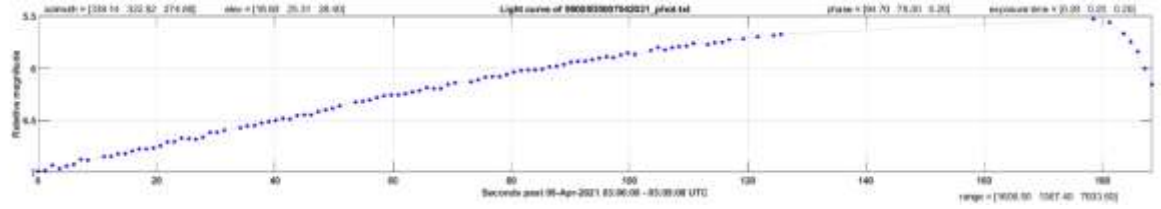

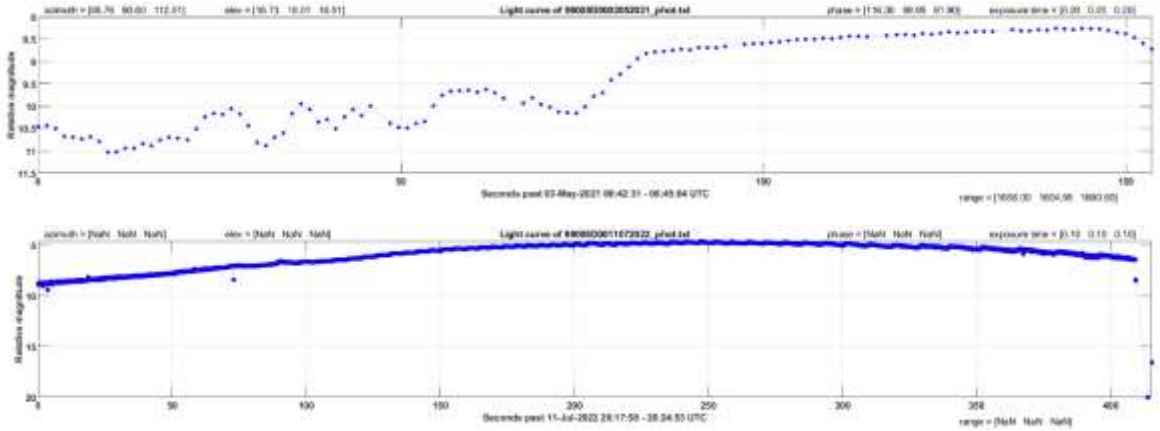

3.3.6 Norad 39198 (13033B)

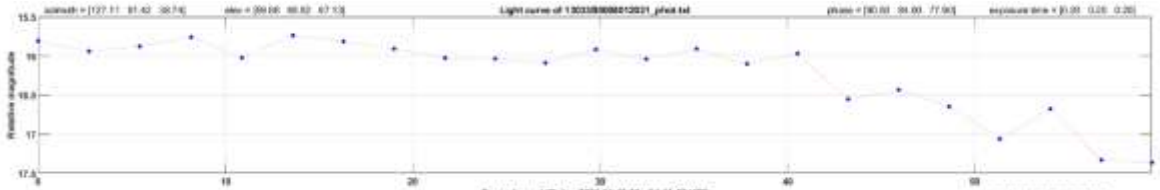

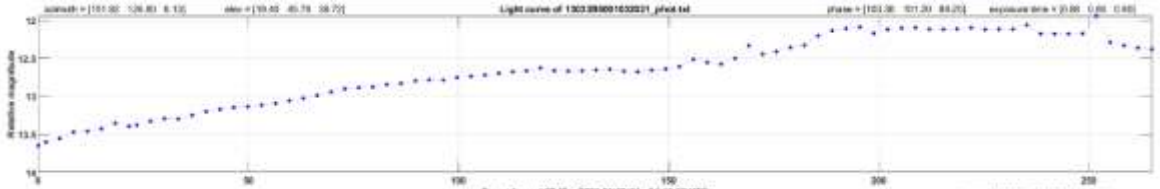

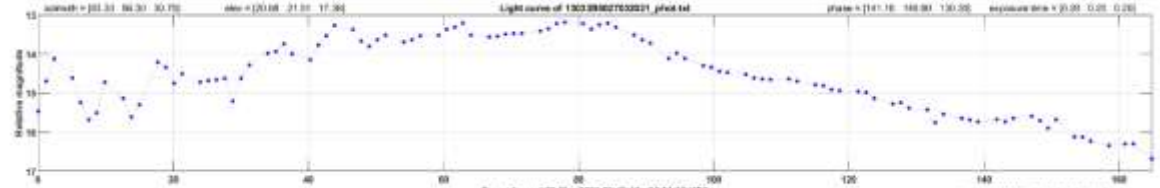

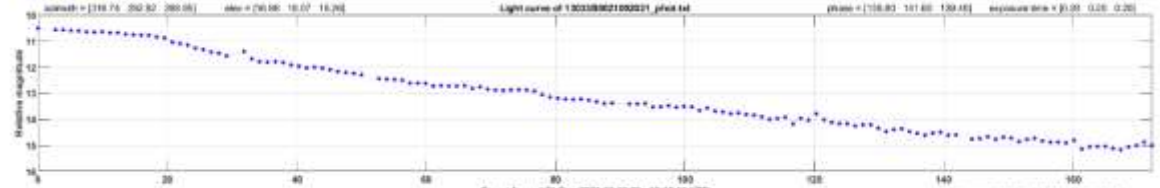

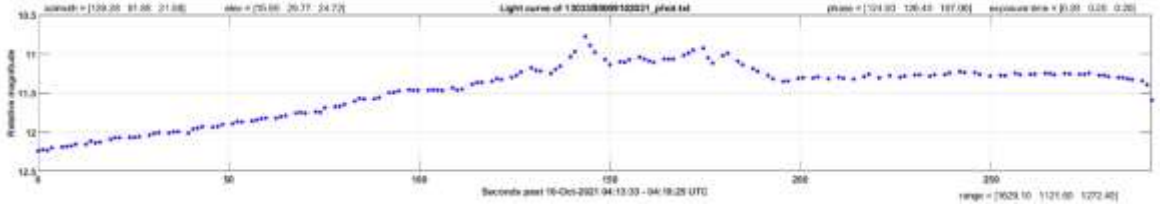

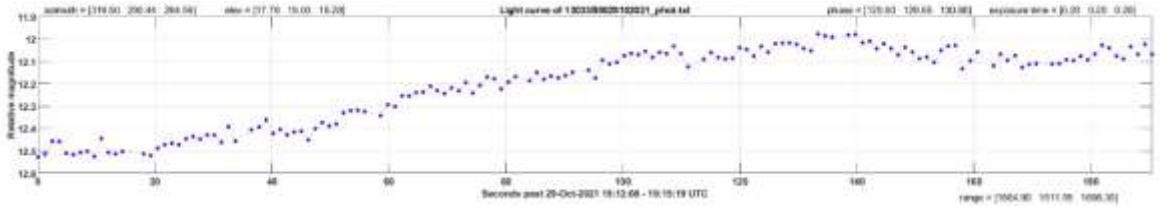
Relative magnitude

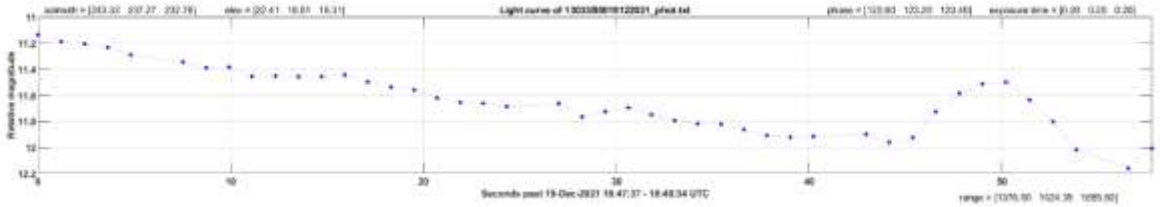
Relative magnitude

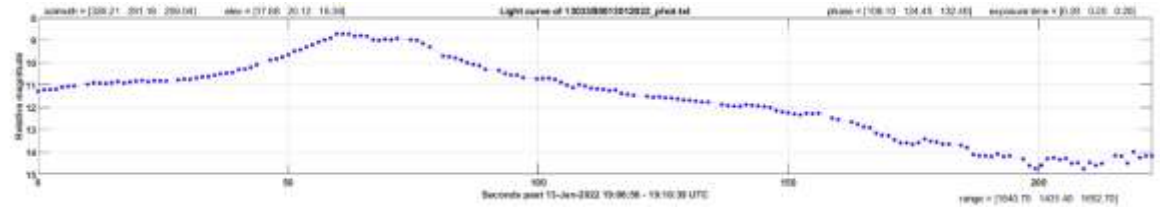
Relative magnitude

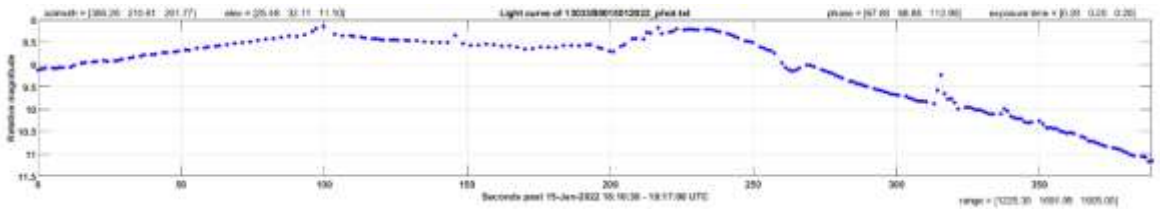
Relative magnitude

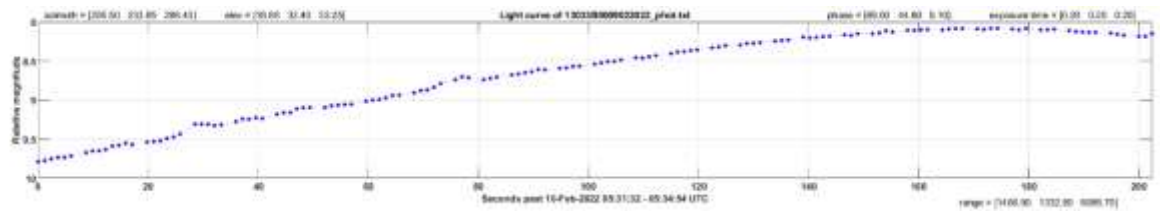
Relative magnitude

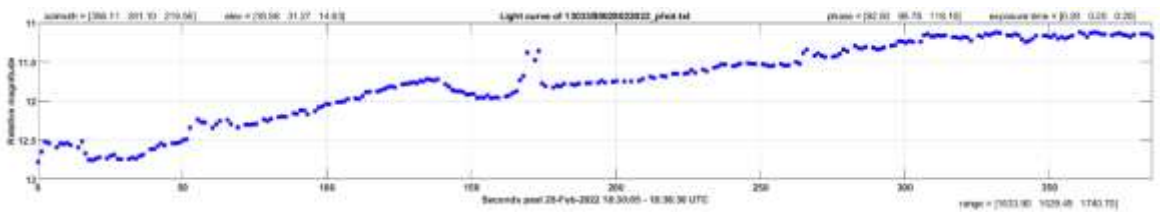
Relative magnitude

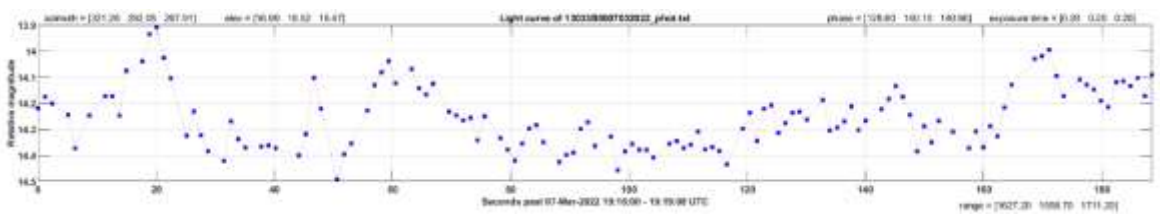
Relative magnitude

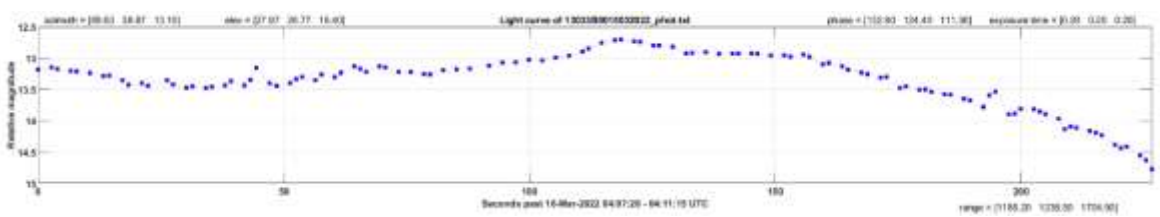
Relative magnitude

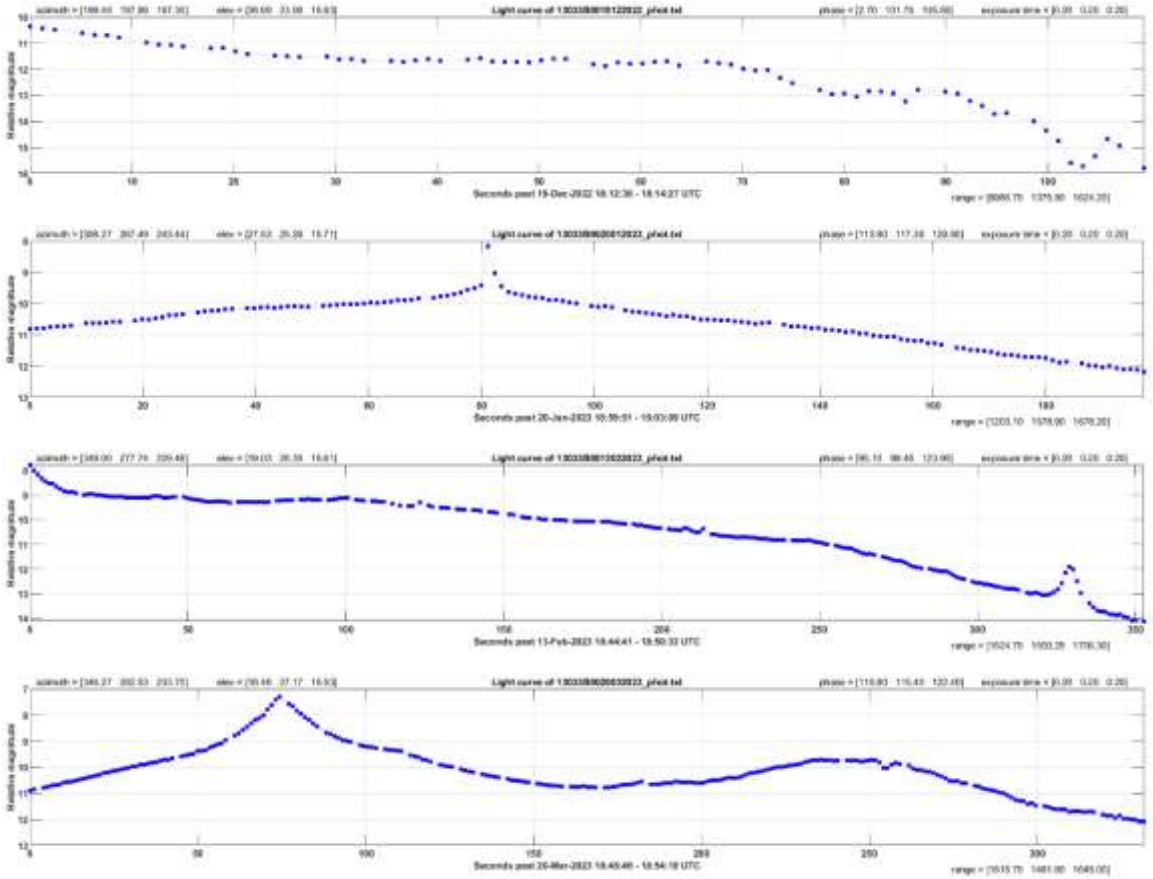

3.3.7 Norad 40879 (15040B)

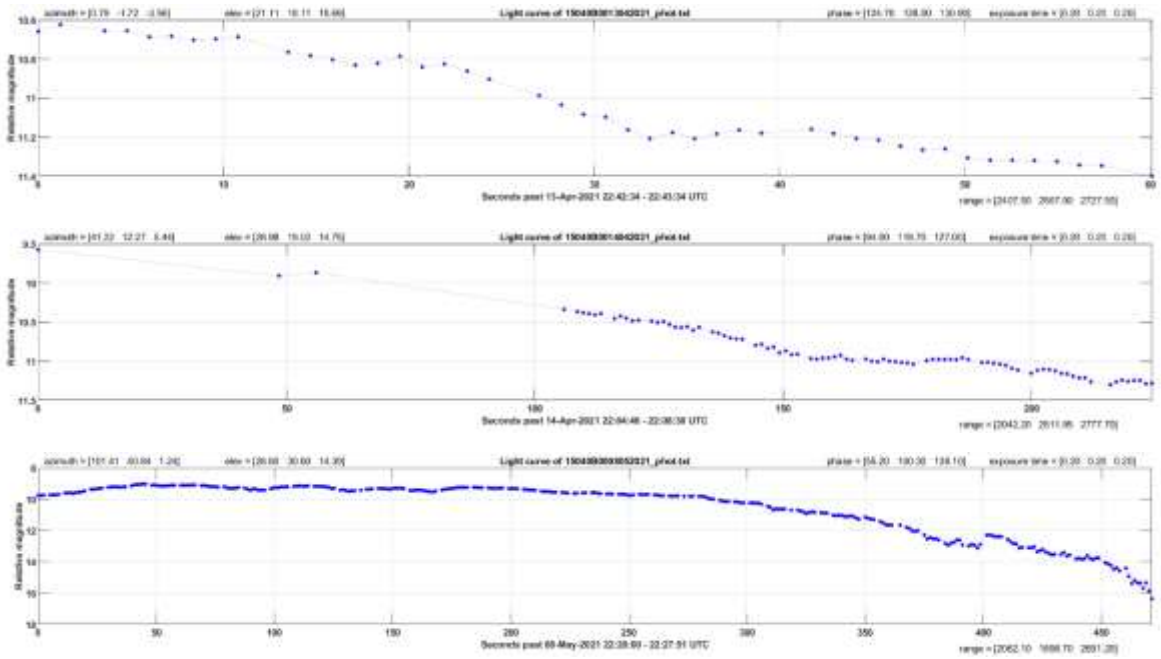

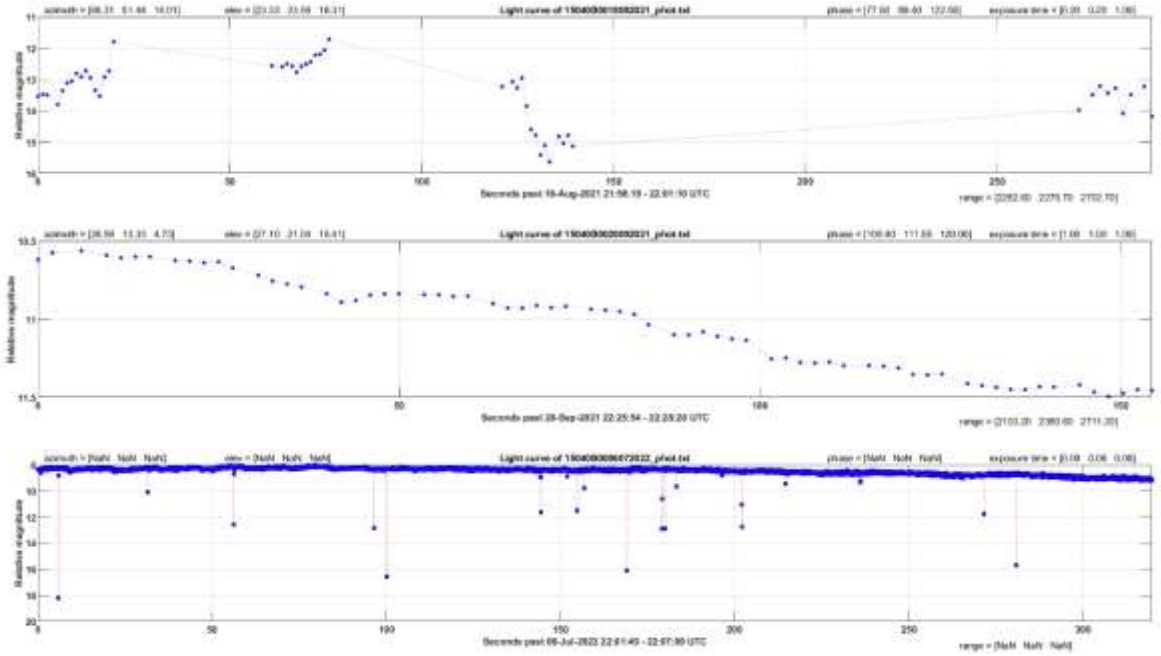

3.3.8 Norad 41847 (16066G)

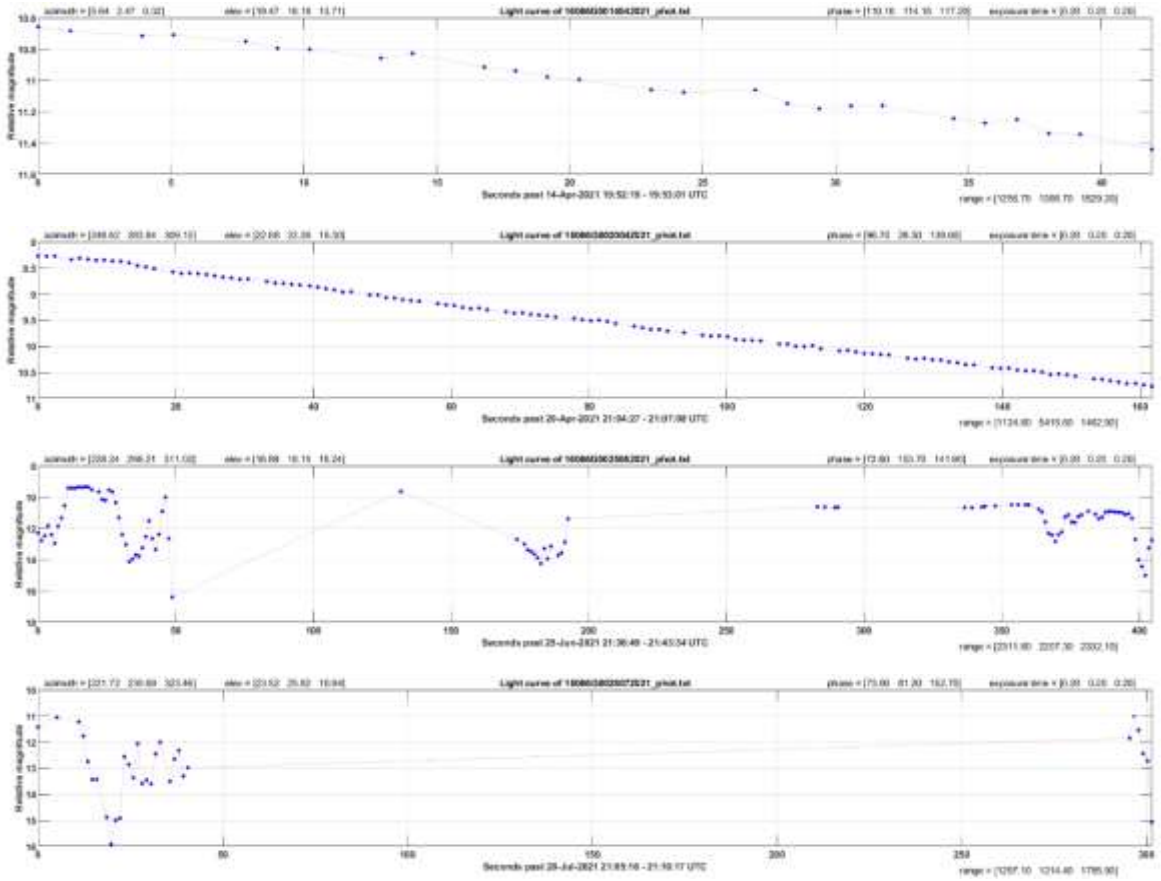

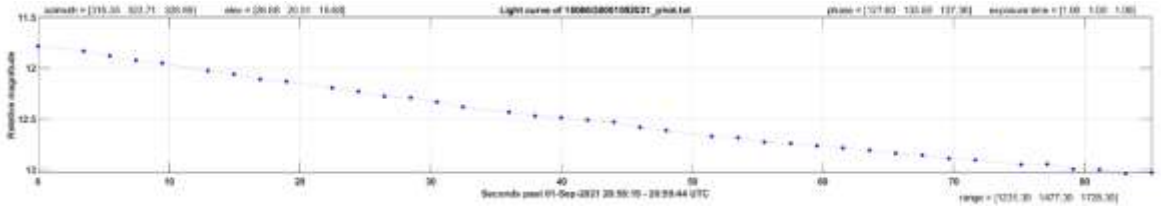
Relative magnitude

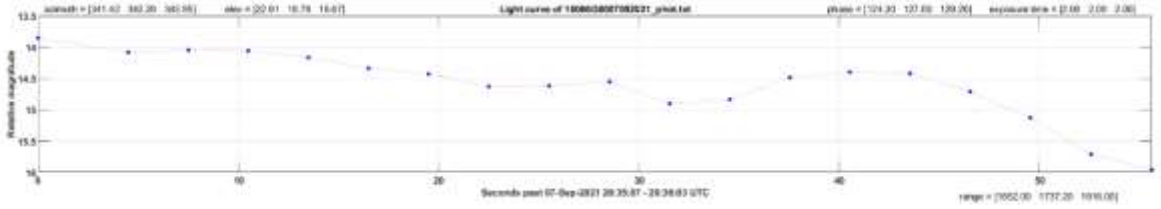
Relative magnitude

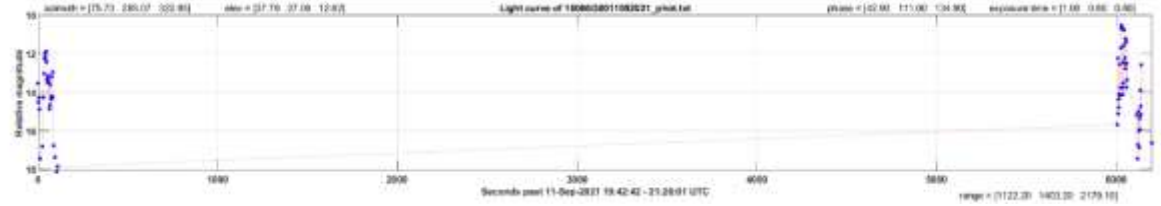
Relative magnitude

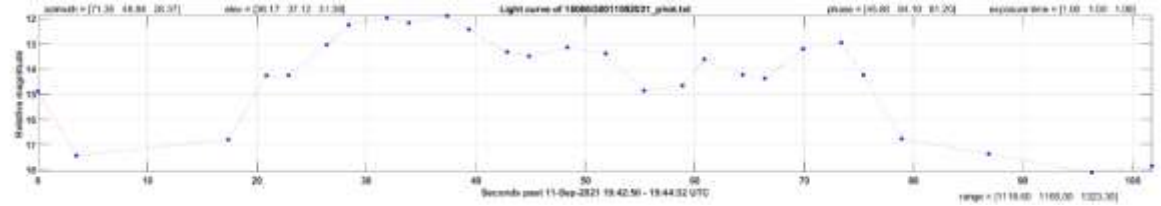
Relative magnitude

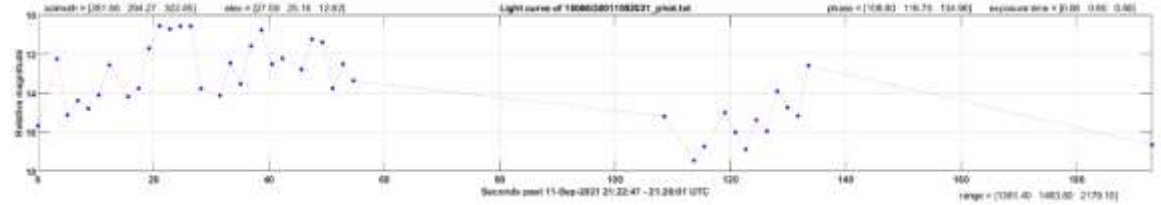
Relative magnitude

Relative magnitude

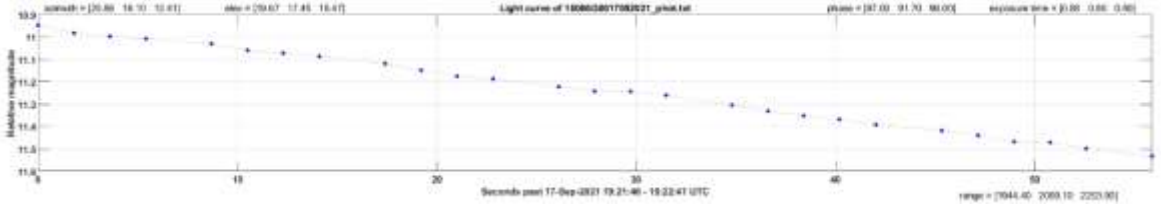
Relative magnitude

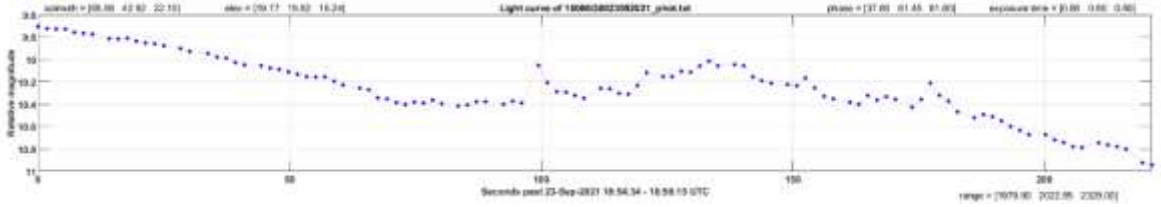
Relative magnitude

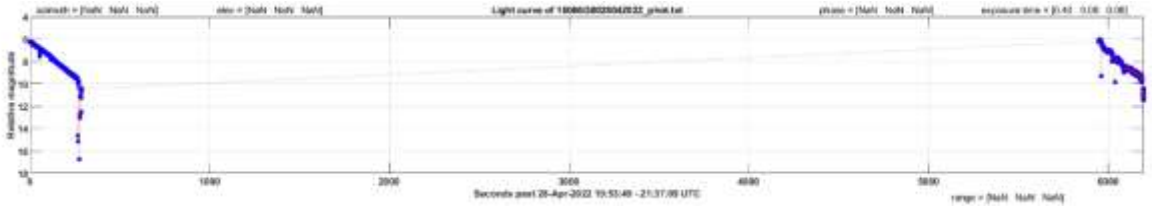

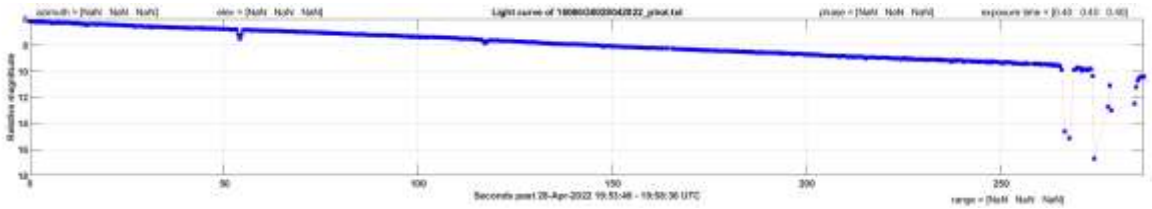

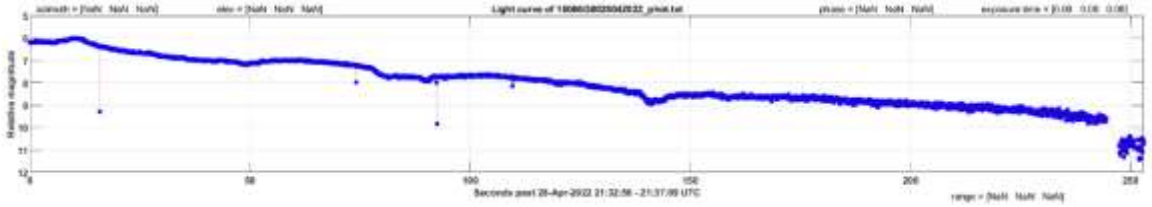

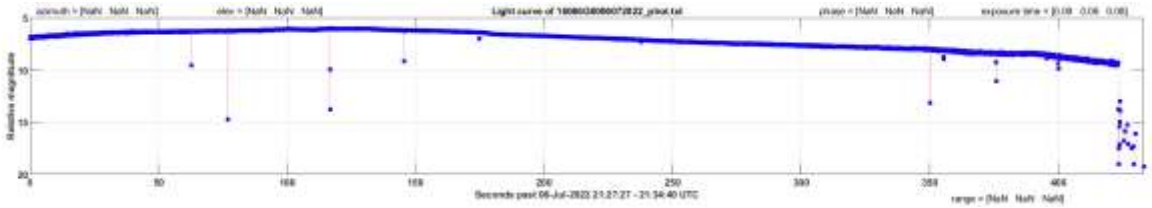

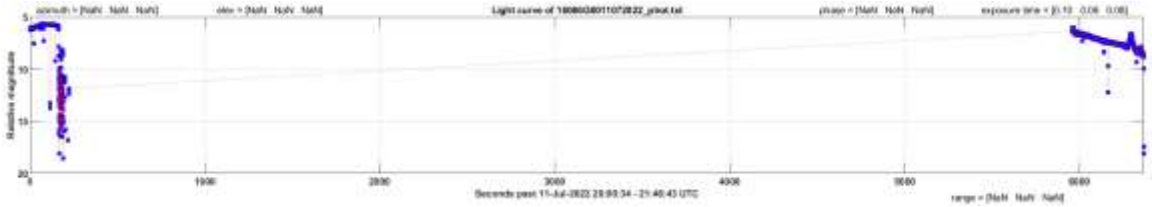

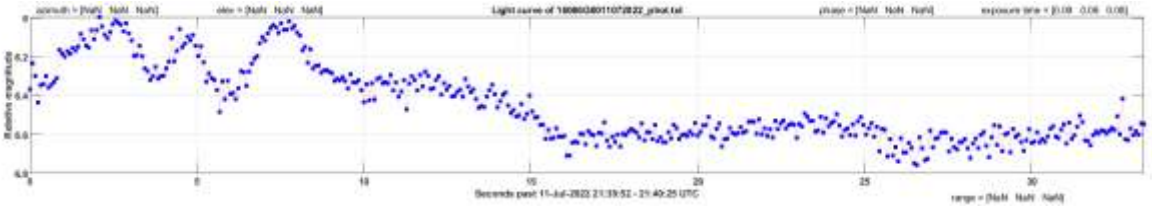

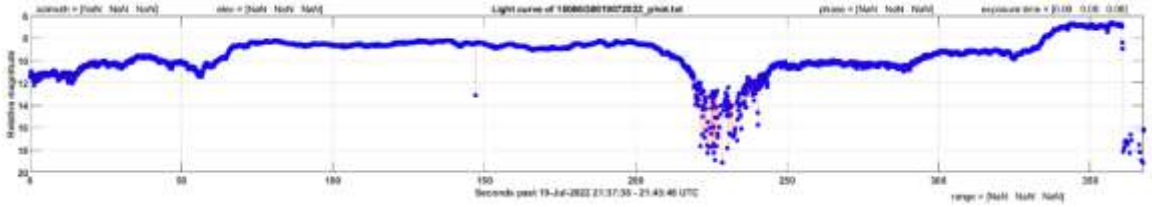

3.3.9 Norad 41858 (16068B)

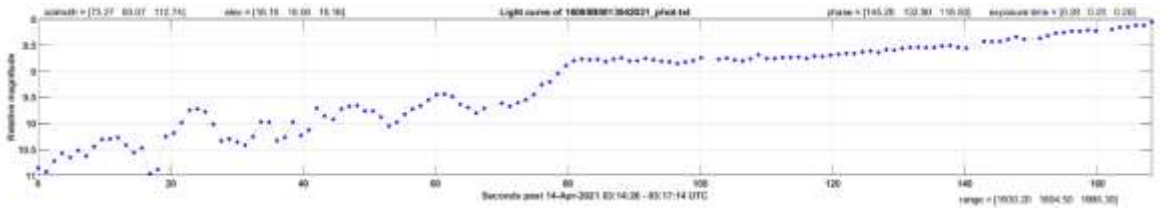

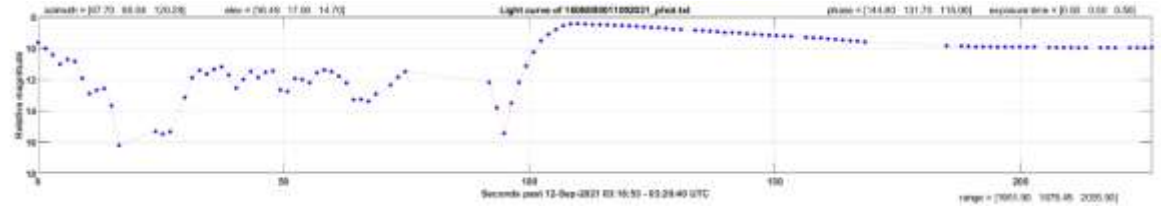
Relative magnitude
Seconds past 12-Sep-2021 03:16:53 - 03:28:40 UTC

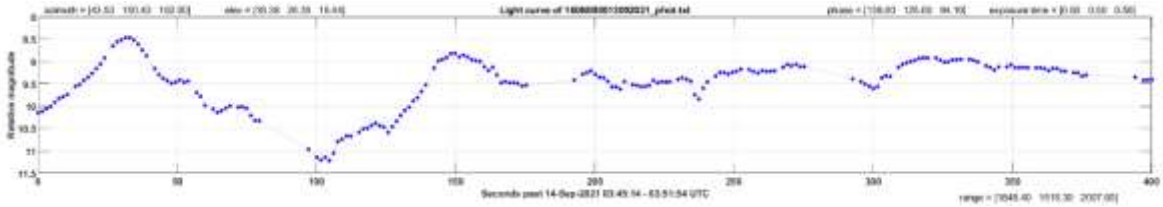
Relative magnitude
Seconds past 14-Sep-2021 03:45:54 - 03:51:54 UTC

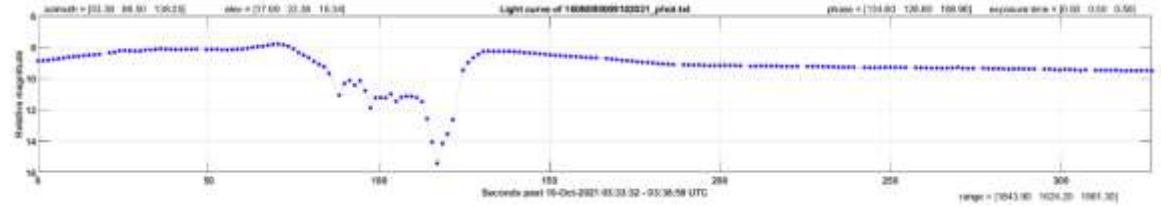
Relative magnitude
Seconds past 16-Oct-2021 03:33:32 - 03:36:58 UTC

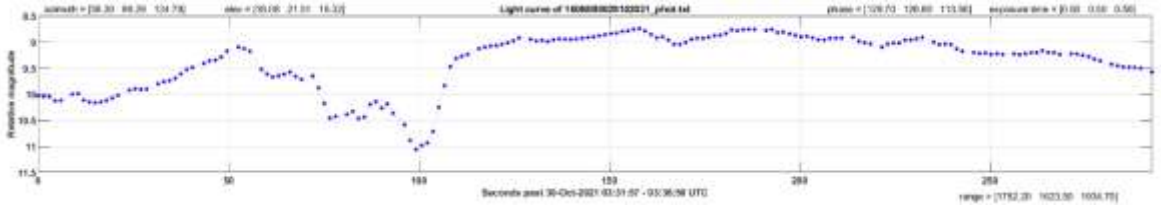
Relative magnitude
Seconds past 30-Oct-2021 03:31:57 - 03:36:58 UTC

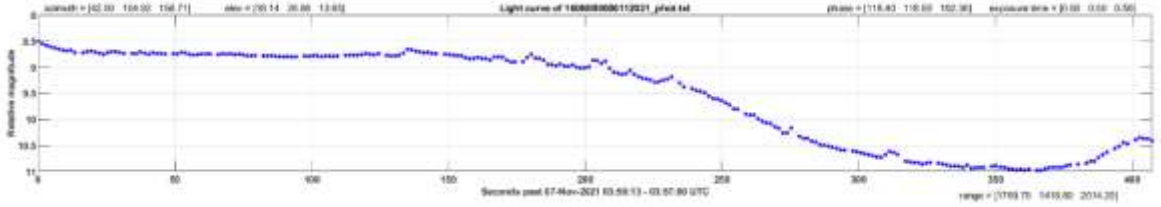
Relative magnitude
Seconds past 07-Nov-2021 03:59:13 - 03:57:50 UTC

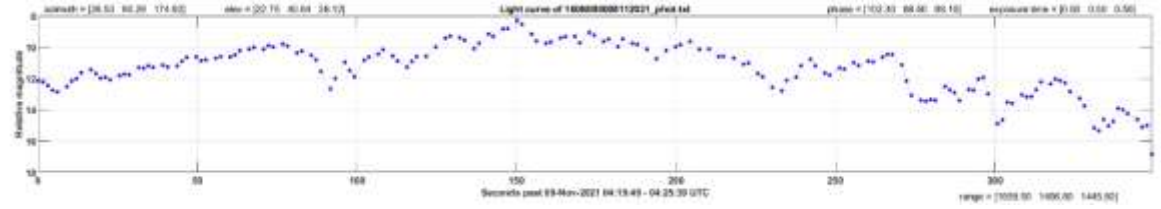
Relative magnitude
Seconds past 09-Nov-2021 04:19:49 - 04:25:39 UTC

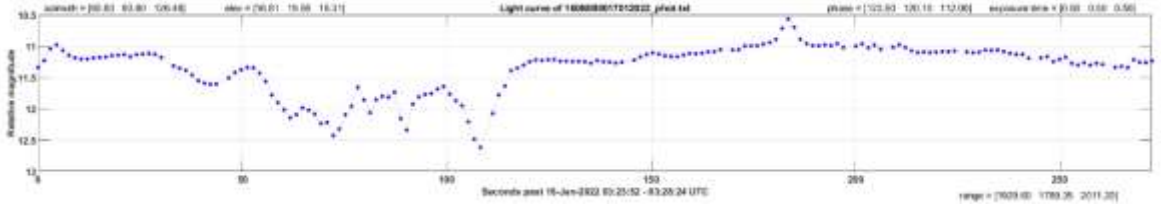
Relative magnitude
Seconds past 16-Jan-2022 03:25:52 - 03:28:24 UTC

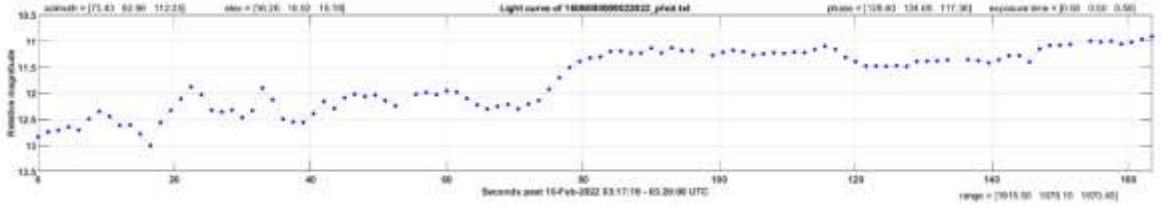
Relative magnitude
Seconds past 16-Feb-2022 03:17:18 - 03:20:00 UTC

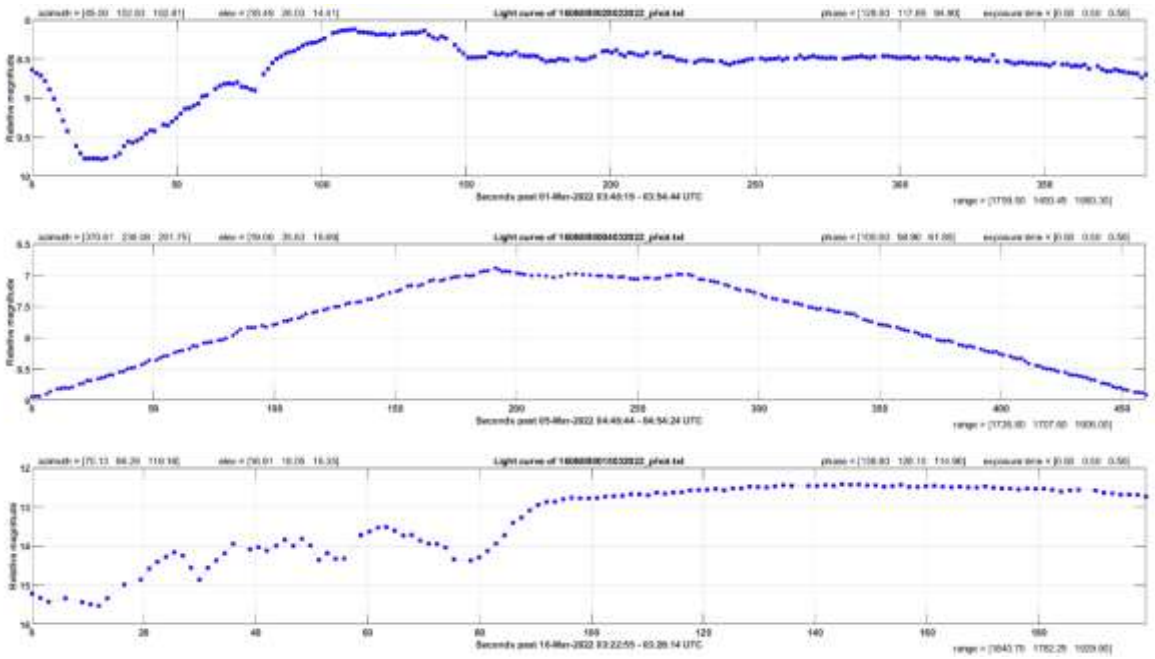

3.4 Lightcurve graphs from JAXA

3.4.1 Norad 11840

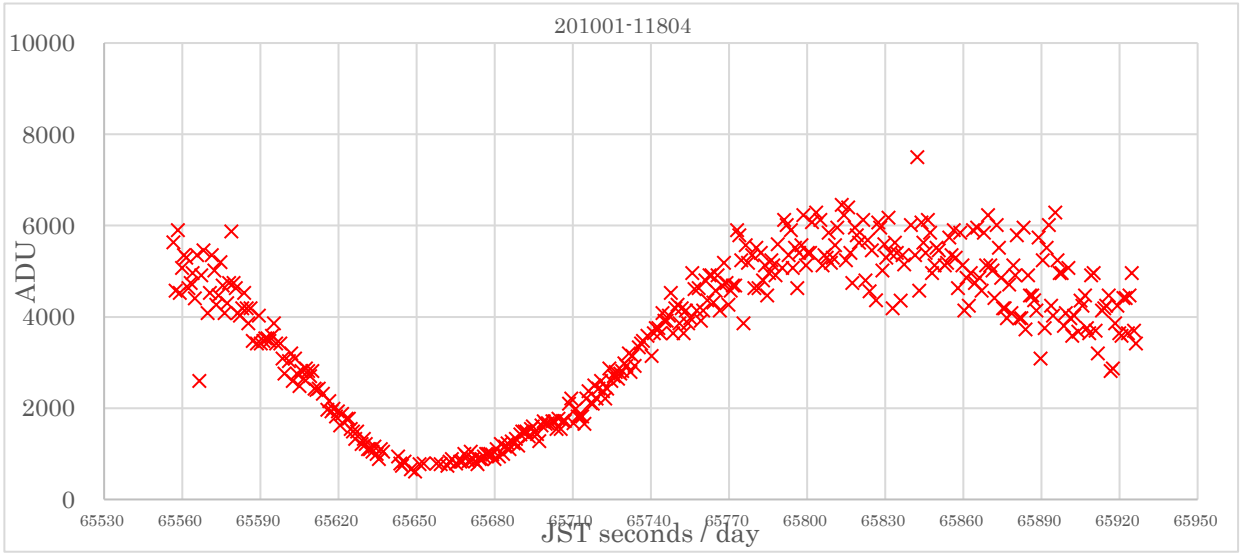

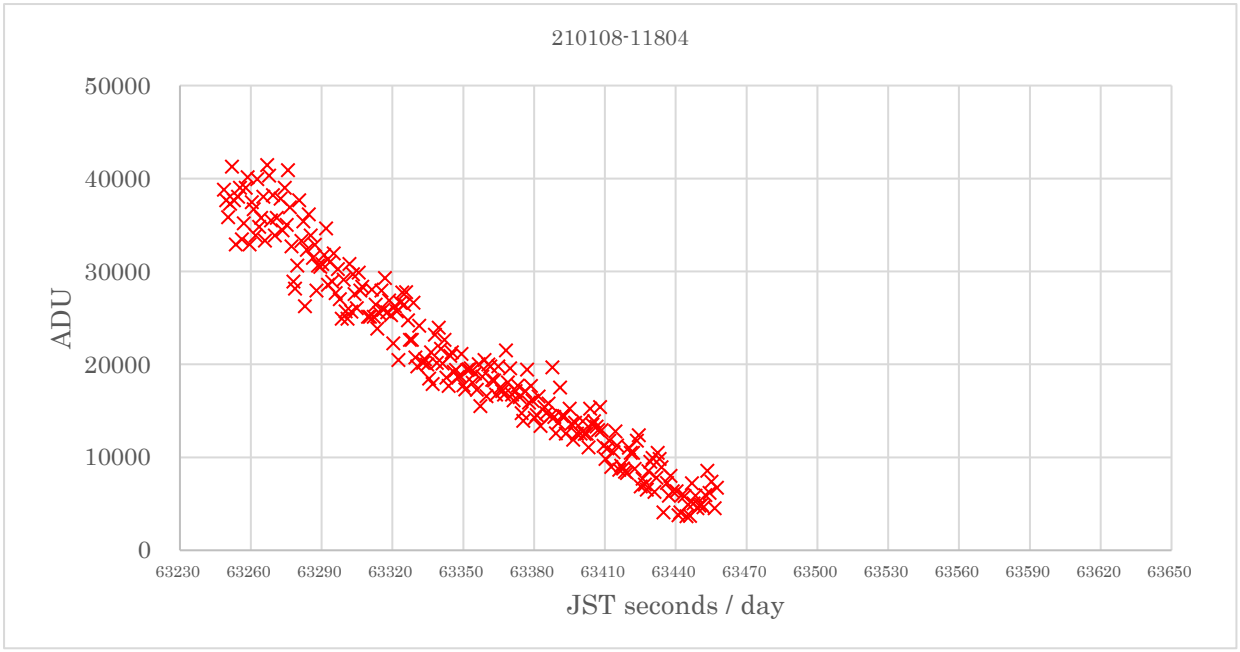
210108-11804
50000
40000
30000
20000
10000
0
ADU
63230
63260
63290
63320
63350
63380
63410
63440
63470
63500
63530
63560
63590
63620
63650
JST seconds / day

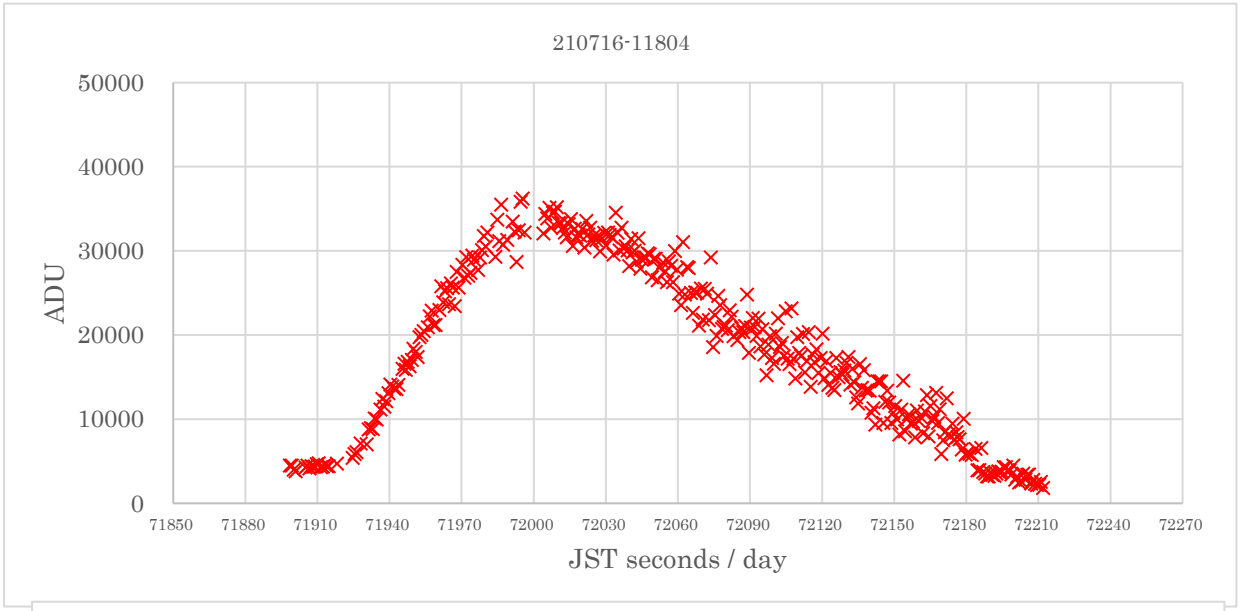
210716-11804
50000
40000
30000
20000
10000
0
ADU
71850
71880
71910
71940
71970
72000
72030
72060
72090
72120
72150
72180
72210
72240
72270
JST seconds / day

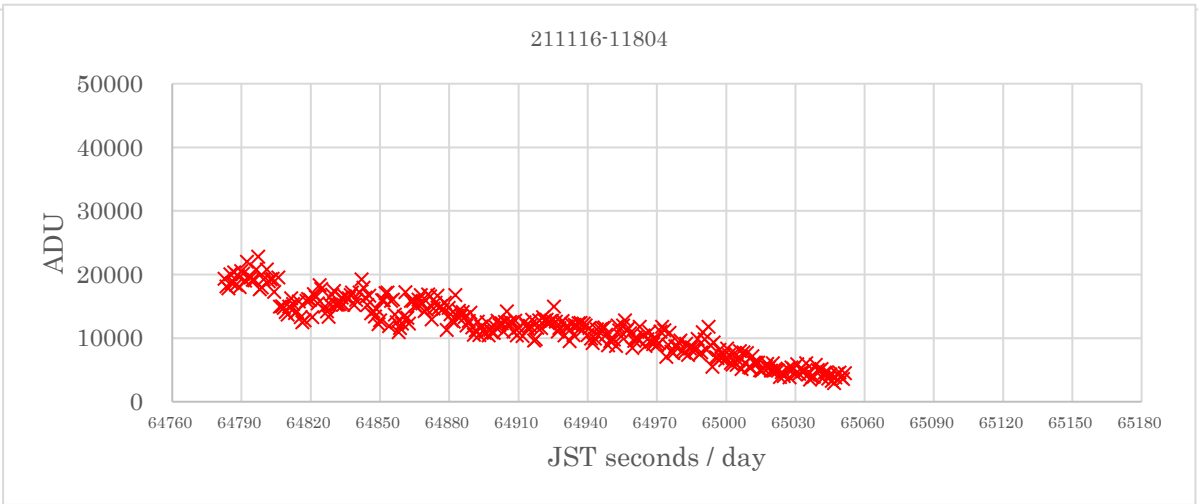
211116-11804
50000
40000
30000
20000
10000
0
ADU
64760
64790
64820
64850
64880
64910
64940
64970
65000
65030
65060
65090
65120
65150
65180
JST seconds / day

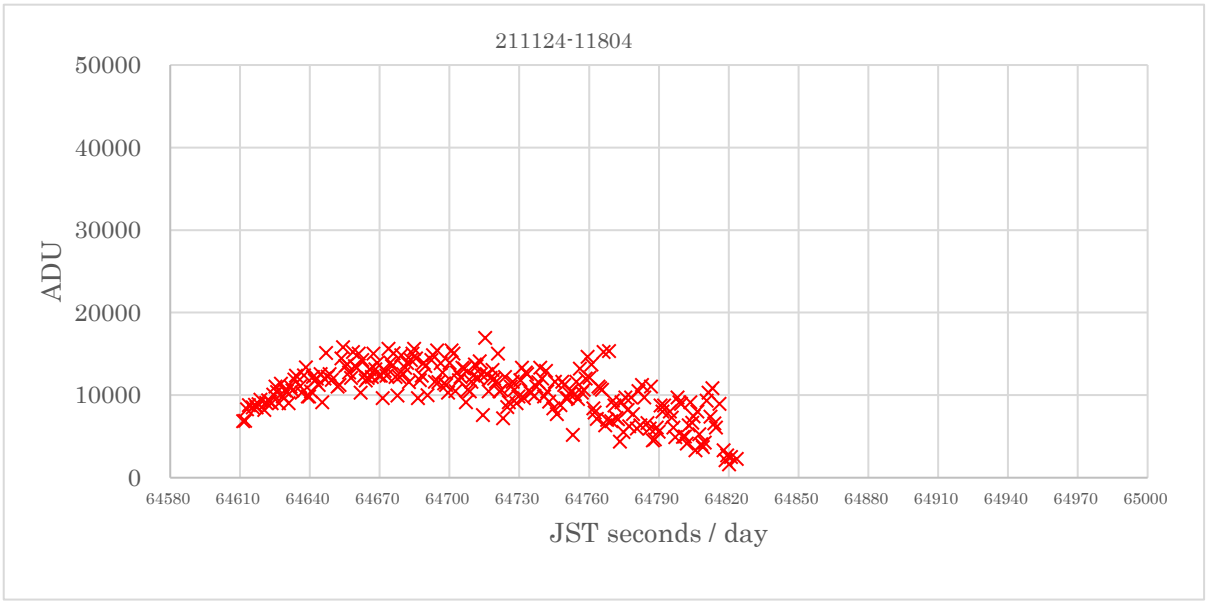

3.4.2 Norad 18340

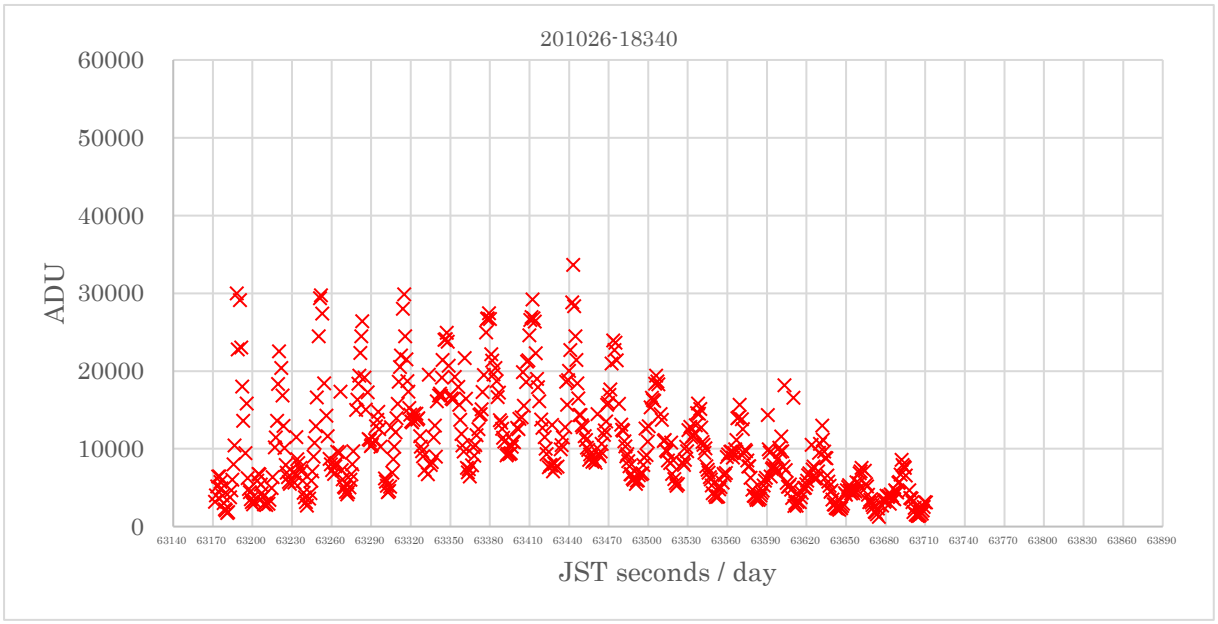

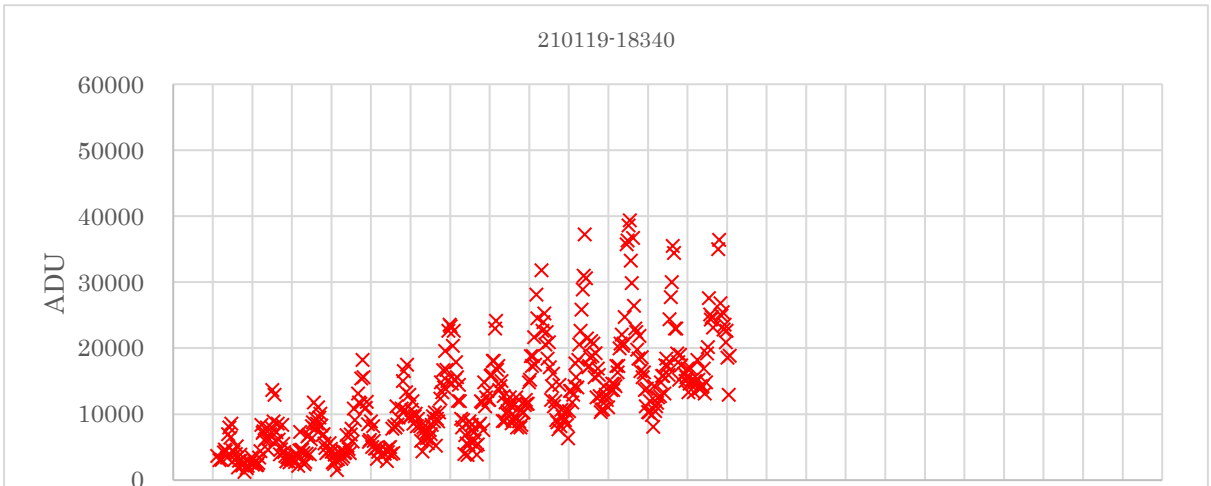

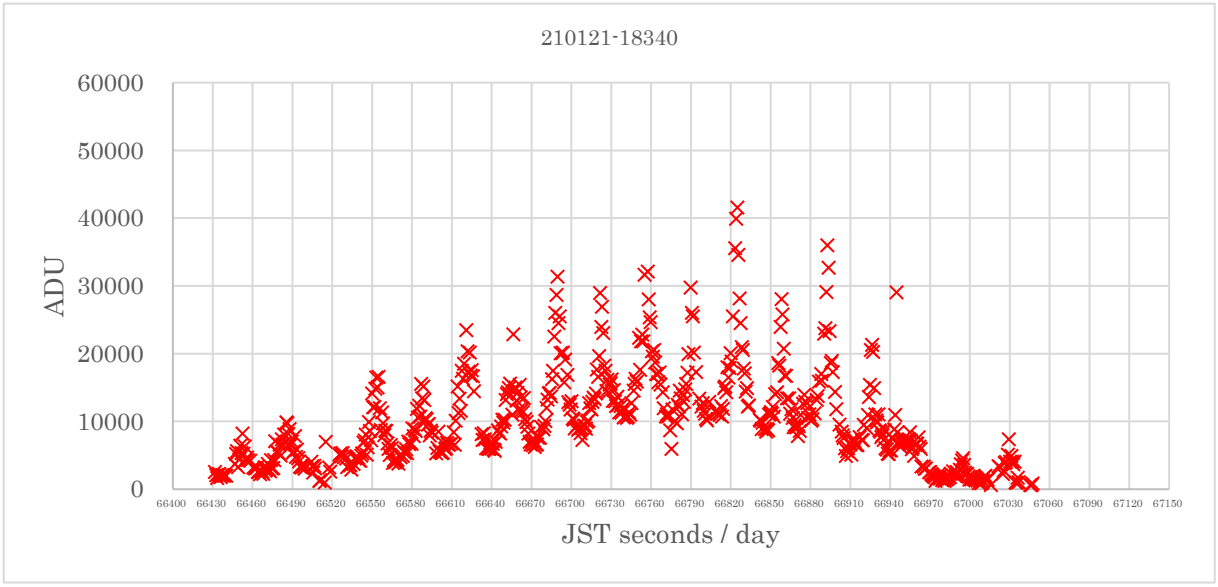
210121-18340
60000
50000
40000
30000
20000
10000
0
ADU
66400 66430 66460 66490 66520 66550 66580 66610 66640 66670 66700 66730 66760 66790 66820 66850 66880 66910 66940 66970 67000 67030 67060 67090 67120 67150
JST seconds / day

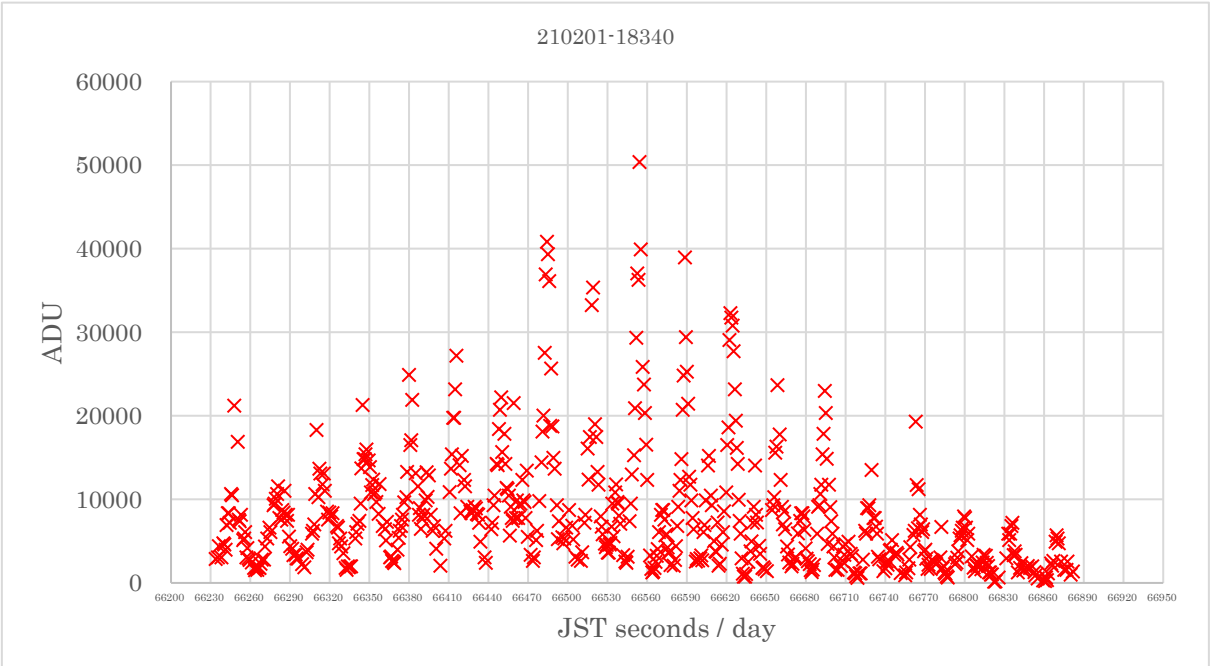
210201-18340
60000
50000
40000
30000
20000
10000
0
ADU
66200 66230 66260 66290 66320 66350 66380 66410 66440 66470 66500 66530 66560 66590 66620 66650 66680 66710 66740 66770 66800 66830 66860 66890 66920 66950
JST seconds / day

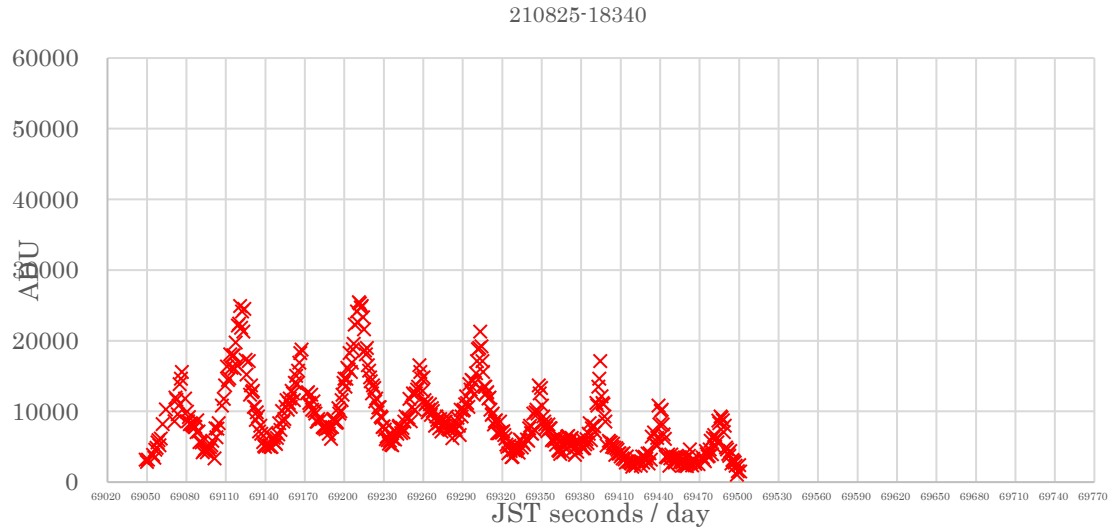
210825-18340
60000
50000
40000
30000
20000
10000
0
ADU
69020 69050 69080 69110 69140 69170 69200 69230 69260 69290 69320 69350 69380 69410 69440 69470 69500 69530 69560 69590 69620 69650 69680 69710 69740 69770
JST seconds / day

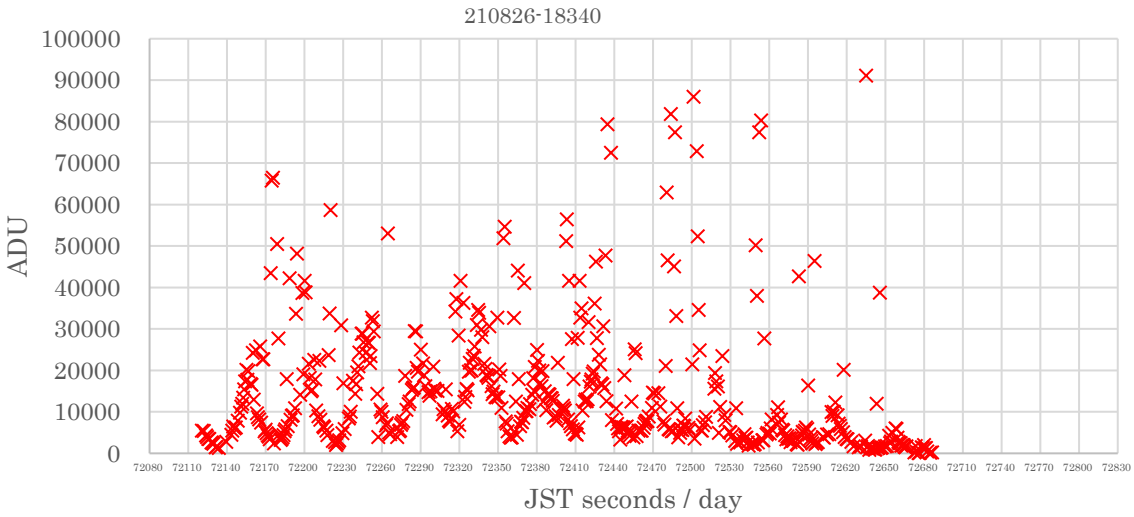
210826-18340
100000
90000
80000
70000
60000
50000
40000
30000
20000
10000
0
ADU
72080 72110 72140 72170 72200 72230 72260 72290 72320 72350 72380 72410 72440 72470 72500 72530 72560 72590 72620 72650 72680 72710 72740 72770 72800 72830
JST seconds / day

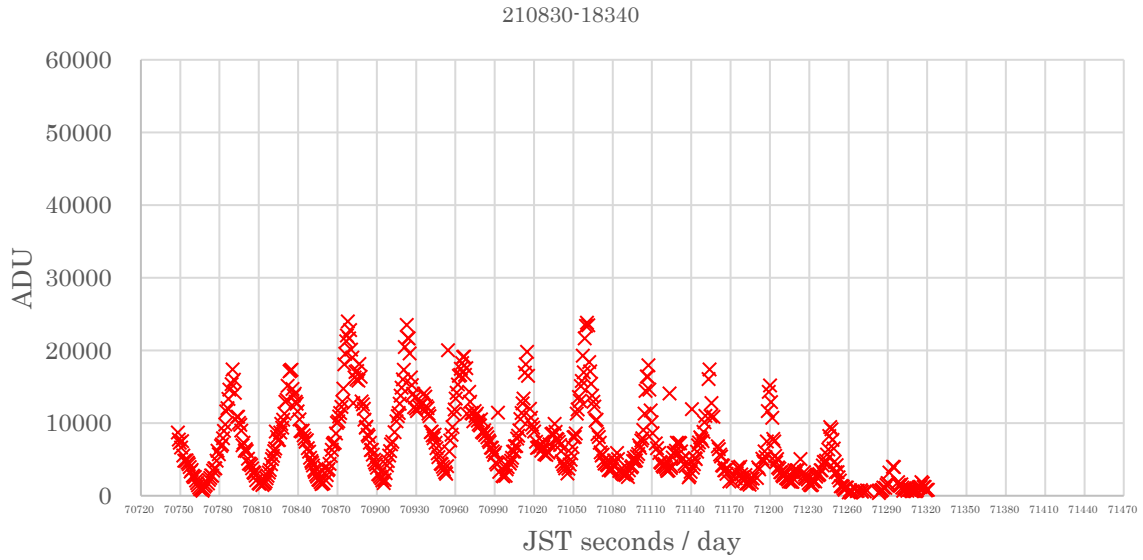

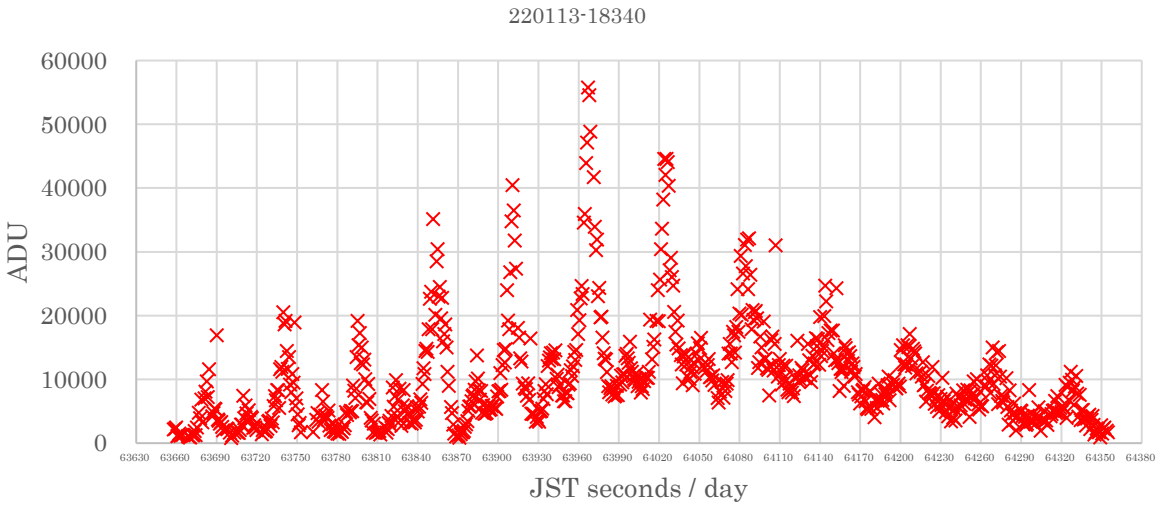

3.4.3 Norad 23088

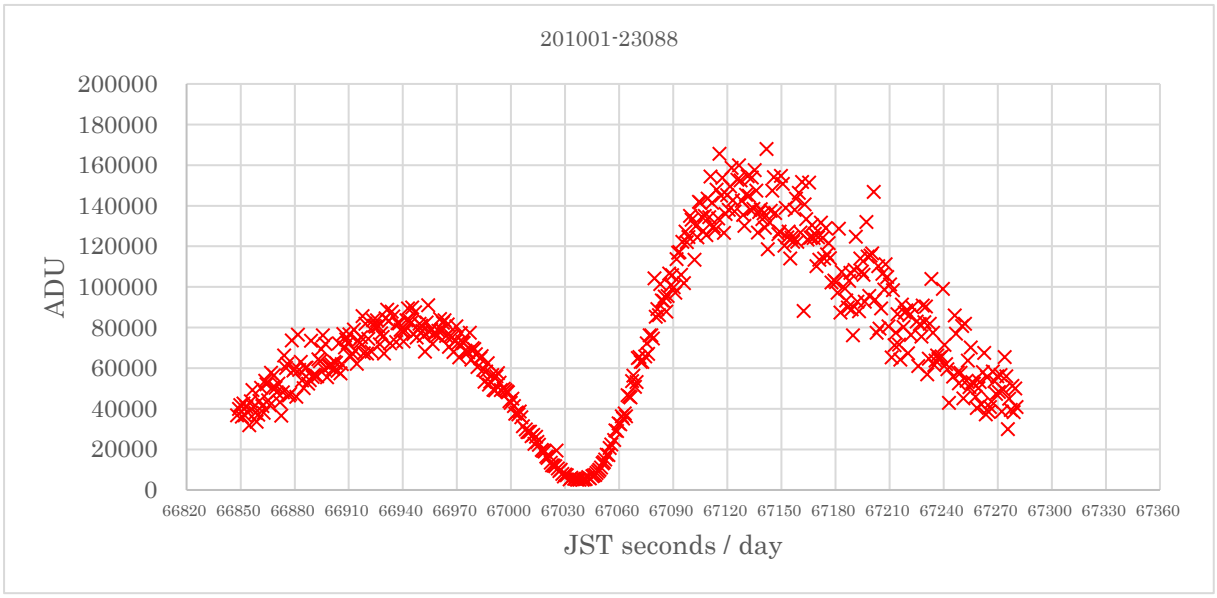
201001-23088
ADU
200000
180000
160000
140000
120000
100000
80000
60000
40000
20000
0
66820 66850 66880 66910 66940 66970 67000 67030 67060 67090 67120 67150 67180 67210 67240 67270 67300 67330 67360
JST seconds / day

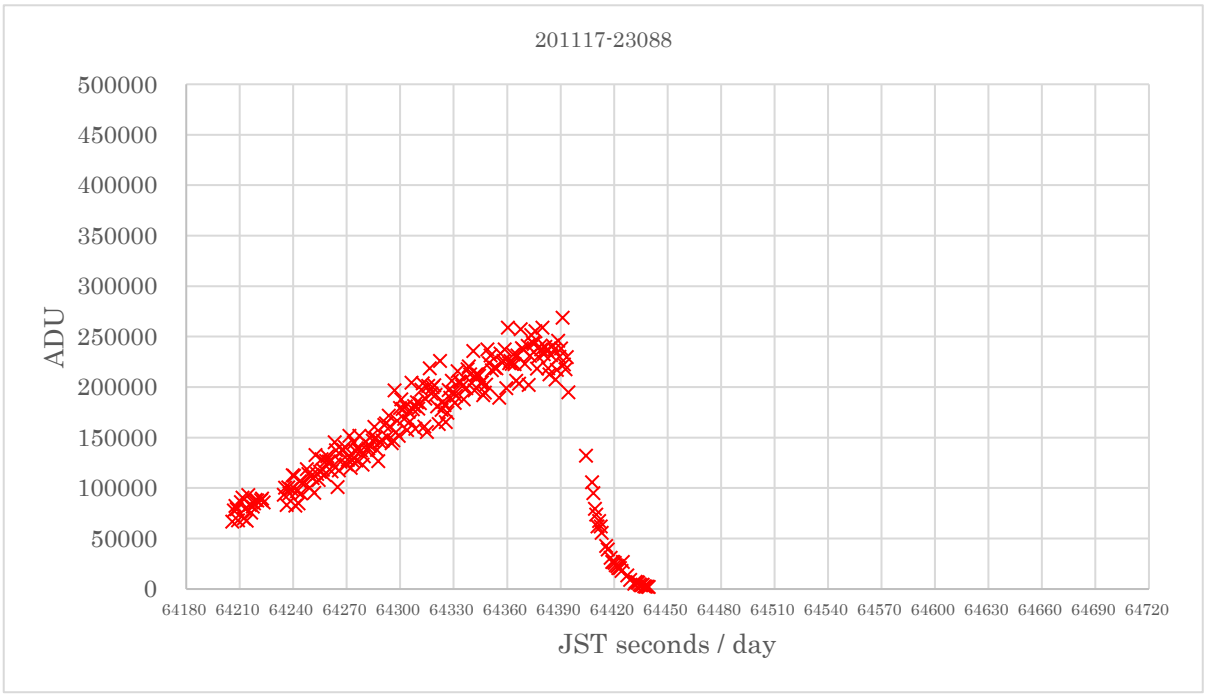
201117-23088
ADU
500000
450000
400000
350000
300000
250000
200000
150000
100000
50000
0
64180 64210 64240 64270 64300 64330 64360 64390 64420 64450 64480 64510 64540 64570 64600 64630 64660 64690 64720
JST seconds / day

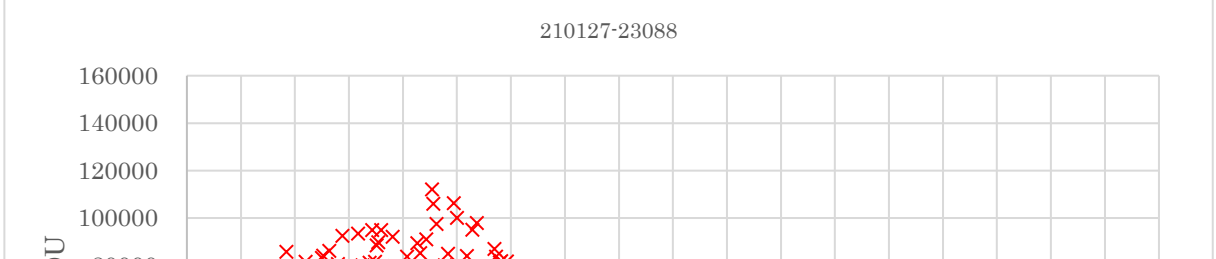
210127-23088
160000
140000
120000
100000

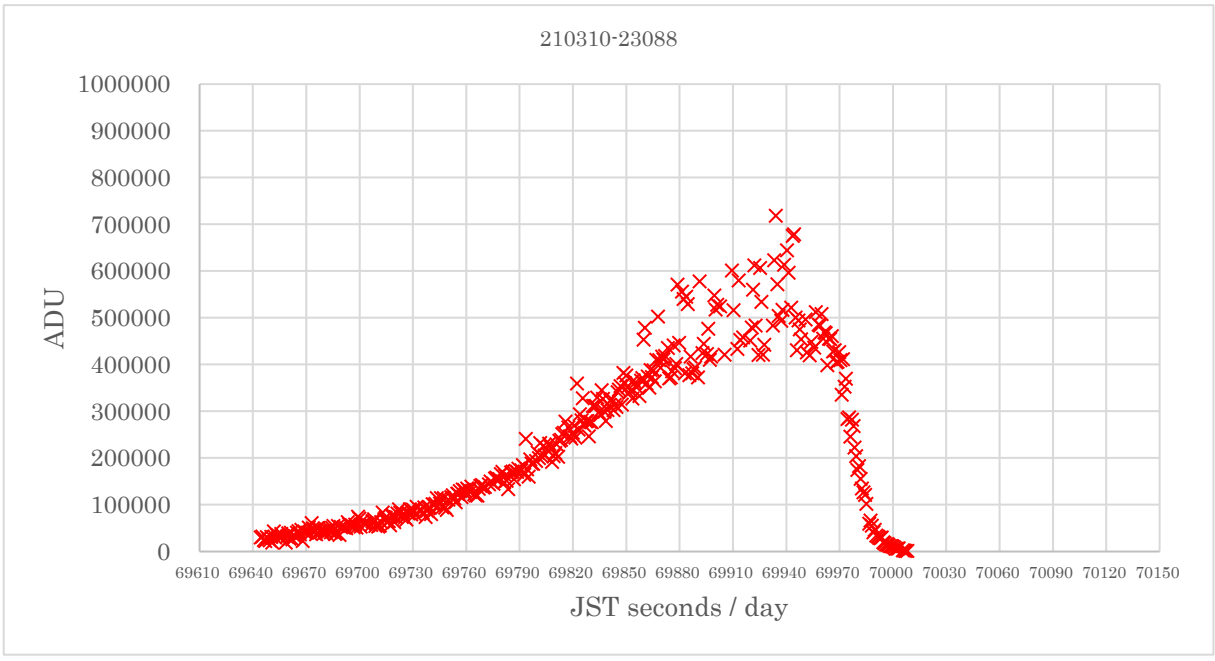
210310-23088
1000000
900000
800000
700000
600000
500000
400000
300000
200000
100000
0
ADU
69610 69640 69670 69700 69730 69760 69790 69820 69850 69880 69910 69940 69970 70000 70030 70060 70090 70120 70150
JST seconds / day

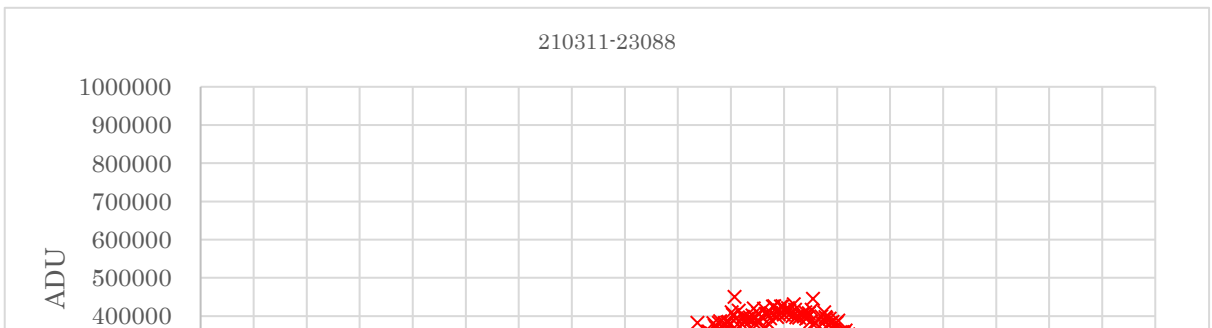
210311-23088
1000000
900000
800000
700000
600000
500000
400000
ADU

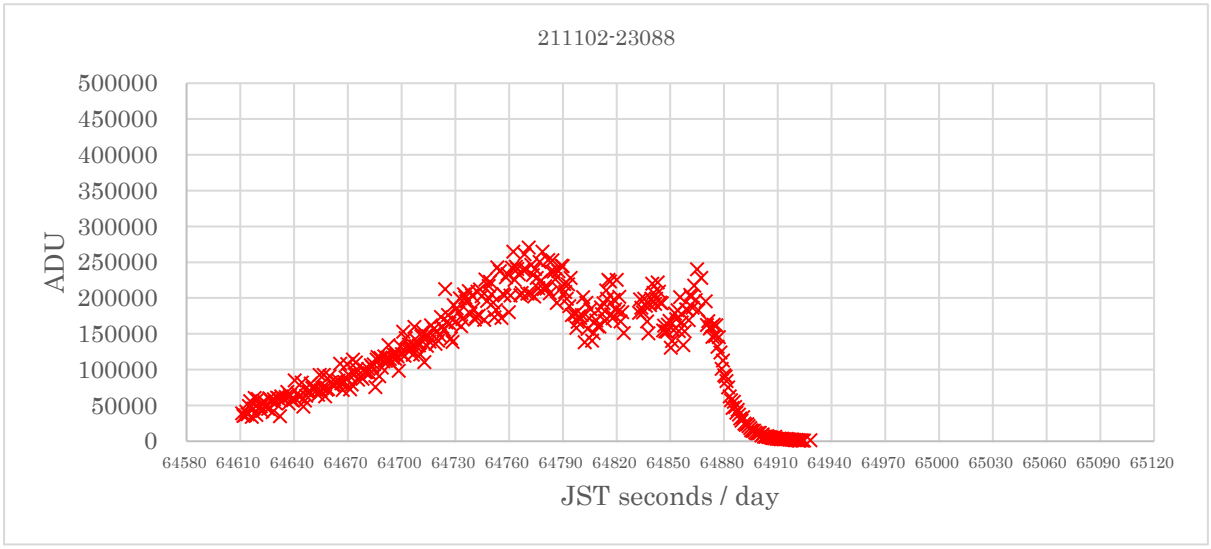
211102-23088
500000
450000
400000
350000
300000
250000
200000
150000
100000
50000
0
ADU
64580 64610 64640 64670 64700 64730 64760 64790 64820 64850 64880 64910 64940 64970 65000 65030 65060 65090 65120
JST seconds / day

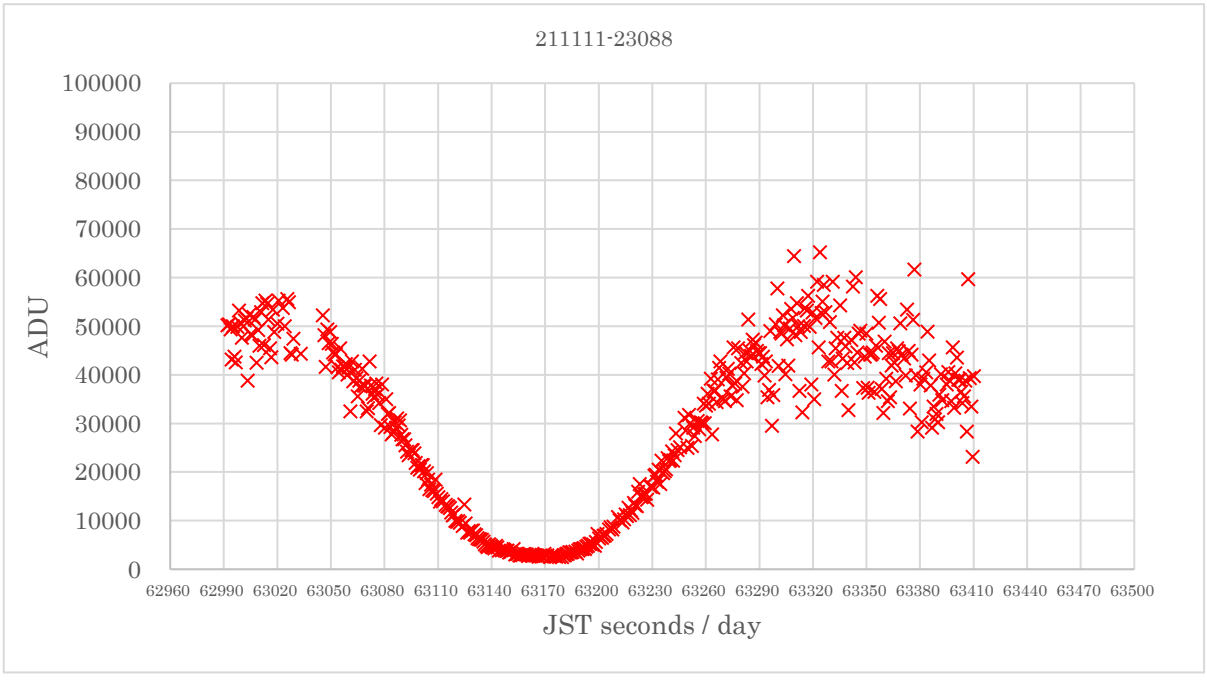
211111-23088
100000
90000
80000
70000
60000
50000
40000
30000
20000
10000
0
ADU
62960 62990 63020 63050 63080 63110 63140 63170 63200 63230 63260 63290 63320 63350 63380 63410 63440 63470 63500
JST seconds / day

3.4.4 Norad 23405

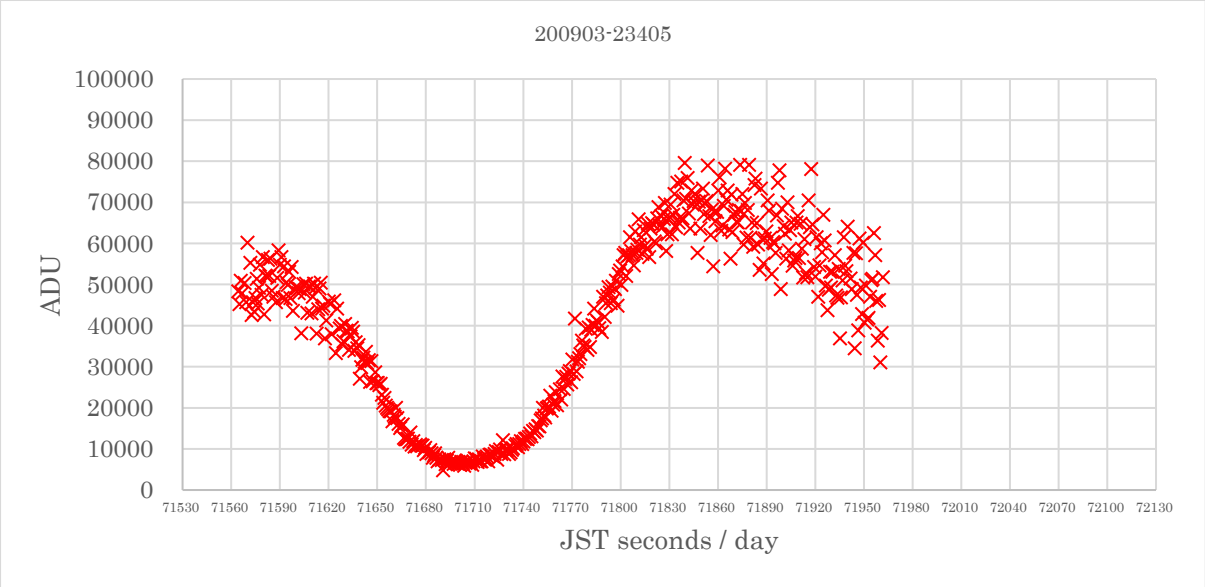

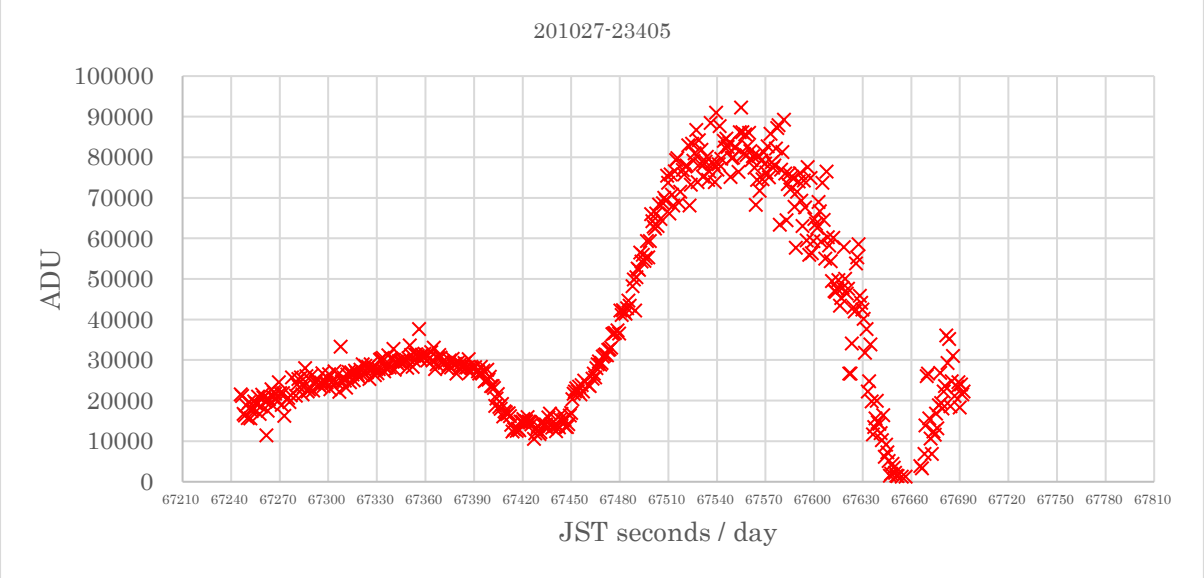

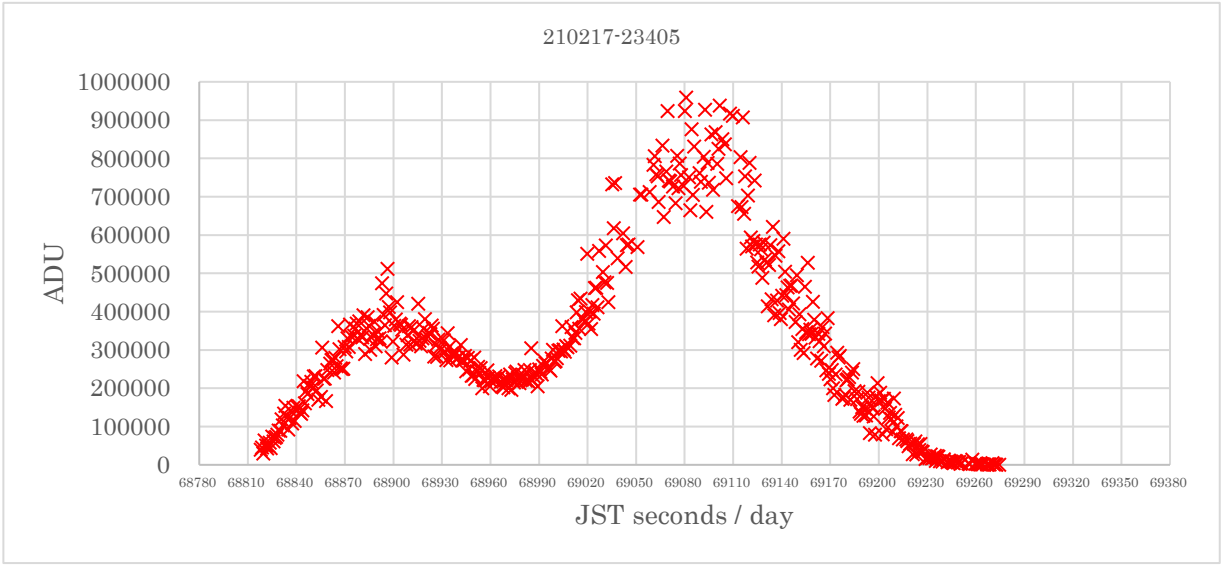
210217-23405
ADU
1000000
900000
800000
700000
600000
500000
400000
300000
200000
100000
0
68780 68810 68840 68870 68900 68930 68960 68990 69020 69050 69080 69110 69140 69170 69200 69230 69260 69290 69320 69350 69380
JST seconds / day

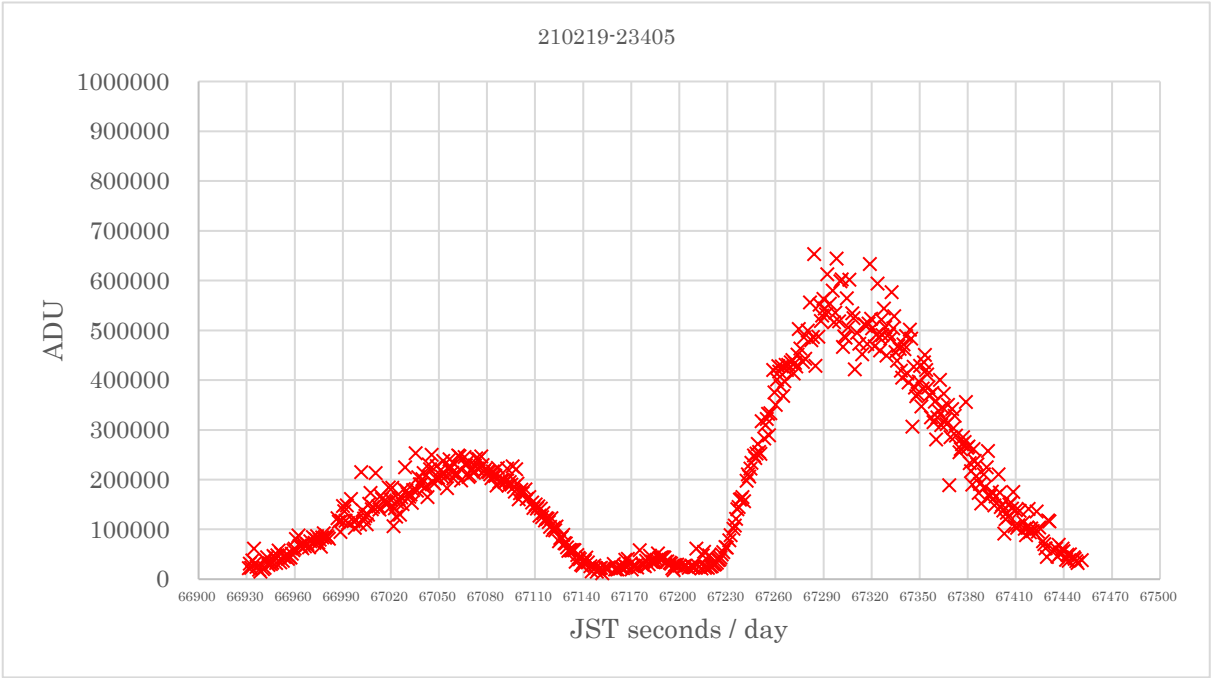
210219-23405
ADU
1000000
900000
800000
700000
600000
500000
400000
300000
200000
100000
0
66900 66930 66960 66990 67020 67050 67080 67110 67140 67170 67200 67230 67260 67290 67320 67350 67380 67410 67440 67470 67500
JST seconds / day

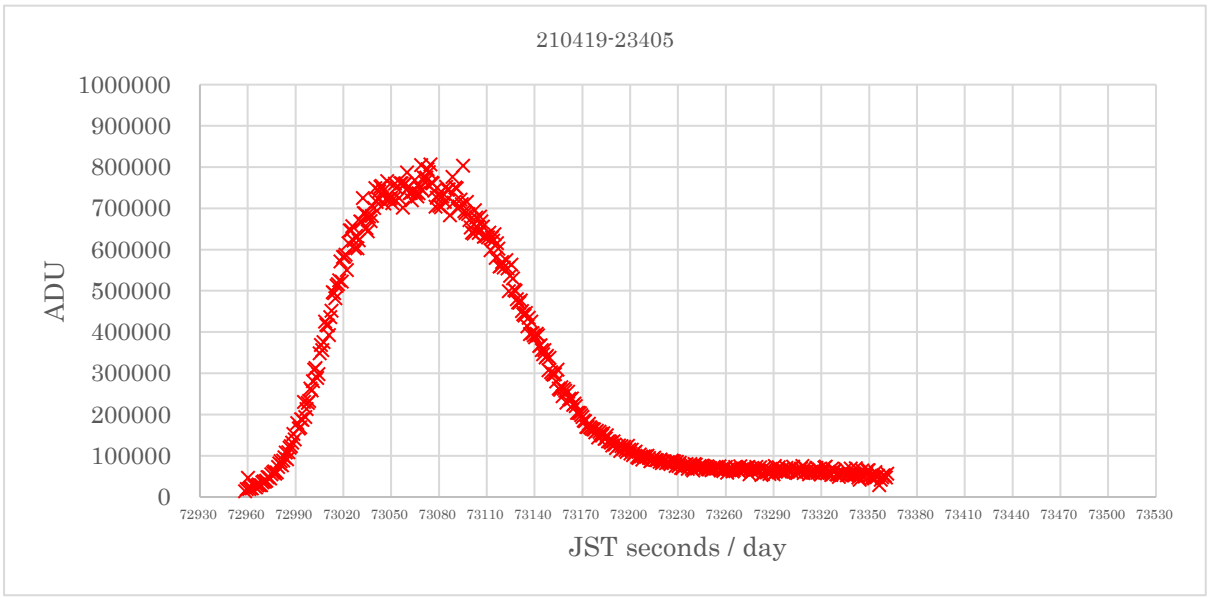
210419-23405
ADU
1000000
900000
800000
700000
600000
500000
400000
300000
200000
100000
0
72930 72960 72990 73020 73050 73080 73110 73140 73170 73200 73230 73260 73290 73320 73350 73380 73410 73440 73470 73500 73530
JST seconds / day

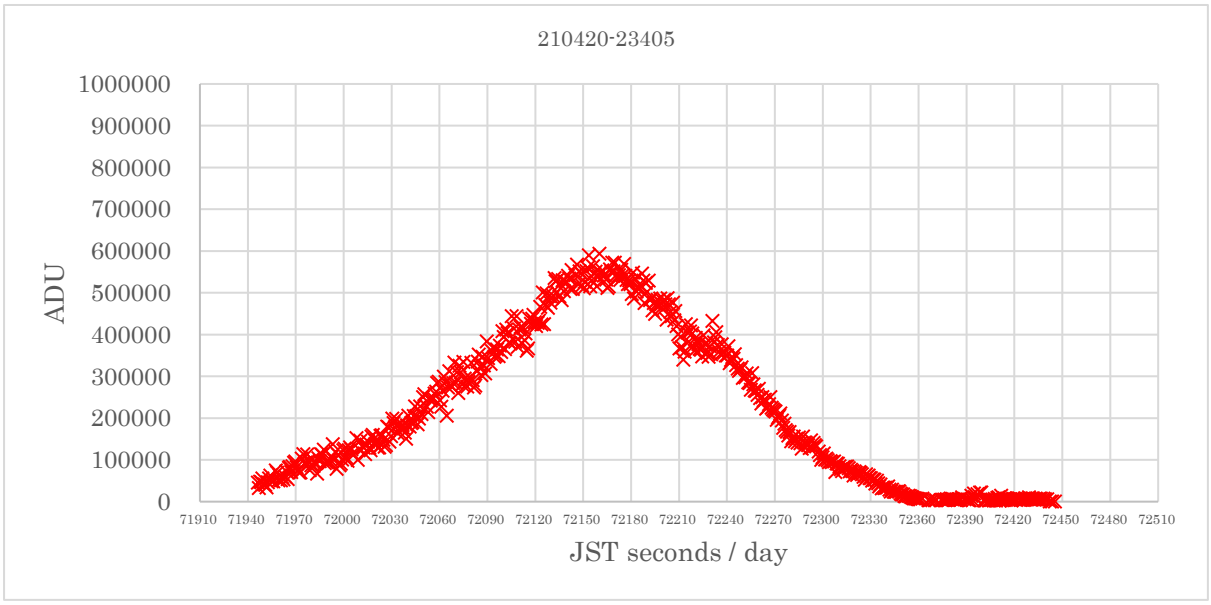
210420-23405
ADU
1000000
900000
800000
700000
600000
500000
400000
300000
200000
100000
0
71910 71940 71970 72000 72030 72060 72090 72120 72150 72180 72210 72240 72270 72300 72330 72360 72390 72420 72450 72480 72510
JST seconds / day

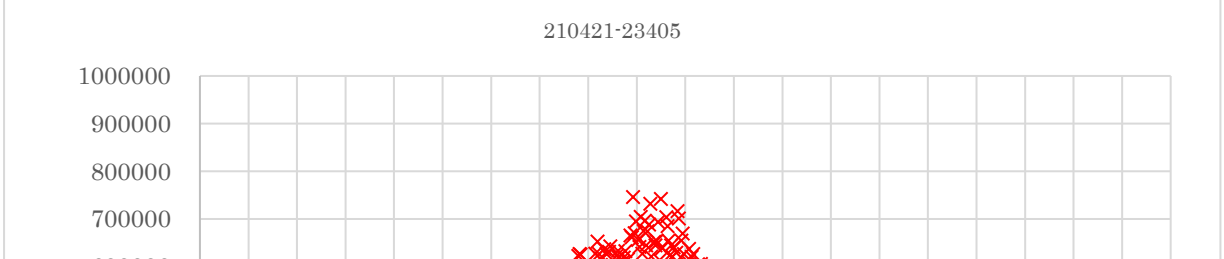
210421-23405
1000000
900000
800000
700000

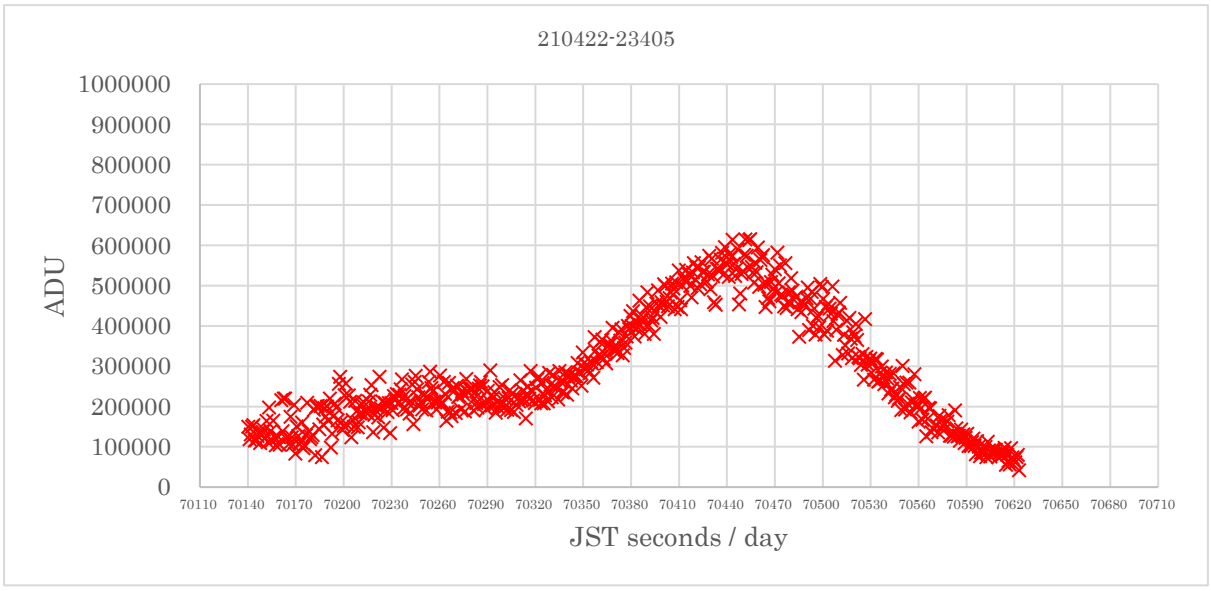
210422-23405
ADU
1000000
900000
800000
700000
600000
500000
400000
300000
200000
100000
0
70110 70140 70170 70200 70230 70260 70290 70320 70350 70380 70410 70440 70470 70500 70530 70560 70590 70620 70650 70680 70710
JST seconds / day

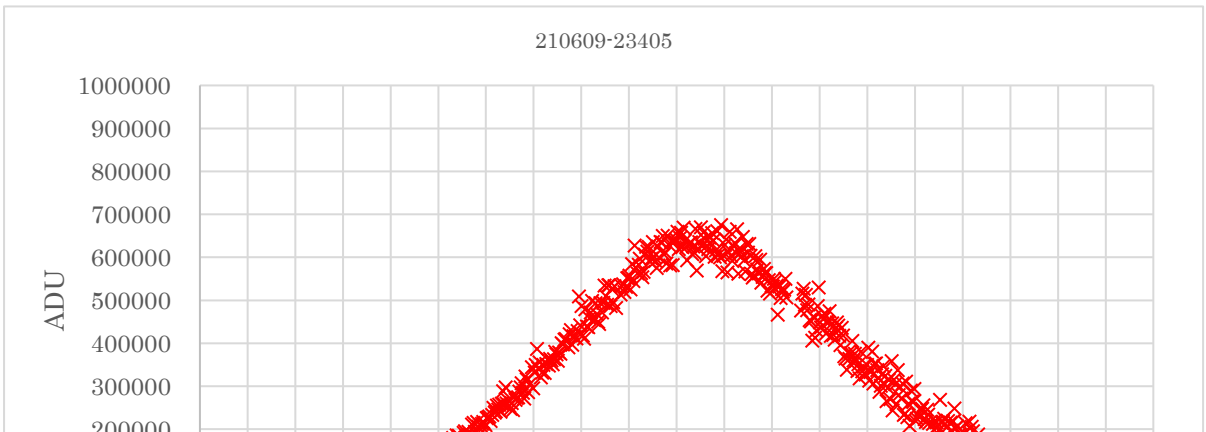
210609-23405
ADU
1000000
900000
800000
700000
600000
500000
400000
300000

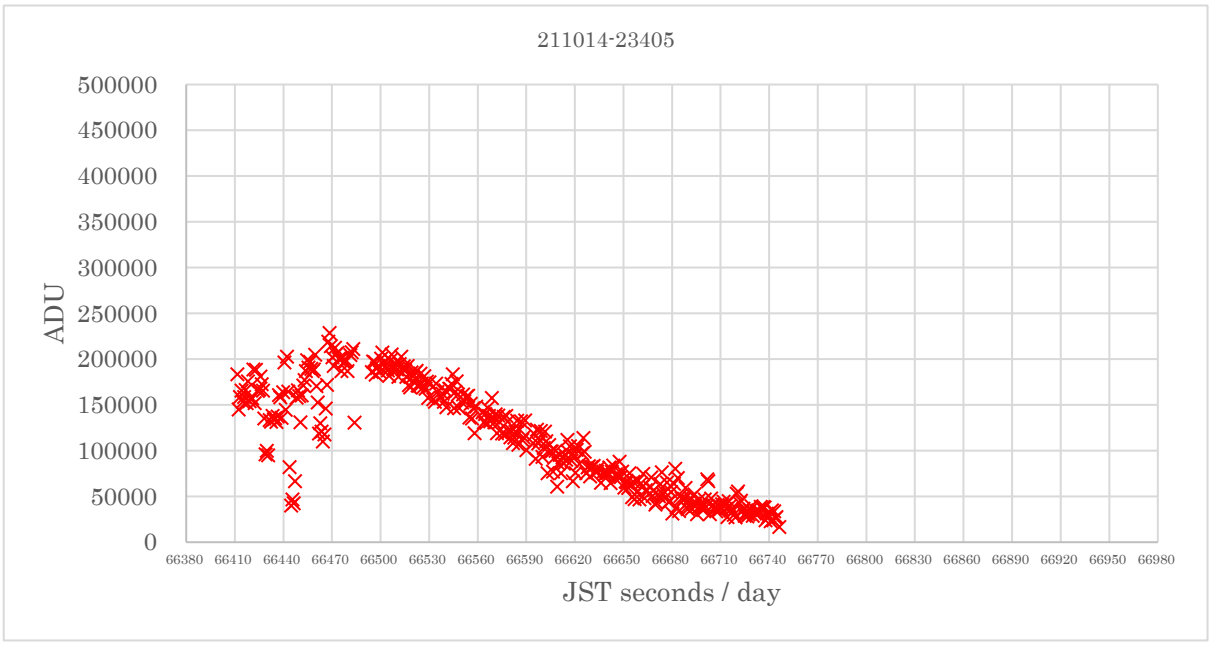
211014-23405
ADU
500000
450000
400000
350000
300000
250000
200000
150000
100000
50000
0
66380 66410 66440 66470 66500 66530 66560 66590 66620 66650 66680 66710 66740 66770 66800 66830 66860 66890 66920 66950 66980
JST seconds / day

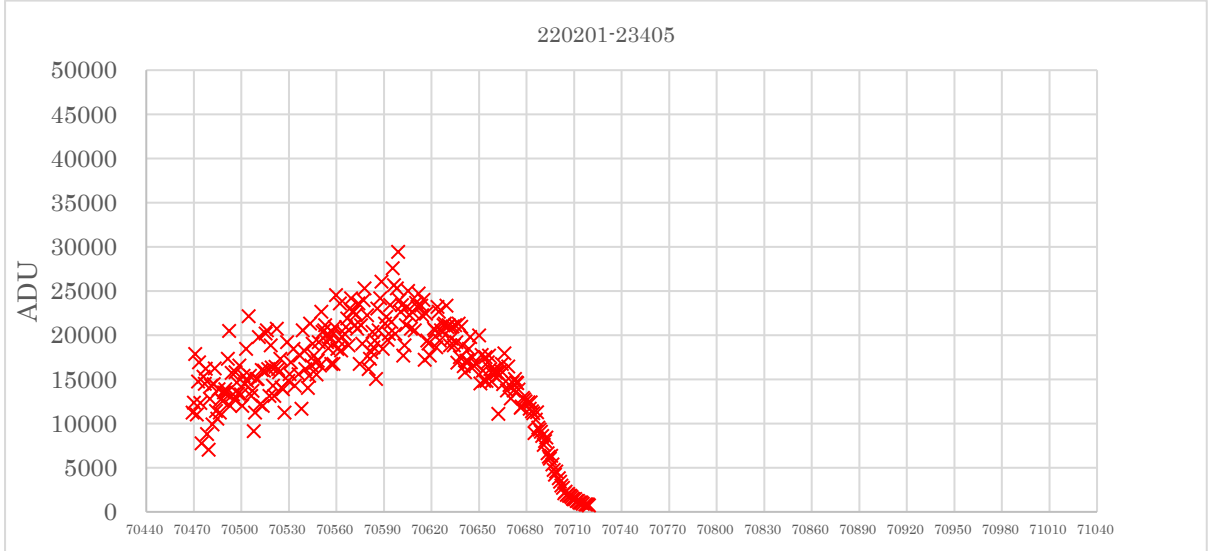
220201-23405
ADU
50000
45000
40000
35000
30000
25000
20000
15000
10000
5000
0
70440 70470 70500 70530 70560 70590 70620 70650 70680 70710 70740 70770 70800 70830 70860 70890 70920 70950 70980 71010 71040

3.4.5 Norad 39198

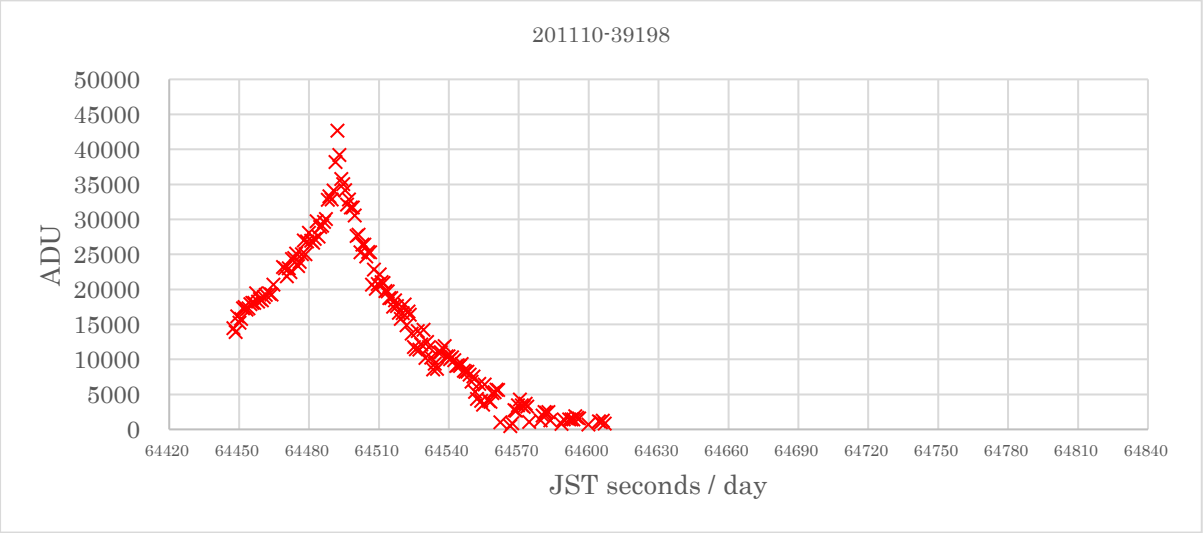

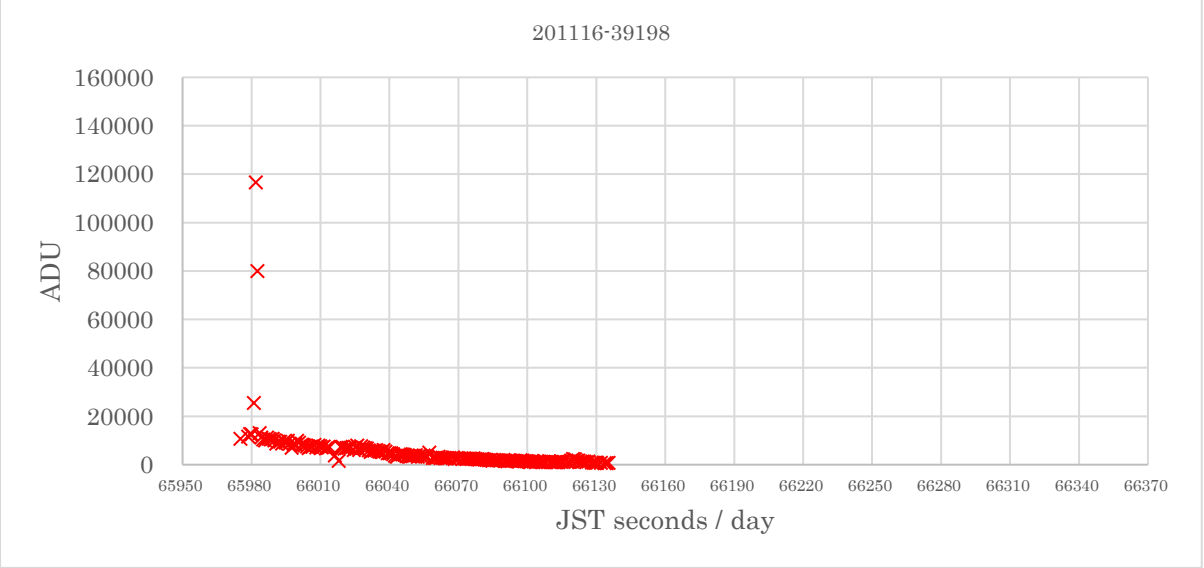

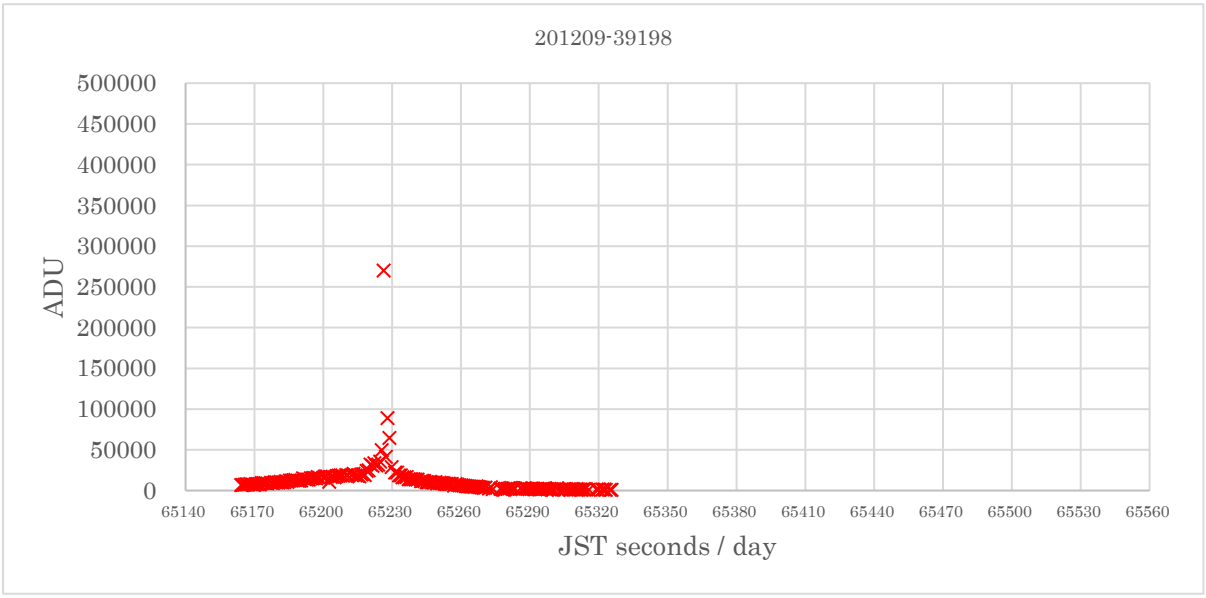
201209-39198
500000
450000
400000
350000
300000
250000
200000
150000
100000
50000
0
ADU
65140
65170
65200
65230
65260
65290
65320
65350
65380
65410
65440
65470
65500
65530
65560
JST seconds / day

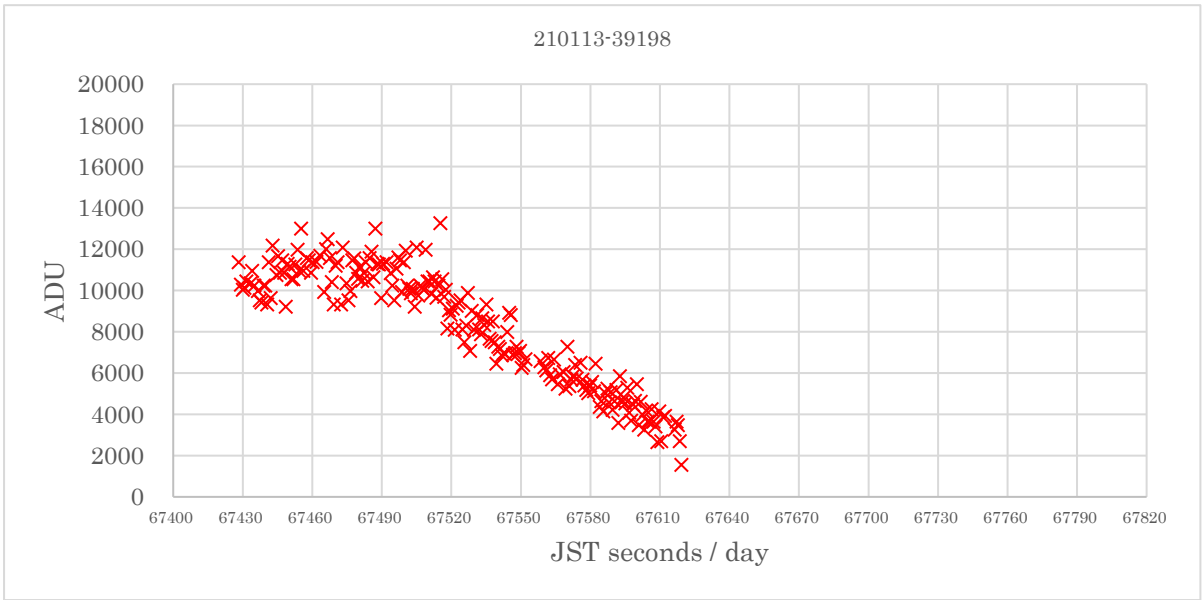
210113-39198
20000
18000
16000
14000
12000
10000
8000
6000
4000
2000
0
ADU
67400
67430
67460
67490
67520
67550
67580
67610
67640
67670
67700
67730
67760
67790
67820
JST seconds / day

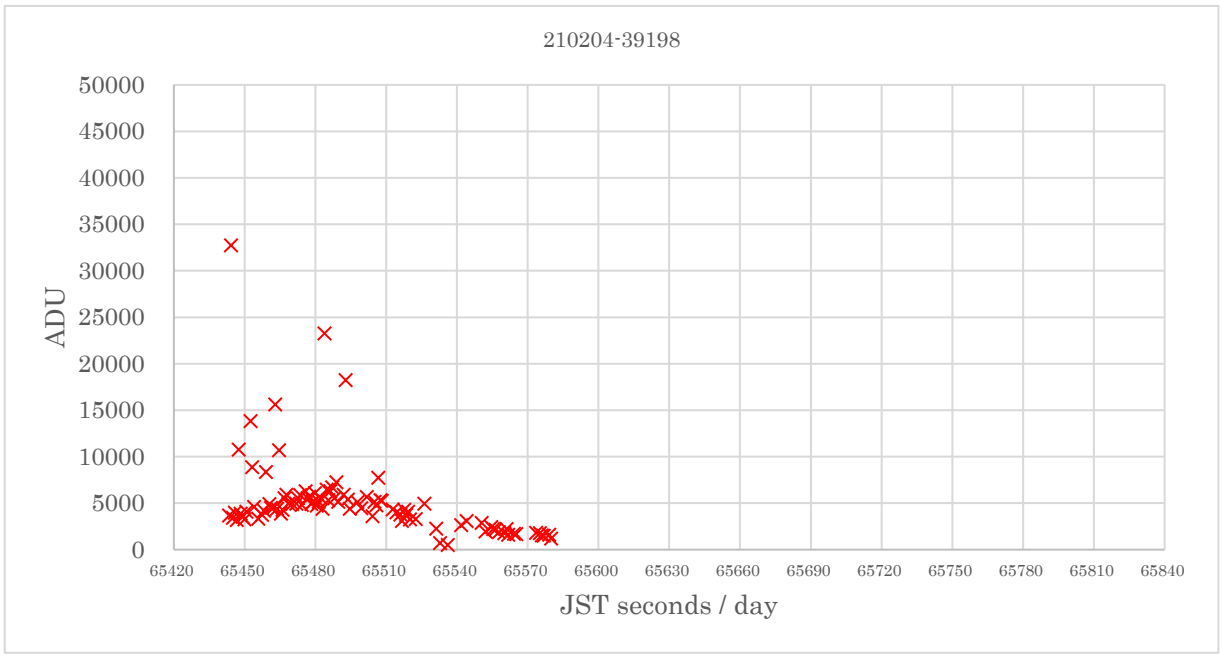
210204-39198
ADU
50000
45000
40000
35000
30000
25000
20000
15000
10000
5000
0
65420
65450
65480
65510
65540
65570
65600
65630
65660
65690
65720
65750
65780
65810
65840
JST seconds / day

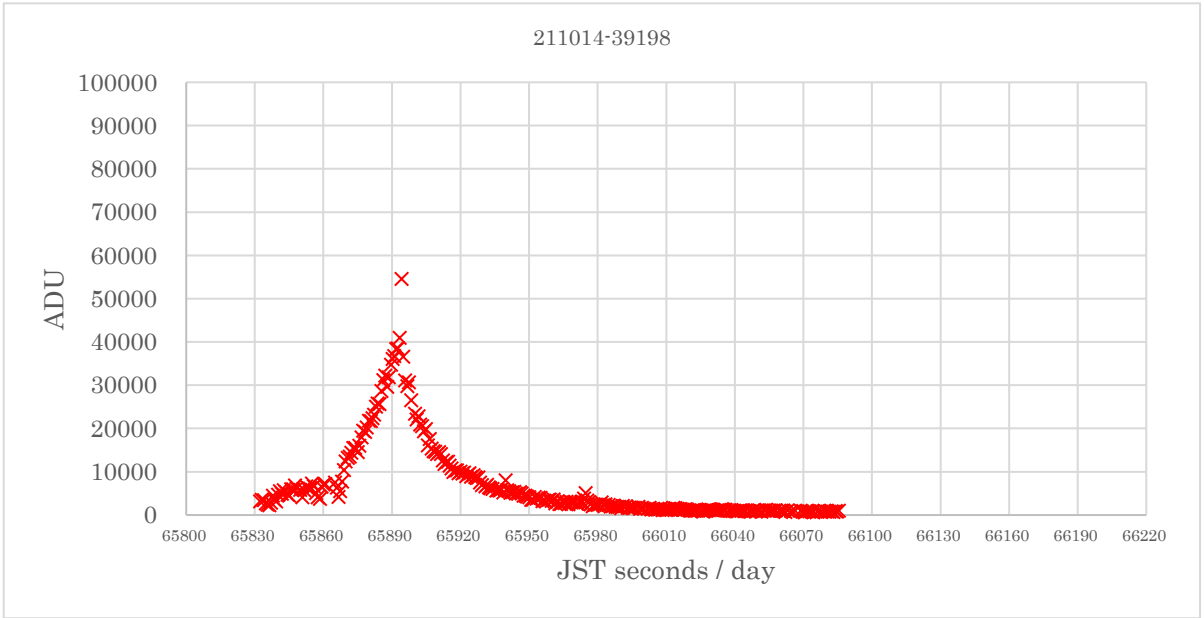
211014-39198
ADU
100000
90000
80000
70000
60000
50000
40000
30000
20000
10000
0
65800
65830
65860
65890
65920
65950
65980
66010
66040
66070
66100
66130
66160
66190
66220
JST seconds / day

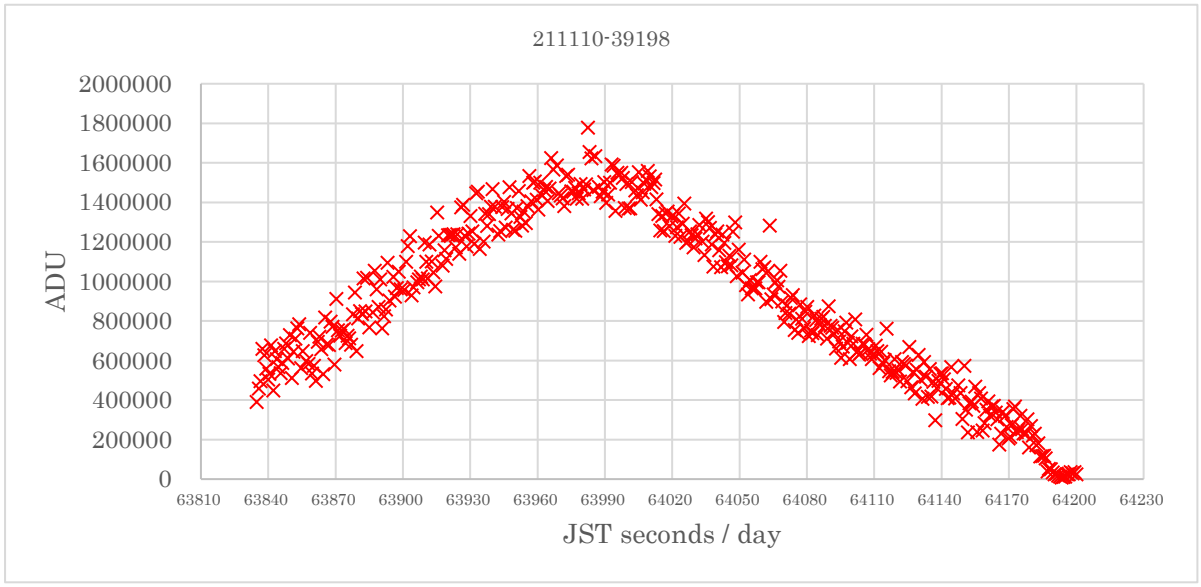
211110-39198
2000000
1800000
1600000
1400000
1200000
1000000
800000
600000
400000
200000
0
ADU
63810
63840
63870
63900
63930
63960
63990
64020
64050
64080
64110
64140
64170
64200
64230
JST seconds / day

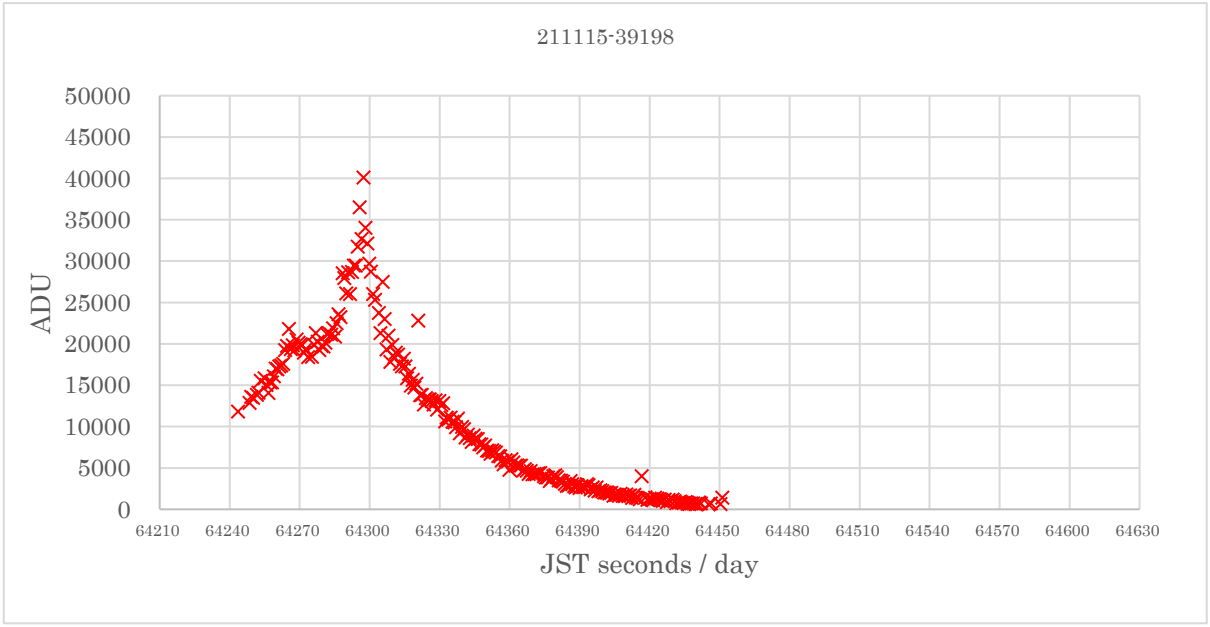
211115-39198
50000
45000
40000
35000
30000
25000
20000
15000
10000
5000
0
ADU
64210
64240
64270
64300
64330
64360
64390
64420
64450
64480
64510
64540
64570
64600
64630
JST seconds / day

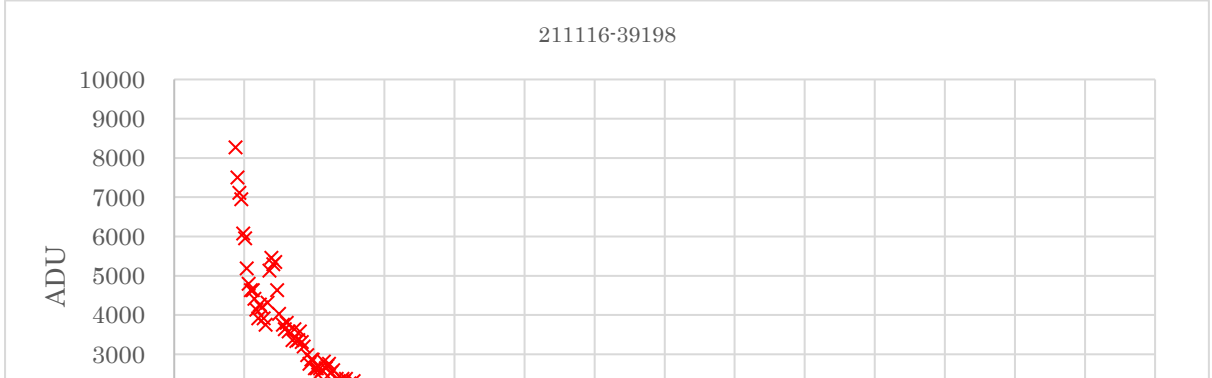
211116-39198
10000
9000
8000
7000
6000
5000
4000
3000
ADU

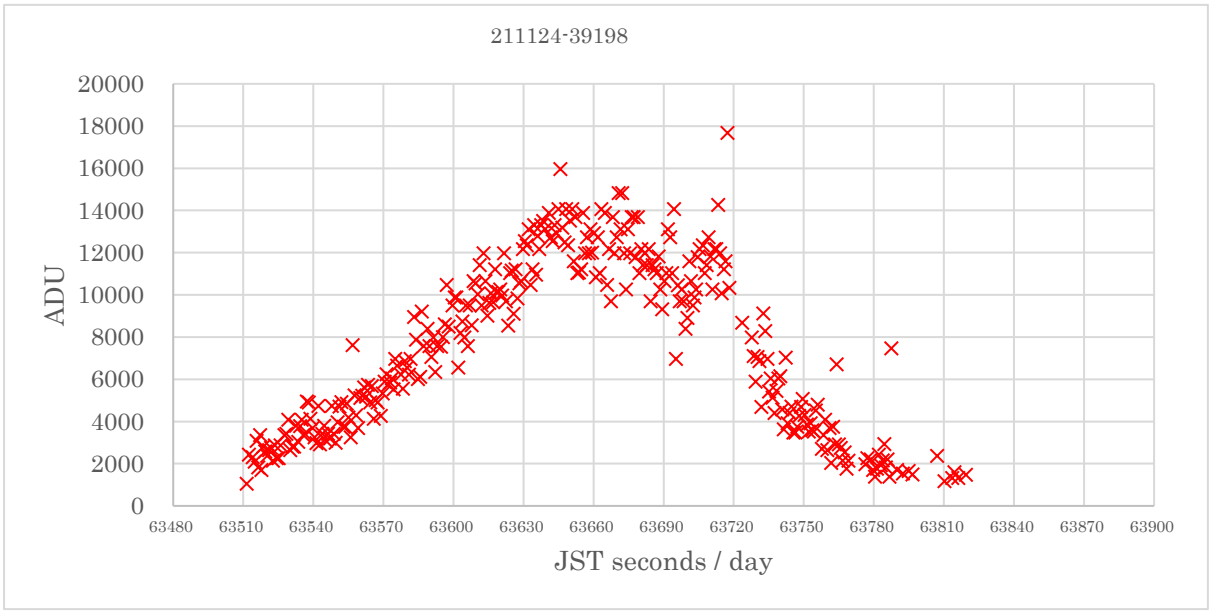
211124-39198
ADU
20000
18000
16000
14000
12000
10000
8000
6000
4000
2000
0
63480
63510
63540
63570
63600
63630
63660
63690
63720
63750
63780
63810
63840
63870
63900
JST seconds / day

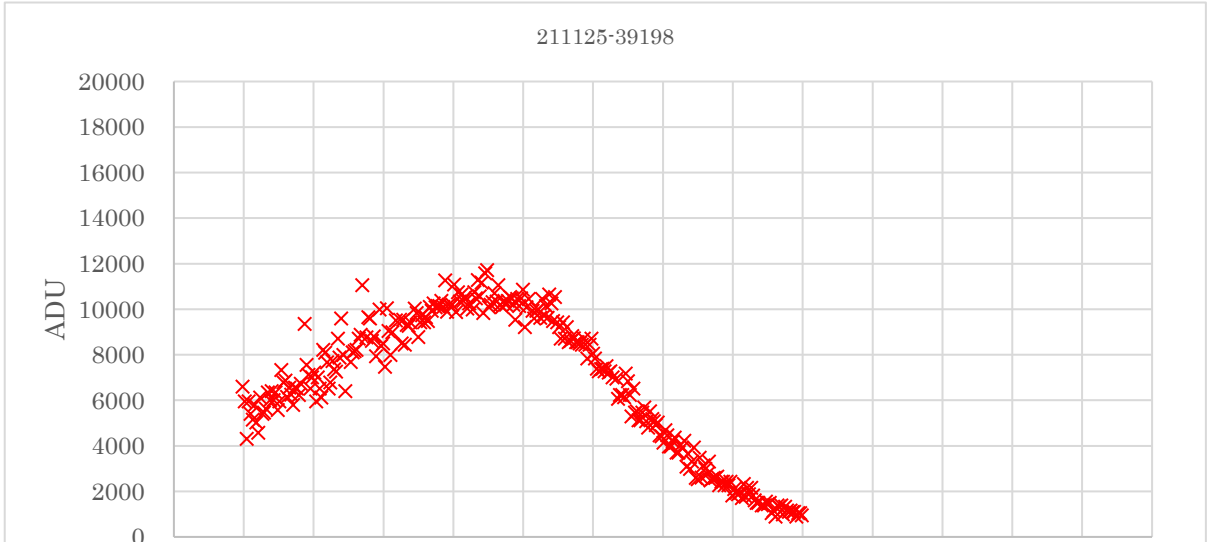
211125-39198
ADU
20000
18000
16000
14000
12000
10000
8000
6000
4000
2000
0

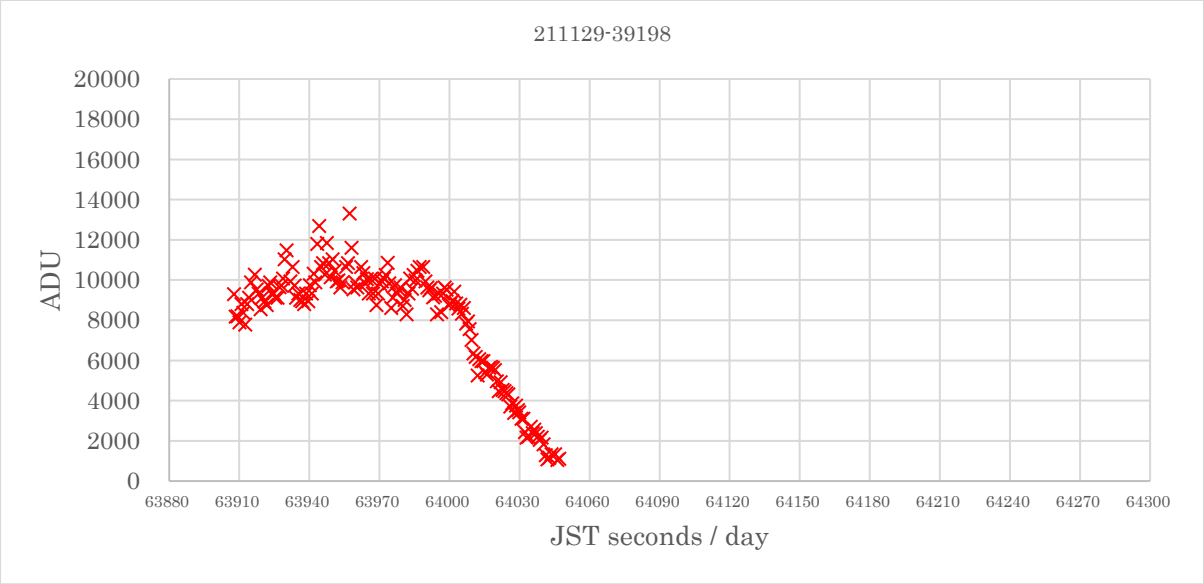
211129-39198
20000
18000
16000
14000
12000
10000
8000
6000
4000
2000
0
ADU
63880
63910
63940
63970
64000
64030
64060
64090
64120
64150
64180
64210
64240
64270
64300
JST seconds / day

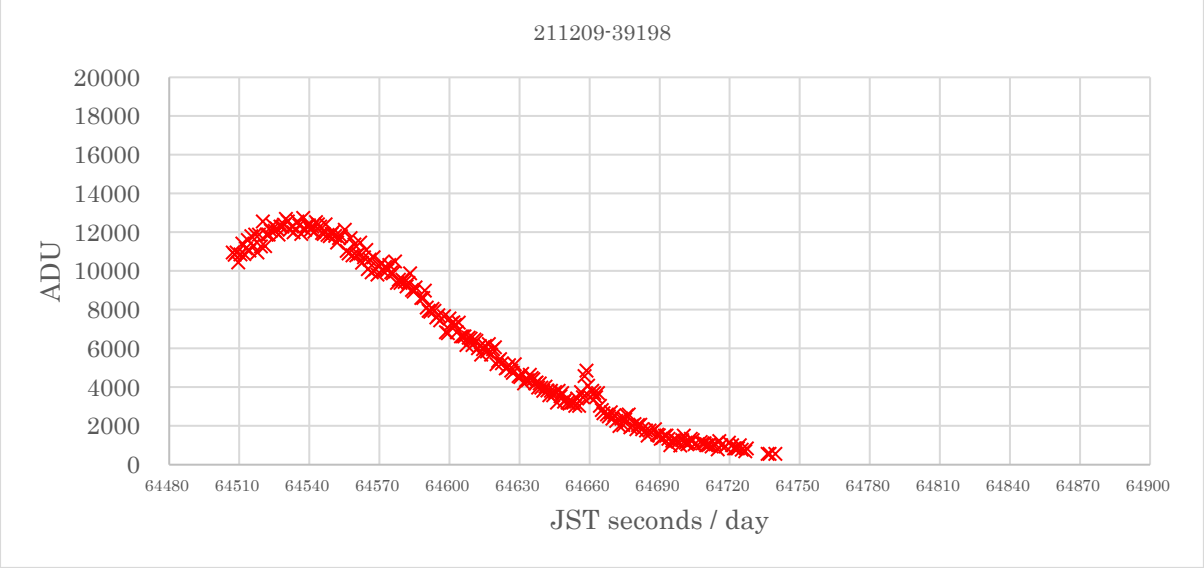
211209-39198
20000
18000
16000
14000
12000
10000
8000
6000
4000
2000
0
ADU
64480
64510
64540
64570
64600
64630
64660
64690
64720
64750
64780
64810
64840
64870
64900
JST seconds / day

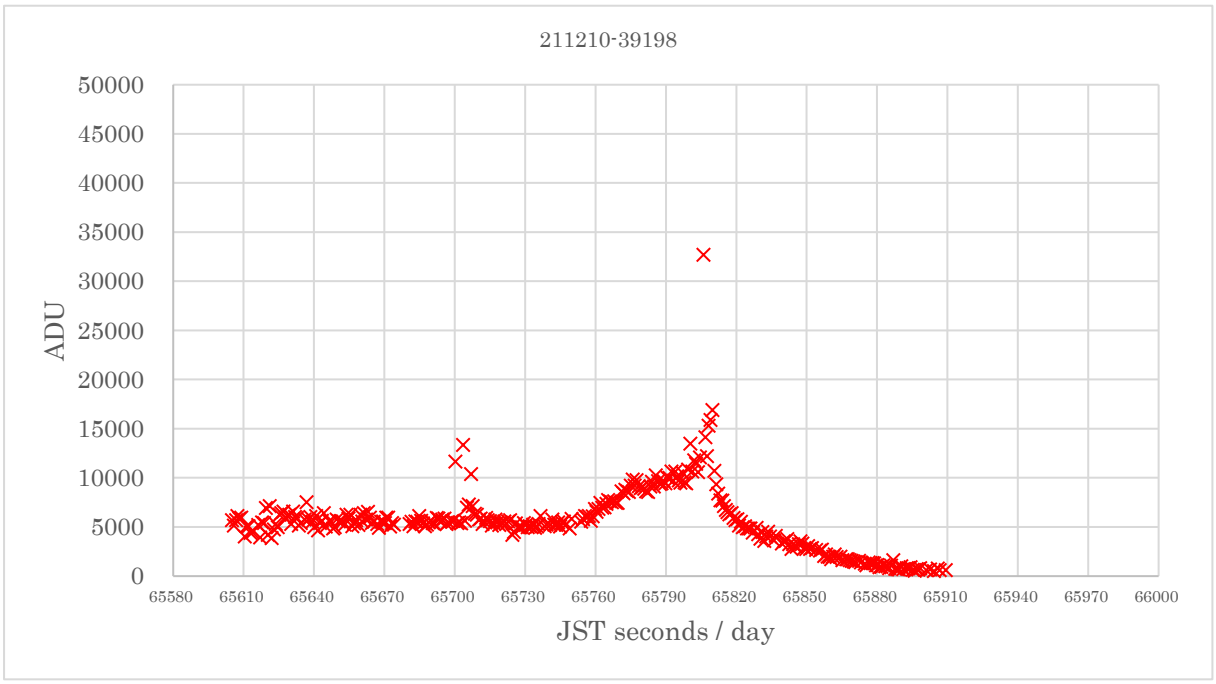
211210-39198
50000
45000
40000
35000
30000
25000
20000
15000
10000
5000
0
ADU
65580
65610
65640
65670
65700
65730
65760
65790
65820
65850
65880
65910
65940
65970
66000
JST seconds / day

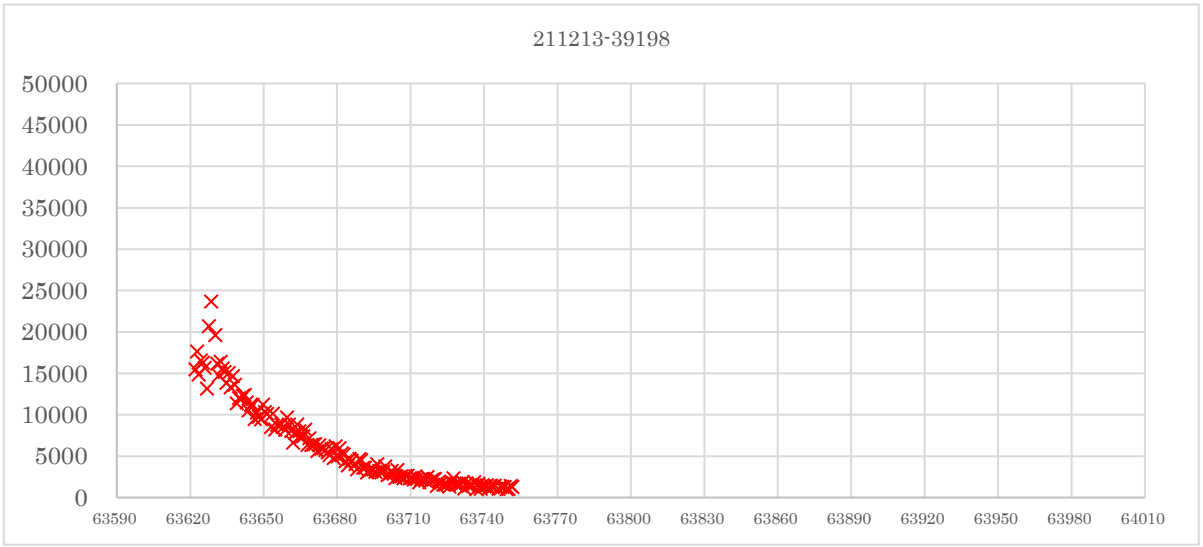
211213-39198
50000
45000
40000
35000
30000
25000
20000
15000
10000
5000
0
63590
63620
63650
63680
63710
63740
63770
63800
63830
63860
63890
63920
63950
63980
64010

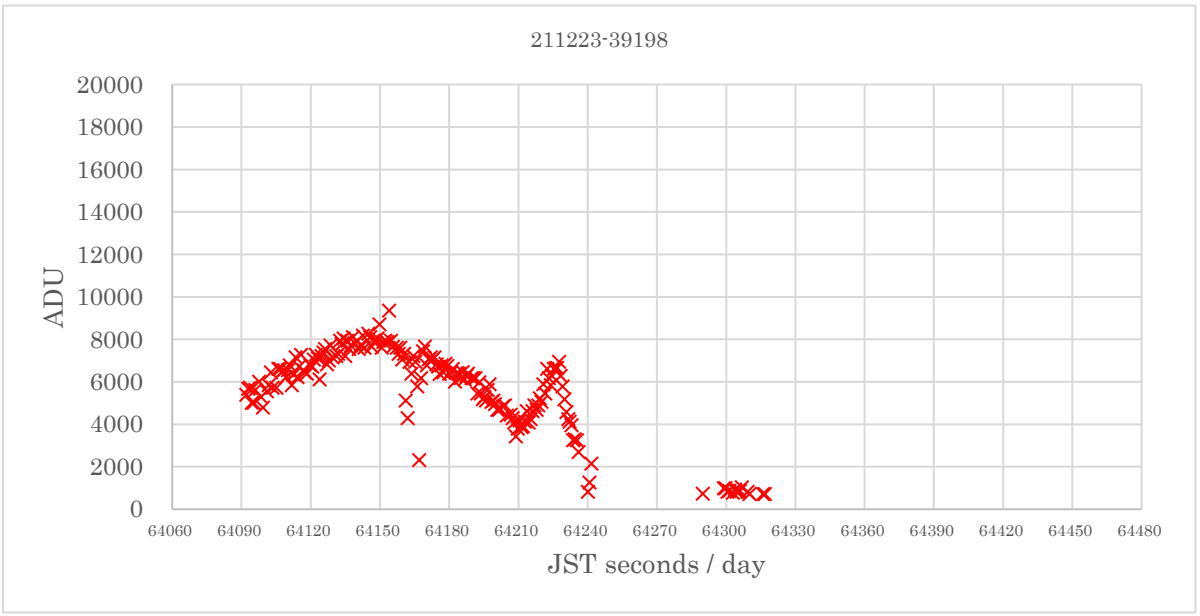
211223-39198
ADU
20000
18000
16000
14000
12000
10000
8000
6000
4000
2000
0
64060
64090
64120
64150
64180
64210
64240
64270
64300
64330
64360
64390
64420
64450
64480
JST seconds / day

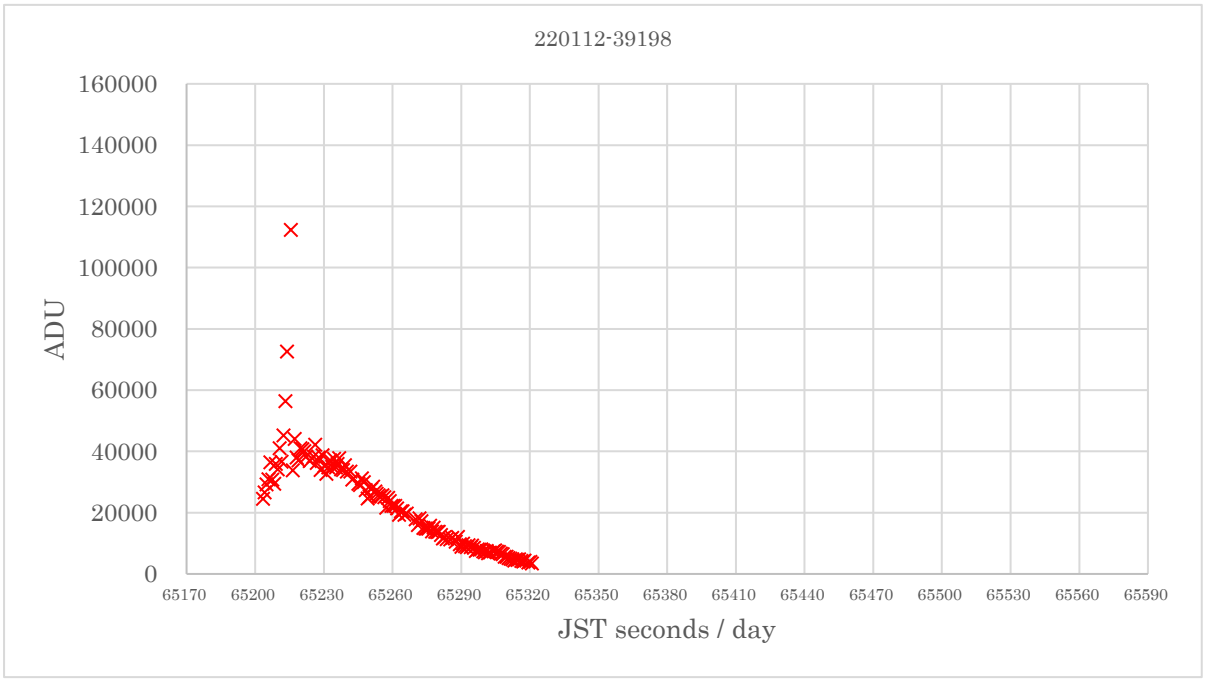
220112-39198
ADU
160000
140000
120000
100000
80000
60000
40000
20000
0
65170
65200
65230
65260
65290
65320
65350
65380
65410
65440
65470
65500
65530
65560
65590
JST seconds / day

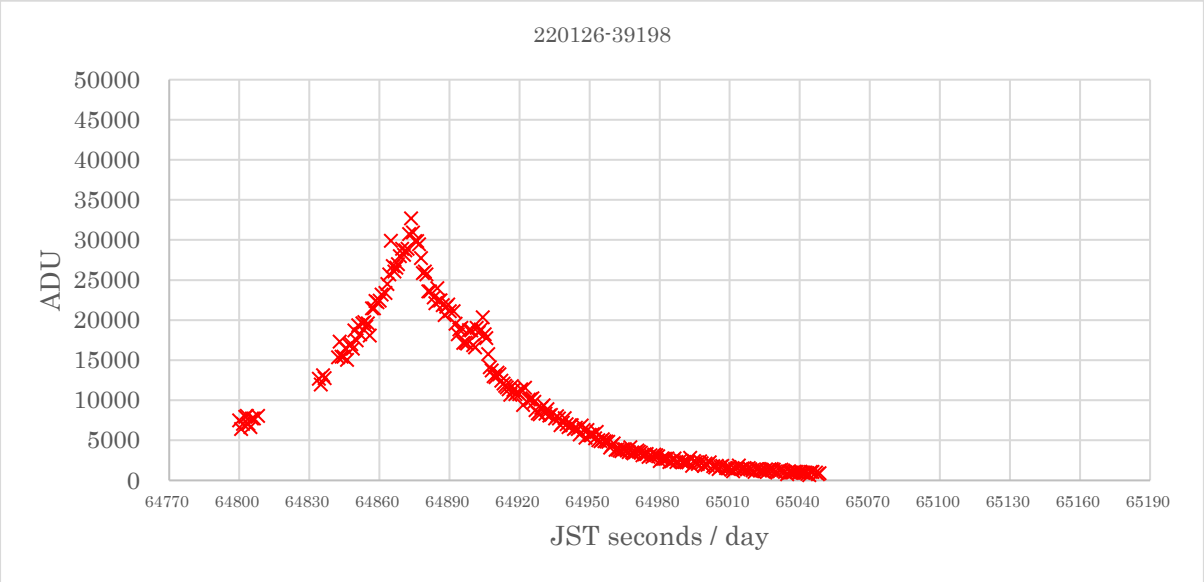

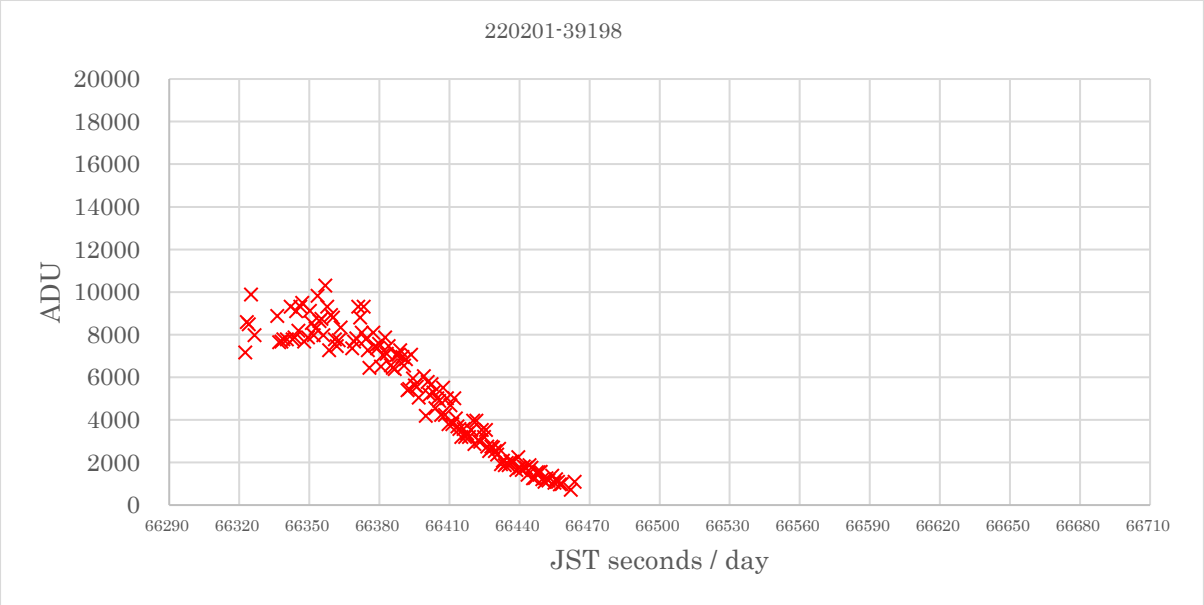

3.4.6 Norad 41847

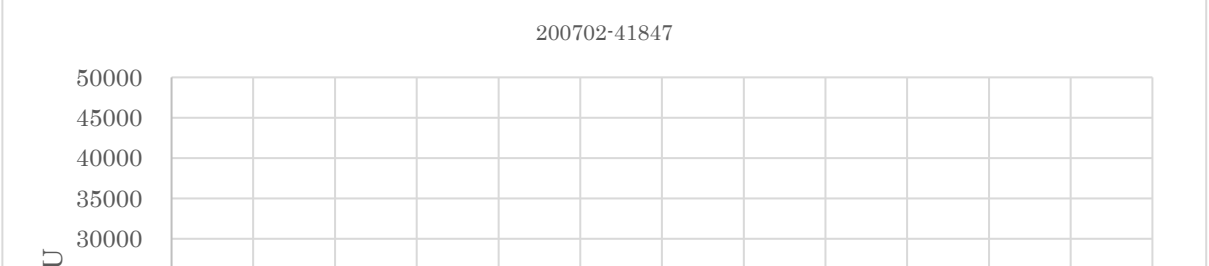

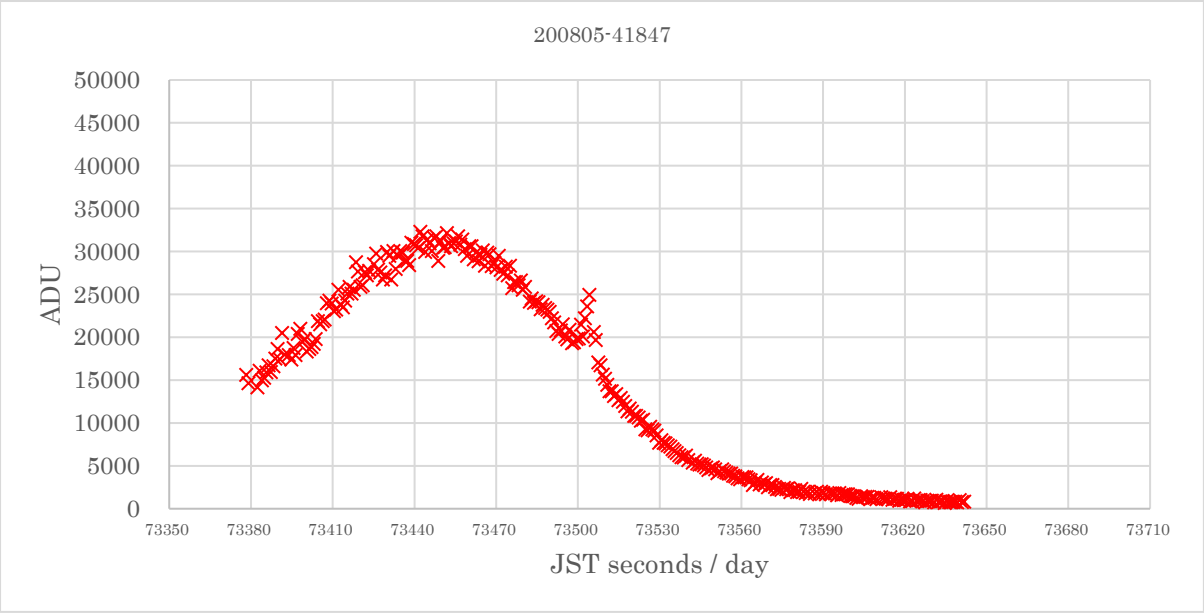
200805-41847
50000
45000
40000
35000
30000
25000
20000
15000
10000
5000
0
ADU
73350
73380
73410
73440
73470
73500
73530
73560
73590
73620
73650
73680
73710
JST seconds / day

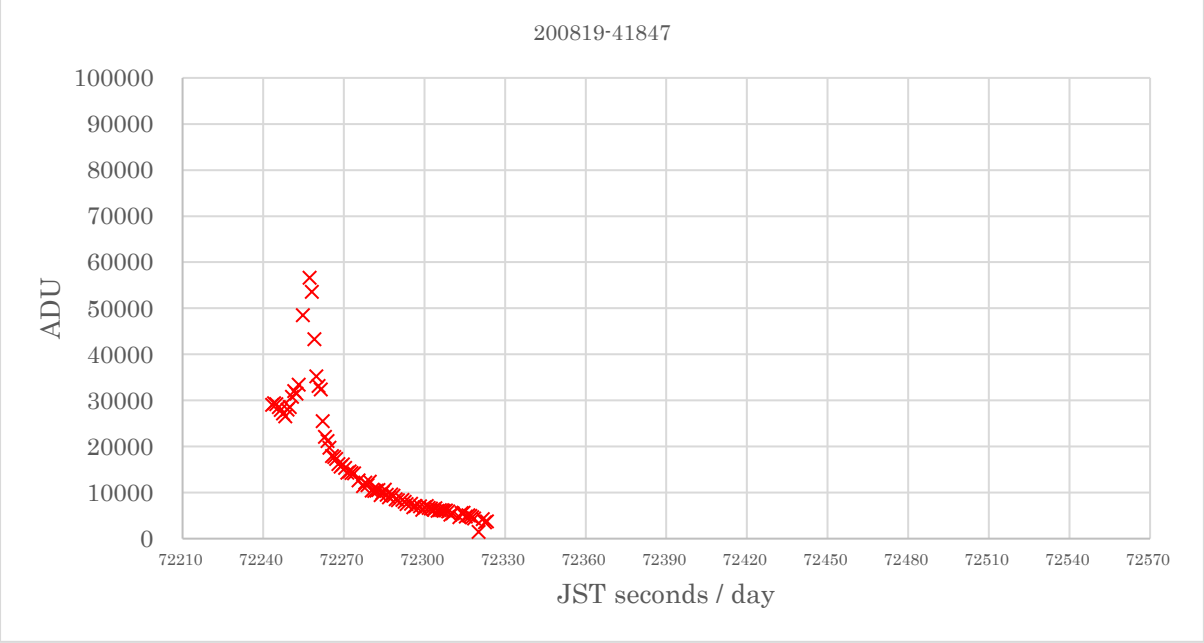
200819-41847
100000
90000
80000
70000
60000
50000
40000
30000
20000
10000
0
ADU
72210
72240
72270
72300
72330
72360
72390
72420
72450
72480
72510
72540
72570
JST seconds / day

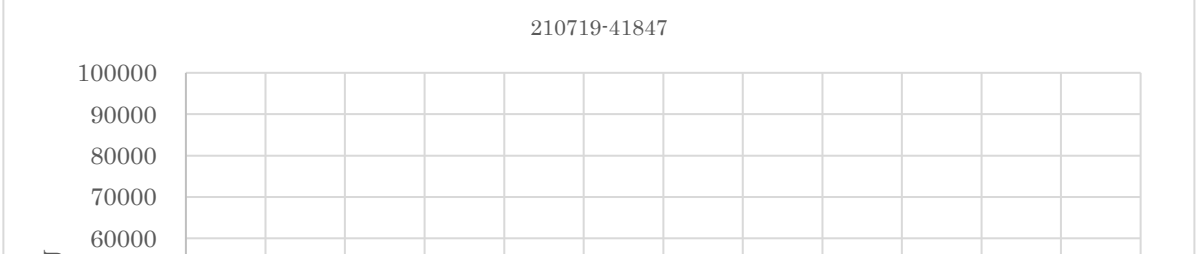
210719-41847
100000
90000
80000
70000
60000

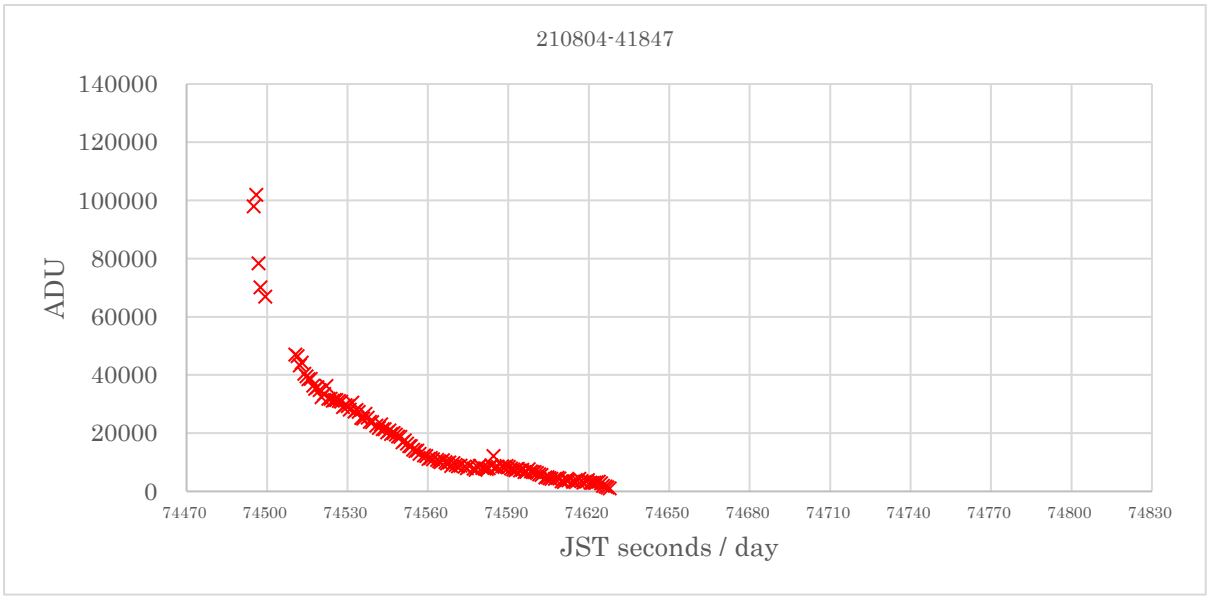
210804-41847
140000
120000
100000
80000
60000
40000
20000
0
ADU
74470
74500
74530
74560
74590
74620
74650
74680
74710
74740
74770
74800
74830
JST seconds / day

3.5 Lightcurve graphs from SSAU

3.5.1 Norad 11804

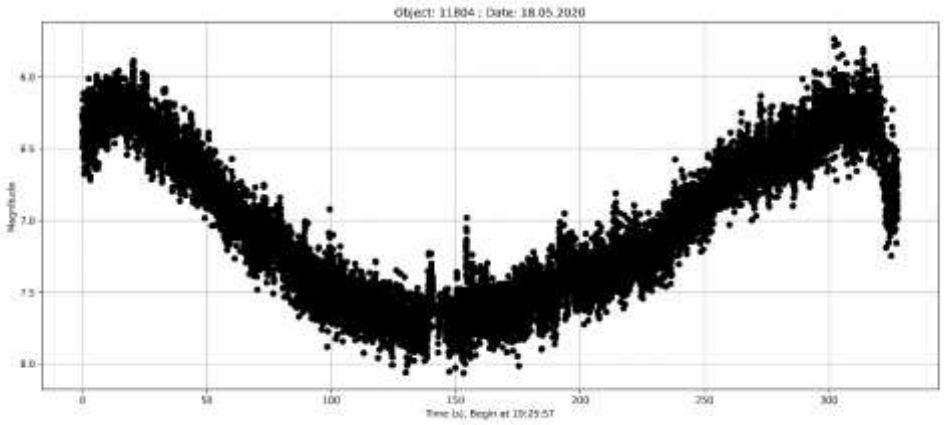

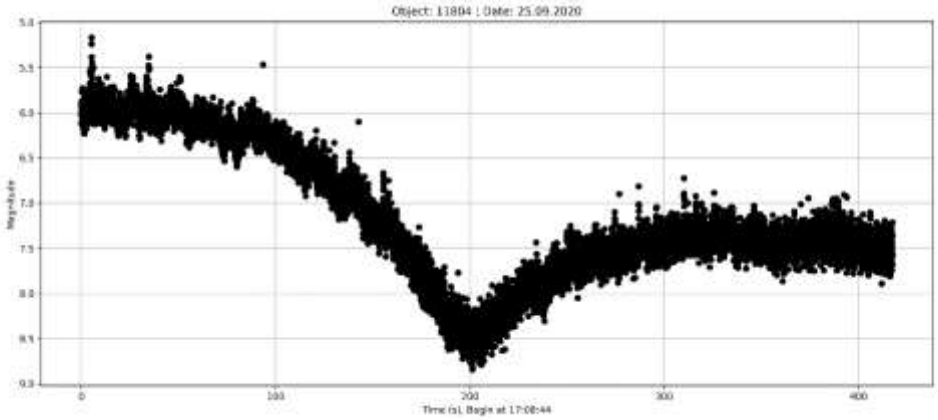

3.5.2 Norad 18340

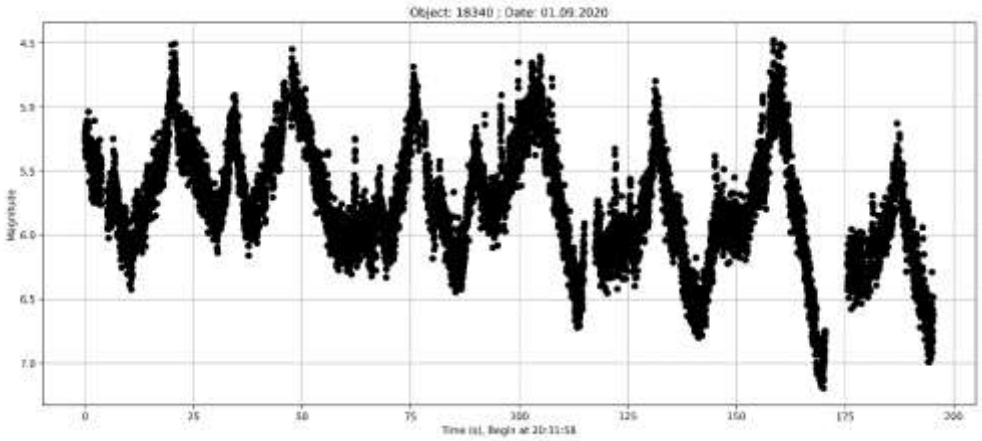

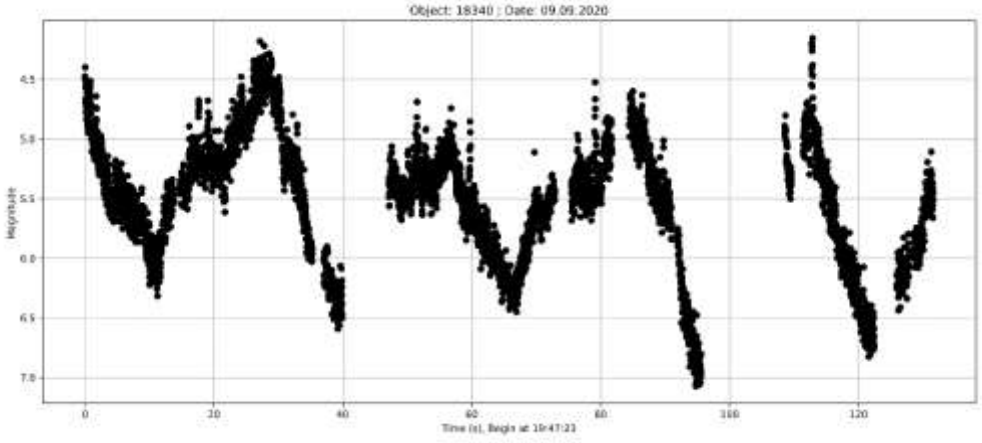

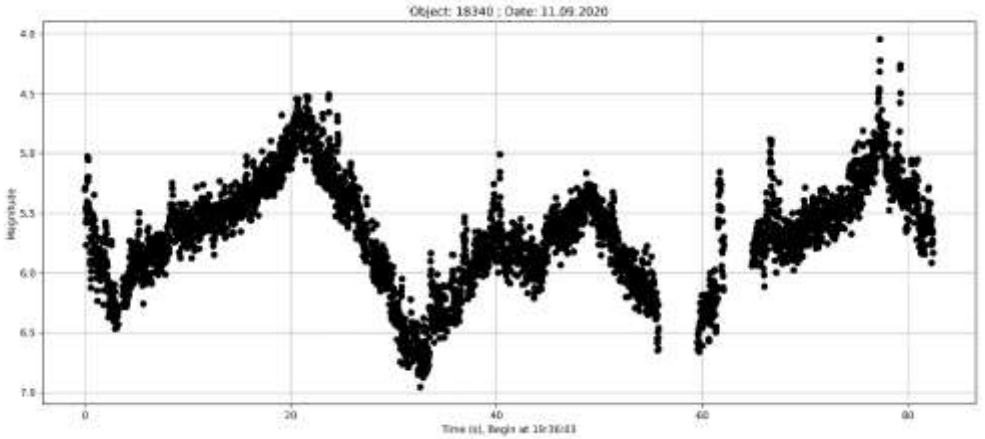
Object: 18340 ; Date: 11.09.2020
Magnitude
Time (s), Begin at 19:30:03

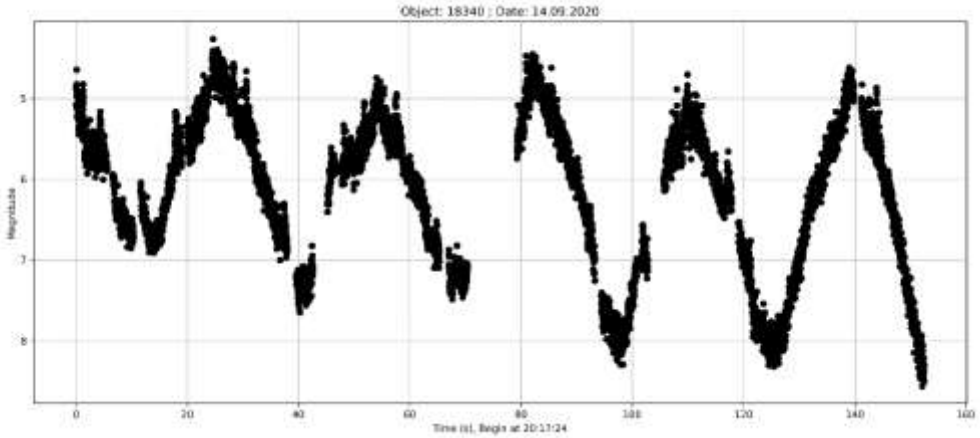
Object: 18340 ; Date: 14.09.2020
Magnitude
Time (s), Begin at 20:17:24

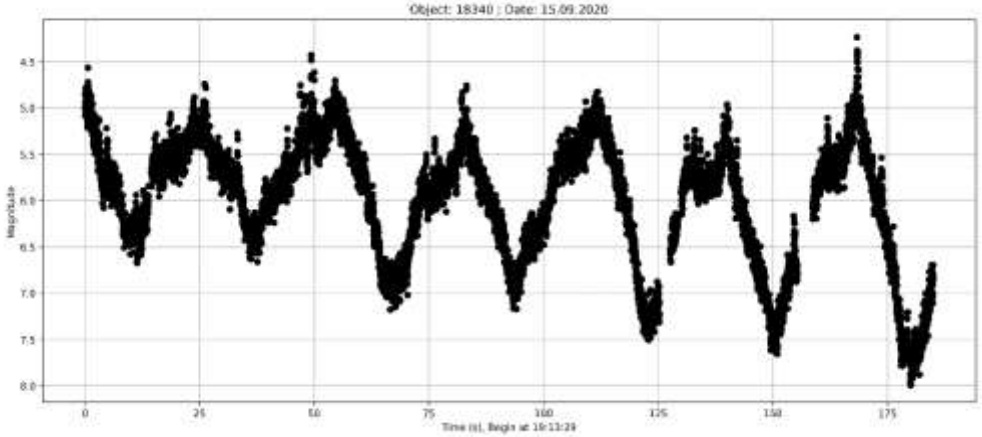
Object: 18340 ; Date: 15.09.2020
Magnitude
Time (s), Begin at 19:13:29

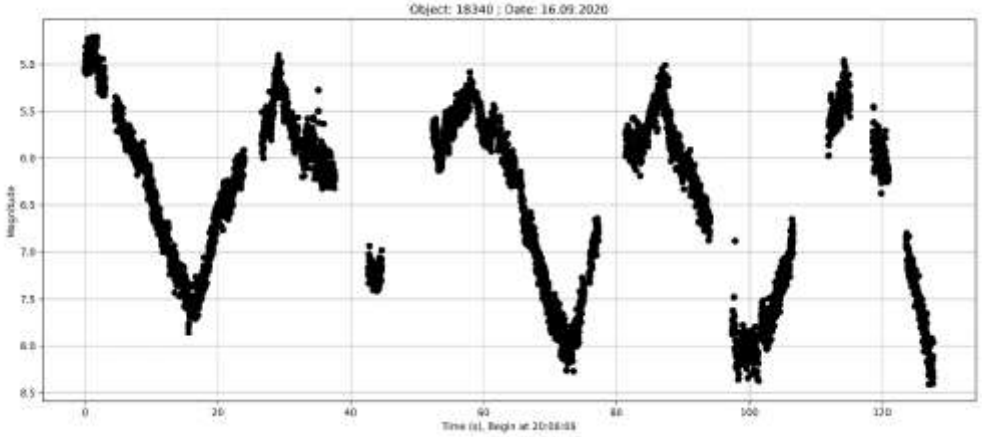
Object: 18340 ; Date: 16.09.2020
Magnitude
Time (s), Begin at 20:08:08

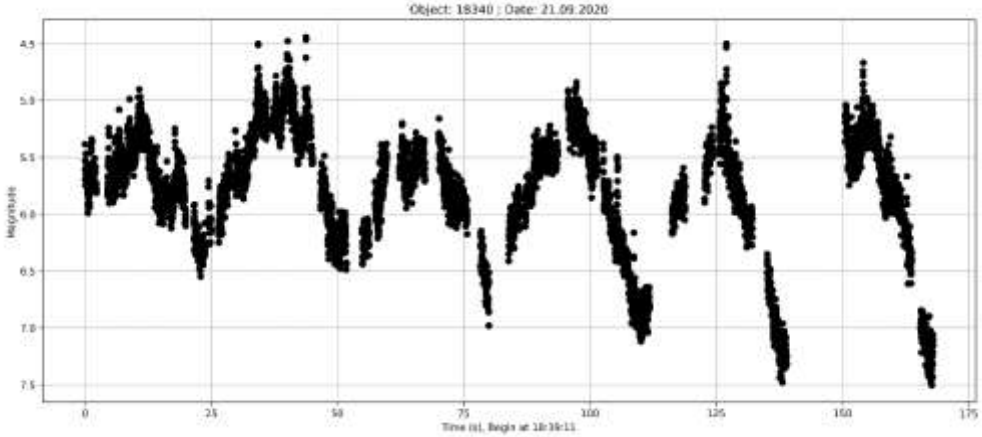
Object: 18340 ; Date: 21.09.2020
Magnitude
Time (s), Begin at 18:39:11

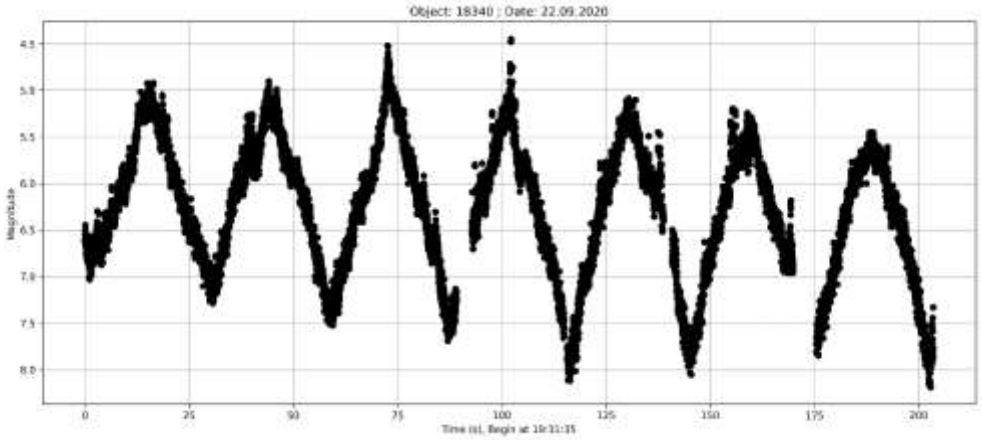
Object: 18340 ; Date: 22.09.2020
Magnitude
Time (s), Begin at 18:11:35

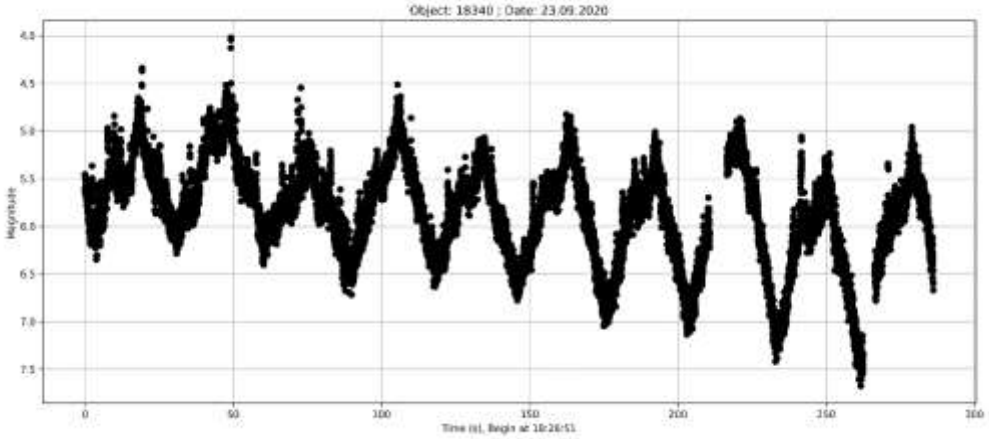
Object: 18340 ; Date: 23.09.2020
Magnitude
Time (s), Begin at 18:26:51

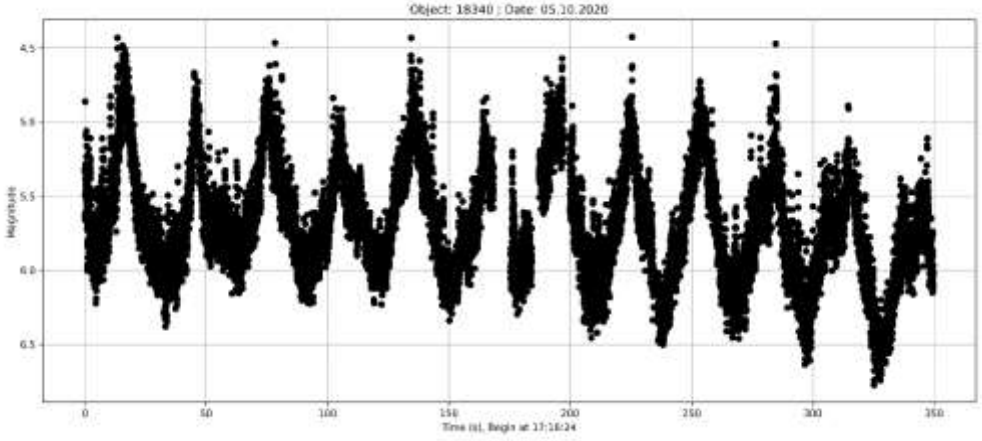
Object: 18340 ; Date: 05.10.2020
Magnitude
Time (s), Begin at 17:16:24

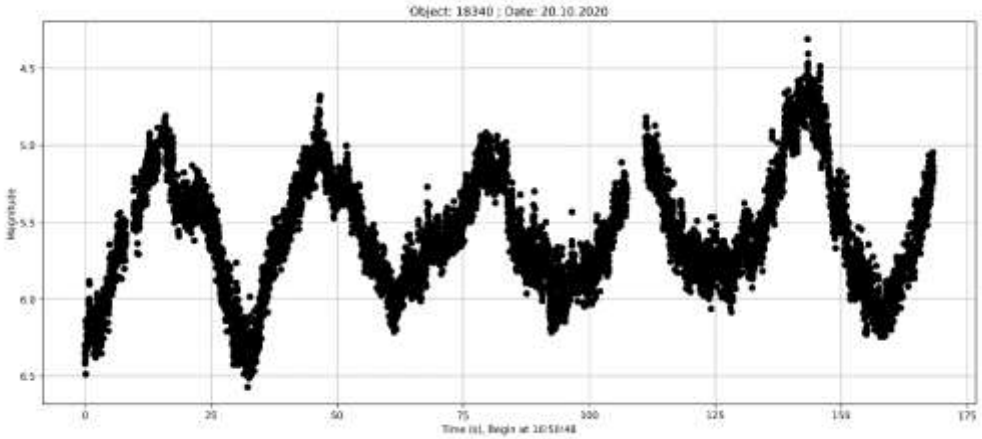
Object: 18340 ; Date: 20.10.2020
Magnitude
4.5
5.0
5.5
6.0
6.5
0
20
50
75
100
125
150
175
Time (s), Begin at 10:50:48

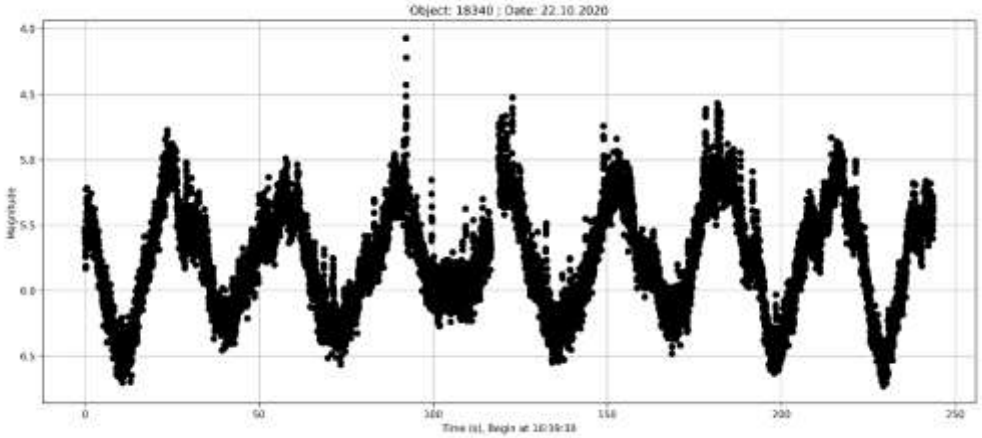
Object: 18340 ; Date: 22.10.2020
Magnitude
4.0
4.5
5.0
5.5
6.0
6.5
0
50
100
150
200
250
Time (s), Begin at 10:59:18

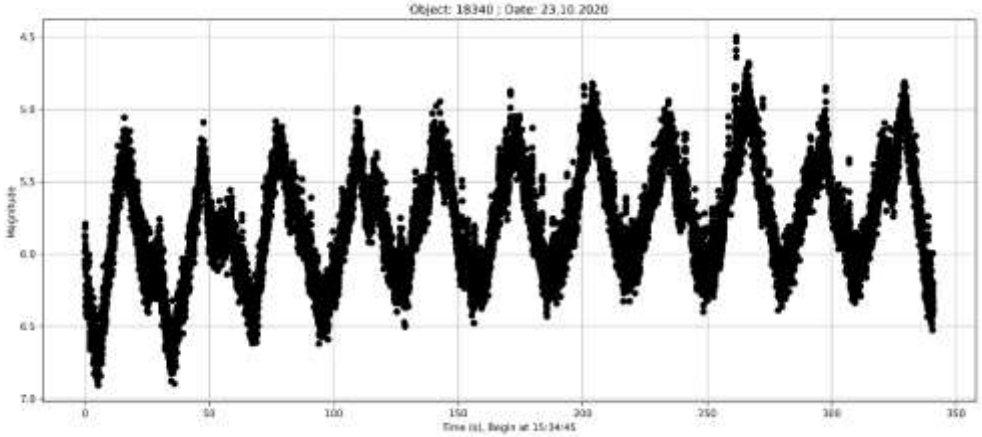
Object: 18340 | Date: 23.10.2020
Magnitude
Time (s), Begin at 15:34:45

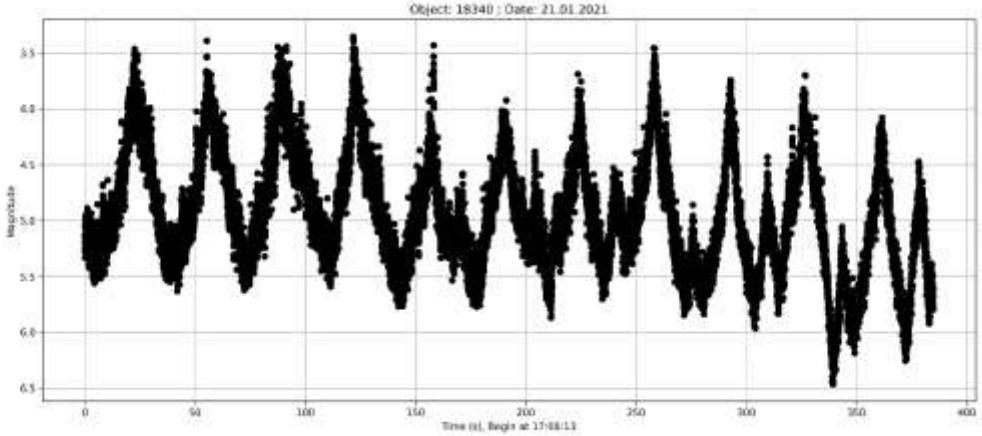
Object: 18340 | Date: 21.01.2021
Magnitude
Time (s), Begin at 17:08:13

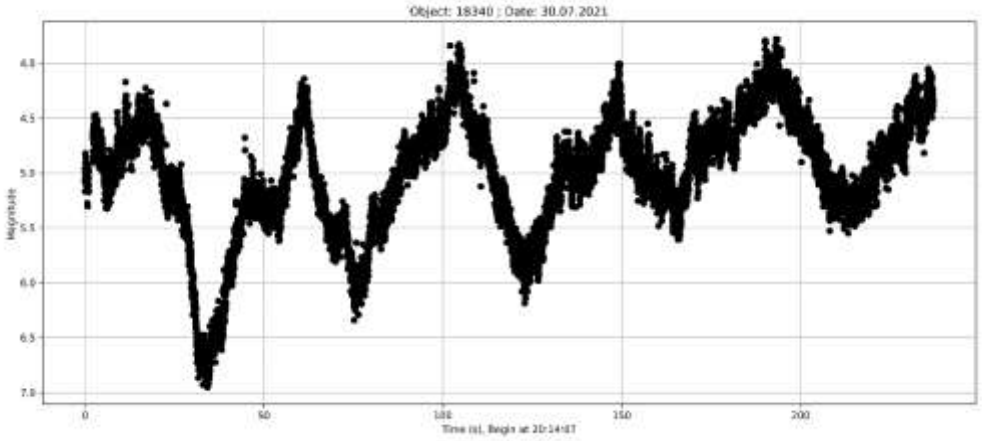
Object: 18340 ; Date: 30.07.2021
Magnitude
4.0
4.5
5.0
5.5
6.0
6.5
7.0
0
50
100
150
200
Time (s), Begin at 20:14:07

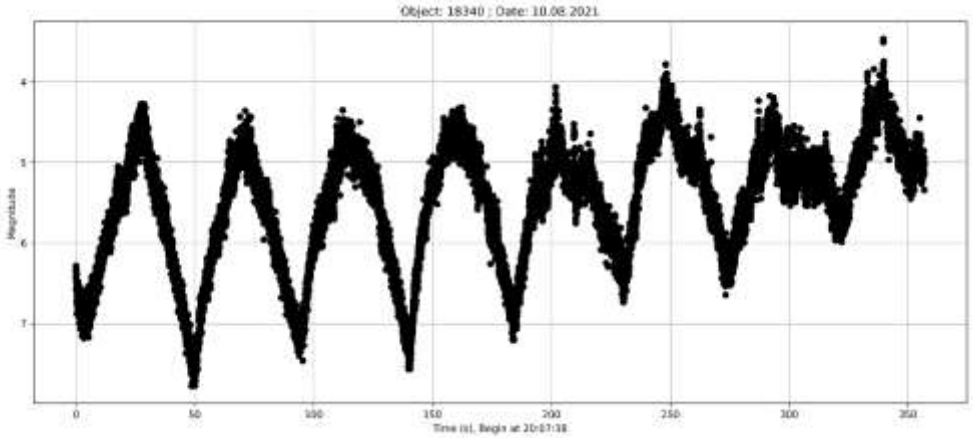
Object: 18340 ; Date: 10.08.2021
Magnitude
4
5
6
7
0
50
100
150
200
250
300
350
Time (s), Begin at 20:17:18

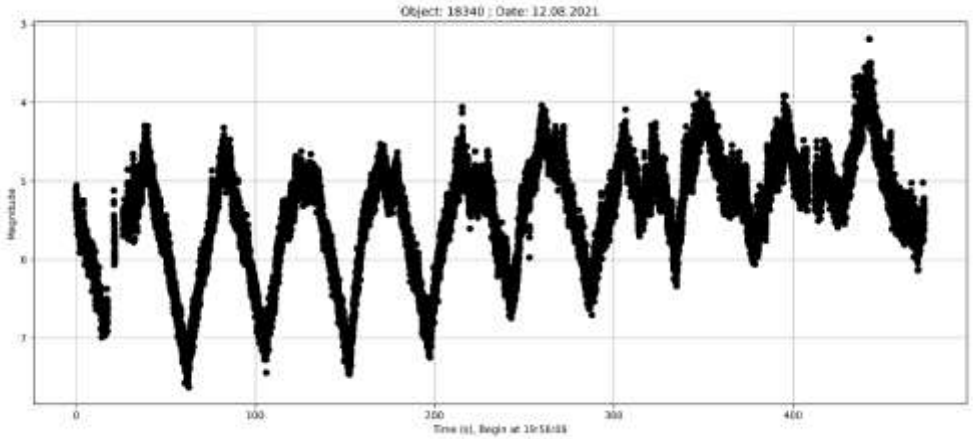
Object: 18340 ; Date: 12.08.2021
Magnitude
Time (s), Begin at 19:58:08

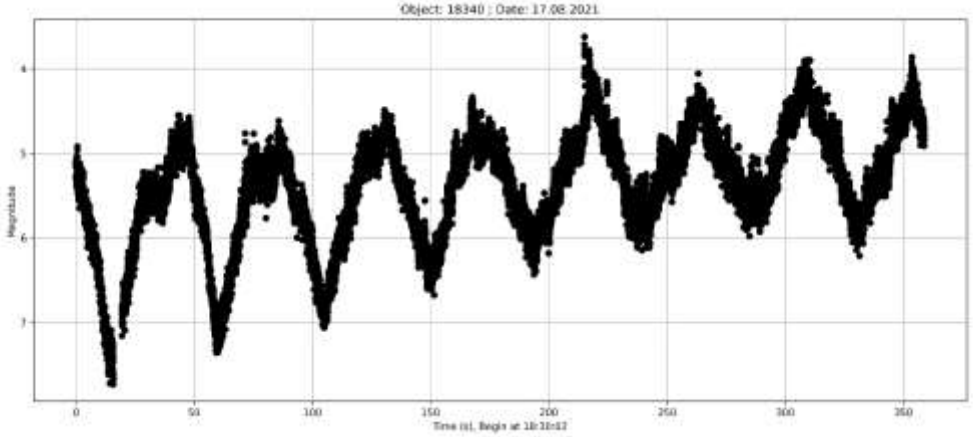
Object: 18340 ; Date: 17.08.2021
Magnitude
Time (s), Begin at 18:30:02

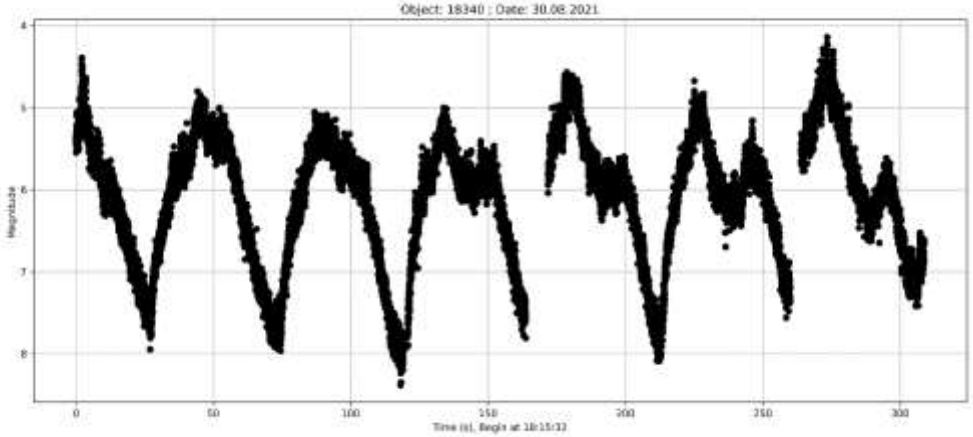
Object: 18340 ; Date: 30.08.2021
Magnitude
Time (s), Begin at 18:15:32

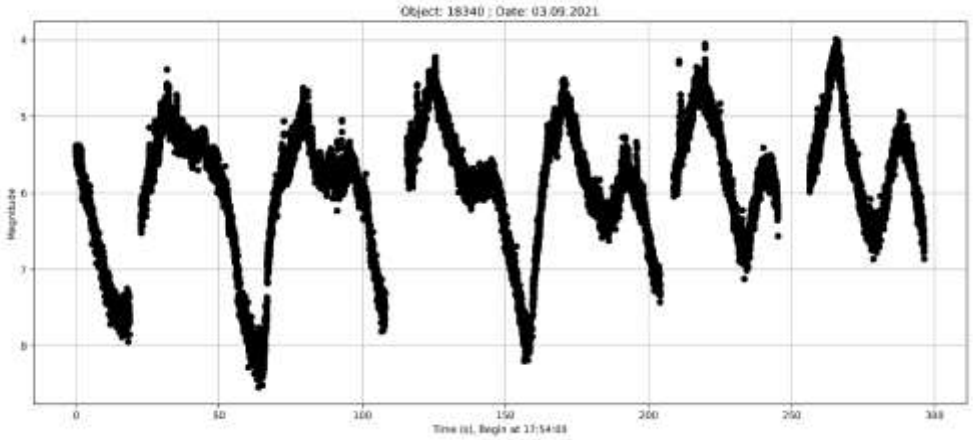
Object: 18340 ; Date: 03.09.2021
Magnitude
Time (s), Begin at 17:54:03

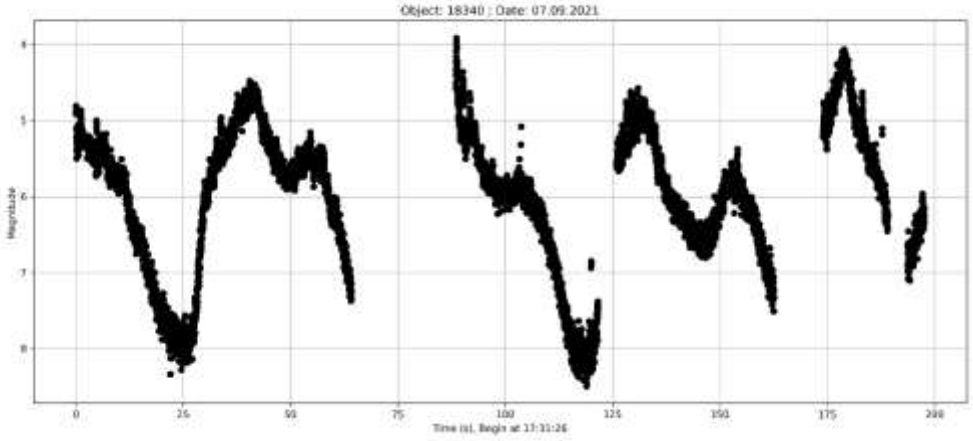
Object: 18340 ; Date: 07.09.2021
Magnitude
Time (s), Begin at 17:31:26

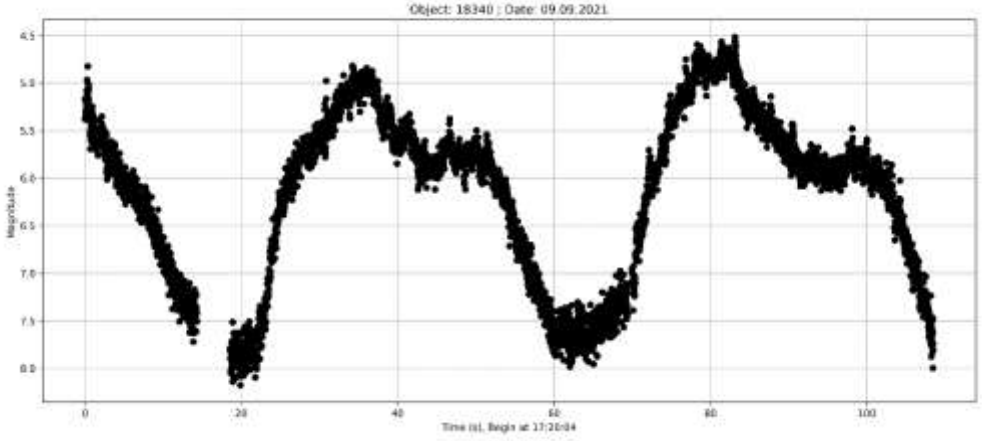
Object: 18340 ; Date: 09.09.2021
Magnitude
Time (s), Begin at 17:20:04

3.5.3 Norad 23088

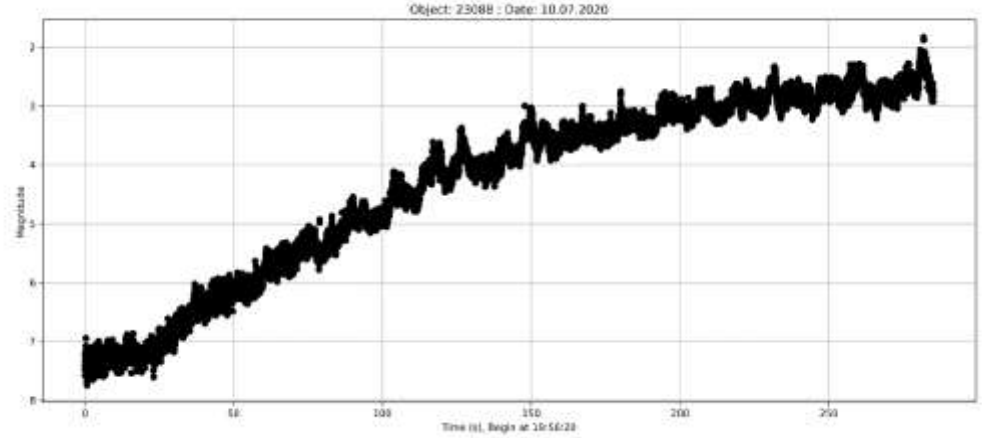

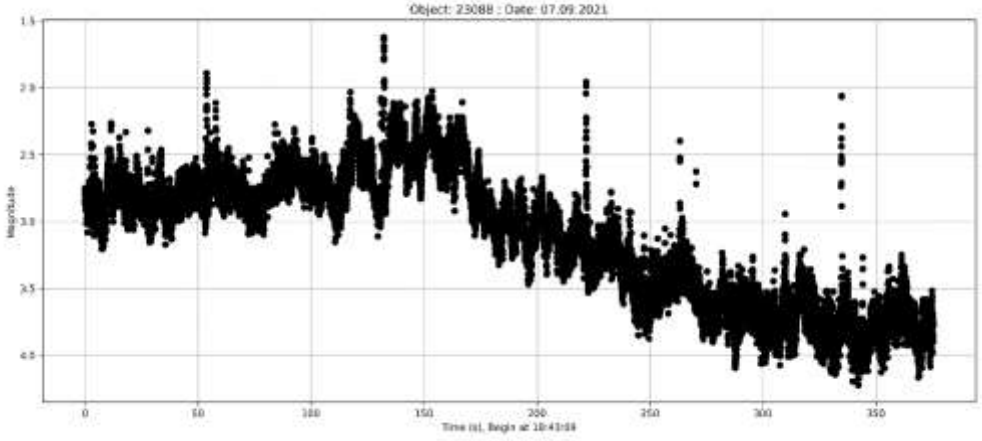

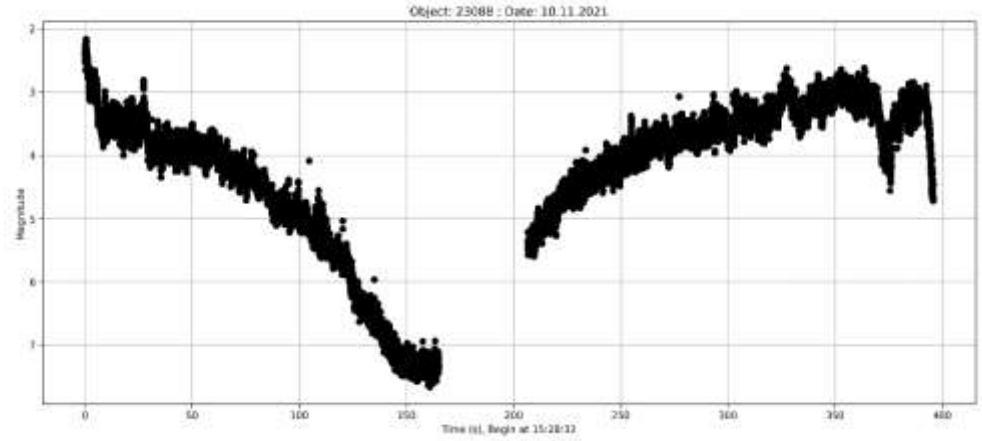

3.5.4 Norad 23405

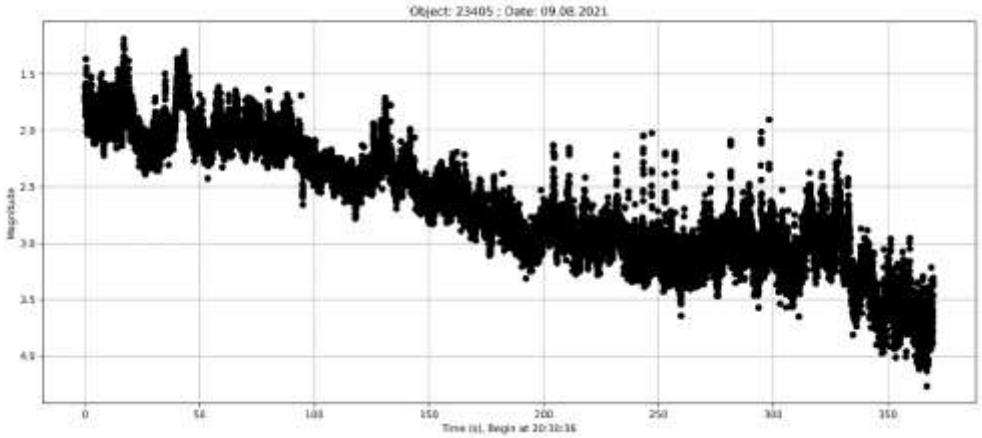

3.5.5 Norad 39198

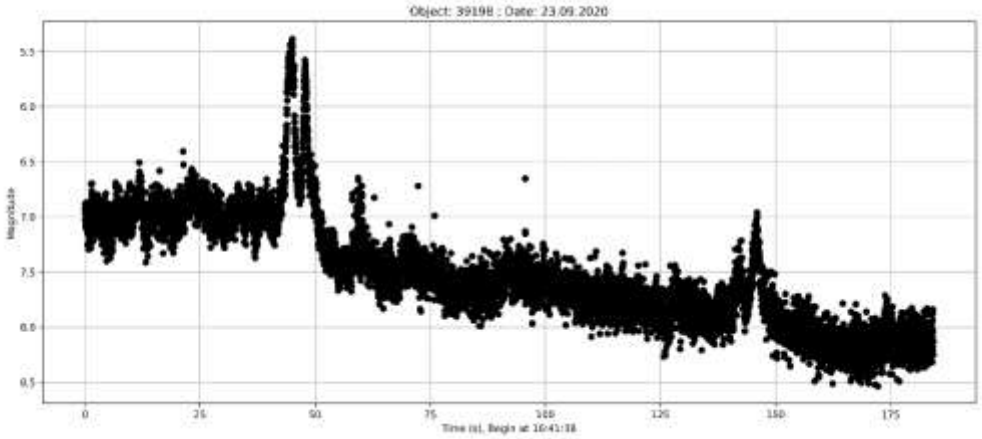

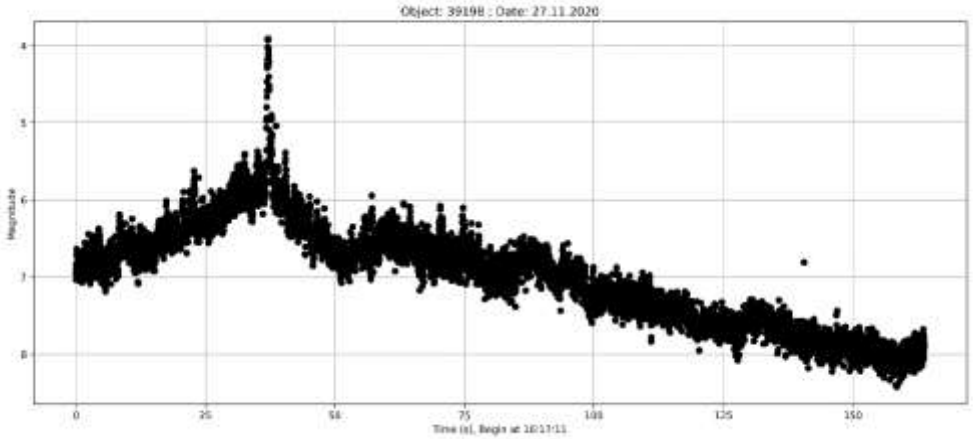

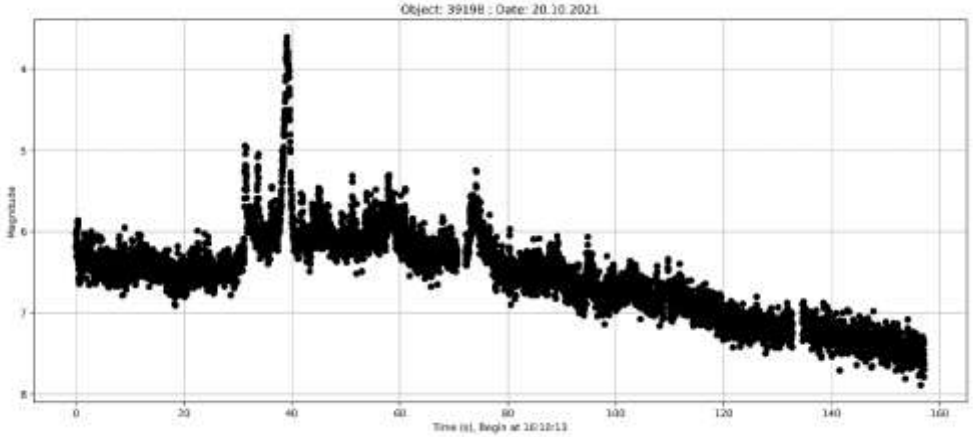

3.5.6 Norad 40879

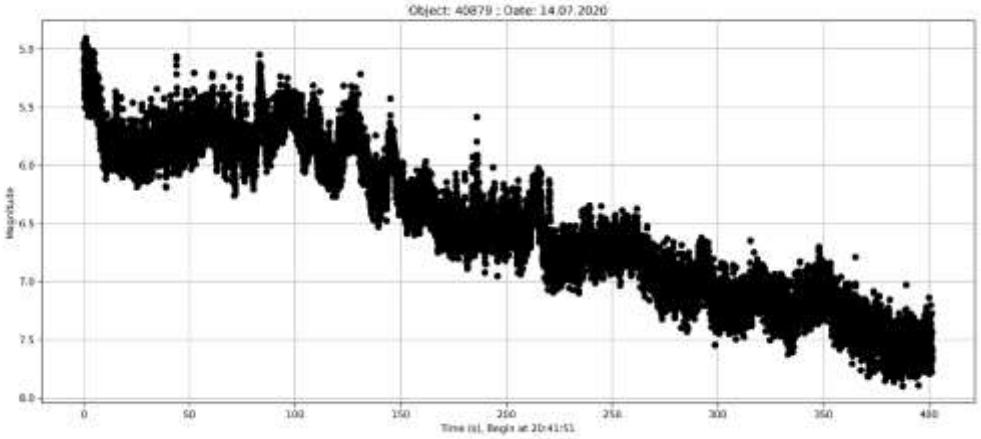
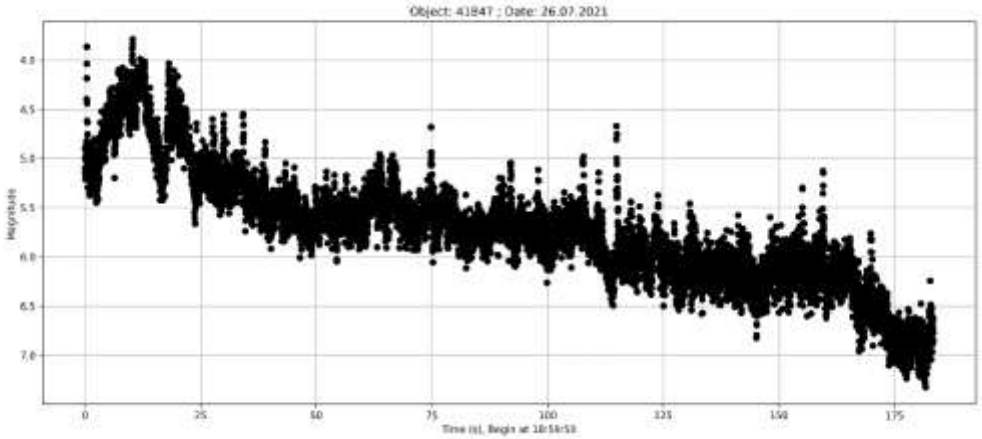
3.5.7 Norad 41847